67-12,565

PELTZMAN, Alan, 1937-

THE EFFECT OF A SMALL NUMBER OF INERT PARTICLES ON THE LOCAL AND OVERALL MASS TRANSFER RATES FROM A SINGLE SPHERE AT LOW REYNOLDS NUMBERS.

The City University of New York, Ph.D., 1967
Engineering, chemical

University Microfilms, Inc., Ann Arbor, Michigan

Copyright by
ALAN PELTZMAN

1967

THE EFFECT OF A SMALL NUMBER OF INERT PARTICLES ON THE LOCAL AND OVERALL MASS TRANSFER RATES FROM A SINGLE SPHERE AT LOW REYNOLDS NUMBERS

by

Alan Peltzman

A dissertation submitted to the
Graduate Faculty in Engineering in partial
fulfillment of the requirements for the
degree of Doctor of Philosophy,
The City University of New York.

1967

This manuscript has been read and accepted for the University Committee in Engineering in satisfaction of the dissertation requirement for the degree of Doctor of Philosophy.

May 25, 1967
Date

Robert Pfeffer
Chairman of Examining Committee

May 25, 1967
Date

Executive Officer

Prof. R. A. Graff

Prof. N. C. Jen

Prof. S. B. Menkes

Prof. R. Pfeffer, Chairman

Supervisory Committee

The City University of New York

ACKNOWLEDGEMENTS

The author is greatly indebted to Professor Robert Pfeffer for his continuous encouragement, guidance and advice during the progress of this research. Special thanks are extended to Professor Alois X. Schmidt for his confidence and interest and to the members of the advisory committee and the Chemical Engineering Department for their valuable suggestions.

Acknowledgement is also due to the Sethco Manufacturing Company for its donation of equipment, to the City College Computation Center for the use of its IBM computer, and to the Mechanical Engineering Department for the use of its optical comparator. The technical assistance of Gabriel Kousourou, John Bodnaruk and the other members of the shop staff was especially helpful and is much appreciated. Heartfelt gratitude is expressed to my wife for her inspiration and understanding and to our families for their warm-hearted encouragement.

This research was supported by a grant from the National Science Foundation and at various times by the City University of New York. Grateful acknowledgement is hereby made to these organizations and their supporters.

TABLE OF CONTENTS

Subject	Page No.
ABSTRACT	1
INTRODUCTION	2
CRITICAL REVIEW OF PERTINENT PRIOR WORK	4
Heat and Mass Transfer from a Single Particle	4
Heat and Mass Transfer in Multiparticle Systems	31
DESCRIPTION OF MATERIALS, APPARATUS AND EXPERIMENTAL METHOD	62
Materials	62
Apparatus	62
Flow System	62
Particle Measurement System	74
Particle Preparation Apparatus	80
Test Section	84
Experimental Method	85
Particle Preparation	85
Initial Particle Measurement	86
Mounting of Active and Inert Spheres	86
Run Procedure	92
Final Particle Measurement	93
RESULTS AND DISCUSSIONS	94
Single Sphere Studies	94
Multiparticle System Studies	108
Axial Configurations	108
Equilateral Triangular Configurations	129
Hexagonal Configurations	140
Relationship Between Local and Overall Mass Transfer Rates for All Studies	157
CONCLUSIONS AND RECOMMENDATIONS	161
Single Sphere Studies	161
Multiparticle System Studies	162
Axial Configurations	162
Equilateral Triangular Configurations	163
Hexagonal Configurations	163
Recommendations	165

NOMENCLATURE 166

LITERATURE CITED 170

ADDENDUM 174

PRESENTATION AND PUBLICATION 178

VITA 179

APPENDICES

Physical Properties of Experimental Materials A - 1
Grashof Number Calculation B - 1
Rotameter Calibration C - 1
Density Determination Data D - 1
Vibrational Considerations E - 1
Method of Data Analysis F - 1
Calculation of Estimated Required Run Times G - 1
Error Analysis H - 1
Flux Effect Calculations I - 1

LIST OF FIGURES

		Page No.
Figure 1.	Heat and Mass Transfer for Single Spheres as Proposed by Friedlander	9
Figure 2.	Gas Phase Heat and Mass Transfer Data for a Single Sphere.	20
Figure 3.	Heat and Mass Transfer Data for Single Spheres to Liquids.	23
Figure 4.	Correlations of Mass Transfer Rates from Separate Regions of Single Sphere Surface.	26
Figure 5.	Local Values of $Sh/Sc^{1/3}$ for Single Spheres vs. Position on Sphere.	28
Figure 6.	Location of Minimum Mass Transfer Rate vs. Reynolds Number.	30
Figure 7.	Average Sherwood Numbers from the Work of Pfeffer, et. al. vs. Peclet Number with Void Fraction as Parameter.	36
Figure 8.	Sherwood (Nusselt) Numbers of Pfeffer, et. al. vs. ϵ, Pe is the Parameter.	37
Figure 9.	Theoretical Values of Sh vs. Re at Sc = 1000, ϵ = 0.5.	38
Figure 10.	Mass Transfer Factor for Packed Beds	40
Figure 11.	Mass Transfer Factors for Packed Beds.	43
Figure 12.	Mass Transfer Factors for Packed Beds.	44
Figure 13.	Heat Transfer Factors for Packed Beds.	47
Figure 14.	Relationship Between Mass Transfer Modulus and Modified Reynolds Number for Spheres and Other Packings.	49

Figure 15.	Relationship Between Heat Transfer Moduli and Modified Reynolds Number for Spheres, Cylinders, and Cubes.	50
Figure 16.	Generalized Relationship Between j_H and Re for Both Heat and Mass Transfer in the Flow of Fluids Through Packed and Distended Beds of Spheres.	53
Figure 17.	Local Heat Transfer Profiles for Single Spheres from Reference (66).	57
Figure 18.	Local Heat Transfer Profiles for a Sphere in a Dense Cubic Array.	59
Figure 19.	Schematic Flow Diagram.	64
Figure 20.	Flow System (Pictures).	65
Figure 21.	Drawing of Flow System Main.	66
Figure 22.	Drawing of Test Section.	68
Figure 23.	Test Section (Pictures).	69
Figure 24.	Rotameter Calibration - Low Flow Range.	72
Figure 25.	Rotameter Calibration - High Flow Range.	73
Figure 26.	Drawing of Rotary Stage.	76
Figure 27.	Drawing of Particle Locking Device.	77
Figure 28.	Optical Comparator (Pictures).	78
Figure 29.	Measuring Assembly (Picture).	79
Figure 30.	Detail Drawing of Molds Used.	81
Figure 31.	Mold for Casting Active Spheres (Pictures).	82
Figure 32.	Sphere Positioner (Picture).	87
Figure 33.	Mounting of the Active Sphere.	89
Figure 34.	Centering and Location Guides.	90

Figure 35. Local Mass Transfer Profiles, Single Spheres of Benzoic Acid. 96

Figure 36. Local Mass Transfer Profiles, Single Spheres of Benzoic Acid. 97

Figure 37. Local Mass Transfer Profiles, Single Spheres of Beta Naphthol. 98

Figure 38. Local Mass Transfer Profiles, Single Spheres of Beta Naphthol. 99

Figure 39. Comparison of Present Local Mass Transfer Profiles with those Reported in (55) and (46). 101

Figure 40. Single Sphere Results, Sh_o vs. $Re^{1/2} Sc^{1/3}$. 103

Figure 41. Single Sphere Results - Sh_o vs. Pe. 104

Figure 42. Single Sphere Results - Sh_o vs. Pe. 109

Figure 43. Axial Configurations Used. 110

Figure 44. Local Mass Transfer Profiles - Series II - Benzoic Acid Results - Sh_L vs. ξ. 114

Figure 45. Local Mass Transfer Profiles - Series II - Beta Naphthol Results - Sh_L vs. ξ. 115

Figure 46. Local Sherwood Number Profiles - Series III - Benzoic Acid Results - Sh_L vs. θ. 116

Figure 47. Local Sherwood Number Profiles - Series III - Beta Naphthol Results - Sh_L vs. θ. 117

Figure 48. Local Sherwood Number Profiles - Series V - Benzoic Acid Results - Sh_L vs. ξ. 118

Figure 49. Local Sherwood Number Profiles - Series V - Beta Naphthol Results - Sh_L vs. ξ. 119

Figure 50. Local Sherwood Number Profiles - Series VI - Benzoic Acid Results - Sh_L vs. ϑ. 120

Figure 51. Local Sherwood Number Profiles - Series VI - Beta Naphthol Results - Sh_L vs. ϑ. 121

Figure 52.	Series II Results - Sh_o vs. Pe.	122
Figure 53.	Series III Results - Sh_o vs. Pe.	123
Figure 54.	Series V Results - Sh_o vs. Pe.	124
Figure 55.	Series VI Results - Sh_o vs. Pe.	125
Figure 56.	Comparison of Local Mass Transfer Profiles - Series I, II and III - Benzoic Acid - $Re_p \doteq 75$ - Sh_L vs. θ.	127
Figure 57.	Comparison of Local Mass Transfer Profiles - Series I, V and VI - Benzoic Acid - $Re_p \doteq 75$ - Sh_L vs. ξ.	128
Figure 58.	Comparison of Overall Mass Transfer Results - Series I, II and III.	130
Figure 59.	Comparison of Overall Mass Transfer Results - Series I, V and VI.	131
Figure 60.	Equilateral Triangle Configurations Used.	132
Figure 61.	Local Sherwood Number Profiles - Series VIII - Benzoic Acid Results - Sh_L vs. θ.	135
Figure 62.	Local Sherwood Number Profiles - Series VIII - Beta Naphthol Results - Sh_L vs. θ.	136
Figure 63.	Local Sherwood Number Profiles - Series IX - Benzoic Acid Results - Sh_L vs. θ.	137
Figure 64.	Local Sherwood Number Profiles - Series IX - Beta Naphthol Results - Sh_L vs. ξ.	138
Figure 65.	Overall Mass Transfer Results - Series VIII and IX - Sh_o vs. Pe.	139
Figure 66.	Hexagonal Geometries Used.	141
Figure 67.	Local Sherwood Number Profiles - Series VII - Pseudo Voidage of 0.85 - Sh_L vs. ξ.	144
Figure 68.	Local Sherwood Number Profiles - Series VII - Pseudo Voidage of 0.73 - Sh_L vs. θ.	145

Figure 69. Local Sherwood Number Profiles - Series VII - Pseudo Voidage of 0.40 - Sh_L vs. θ. 146

Figure 70. Series I (BA) Results and Series VII Results - Sh_o vs. Pe, ϵ' is Parameter. 148

Figure 71. Local Sherwood Number Profiles - Series X - Pseudo Voidage of 0.85 - Sh_L vs. θ . 149

Figure 72. Local Sherwood Number Profiles - Series X - Pseudo Voidage of 0.82 - Sh_L vs. θ . 150

Figure 73. Local Sherwood Number Profiles - Series X - Pseudo Voidage of 0.40 - Sh_L vs. θ . 151

Figure 74. Series I (BA) Results and Series X Results - Sh_o vs. Pe, ϵ' is Parameter. 153

Figure 75. Series I (BA) Results and Series X Results - Sh_o vs. ϵ', Pe is Parameter. 154

Figure 76. Comparison of Benzoic Acid Results - Series I, II, VII ($\epsilon' = 0.85$) and X ($\epsilon' = 0.85$) - Sh_o vs. Pe. 155

Figure 77. Comparison of Benzoic Acid Results - Series I, II, VII ($\epsilon' = 0.40$) and X ($\epsilon' = 0.40$) - Sh_o vs. Pe. 156

Figure 78. Results of Roughness Tests. 176

Figure App. 1. Solubility of 2-Naphthol in Water. A-4

Figure App. 2. Diffusivity of 2-Naphthol in Water. A-5

Figure App. 3. Schmidt Number of 2-Naphthol in Water. A-6.

Figure App. 4. Solubility of Benzoic Acid in Water. A-7

Figure App. 5. Schmidt Number of Benzoic Acid in Water. A-8

Figure App. 6. Diffusivity of Benzoic Acid in Water. A-9

Figure App. 7. Gr vs. t for Benzoic Acid - Water and Beta Naphthol -Water. B-4

Figure App. 8. Simplification of Sphere Support System for Vibration Calculations. E-2

Figure App. 9.	Simplification of Sphere Support System for Vibration Calculations.	E-6
Figure App. 10.	Estimated Required Run Times - Single Sphere Studies.	G-7
Figure App. 11a.	Estimated Required Run Times - Multiparticle Studies - Benzoic Acid.	G-8
Figure App. 11b.	Estimated Required Run Times - Multiparticle Studies - Beta Naphthol.	G-9

LIST OF TABLES

		Page No.
Table I.	A Numerical Comparison of Average Nusselt Numbers at Low Peclet Numbers	11
Table II.	Comparison of Experimental and Calculated Values of M at a Reynolds Number of 500	15
Table III.	Overall Mass Transfer for Spheres	16
Table IV.	Mass Transfer from the Forward Stagnation Point of 3/8 Inch Diameter Benzoic Acid Spheres in Water	17
Table V.	Correlations of Garner, et. al. for Mass Transfer Rates from Separate Regions of Sphere Surface	25
Table VI.	American Chemical Society Certified Analysis of the Benzoic Acid and BetaNaphthol Used Throughout this Work	63
Table VII.	Overall Mass Transfer Rates for Single Spheres of BetaNaphthol and Benzoic Acid	95
Table VIII.	Overall Mass Transfer Results - Axial Studies	111
Table IX.	Overall Mass Transfer Results - Equilateral Triangular Studies	133
Table X.	Overall Mass Transfer Results - Benzoic Acid Test Spheres - Hexagonal Studies	142
Table XI.	Comparison Between Overall Sherwood Numbers Calculated from Local Mass Transfer Profiles and Particle Weight Loss	158

Table App. I.	Density of Water	A-2
Table App. II.	Viscosity of Water	A-3
Table App. III.	Grashof Numbers for Benzoic Acid and Beta Naphthol as a Function of Temperature	B-3
Table App. IV.	Calibration Data - Low Flow Range Rotameter	C-3
Table App. V.	Calibration Data - High Flow Range Rotameter	C-4
Table App. VI.	Particle Density Data	D-2
Table App. VII.	Estimated Required Run Times - Single Sphere Studies	G-4
Table App. VIII.	Estimated Required Run Times - Multiparticle Studies	G-5

ABSTRACT

An investigation was undertaken to study the phenomenon of particle-to-fluid mass transfer in multiparticle systems. Local and overall mass transfer rates from a single active sphere either alone or in the presence of one or more inert spheres were determined experimentally, at low Reynolds number (5-150), high Peclet number (3,500-150,000) flow. Data were obtained by measuring the diminution profile of a spherical particle of either benzoic acid or beta naphthol due to water flowing past the rigidly held particles in a cylindrical tube.

Single sphere results show that flow separation does not appear to occur at a Reynolds number of 5 but is striking at a Reynolds number of 25. The location of the separation ring is dependent upon Reynolds number, in agreement with the results of previous investigators. The local mass transfer rate profiles for single spheres are in agreement with those predicted by boundary layer theory and the overall mass transfer results can be represented as a function of $Re^{1/2}\ Sc^{1/3}$ or $Pe^{1/3}$.

Numerous results were obtained for spheres in axial, equilateral triangular and hexagonal configurations. They show the marked effect particle-to-particle interactions have on particle-to-fluid mass transfer and on the hydrodynamic flow pattern around particles.

INTRODUCTION

The phenomenon of particle-to-fluid heat and mass transfer is widely encountered in the chemical and nuclear industries. An example of this is the diffusion controlled catalytic reaction, such as might occur in a fixed or fluidized reactor. This involves diffusion of the reactants from the bulk fluid stream to the surface of the solid catalyst particles where the chemical reaction occurs, and then back diffusion of the products. Chemical reactions are invariably accompanied by enthalpy changes, therefore we have simultaneous particle-to-fluid heat and mass transfer.

Other examples include: fixed or moving bed pebble heaters, heat recovery operations in which a particulate catalyst is cooled by direct contact with a flowing gas, drying of a gas by a granular adsorbent, regeneration of a used adsorbent and spent catalyst, destruction of nuclear wastes, sublimation of solid particles into a gaseous stream, solution of solid particles into a liquid stream, roasting of ores, solid-liquid extraction and leaching, etc.

When one considers the widespread occurence of particle-to-fluid heat and mass transfer, it is easily understood why such a large number of experimental and theoretical studies have been reported in recent years. However, the correlations resulting from these investigations, for the most part, do not agree with each other; especially in the low Reynolds number range. In addition, almost all of the experimental data were obtained in the void fraction range

$\epsilon = 0.4$ to $\epsilon = 0.6$ so that the effect of fractional void volume on heat and mass transfer rates is not well established. The theoretical investigators are faced with the problem of adequately describing, mathematically, the flow behavior around particles and the effects of particle-to-particle interactions. Recently, great interest has developed in the local mass and heat transfer rates from particles-to-fluids in packed and fluidized beds.

The purpose of this investigation was to obtain experimental data at low Reynolds number, high Peclet number flow which would help to establish the effect of particle-to-particle interactions (hydrodynamic or void volume effect) on the local and overall mass transfer rates in multiparticle systems. To this end, axial and axial-radial configurations of a small number of inert spheres, surrounding a single active sphere, were used. For these configurations, local radius diminution profiles, which in turn are related to the local mass transfer process, were obtained optically. Overall mass transfer rates were obtained by integration of the local profiles.

CRITICAL REVIEW OF PERTINENT PRIOR WORK

The transfer of heat and mass between particles and fluids has been widely investigated both experimentally and theoretically in recent years because of the growing importance of fluid-particle operations in the chemical and nuclear industries. These investigations were concerned with heat and mass transfer from single particles as well as heat and mass transfer in multiparticle systems such as packed, distended, and fluidized beds. This review will summarize the present state of knowledge pertinent to this thesis.

Heat and Mass Transfer from a Single Particle

Theoretical Studies

The transfer of heat and mass from a sphere to an infinite stagnant fluid has been treated theoretically by Langmuir,[33] Rudenberg,[48] and Fuchs,[17] all of whom have shown that

$$Sh = Nu = 2 \qquad (1)$$

If the fluid is allowed to flow past the particle at low Reynolds numbers, heat or mass will be transferred by convection as well as by molecular transport and the value of the Nusselt number or Sherwood number will become greater than two.

Kronig and Bruijsten,[31] in a theoretical study, developed an expression for the Nusselt (or Sherwood) number around a sphere by a perturbation

technique which expanded the temperature field around the sphere in powers of the Peclet number, Pe. They found that a perturbation procedure starting with a finite sphere in a stationary medium as a zeroth approximation was unsuitable. However, using a point source in a flowing medium as a basis, a solution was obtained which satisfied the boundary condition at infinity except at $\theta = 0$ (the direction of flow). Their result is applicable only at low values of the Reynolds number since they used Stokes' field for the velocity profile in the solution of the energy equation. They found that

$$Nu_{avg} = 2 + \frac{1}{2} Pe + \frac{581}{1920} Pe^2 + \cdots \qquad (2)$$

Breiman[5] considered the same physical situation as Kronig and Bruijsten. However, he used a Green's function technique to transform the problem into an integral equation which was then solved by iteration. He concluded that, for small Peclet numbers,

$$Nu_{avg} = 2 + \frac{1}{2} Pe - \frac{1}{4} Pe^2 \ln Pe - 0.0334\, Pe^2 + \cdots \qquad (3)$$

That this does not agree with equation (2) is surprising, since the two investigations were concerned with the same mathematical model and differed only in the method of solution.

Frisch[14] considered the same problem but assumed the sphere to be falling in a stationary fluid with diffusion occurring from the fluid to the particle. He also expanded the concentration field around the sphere in terms of the Peclet number by a perturbation method. However, he assumed, for some reason,

that $C(\cdot^{\cdot},0) = C(\cdot,\cdot)$ as one of his boundary conditions. This seems to invalidate the result he obtained for the Sherwood number around the sphere.

Illingworth,[29] in a study of the hot wire anemometer, developed an expression relating the Nusselt number and the Peclet number by assuming that the fluid flows past the sphere in simple harmonic motion about a mean velocity. Using an Oseen-type approximation he solved the energy equation. He represented the velocity profile by the main-stream velocity, V_∞. Illingworth's result, without regard to the effect of velocity fluctuations, is

$$Nu_{avg} = 2 + \frac{1}{2} Pe + O(Pe)^2 \qquad (4)$$

Ogiwara,[43] using a similar approximation obtained the same result.

Nielson[39] also utilized Stokes' field to describe the fluid velocity profile. However, he solved the energy equation numerically by a relaxation procedure. His result is

$$Sh_{avg} = 2\left(1 + \frac{Pe}{2}\right)^{.285} \approx 2 + .285\,Pe - .05095\,Pe^2 \qquad (5)$$

This shows a smaller coefficient, than was previously obtained, for the first order Peclet number term.

Friedlander[12] using boundary-layer theory solved the same problem. The existence of a thermal boundary layer, which is a limited region of the flow that is affected by the presence of the heated surface, was assumed. At the edge of the layer the temperature reaches that of the bulk of the fluid and all the temperature derivatives with respect to the normal to the surface vanish. The Nusselt number can be calculated by use of the known velocity

profile if a temperature distribution is assumed. Friedlander used the velocity profile derived by Tomotika and Aoi[60] from the linearized Navier-Stokes equations. His result for large Peclet numbers is

$$Nu_{avg} = 0.975\ (Pe)^{1/3} \tag{6}$$

and for very small Peclet numbers is

$$Nu_{avg} = 2 + \frac{Pe}{2} + \frac{Pe^2}{6} + \cdots \tag{7}$$

Yuge[64] also conducted a theoretical study of heat and mass transfer from a single sphere to a fluid flowing at low Reynolds numbers. He solved the energy equation numerically by a set of approximations in which he assumed that the temperature profile was expandable in even powered terms of the spherical angle θ. The fluid velocity profile used was Stokes' field. He succeeded in showing that his expansion converged extremely rapidly, and also satisfied all the boundary conditions. The previous expansions in terms of the Peclet number[5, 12, 14, 29, 31, 39, 43] were restricted to Peclet values less than unity. Yuge's results are not restricted to values of $Pe \lesssim 1$ and were calculated for a Peclet number as high as 10. His results for different values of the Peclet number are tabulated below.

Pe	g_o'	g_2'	f_4'	Nu_{avg}
0.3	1.0939	-0.0327	0.0001	2.00
1.0	1.2733	-0.0591	0.0000	2.20
3.0	1.5510	-0.0927	-0.0001	2.55
10.0	2.0301	-0.1450	-0.0003	3.20

In the last column are presented the average Nusselt number for different values of the Peclet number. In order to obtain the local Nusselt number at any location on the sphere's surface, use must be made of the following equation given in Yuge's paper:

$$Nu = 2 (g_o' + g_2' \Theta^2 + f_4' \Theta^4) \tag{8}$$

where the constants g_o', g_2', and f_4' are those tabulated above.

Friedlander [13] combined the theoretical results of Yuge for low Pe number with a Levich-Lighthill[34] thin boundary-layer method solution of the energy equation at high Peclet number to obtain a curve which represents the relation between the Sherwood number and the Peclet number for all values of Pe. Equation (9) is the result he obtained for Pe approaching infinity.

$$Sh = 0.991\ Pe^{1/3} \tag{9}$$

Figure 1 presents the complete Sh vs. Pe curve drawn by Friedlander based on equation (9) and the results of Yuge. It should be noted that this curve applies only for low Reynolds numbers since the velocity field which was used neglects all inertial effects.

Acrivos and Taylor[1] made a theoretical study of heat and mass transfer rates from a single sphere at low Peclet numbers, where the velocity field was also assumed to be given by Stokes' formula. Using a singular perturbation technique they derived the following expression for the average Nusselt number in terms of the Peclet number, in the Peclet number range 0 to 1.

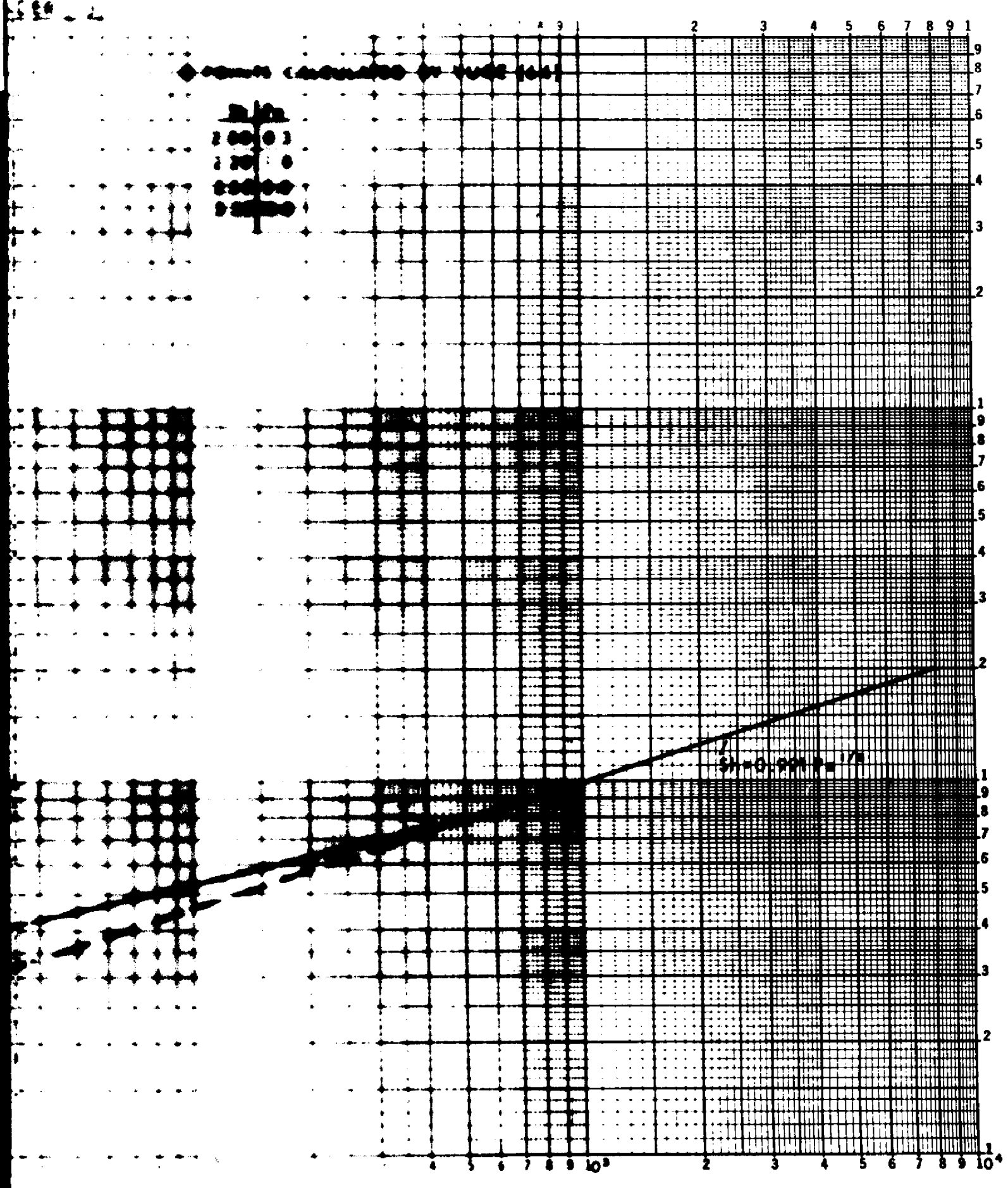

(8)

w Pe number

the energy

the relation

of Pe

ty

(9)

Friedlander based

that this curve

ty field which was

heat and mass transfer

where the velocity field was

a singular perturbation

the average Nusselt

let number range 0 to 1.

FIGURE 1 - HEAT & MASS TRANSFER FOR SINGLE SPHERES AS PROPOSED BY FRIEDLANDER (13)

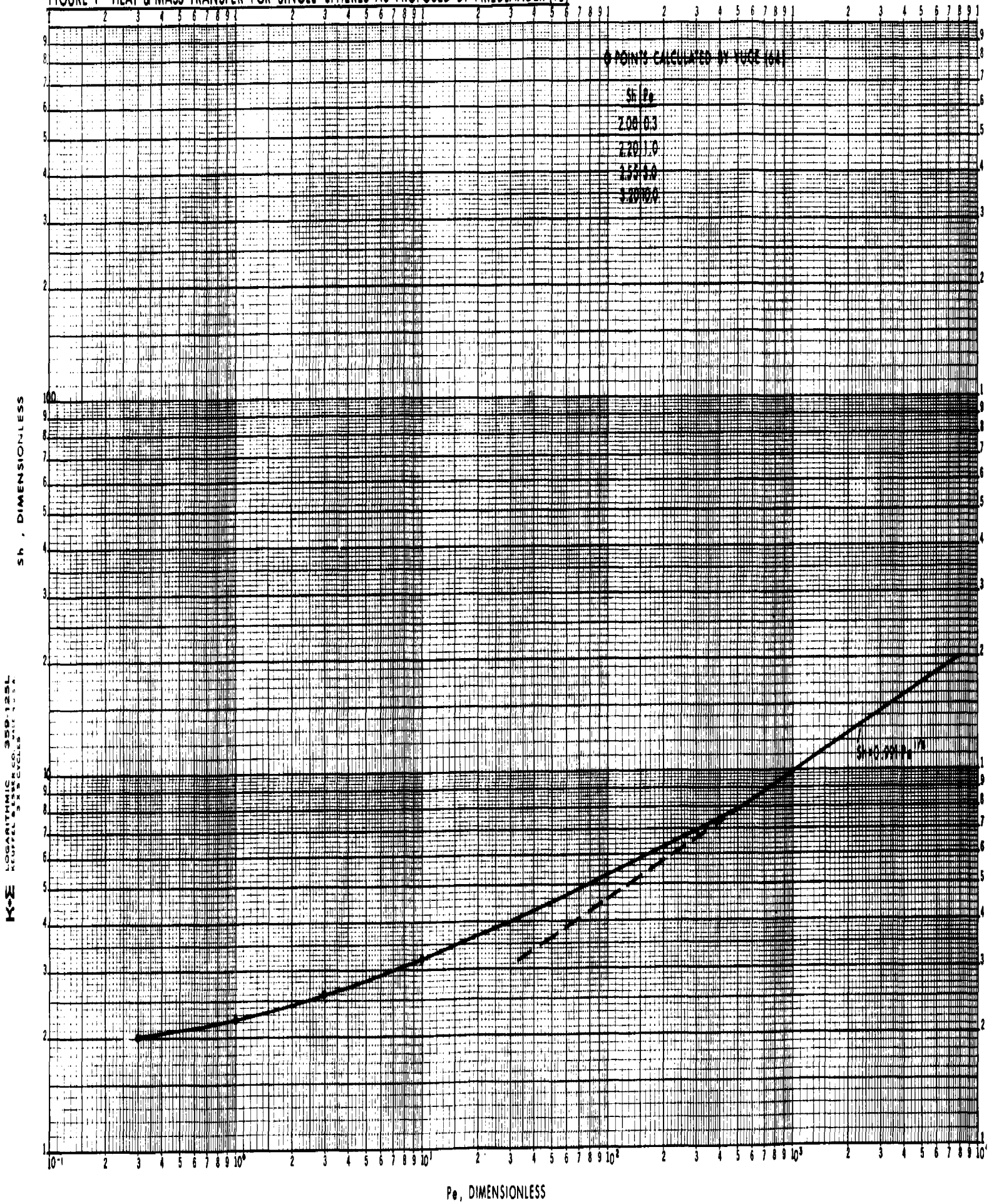

$$Nu_{avg} = 2 + \frac{1}{2} Pe + \frac{1}{4} Pe^2 \ln Pe + 0.03404\, Pe^2 + \frac{1}{16} Pe^3 \ln Pe + \cdots \quad (10)$$

Table I presents the numerical values of the average Nusselt number, as computed from equations (2), (3), and (10) and those reported by Yuge, for the range $0 \leq Pe < 1$.

The "matching" solution used by Acrivos and Taylor in deriving equation (10) seems mathematically rigorous at very low Pe, but at what value of Pe it will break down cannot be determined.

Brenner,[6] using the singular perturbation technique of Acrivos and Taylor, solved the steady-state energy equation for the streaming flow of an incompressible fluid of infinite extent past an isothermal, stationary, three dimensional body of arbitrary shape. He found that at small Peclet numbers the average Nusselt number could be expressed in the form

$$\frac{Nu}{Nu'_o} = 1 + \frac{1}{8} Nu\, Pe + O(Pe) \quad (11)$$

where Nu'_o is the Nusselt number for heat transfer to a stagnant fluid. This relation was shown to be independent of the particle Reynolds number, the orientation of the body relative to the free-stream velocity and the dynamical boundary condition satisfied by the velocity at the surface of the body. These variables do, however, have an effect in higher approximations.

Brenner also made an explicit calculation of the next term in the expansion of equation (11) for the case of Stokes' flow relative to the arbitrary

TABLE I. A Numerical Comparison of Average Nusselt Numbers at Low Peclet Numbers

Pe	Equation (2)	Equation (3)	Equation (10)	Reference (64)
0.1	2.053	2.055	2.044	—
0.2	2.112	2.115	2.084	—
0.3	2.177	2.174	2.124	2.00
0.4	2.248	2.231	2.165	—
0.5	2.326	2.284	2.209	—
0.6	2.409	2.334	2.259	—
0.7	2.498	2.377	2.315	—
0.8	2.594	2.414	2.379	—
0.9	2.695	2.444	2.451	—
1.0	2.803	2.467	2.534	2.20

shaped body. The results of this analysis yields the relation

$$\frac{Nu}{Nu'_o} = 1 + \frac{1}{8} Nu'_o Pe + \frac{1}{16} Nu'_o f_{ox} Pe^2 \ln Pe + O(Pe^2) \qquad (12)$$

where f_{ox} is the dimensionless drag on the body. It was further concluded that the O (Pe^2) term in this expansion for the Nusselt number depends explicitly on the shape of the body and cannot be given in general form.

It is notable that for the case of a solid sphere of radius "a" ($Nu'_o = 2$, $f_{ox} = 1$) equation (12) yields

$$Nu = 2 + \frac{1}{2} Pe + \frac{1}{4} Pe^2 \ln Pe + O(Pe^2) \qquad (13)$$

which is in agreement with the first three terms of the expansion of Acrivos and Taylor; (equation 10).

Grafton[25] considered the transfer of mass from solid spheres due to forced convection of a continuous incompressible fluid, where there was no effect of natural convection and where negligible molecular diffusion occurred outside the boundary layer. This approach was to relate the mass transfer process to the hydrodynamic conditions existing over the entire surface of the sphere. It was assumed, in order to analyze the hydrodynamic conditions, that the boundary layer is laminar.

In order to describe the hydrodynamic conditions over the sphere surface in the forward flow area, Grafton used the method of Tomotika[59] which

requires a knowledge of the pressure variations normal to the particle surface. He then used a boundary layer theory approach to obtain a relation for the hydrodynamic conditions in the wake area of the sphere. This requires a knowledge of the wake contours of the sphere. Both of these descriptions for the hydrodynamic conditions are in terms of the dimensionless parameter Z which is defined as

$$Z = \frac{U_a \xi^2 \rho}{a \mu} \tag{14}$$

A boundary layer theory analysis of the mass transfer process results in the following relationship

$$M = \frac{Sh}{Sc^{0.33} Re^{0.5}} = \left(\frac{8}{Z}\right)^{0.5} \tag{15}$$

which permits calculation of the local value of the Sherwood number from a knowledge of the local value of Z. One could then obtain the average Sherwood number by integration over the sphere surface.

Grafton showed that for the forward stagnation point the forced convection transfer group M is independent of Reynolds number but for the over-all or partial surfaces the value of M is dependent on Reynolds number. He offered no general form of this dependency because of its complexity but these observations explain the reason for various investigators obtaining different constants, for different ranges of Reynolds numbers, in the usual

dimensionless expressions.

The result obtained by Grafton is obviously more applicable at higher Reynolds numbers than the previously discussed theoretical works because Stokes' field was not assumed as the velocity profile around the sphere. Table II presents a comparison between calculated values of M and experimentally determined values for a Reynolds number of 500. The results of several experimental studies are compared with the overall value of M calculated through equation (14) in Table III. The experimental data of Garner and Hoffman[21] for mass transfer from the forward stagnation point of benzoic acid spheres to water at low Reynolds numbers are presented in Table IV to show the disturbance due to natural convection upon the mass transfer group M.

Lochiel and Calderbank[35] developed a theoretical equation to describe the mass transfer rate around any axisymmetric body of revolution when the Peclet and Schmidt numbers are large in value. They then solved this equation for several bodies which are of interest to chemical engineers. For solid spheres at Reynolds numbers less than 1 (creeping flow) they applied Stokes' law and obtained the same result as Friedlander,[13] i.e.

$$Sh = 0.99\ Pe^{1/3} \tag{16}$$

with the additional stipulation that the Peclet number must be greater than 100.

TABLE II. Comparison of Experimental and Calculated Values of M at a Reynolds Number of 500

$$M = Sh/Sc^{0.33} Re^{0.5}$$

	Experimental Values of Garner and Suckling (23)	Experimental Values of Garner and Grafton (20)	Calculated Values
Entire Surface	0.95	0.91	0.90
Forward Flow Area	1.08	1.04	1.01
Wake Area	0.67	0.77	0.63
Forward Stagnation Point	1.68	1.39	1.60
Rear Stagnation Point	0.87	0.56	0.875

TABLE III. Overall Mass Transfer for Spheres

Experimenter	Re Range	Value of M $M = Sh/Sc^{0.33}Re^{0.5}$
Garner and Grafton (20)	500	0.91
Garner and Keey (22)	250 - 750	0.94
Garner and Suckling (23)	500	0.95
Frossling (15)	2 - 1000	0.55
McCune and Wilhelm (38)	30 - 130	1.38
Rowe, Claxton and Lewis (47)	500	0.80
Calculated	500	0.90

TABLE IV. Mass Transfer from the Forward Stagnation Point of 3/8 Inch Diameter Benzoic Acid Spheres in Water

$$M = \frac{Sh}{Sc^{0.33} Re^{0.5}}$$

Re	Up Flow	Down Flow
3	3.1	3.2
10	2.1	1.8
20	1.8	1.3
40	1.4	1.1
70	1.4	1.2
100	1.4	1.3
Calculated Value	1.6	1.6

For solid spheres at Reynolds numbers much larger than 1 (boundary layer flow) they applied boundary layer theory and found that for the forward flow area, $0^{o} \leq \theta \leq 108^{o}$, the relation was

$$Sh = 0.7\ Re^{1/2}\ Sc^{1/3} \tag{17}$$

Assuming that the transfer occurring in the wake area amounts to twenty percent of the forward flow area transfer, see reference (15), the overall transfer rate may be described approximately as

$$Sh = 0.84\ Re^{1/2}\ Sc^{1/3} \tag{18}$$

Their analysis yielded a value of $Sh/Sc^{1/3}\ Re^{1/2}$, M, at the forward stagnation point of 1.34 which compares to 1.47 found for this group by Frossling[16] and to 1.6 found by Grafton.

Experimental verification of the theoretical studies which are applicable at low Reynolds and Peclet numbers has been limited, due to the difficulty in obtaining accurate heat or mass transfer data at very low Reynolds numbers because of natural convection effects. In the next section a critical study is presented of the experimental single sphere data available in the literature.

Experimental Studies

Heat and mass transfer rates from single particles to both gases and liquids have been measured experimentally by many different investigators.

All of the solid-gas data were obtained using an air stream. The solid-liquid investigations were carried out mainly by using water as the solvent medium.

For Reynolds numbers of 1000 or less, experimental data have been reported by Kramers,[30] Ranz and Marshall,[44] Tang, Duncan, and Schweyer,[57] Yuge[65], Allander,[2] Frossling,[15] and most recently by Rowe, Claxton, and Lewis[47] for solid-gas systems. These data together with the theoretical results of Kronig and Bruijsten, Friedlander, Yuge, Acrivos and Taylor, and Lochiel and Calderbank are shown in Figure 2 so as to offer a convenient comparison. It appears from Figure 2 that equation (2) overestimates the convection effect whereas Yuge's theoretical result underestimates this effect. Inspection of Figure 2 indicates that both equations (7) and (10) seem to extrapolate the experimental data down to low Reynolds numbers. Figure 2 also indicates that Friedlander's result for high Pe, equation (6), as well as equation (16) underestimate the experimental observations. Furthermore, it clearly shows that the combined Friedlander-Yuge curve underestimates the experimental data over the entire range of Pe or Re under consideration.

Upon further inspection of Figure 2, it seems that a combination of the data leading to curves F and H with the theoretical results of curves B and C will yield a correlation between Nu and Pe. This will satisfactorily represent the single sphere gas phase heat and mass transfer phenomenon up to a Peclet number of 3000.

FIGURE 2 - GAS PHASE HEAT AND MASS TRANSFER DATA FOR A SINGLE SPHERE

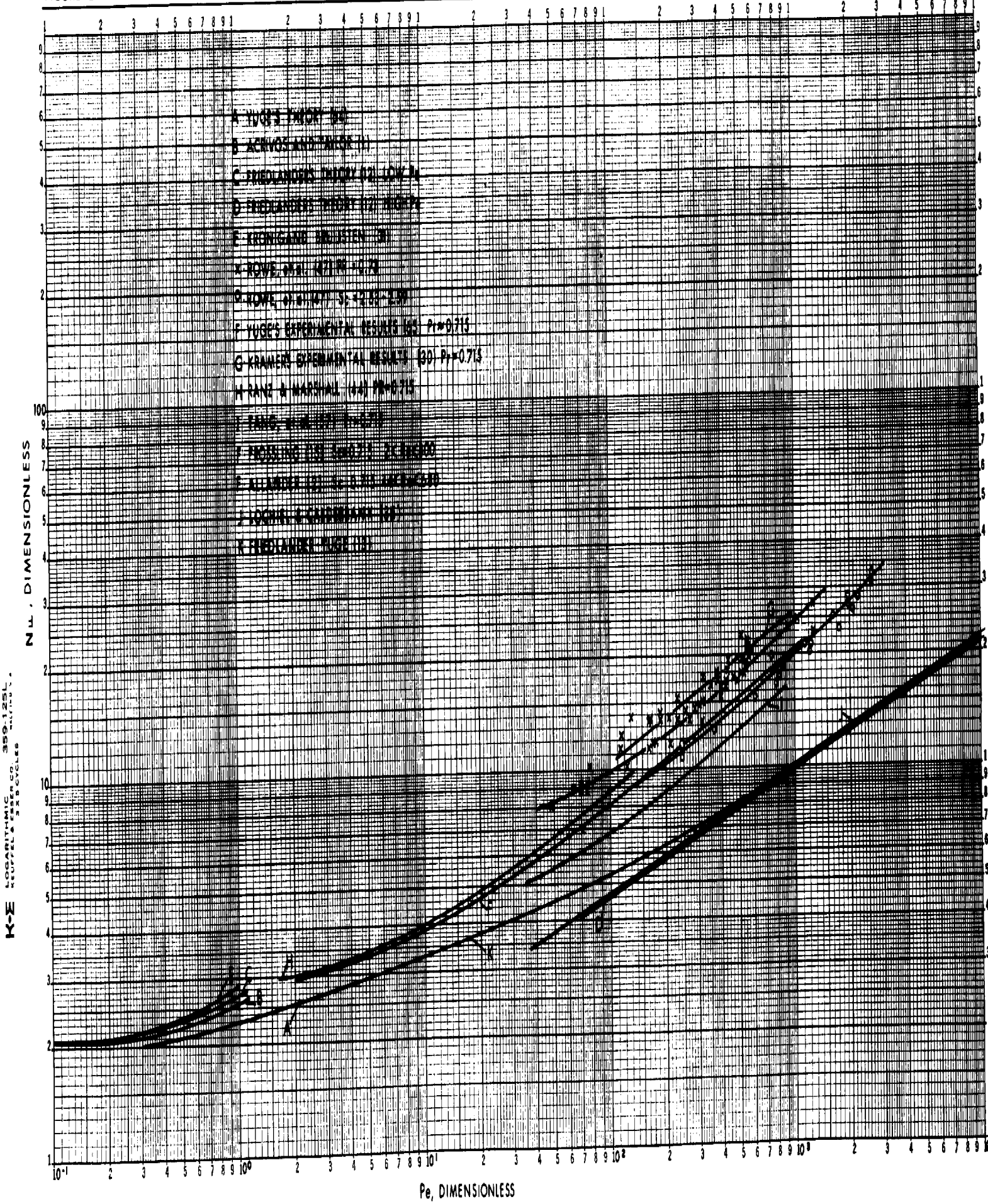

Comparatively little experimental data for liquid systems are available. This is especially the case at low Reynolds numbers. Garner, et. al.[20, 22, & 23] measured the rate of solution of cast benzoic acid and adipic acid spheres in water flowing in a pipe. Their results were correlated by the equation

$$Sh_{avg} = 2.0 + 0.95\ Re^{1/2}\ Sc^{1/3} \qquad (19)$$

This equation is identical to that used by Frossling to correlate his gas phase data, see Figure 2, except that Frossling's constant was 0.552 instead of 0.95. Therefore, the liquid stream data of Garner, et. al. (Sc = 1,100 to 3,200) appear to give average Sherwood numbers nearly twice those of the gas stream experiments (Sc = .715) at the same value of $Re^{1/2}\ Sc^{1/3}$. Garner and coworkers conducted their investigations in the Reynolds number range of 2 to 1000 and equation (19) represents their results over the Re range of 100 to 700.

Steinberger and Treybal[54] have also measured mass transfer rates from single spheres to liquid streams and have correlated their results based on the additivity of natural and forced convection effects. Their correlation is in agreement with previous heat and mass transfer data for both liquid and gaseous systems and is given by

$$Sh_{avg} = Sh'_o + 0.347\ (Re\ Sc^{1/2})^{0.62} \qquad (20)$$

where Sh'_o is a Sherwood number due to molecular diffusion and natural convection only (i.e. Sh at Re = 0). The value of Sh'_o may be found from

either of the following relations depending upon the value of the product of the Grashoff, Gr, and Schmidt numbers for the system:

$$Sh'_o = 2 + 0.569\ (Gr\ Sc)^{0.250},\ Gr\ Sc < 10^8 \qquad (21)$$

$$Sh'_o = 2 + 0.0254\ (Gr\ Sc)^{1/3}\ Sc^{.244},\ Gr\ Sc > 10^8 \qquad (22)$$

Recently, Rowe, Claxton, and Lewis reported rates of single sphere heat and mass transfer to water in the Reynolds number range 30 to 1,750. Their data along with the correlating equation and some of the data of Garner, et. al. are given in Figure 3.

Rhodes and Peebles,[46] as a small phase of their investigation, conducted some single sphere studies. Their results are in agreement with those of Garner, et. al. and are also shown in Figure 3. McCune and Wilhelm[38] also reported several data for the dissolution of single spheres of beta naphthol in water. Their data are included in Figure 3.

Figure 3 clearly shows the dearth of experimental liquid phase single sphere heat and mass transfer data at low Reynolds numbers.

The work of Garner and Suckling[23] as well as the single sphere work of Rhodes and Peebles[46] are of particular pertinence to the present investigation.

Garner and Suckling measured optically, both local and overall mass

FIGURE 3 - HEAT AND MASS TRANSFER DATA FOR SINGLE SPHERES TO LIQUIDS

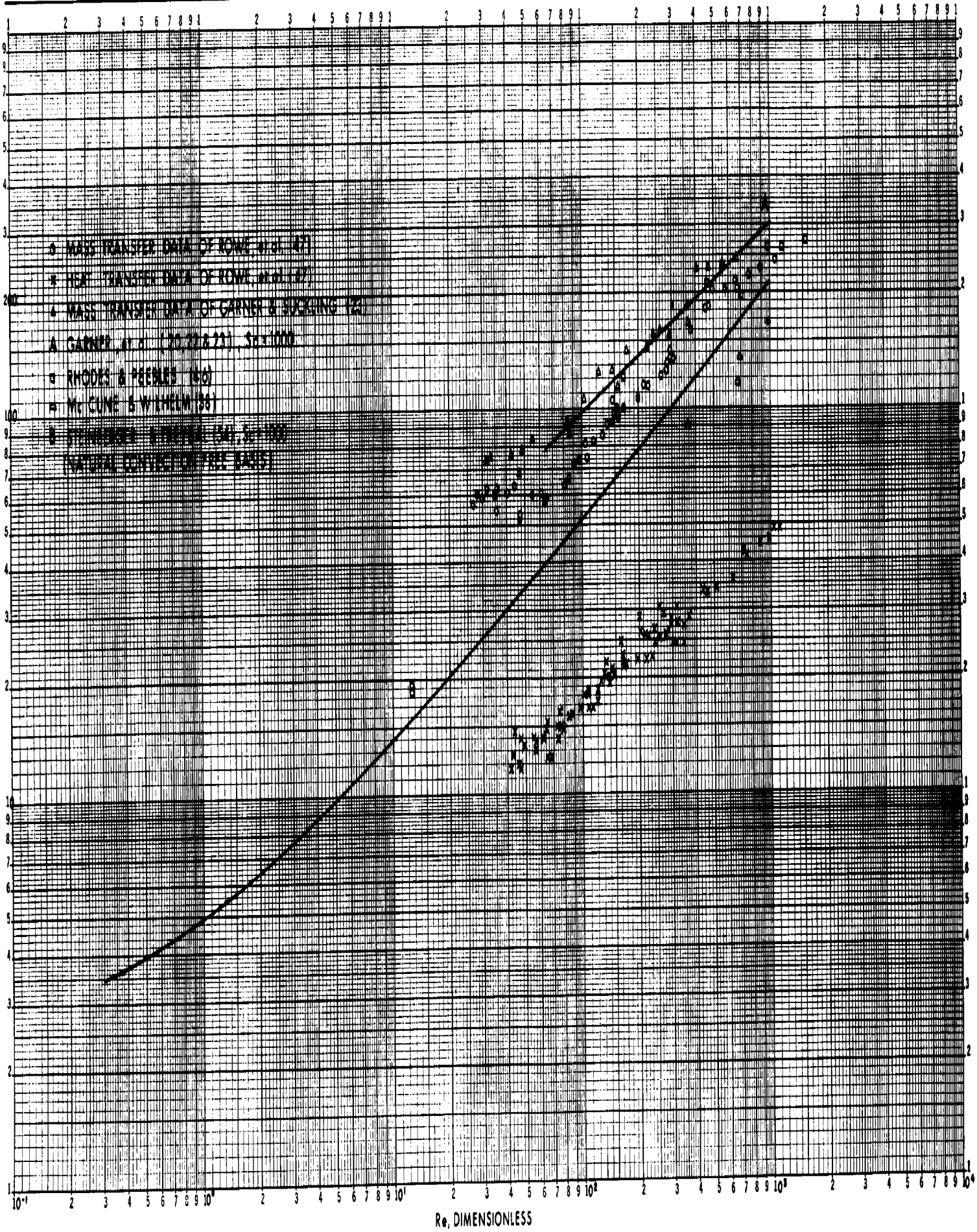

transfer rates from various diameter single spheres of adipic and benzoic acids into a laminar stream of water flowing in a horizontal pipe. A single equation

$$Sh_o = 2 + 0.95\, Re^{1/2}\, Sc^{1/3} \qquad (23)$$

was found to correlate their data and that of Garner, et. al.[20, 22] for particle Reynolds numbers between 100 and 700. They also correlated their data for separate regions of the sphere surface. Table V presents a summary of their correlations and Figure 4 shows the same information graphically.

Inspection of Figure 4 indicates that the maximum transfer on the sphere surface occurs at the forward stagnation point. It is seen that the transfer occurring in the forward flow area is considerably greater than that which occurs in the wake area. Figure 4 also shows that the transfer from the rear stagnation point is less than the average transfer rate, considerably less than that from the forward stagnation point, but greater than the average transfer from the wake area.

These authors admit that their data, which were obtained photographically, show considerable scatter and explain that this is due to small errors in analyzing the photographs which become magnified since they are of the order of magnitude of the diminutions being sought. They contend that better photographic techniques would tend to lessen this error. They

TABLE V. Correlations of Garner, et.al. for Mass Transfer Rates from Separate Regions of Sphere Surface

Equation: $Sh = 2 + B\ Re^{1/2}\ Sc^{1/3}$

Region	B
Forward Flow Area	1.08
Wake Area	0.67
Forward Stagnation Point	1.68
Rear Stagnation Point	0.87

Range of $Re^{1/2}\ Sc^{1/3}$ in which applicable: 100 - 300

FIGURE 4 - CORRELATIONS OF MASS TRANSFER RATES FROM SEPARATE REGIONS OF SINGLE SPHERE SURFACE

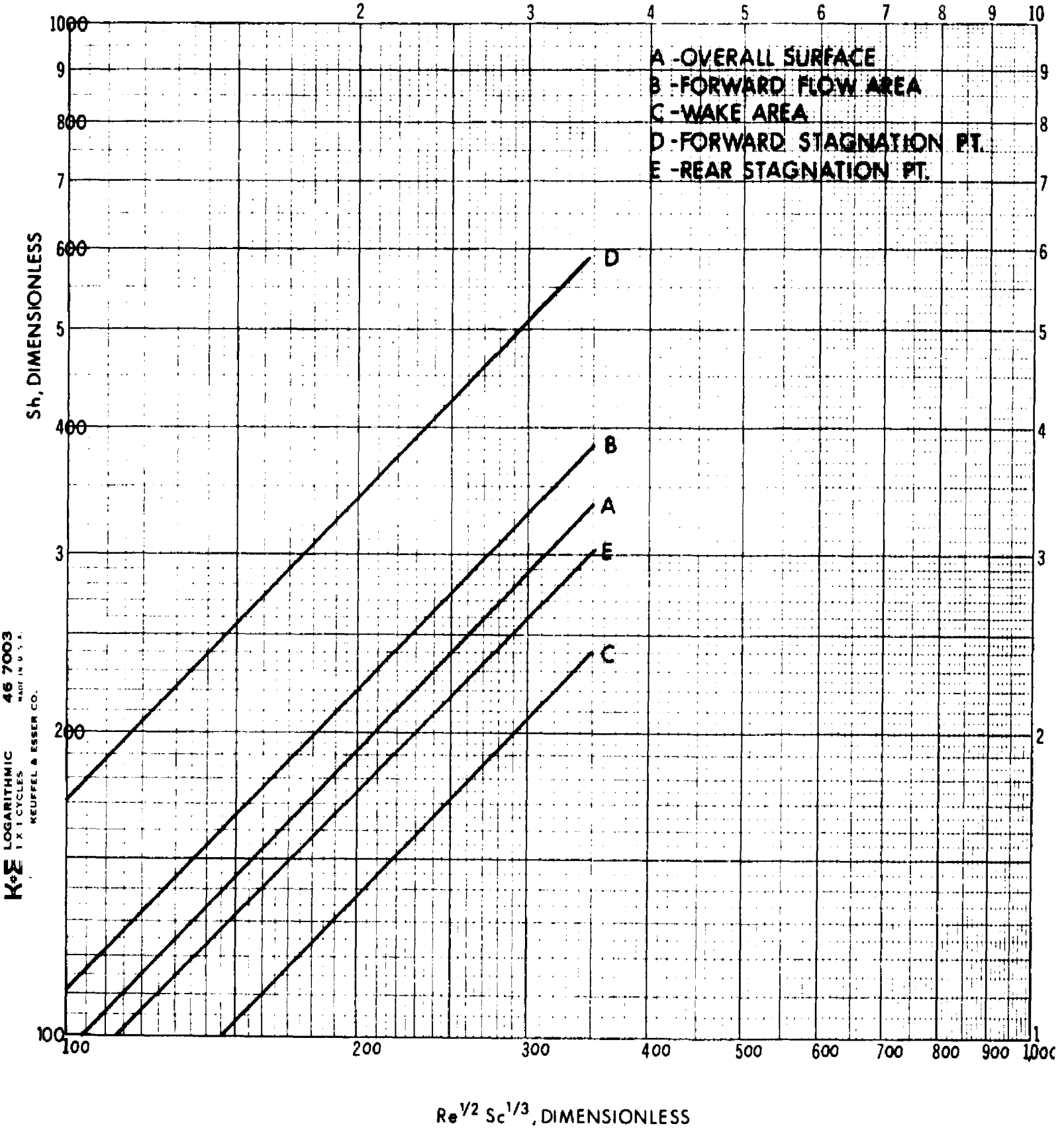

further contend that location of initial and final silhouettes lead to additional errors.

Garner, et. al. did not present plots of local Sherwood number versus position on the sphere surface. However, Suckling[55] presented sufficient information to enable Figure 5 to be prepared.

Rhodes and Peebles,[46] in the initial portion of their study of local transfer rates from spheres in ordered arrays, did some single particle runs. They worked at Reynolds numbers from 166 to 1,560 and found excellent agreement with the results of Garner, et. al. for their average Sherwood numbers. Their data are also presented in Figure 5.

Inspection of Figure 5 shows the increasing importance of the wake area in the transfer process as Re increases. The figure also clearly shows how the forward flow area transfer increases very sharply with increasing Reynolds number. There seems to be some disagreement between the profiles of Garner, et. al. and those of Rhodes and Peebles. Curves B, D, E, and G, after Garner and Suckling, show a steady change with the increasing Reynolds number. Curves A, C, and F show this change in the forward flow area but do not fit into the pattern of the other curves in the wake area. The poor behavior of the wake region of curve A, Re = 1560, was explained by an unstable flow at the rear of the particle.

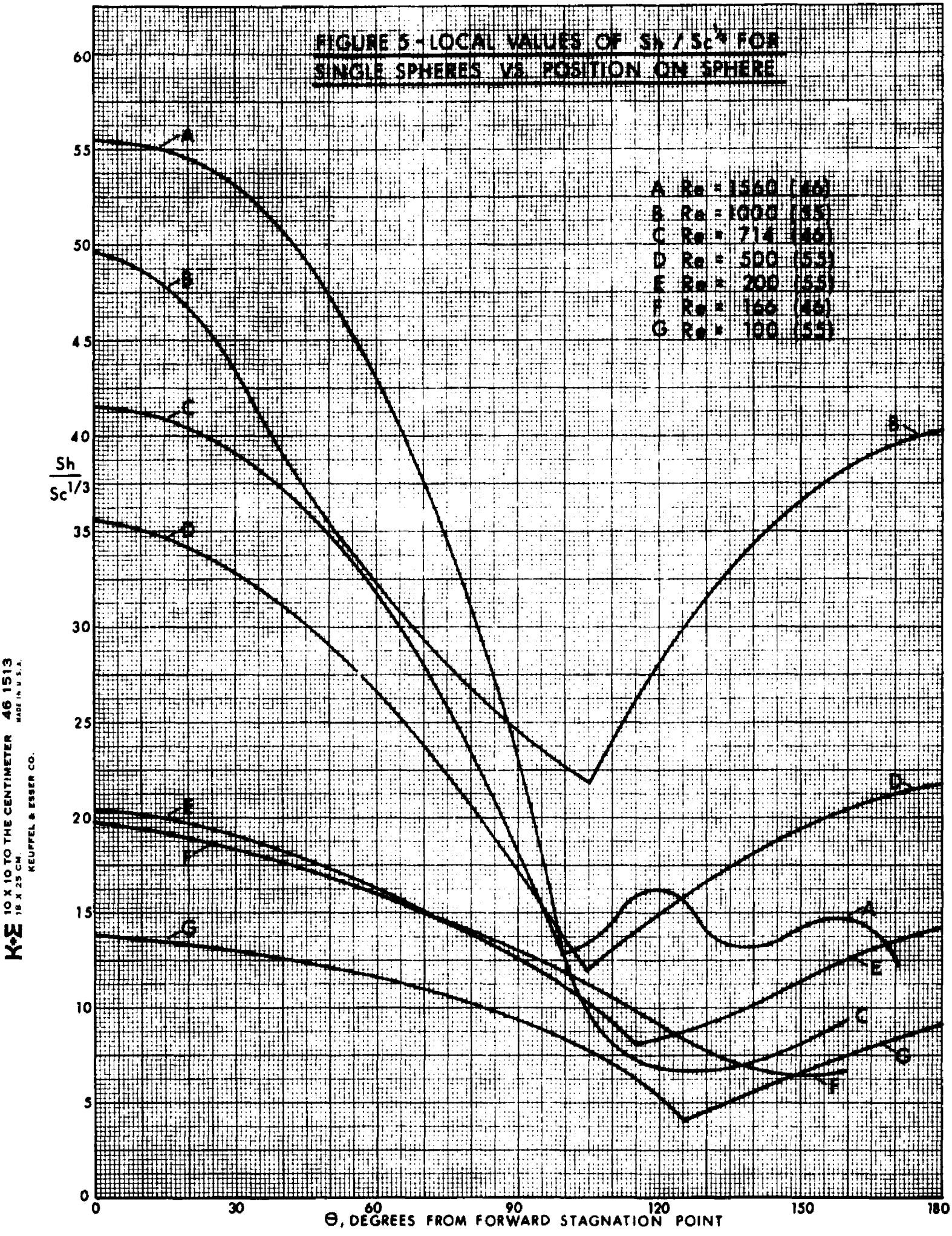
FIGURE 5 - LOCAL VALUES OF Sh / Sc^1/3 FOR SINGLE SPHERES VS. POSITION ON SPHERE
A Re = 1560 (±6)
B Re = 1000 (±5)
C Re = 714 (±6)
D Re = 500 (±5)
E Re = 200 (±5)
F Re = 166 (±6)
G Re = 100 (±5)
Sh / Sc^1/3
Θ, DEGREES FROM FORWARD STAGNATION POINT
0
5
10
15
20
25
30
35
40
45
50
55
60
0
30
60
90
120
150
180
K&E 10 X 10 TO THE CENTIMETER 46 1513
18 X 25 CM.
KEUFFEL & ESSER CO.
MADE IN U.S.A.

Garner, et. al. explained the distributions of mass transfer rate obtained by means of boundary layer concepts, assuming that the mass and momentum boundary-layer thicknesses are in a constant ratio under a given set of flow conditions.

The location of the pronounced minima in the mass transfer profiles of Figure 5 and the location of the minima of the data of Garner, et. al. are plotted in Figure 6, against the Reynolds number. These minima are also indicative of the location of the hydrodynamic separation point. The separation point and the point of minimum transfer should coincide since the hydrodynamic boundary layer attains its maximum thickness at the separation point. Also plotted in Figure 6 is the curve reported by Garner and Grafton[20] for the movement of the hydrodynamic separation point with Reynolds number.

The coincidence of these separation locations (Figure 6) is observed in the Reynolds number range 200 to 400. Above Re of 400 and below Re of 200 the minimum mass transfer rate occurs a few degrees behind the flow separation point. Garner and Grafton believe that at the higher Reynolds numbers, a small stagnant pocket of fluid exists behind the flow separation point in which transfer occurs only very slowly. As the separation point moves further back over the surface with a decrease in Reynolds number, the angle between the surface and the separating streamline becomes greater and there is less tendency for the stagnant pocket to form. This explanation is quite plausible.

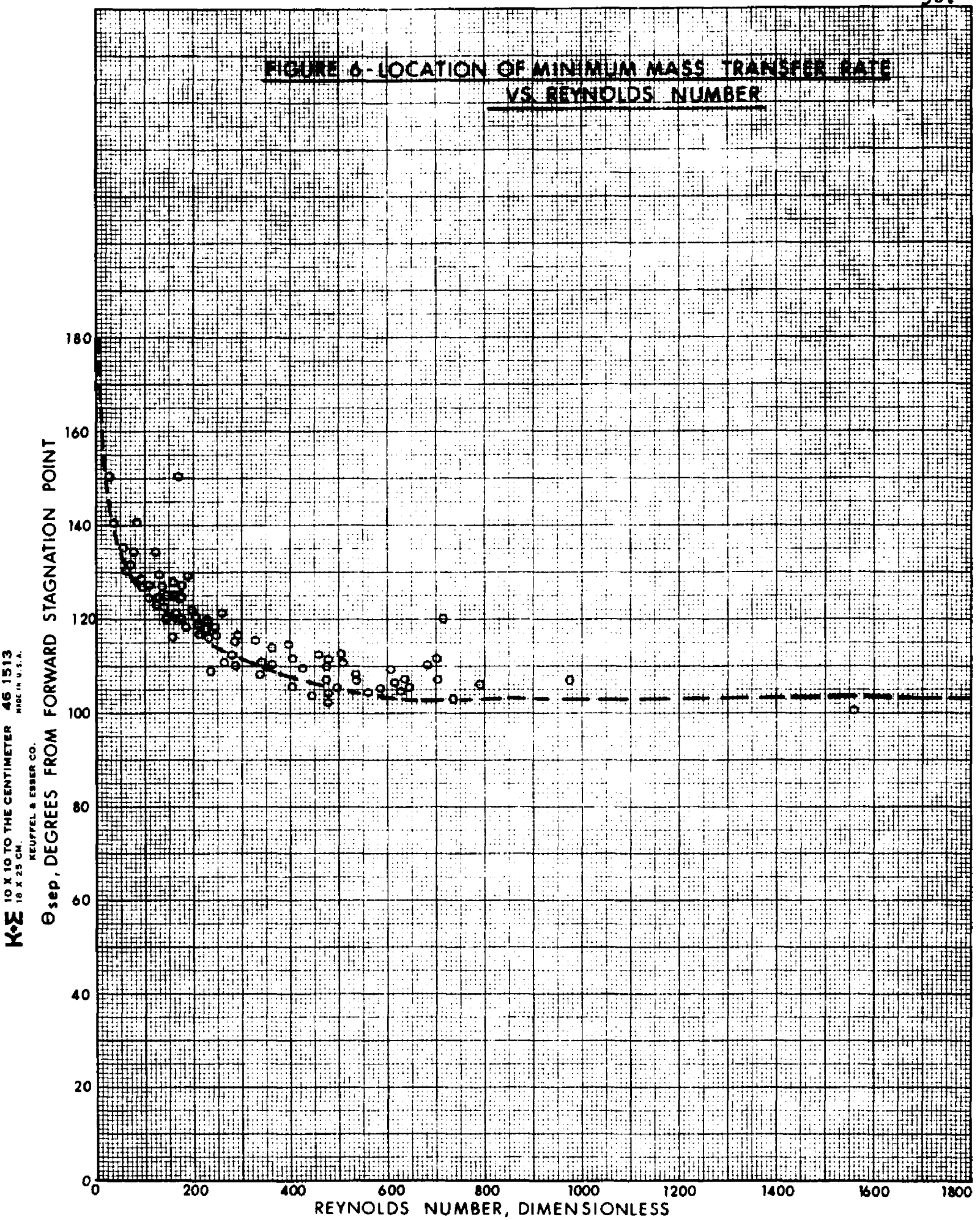
FIGURE 6 - LOCATION OF MINIMUM MASS TRANSFER RATE VS. REYNOLDS NUMBER
θsep, DEGREES FROM FORWARD STAGNATION POINT
REYNOLDS NUMBER, DIMENSIONLESS
0
20
40
60
80
100
120
140
160
180
0
200
400
600
800
1000
1200
1400
1600
1800
K+E 10 X 10 TO THE CENTIMETER 46 1513
18 X 25 CM.
KEUFFEL & ESSER CO.
MADE IN U.S.A.

The disparity at low Reynolds numbers is said to be due to natural convection effects. It seems that this difference at low Reynolds numbers might also be explained by inaccuracies in the data of these authors, particularly since their work involved the measurement of pressure differences over the particle surface at low flow rates.

In the above papers, the relative importance of the wake in mass transfer has been shown. At a Reynolds number of 70 the wake contributes about 80% of the total transfer; while at a Reynolds number of about 500 the wake contributes about 25% of the total. The controlling factor in the transfer from the wake was found to be the solid surface within the wake region. It is determined by the location of the separation point.

Due to the lack of low Reynolds number experimental data for both local and overall mass transfer rates from solids to liquids, it seems worthwhile to expand upon the investigations of Garner, et. al.

Heat and Mass Transfer in Multiparticle Systems

Due to the far greater complexity involved in treating multiparticle systems, very few theoretical studies have been made of heat and mass transfer in packed and fluidized beds. However, a great deal of experimental data have been reported. First, we will examine the pertinent theoretical studies.

Theoretical Studies

Ergun[11] extended the Reynolds analogy to fixed beds to show that the friction factor "f" (a well established experimental quantity) should be identically equal to a modified "j" factor defined by

$$f = j_E = \frac{6 \epsilon \, Sh}{Re} = \frac{150 \, \mu (1-\epsilon)}{D_p G} + 1.75 \qquad (24)$$

He compared his theoretical result to the experimental data of (18), (19), (26), (28), (38), and (45) and found fairly good agreement for liquid-solid systems. His attempts to extend the result to gas-solid systems were unsuccessful; lack of reliable voidage and pressure-drop data were given as reasons. It is interesting to note, however, that the Reynolds analogy indicates an exponent of unity rather than 2/3 on the Sc number term in the conventional definition of "j" (see equation (29)).

Carberry[7] analyzed the process of fluid-particle mass transfer in fixed beds in terms of unsteady state molecular diffusion within a boundary layer which is developed and destroyed repeatedly as the fluid travels through the bed. By assuming that the boundary layer develops and collapses over a distance equal to one particle diameter, he was able to obtain an expression for the mass transfer coefficient by solving the differential equation obtained from the boundary-layer model first proposed by Higbie. His

result in terms of j_ϵ and Re_ϵ is given by

$$j_\epsilon = 1.15\ Re_\epsilon^{-1/2} \tag{25}$$

Kusik and Happel[32] combined boundary layer theory with the "free surface model" (spherical particle surrounded by a spherical envelope) to obtain a theoretical correlation of mass transfer rates and reaction rates in particle beds with heterogeneous catalysis. Their result for void volumes of 0.3 to 1.0 is given by

$$j = 0.93\left[\epsilon - 0.75\,(1-\epsilon)\,(\epsilon - 0.2)\right]^{-1/2} Re^{-1/2} \tag{26}$$

Pfeffer and Happel[41] obtained an analytical solution to the problem of predicting particle-to-fluid heat and mass transfer rates in multiparticle systems at low Reynolds numbers. The energy equation based on the "free surface model" was solved by expanding the fluid temperature profile in even powers of the spherical angle and by assuming that the fluid properties remain relatively constant with temperature. Solutions were obtained for Peclet numbers between 0.1 and 100 and fractional void volumes between 0.4 and 1.0. Their results show that the average Nusselt or Sherwood number in a bed of particles is a function of both ϵ and Pe, the effect of Pe decreasing as ϵ decreases in the low Peclet number range. These authors compared their results with published experimental mass and heat transfer data and found good agreement which indicates that the "j" factor is not independent of the Schmidt

or Prandtl numbers at low Reynolds number, low Peclet number flow.

Pfeffer[40] combined the "free surface model" with the Levich "thin boundary layer solution" of the diffusion equation to obtain an expression relating the Sherwood or Nusselt number to the Peclet number and the fractional void volume of a multiparticle system. His theoretical result is given by

$$Sh = 1.26 \left[\frac{1 - (1-\epsilon)^{5/3}}{2 - 3(1-\epsilon)^{1/3} + 3(1-\epsilon)^{5/3} - 2(1-\epsilon)^2} \right]^{1/3} Pe^{1/3} \qquad (27)$$

or in terms of the "j" factor by

$$j = 1.26 \left[\frac{1 - (1-\epsilon)^{5/3}}{2 - 3(1-\epsilon)^{1/3} + 3(1-\epsilon)^{5/3} - 2(1-\epsilon)^2} \right]^{1/3} Re^{-2/3} \qquad (28)$$

Pfeffer found his theoretical correlation to agree very closely with available experimental mass transfer data for fixed and fluidized beds in the low Reynolds number-high Peclet number range, in which it is applicable.

Pfeffer and Huang[42] in an extension of the earlier work of Pfeffer,[40] combined the "free surface model" with a "von Karman" integral method of solution of the diffusion equation and obtained an analytical solution to the problem of predicting heat and mass transfer rates in multiparticle systems which is applicable for any value of the Peclet number. They computed Sherwood numbers for Peclet numbers between 10 and 10,000 and for fractional void volumes, ϵ, between 0.4 and 1.0. Although the mathematical model used was an extreme over-simplification of the actual physical phenomena occurring in packed and fluidized beds, the results were found to agree quite

well with both theoretical and experimental investigations reported in the literature. The only limitation on the usefullness of these results is that the fluid must be flowing slow enough to make inertial effects negligible.

In Figure 7 are plotted the average Sherwood or Nusselt numbers predicted from the theoretical results of Pfeffer, et. al. against Peclet number with the fractional void volume as the parameter. Inspection of this figure shows that equation (27) gives values of Sh or Nu which agree with those obtained by Pfeffer and Huang at values of greater than 0.9 and at high Peclet numbers. At other values of ϵ, equation (27) either overestimates or underestimates the Sh or Nu numbers, depending on the Peclet number. This disparity is better shown in Figure 8 where Sh or Nu are plotted against ϵ with Peclet number as the parameter. For the sake of completeness, in Figure 9 are plotted the values of Sh obtained from equations (24), (25), (26), and (27) at a Sc of 1000 for ϵ of 0.5 and those of Pfeffer and Happel and Pfeffer and Huang at the same values of Sc and ϵ against the Reynolds number.

In contrast to this small number of theoretical investigations of heat and mass transfer in multiparticle systems, there are numerous experimental papers in the literature. We shall now study those experimental investigations pertinent to the present work.

FIGURE 7 - AVERAGE SHERWOOD NUMBERS FROM THE WORK OF PFEFFER, et al.
VS. PECLET NUMBER WITH VOID FRACTION AS PARAMETER

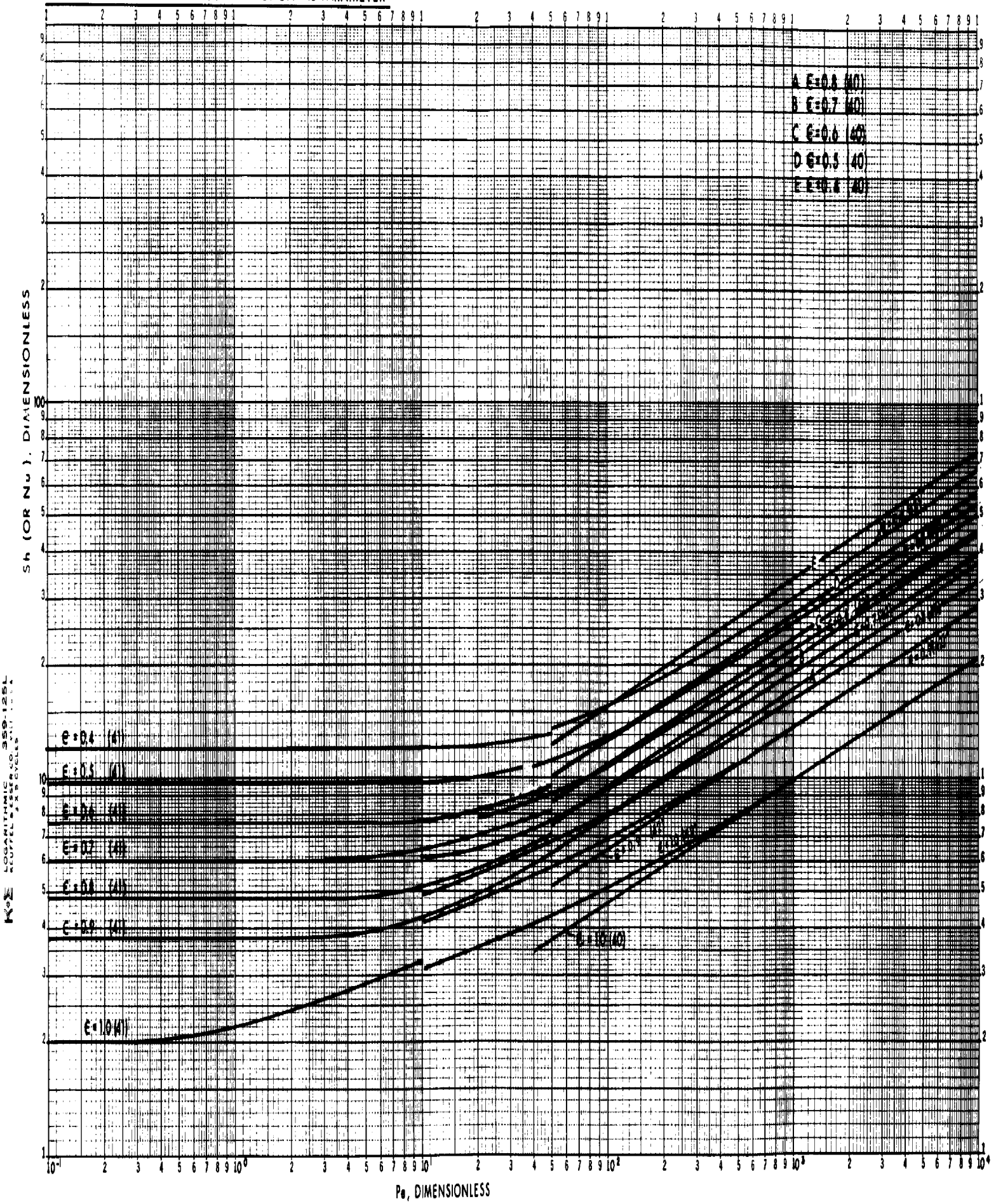

FIGURE 8 SHERWOOD (NUSSELT) NUMBERS OF PFEFFER, ET.AL. VS ϵ_z, P_e IS THE PARAMETER

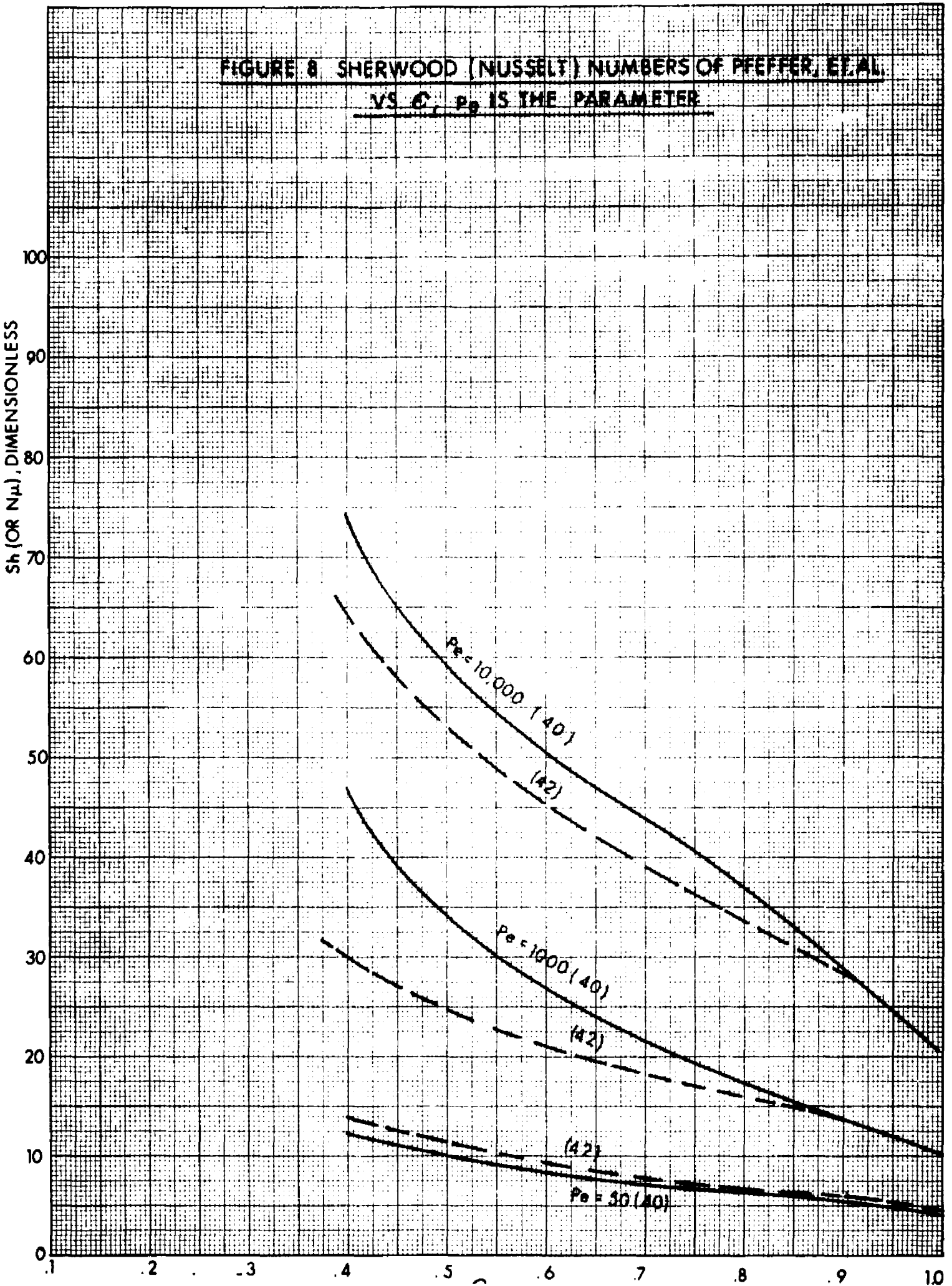

K+E 10 X 10 TO THE CENTIMETER 46 1513
19 X 25 CM.
MADE IN U.S.A.
KEUFFEL & ESSER CO.

FIGURE 9-THEORETICAL VALUES OF Sh VS. Re at Sc = 1000, ϵ = 0.5

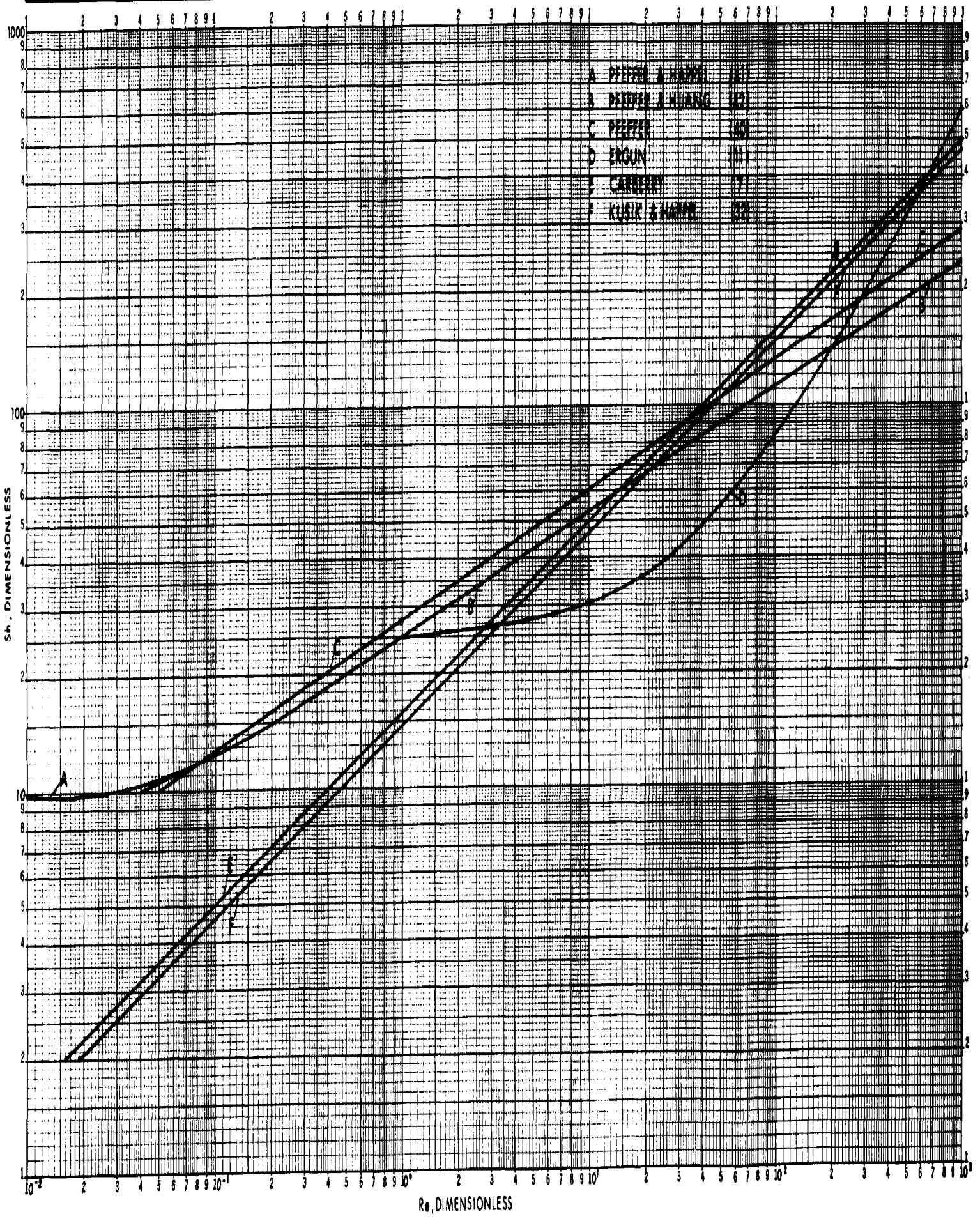

Experimental Studies

(Fixed, Distended and Fluidized Beds)

Almost all of the experimental heat and mass transfer data for packed beds are correlated in the literature in terms of the Colburn "j" factor as a function of Reynolds number. Based upon experimental investigations of the vaporization of water into air from the surfaces of spheres and cylinders, Gamson, Thodos, and Hougen[19] proposed the mass transfer factor

$$j_d = \frac{(K_c)_g \rho_g m}{G} (Sc)^{2/3} = \frac{Sh}{Re\, Sc} Sc^{2/3} \qquad (29)$$

as a generalized variable for the estimation of mass transfer coefficients. A mass transfer factor specifically applied to transfer across a liquid film

$$j_d = \frac{(K_c)_l C_l m}{G} (Sc)^{2/3} = \frac{Sh}{Re\, Sc} Sc^{2/3} \qquad (30)$$

was employed by McCune and Wilhelm[38] and Hobson and Thodos[26] to correlate the results of studies in solid-to-liquid and liquid-to-liquid transfer, respectively. The results of these investigations, together with additional gas phase data obtained by evaporating many different organic liquids into air, N_2, H_2, and CO_2 were all correlated in a second paper by Hobson and Thodos[27] by a single plot of jd vs. Reynolds number. This curve has been reproduced in Figure 10.

Examination of Figure 10 shows that for Reynolds numbers less than 50,

FIGURE 10 - MASS TRANSFER FACTOR FOR PACKED BEDS

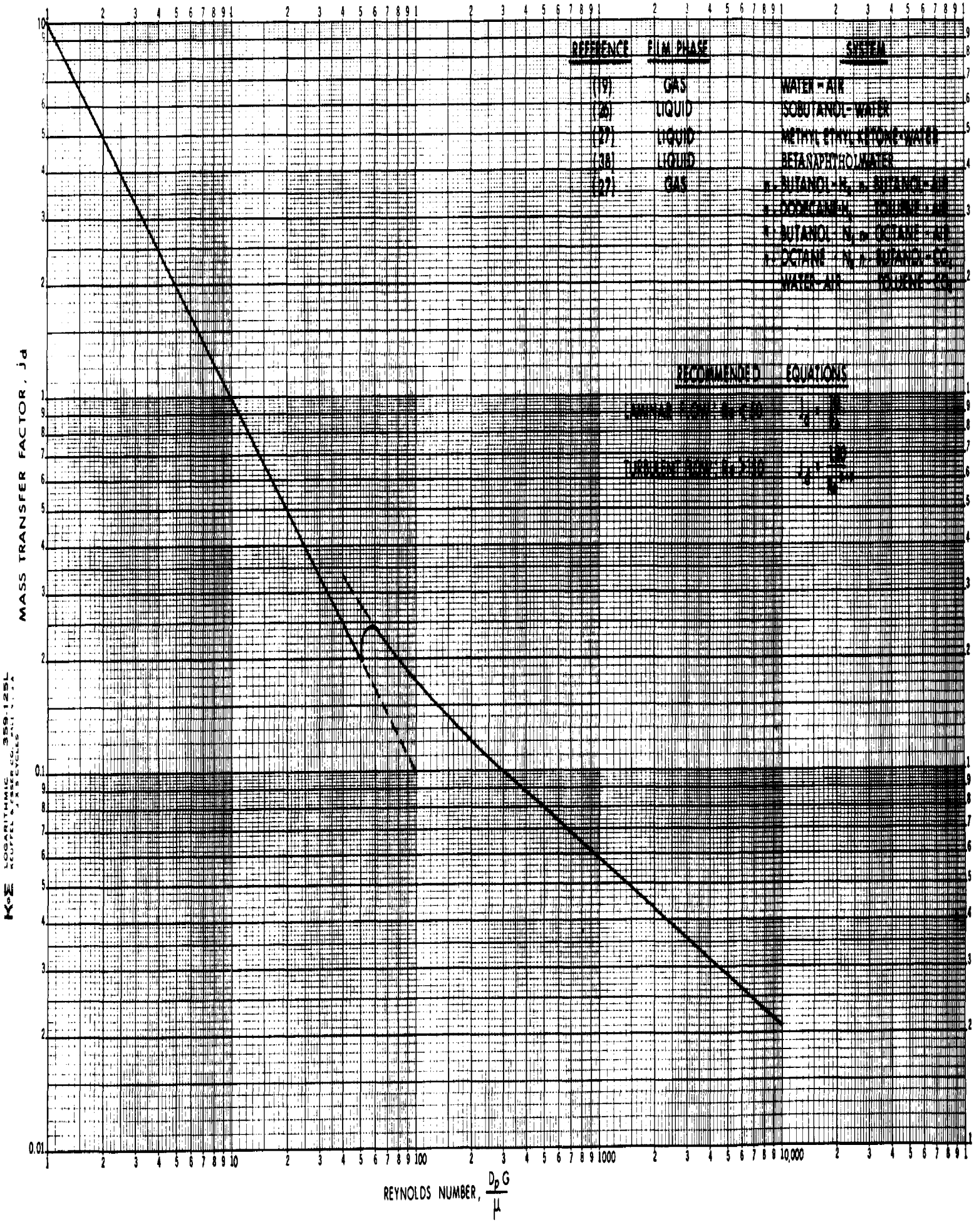

the jd vs. Re curve is a straight line with a slope of negative unity. This is in complete agreement with the established characteristics of laminar flow and the mathematical representation of the data for values of Re < 50 is

$$jd = \frac{10}{Re} \tag{31}$$

In the transition region ($50 < Re < 150$), an exact correlation of the data is not readily apparent, but at $Re > 150$, the correlation is represented by

$$jd = \frac{1.30}{Re^{0.45}} \tag{32}$$

Dryden, Strang, and Withrow[9] also studied the rate of mass transfer from solid pellets in packed beds to water flowing at low velocities, but correlated their data in terms of a modified Reynolds number, $Re_\epsilon = \frac{D_p G}{\mu \epsilon}$, and a modified "j" factor, $j_\epsilon = \frac{Sh}{Re_\epsilon Sc} Sc^{2/3}$. This method of correlation was suggested previously in an earlier paper by Gaffney and Drew,[18] although these authors had found that the exponent of the Schmidt number should be taken as 0.58 rather than 2/3 for liquid systems.

The data of Dryden, et. al. were obtained in the Re_ϵ range of 0.0125 to 7.21 using pelletts made of beta naphtholand benzoic acid ($814 < Sc < 1147$); mass transfer coefficients were computed assuming that axial diffusion and natural convection were nonexistent. At very low Re_ϵ values, these assumptions were not valid, and therefore the authors extrapolated their correlation curve rather than have it show a marked reversal of curvature at

low Re_ϵ values. The benzoic acid data form a smooth curve with a slope of -1, but the curve lies above the corresponding betanaphtholdata; the two curves appear to converge at Re_ϵ equal to 5. The authors explained that this phenomenon was due either to the difference in Grashof number for the two systems, or to the fact that the exponent of the Schmidt number in the "j_ϵ" factor might actually be a function of the Schmidt number rather than the assumed constant. Their results, together with the correlation of Hobson and Thodos converted to j_ϵ vs. Re_ϵ , are given in Figure 11.

Bar-Ilan and Resnick[3] measured mass transfer rates by studying the evaporation ofnaphthaleneparticles into air which passed through the bed of particles. They found that the "j" factor was a function of particle diameter as well as Reynolds number when the particle diameter was very small. This dependence of the "j" factor on particle diameter had been reported earlier by (28) and (45) in mass transfer work and (10) and (36) in heat transfer investigations. The effect was found to occur only for regularly shaped particles whose diameters were less than 4 mm.

Bar-Ilan and Resnick correlated their data by plotting jd vs. $Re/1-\epsilon$. If their data is replotted as j_ϵ vs. Re_ϵ instead, the values of j_ϵ are found to be lower than those obtained by other investigators (see Figure 12), although they agree fairly well with the data of Chu, et. al.[8] at $Re/1-\epsilon$ greater than 30. A comparison of Figures 10, 11, and 12 indicates the large differences between the data of different investigators.

FIGURE 11 MASS TRANSFER FACTORS FOR PACKED BEDS

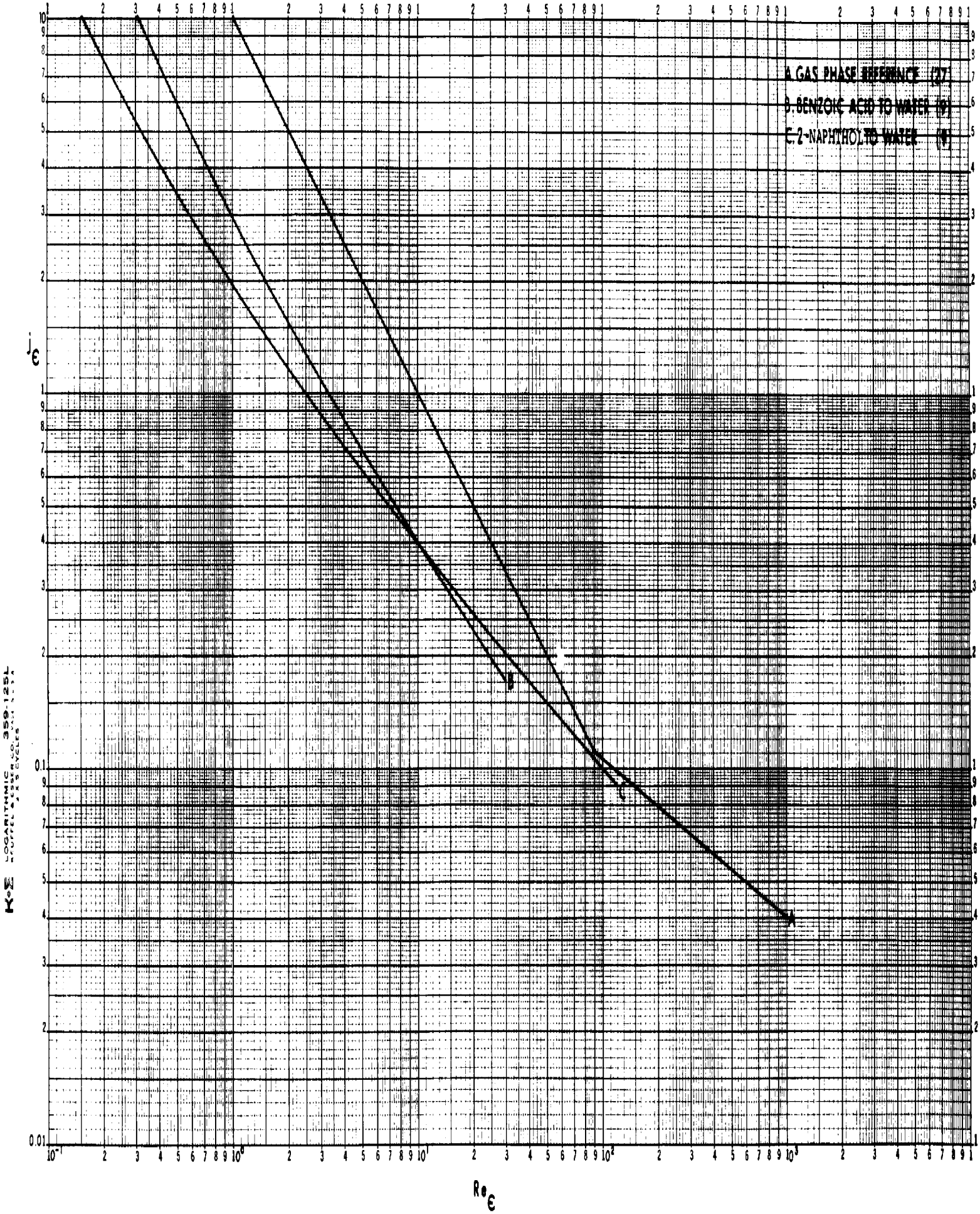

FIGURE 12 - MASS TRANSFER FACTORS FOR PACKED BEDS

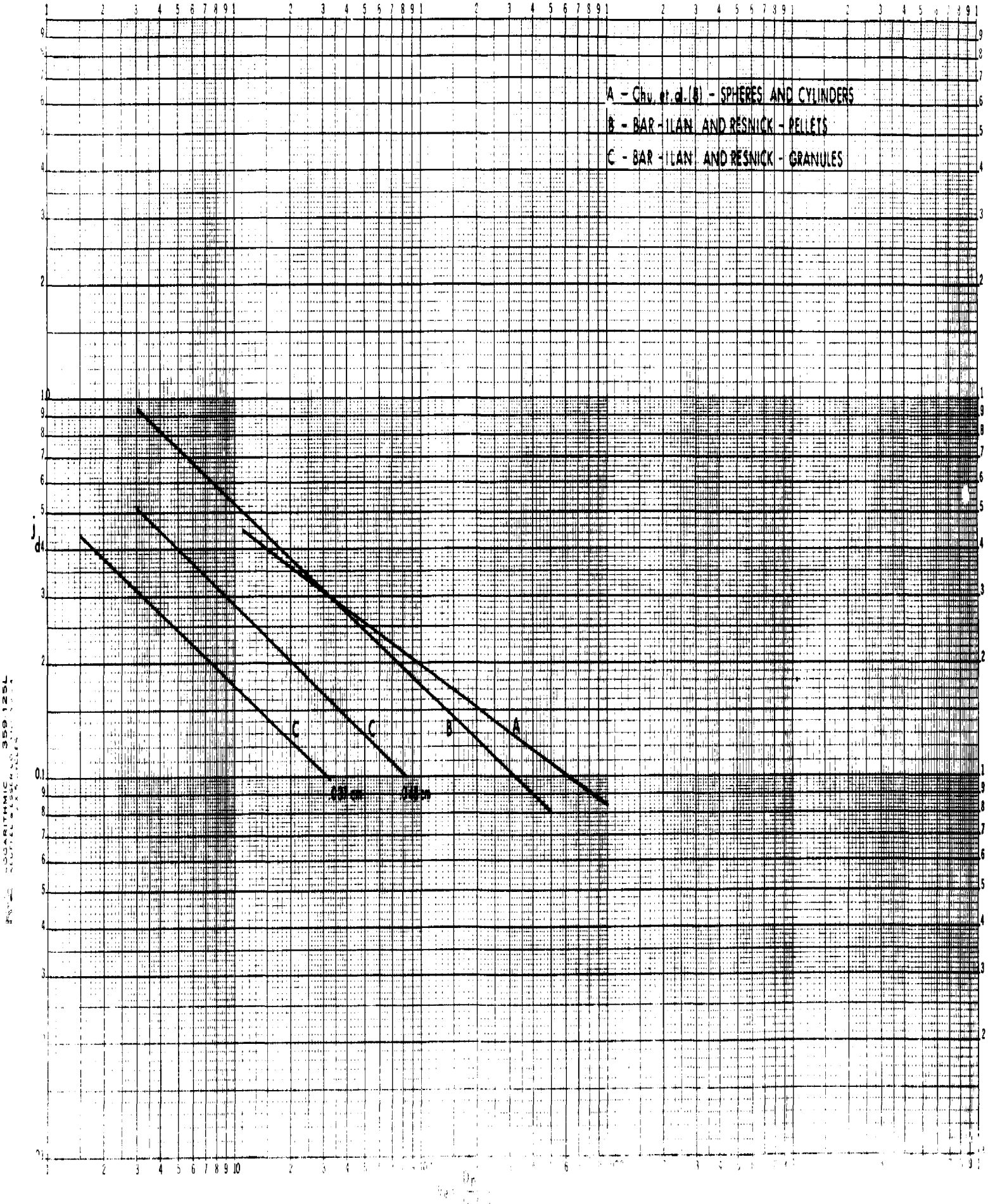

Thoenes and Kramers[58], in an effort to avoid the possible causes of the discrepancies between the published packed bed mass transfer data (bed inhomogeneity, axial diffusion, short bed height, etc.) determined mass transfer coefficients for fluids flowing around single spheres, which were part of a regular arrangement of similar, but inactive spheres. The experiments were carried out with solid spheres dissolving into a stream of water, and with porous spheres soaked with a liquid, which evaporated into a stream of gas. The authors correlated their data by plotting $Sh/Sc^{1/3}$ against Re with both Sh and Re based on a hydraulic diameter defined as $\epsilon d/1-\epsilon$, and an average axial velocity of flow V/ϵ. Their plotted data produce different curves for different packing configurations (fractional void volumes) and show that the influence of Re on $Sh/Sc^{1/3}$ also depends on the value of Sc; the a priori assumption that Sh is proportional to $Sc^{1/3}$ at constant Re is only a rough approximation, particularly for gases at small Reynolds numbers. At values of Re less than 100 the measured values of $Sh/Sc^{1/3}$ are all lower for higher values of Sc and accordingly lowest for liquids.

Heat transfer rates between particles and fluids flowing past them were also correlated in terms of the Colburn "j" factor. For example, Gamson, et. al.[19] and Taecker and Hougen[56] in their mass transfer studies were able to establish gas and particle temperatures with the help of a humidity chart and thus calculated fluid-to-particle heat transfer coefficients as well as mass transfer coefficients. Their results were plotted as

$$j_H = \frac{h}{C_p V \rho}\left(\frac{C_p \mu}{k}\right)^{2/3} = \frac{Nu}{Re\ Pr}Pr^{2/3} \qquad (33)$$

vs. the Reynolds number and because of the analogy between the mechanisms of heat and mass transfer, the heat and mass transfer factors jh and jd were found to be almost numerically equal.

Glaser and Thodos[24] obtained heat transfer data under steady state conditions in the absence of mass transfer by generating heat within metallic particles with an electric current. The heat was continuously removed by gases flowing through the bed and the heat transfer coefficient for the gas film was calculated from temperature measurements of both gases and solids within the bed. The authors correlated their data by plotting jh vs. $Re_m = [A_p] G/\mu(1-\epsilon)$, a modified Reynolds number, and found that jh depended on particle shape and size as well as Reynolds number especially in the region of low Reynolds number (Re_m = 100 to 1000). By taking into account the effect of d_p/d_c (ratio of particle size to column diameter) and adding a shape factor to their modified Reynolds number term, Glaser and Thodos were able to obtain a single correlation for all their data. Their results are found in Figure 13, together with other heat transfer correlations (4), (19), and (24), as a comparison.

Baumeister and Bennett[4] also obtained heat transfer data by generating heat within the particles in a packed bed with an electric current. Their experimental procedure was quite similar to that of Glaser and Thodos, but they correlated their results simply as jh vs. Re with d_p/d_c as a parameter.

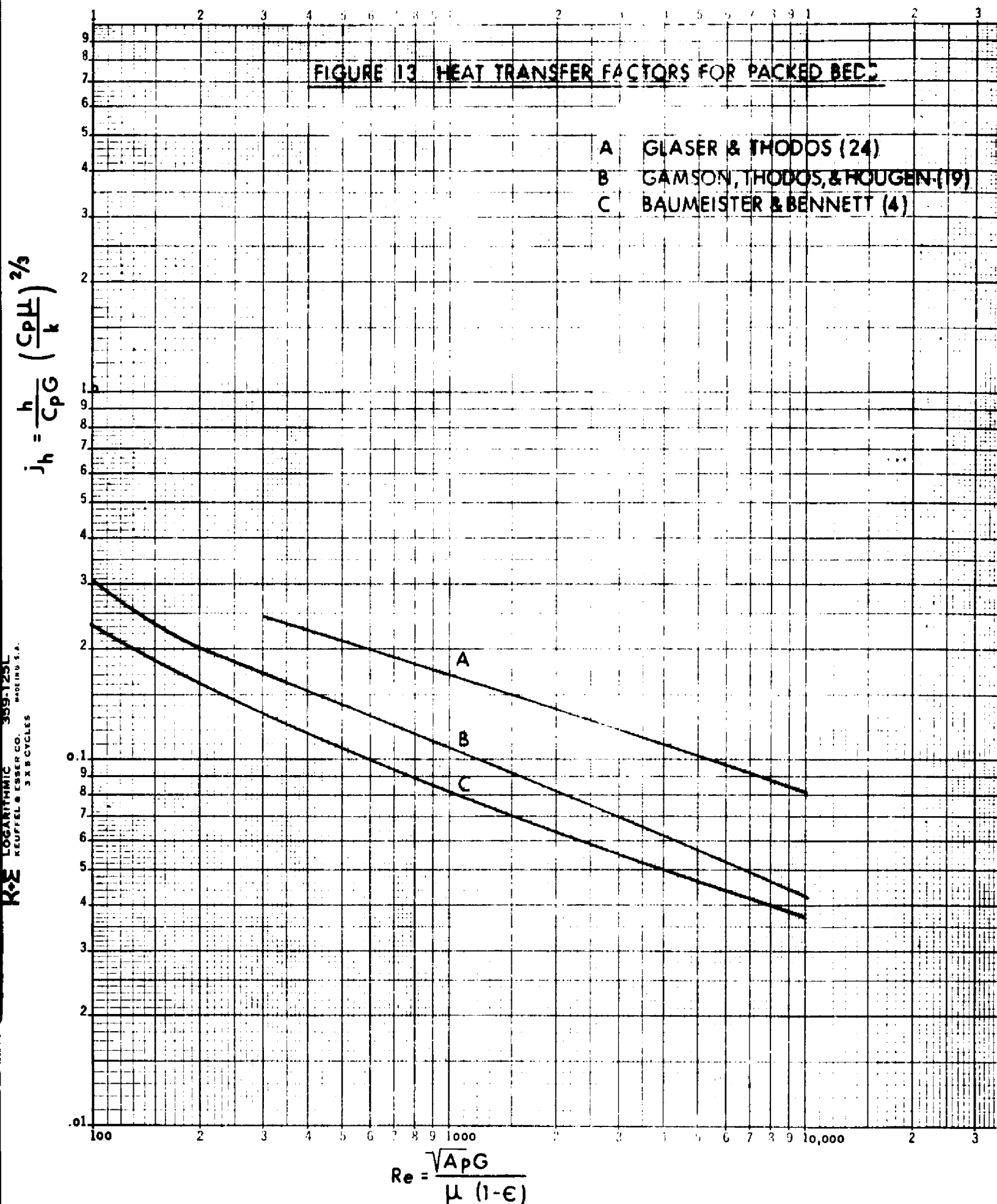
FIGURE 13 HEAT TRANSFER FACTORS FOR PACKED BEDS
A GLASER & THODOS (24)
B GAMSON, THODOS, & HOUGEN (19)
C BAUMEISTER & BENNETT (4)
$j_h = \frac{h}{C_p G} \left(\frac{C_p \mu}{k}\right)^{2/3}$
$Re = \frac{\sqrt{A_p} G}{\mu (1-\epsilon)}$
A
B
C
100
1000
10,000
1
.01

Unfortunately, very little particle-to-fluid heat transfer data has been obtained for Reynolds numbers less than 100.

In several recent studies, Sen Gupta and Thodos[49, 50, 51, and 52] correlated all the available heat and mass transfer data for packed, distended, and fluidized beds. After noting that their correlations also gave discrepancies between jh and jd, they conducted an experimental investigation which attempted to eliminate the sources of the discrepancy. In the earliest of these papers,[49] the authors presented a correlation between the j-(factor) and a modified Reynolds number, $Re' = \sqrt{A_p}\ G/\mu$, for mass and heat transfer through fixed and fluidized beds of all types of packings which required knowledge of an area availability factor, f. It should be noted that the use of $\sqrt{A_p}$ as the characteristic linear dimension of a system had been introduced earlier by Taecker and Hougen[56]. The area availability factor, f, was defined as the ratio of the surface of a particle available for transfer to the surface area of a sphere having the same volume as the particle. The fact that the area available for transfer depends upon the particle geometry and the type of bed used was thus taken into account. It was suggested by these authors that f be evaluated from experimental data. However, a simplified approach was proposed for its estimation, which gave reasonable agreement with experimental values. The correlations obtained by Sen Gupta and Thodos are reproduced in Figures 14 and 15. If one compares the correlating equations for these plots the interesting

FIGURE 14- RELATIONSHIP BETWEEN MASS TRANSFER MODULUS & MODIFIED REYNOLDS NUMBER FOR SPHERES & OTHER PACKINGS.

	GEOMETRY	ε	f	FILM PHASE	SYSTEM	TYPE OF BED
□ CHU, KALIL, & WETTEROTH	CYLINDERS	0.322 - 0.388	0.865	GAS	AIR-NAPHTHALENE	PACKED
◊	CYLINDERS	0.381 - 0.871	1.16	GAS	AIR-NAPHTHALENE	FLUIDIZED
△	CYLINDERS	0.287 - 0.665	1.16	GAS	AIR-P-DICHLOROBENZENE	FLUIDIZED
+ GAMSON, THODOS, & HOUGEN	CYLINDERS	0.357 - 0.410	0.865	GAS	AIR-WATER VAPOR	PACKED
♦ TAECKER & HOUGEN	CYLINDERS	0.390	0.865	GAS	AIR-WATER VAPOR	PACKED
▽ WILKE & HOUGEN	CYLINDERS	0.342 - 0.436	0.865	GAS	AIR-WATER VAPOR	PACKED
▲ TAECKER & HOUGEN	PARTITION RINGS	0.669	1.24	GAS	AIR-WATER VAPOR	PACKED
■	RASHING RINGS	0.631, 0.717	1.34	GAS	AIR-WATER VAPOR	PACKED
▼	BERL SADDLES	0.65	1.36	GAS	AIR-WATER VAPOR	PACKED

○ SPHERES

ALL TYPES OF BEDS

LIQUID AND GAS FILMS

$0.346 > \varepsilon < 0.921$

CHU, KALIL, AND WETTEROTH

DE ACETIS AND THODOS

GAFFNEY AND DREW

GAMSON, THODOS, & HOUGEN

HOBSON AND THODOS

Mc CONNACHIE & THODOS

Mc CUNE AND WILHELM

$$\frac{\varepsilon j_d}{f} = \frac{0.300}{\left(\frac{\sqrt{A_p}G}{\mu}\right)^{0.35} - 1.90}, \quad \text{FOR } \frac{\sqrt{A_p}G}{\mu} > 50$$

$\varepsilon j_d / f$

$Re = \sqrt{A_p}G / \mu$

10 8 6 4 3 2 1.0 0.8 0.6 0.4 0.3 0.2 0.10 0.08 0.06 0.04 0.03 0.02 0.010

10 20 40 60 100 200 400 1000 2000 4000 10,000 30,000

FIGURE 15

RELATIONSHIP BETWEEN HEAT TRANSFER MODULUS & MODIFIED REINOLDS NUMBER FOR SPHERES, CYLINDERS, AND CUBES.

	GEOMETRY	ε	f	FILM PHASE	SYSTEM	TYPE OF BED
+ GAMSON, THODOS, AND HOUGEN	CYLINDERS	0.357 - 0.410	0.865	GAS	AIR-WATER VAPOR	PACKED
♦ GLASSER & THODOS	CYLINDERS	0.477	0.865	GAS	AIR, H_2, CO_2	PACKED
■ GLASER & THODOS	CUBES	0.417 - 0.469	0.825	GAS	AIR, H_2, CO_2	PACKED

O SPHERES

GAS FILM, FIXED BEDS

$0.330 < \varepsilon < 0.778$

BAUMEISTER AND BENNETT

DE ACETIS AND THODOS

GLASER & THODOS

Mc CONNACHIE & THODOS

$$\frac{\varepsilon j_h}{f} = \frac{0.322}{\left(\frac{\sqrt{A_p}G}{\mu}\right) - 1.90}^{0.35} \quad \text{FOR} \quad \frac{\sqrt{A_p}G}{\mu} > 50$$

$\varepsilon j_h / f$

$R_e = \sqrt{A_p}G/\mu$

4 3 2 1.0 0.8 0.6 0.4 0.3 0.2 0.10 0.08 0.06 0.04 0.03 0.03 0.010

2 4 6 8 10 20 40 60 100 200 400 1000 3000 10,000

result

$$\frac{jh}{jd} = 1.073 \tag{34}$$

is obtained.

In their second paper,[58] these authors correlated all of the available mass and heat transfer data for fixed, distended, and fluidized beds of spherical particles. These correlations are of the form

$$\in jd = f\left(\frac{D_p G}{\mu}\right) \tag{35}$$

Since the availability factor, f, for spheres is unity and since the particle diameter completely describes the sphere, this functionality is a natural outgrowth of their earlier work. For mass transfer they found that the relation

$$\in jd = 0.010 + \frac{0.863}{Re^{0.58} - 0.483} \tag{36}$$

best represented the data for Reynolds numbers greater than one. The equation

$$\in jh = 0.0108 + \frac{0.929}{Re^{0.58} - 0.483} \tag{37}$$

was found to best describe the heat transfer data for Re values greater than 20. Plots of equations (36) and (37) are similar in appearance to those presented in Figures 14 and 15 and are, therefore, not included here.

For Reynolds numbers above 20, where both equations (36) and (37) apply dividing $\in jh$ by $\in jd$, one finds that

$$\frac{jh}{jd} = \frac{0.0108\ Re^{.58} + 0.924}{0.0100\ Re^{.58} + 0.858} \qquad (38)$$

which shows that the ratio jh/jd for spherical particles is a function of the Reynolds number. For Re between 20 and 1000 equation (38) gives a value of 1.078 for the ratio jh/jd.

The fact that the discrepancy between jh and jd does exist is quite interesting since theoretical considerations indicate that there should be a direct analogy between these two transfer processes. Sen Gupta and Thodos[51 and 52] presented the results of an experimental study in which they were able to eliminate the factors leading to the discrepancy between jh and jd for multiparticle systems.

These authors found that

$$j = \frac{2.06}{Re^{0.575}} \qquad (39)$$

represents both heat and mass transfer "j" factors for multiparticle systems of spheres when relatively small rates of mass transfer exist, radiation effects are eliminated, and the true-mean driving force is used. Their generalized relationship between ϵj and Re is reproduced in Figure 16.

McConnachie and Thodos,[37] in a study of transfer processes in the flow of gases through packed and distended beds of spheres, found that their mass transfer data was consistent with that obtained by other investigators for

FIGURE 16 – GENERALIZED RELATIONSHIP BETWEEN εj AND Re FOR BOTH MASS & HEAT TRANSFER IN THE FLOW OF FLUIDS THROUGH PACKED & DISTENDED BEDS OF SPHERES.

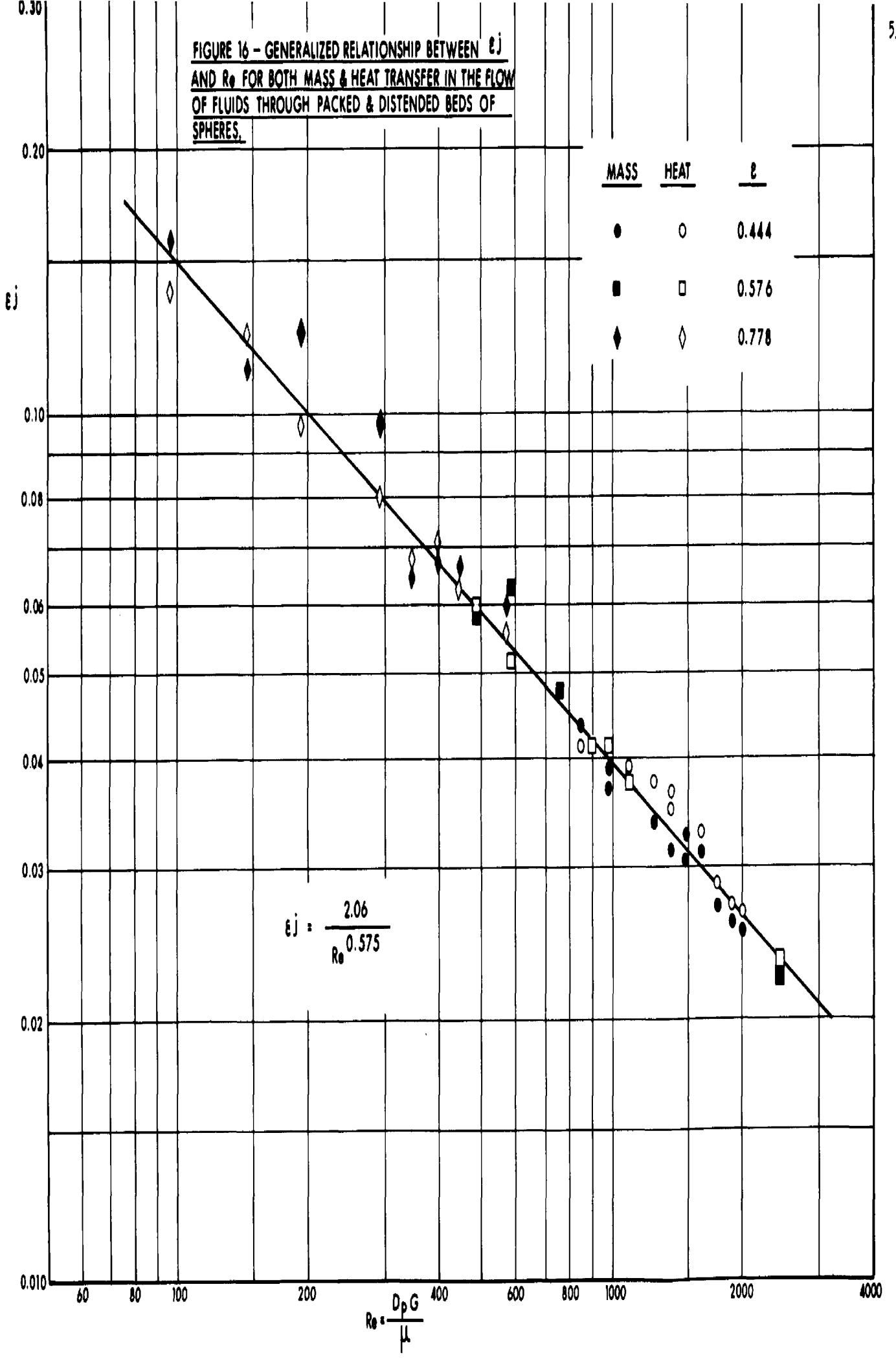

packed and fluidized beds. They concluded that the motion of the particles in a fluidized bed does not seem to have an effect on the mass transfer process. They also found that there was essentially no difference between the jh and jd relationships for expanded fixed beds formed by randomly dispersed solid spheres and those formed by holding the separated spheres in position.

McConnachie and Thodos correlated their results by

$$j_d = \frac{1.127}{\left(\frac{d_p G}{\mu(1-\epsilon)}\right)^{0.41}} \qquad (40)$$

and

$$j_h = \frac{1.192}{\left(\frac{d_p G}{\mu(1-\epsilon)}\right)^{0.41}} \qquad (41)$$

Williamson, Bazaire, and Geankoplis[62] obtained liquid-phase mass transfer coefficients for packed beds of benzoic acid spheres and water in the Reynolds number, $d_p L/\mu\epsilon$, range of 0.08 to 120. They found that the exponent on the Schmidt number for liquids should be 0.58 They also recommend the following equations for the prediction of mass transfer rates in liquid phase packed beds:

$$\left(\frac{k_l}{L}\right) Sc^{0.58} = 2.40\left(\frac{d_p L}{\mu\epsilon}\right)^{-0.66} \qquad 0.08 < \frac{d_p L}{\mu\epsilon} < 125 \qquad (42)$$

and

$$\left(\frac{k_l}{L}\right) Sc^{0.58} = 0.442\left(\frac{d_p L}{\mu\epsilon}\right)^{-0.31} \qquad 125 < \frac{d_p L}{\mu\epsilon} < 5000 \qquad (43)$$

Rhodes and Peebles[46] obtained local mass transfer rates from spheres in ordered arrays by measuring the local radius change of 1.500 inch diameter benzoic acid test spheres after they were immersed in a water stream. Local Sherwood number profiles were reported for spheres in both simple cubic packing and rhombohedral packing over a particle Reynolds number range of 488 to 3410. They found a large variation in local transfer rates over the surface of a sphere in a packed bed. They also found that in regions adjacent to points of contact between spheres, mass transfer rates were nearly zero. The size of these minimum mass transfer regions was strongly dependent upon their location with respect to the flow direction. These authors presented no correlations for any of their results. However, as a first study, their contribution is quite significant.

Recently, Zhitkavich and Zabrodsky[66] experimentally determined both local and overall convective heat transfer rates from a single sphere when either alone or part of a regular cubic arrangement of uniform spheres to air. Both loose and dense arrays were used. Their single sphere work was in the Reynolds number range of 50 to 90,000; their dense array studies were in the Re_p range of 50 to 40,000. Their overall single sphere results were found to agree closely with those of Yuge[65]. For the forward flow area of the sphere they found that their data could be correlated as

$$Nu = 2 + 4.12\ Re^{0.31};\ 50 < Re < 2000 \qquad (44)$$

and

$$Nu = 0.945\ Re^{0.54};\ 1600 < Re < 90,000 \tag{45}$$

Their overall heat transfer data for single spheres were correlated as

$$Nu = 0.84\ Re^{0.48} \tag{46}$$

In Figure 17 are presented their local single sphere results as Nu_L vs. θ. At low Reynolds numbers, they found that the heat transfer rate in the wake area is less than that in the forward flow area. They found that at Re of 50 the local Nusselt number profile was uniform (no apparent separation); while at Re of 1500 the effect of wake turbulence was quite pronounced and the appearance of the separation point was striking. They correlated their local single sphere data as

$$Nu_L = 8.83 \times 10^{-3}\ Re^{0.54}\ (7050 - \theta^2)^{1/2} \tag{47}$$

for θ less than 80°. For their dense packing studies they found that the relations

$$Nu = 2 + 1.18\ Re^{0.53};\ 50 < Re < 3000 \tag{48}$$

and

$$Nu = 0.263\ Re^{0.73};\ 2000 < Re < 50,000 \tag{49}$$

FIGURE 17 LOCAL HEAT TRANSFER PROFILES FOR SINGLE SPHERES FROM REFERENCE (66)

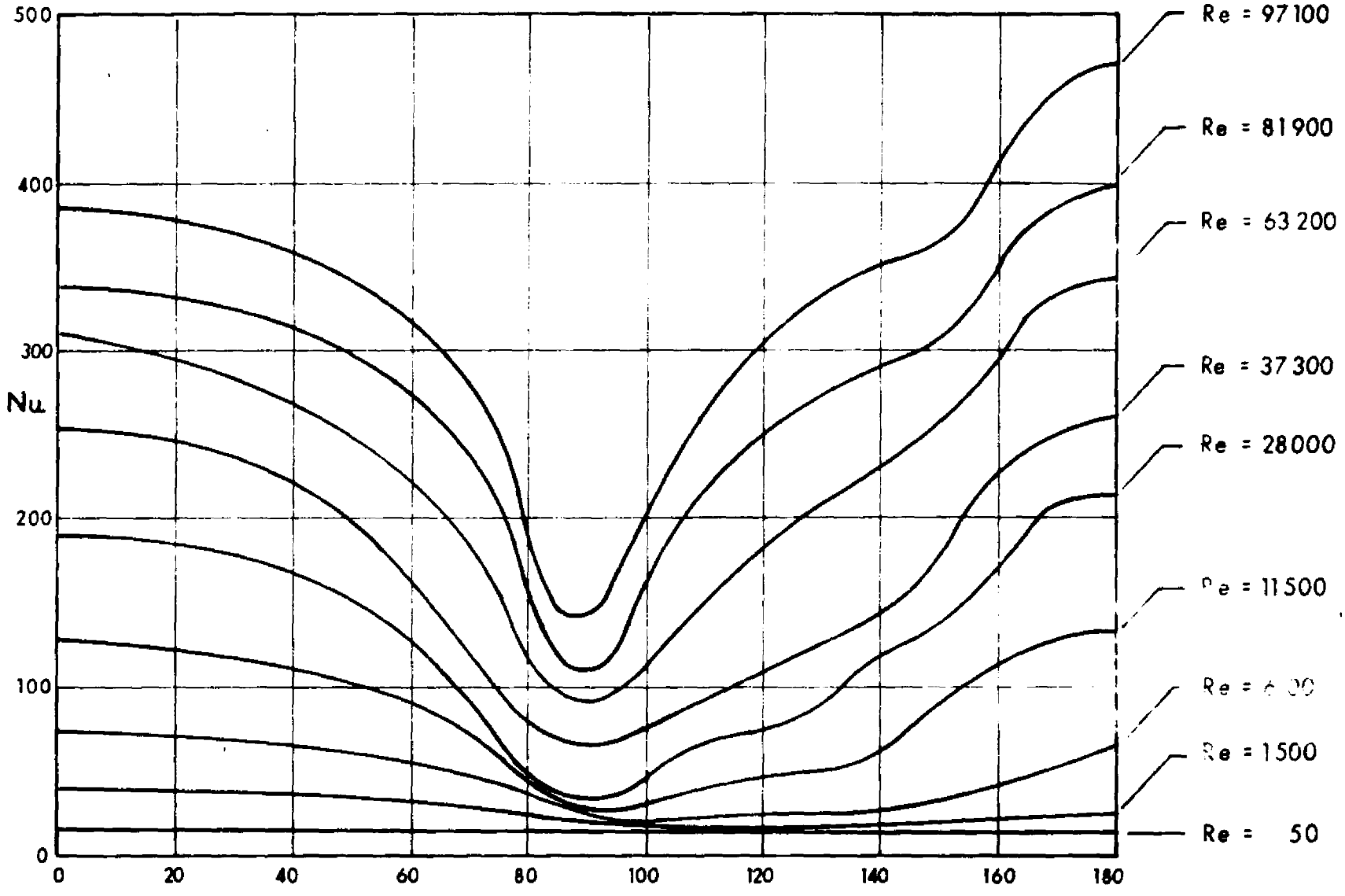

correlated their data. Three kinds of loose packings were studied (separation between spheres being $d_p/4$, $d_p/2$ and d_p) in the Re_p range of 7500 to 40,000. They found that the overall heat transfer rate, for all loose packings, at all Reynolds numbers was greater than that for a single sphere. They correlated the data for all packings as

$$Nu = \left[0.87 \frac{\epsilon_s}{\epsilon_\ell} - .19\right] Re^{0.635} \qquad (50)$$

In Figure 18 are presented their results for local heat transfer rate over the equator of a sphere in a dense cubic array in the Re range of 50 to 33,000. They found that points of contact result in minimum transfer rates and that the value attained is due to the different flow regimes in the neighborhood of these points of contact. The location of minima and maxima in these profiles was found to be a function of the density of the packing. As the particles became more separated, the profiles more and more resembled those obtained for single spheres. The authors tried to extrapolate equation (50) to the limiting case of flow around a single sphere ($\epsilon_\ell = 1$) whereby they arrived at the relation

$$Nu = 0.225\ Re^{0.635} \qquad (51)$$

which they found was in good agreement with the data of Wadsworth[61].

In this manner, an approximate correlation was obtained which is valid over a wide Re range for single spheres, loose packings and for a dense cubic arrangement. However, the authors make no claim on extending their correlation to a fluidized bed. These authors also concluded that

FIGURE 18 LOCAL HEAT TRANSFER PROFILES FOR A SPHERE IN A DENSE CUBIC ARRAY

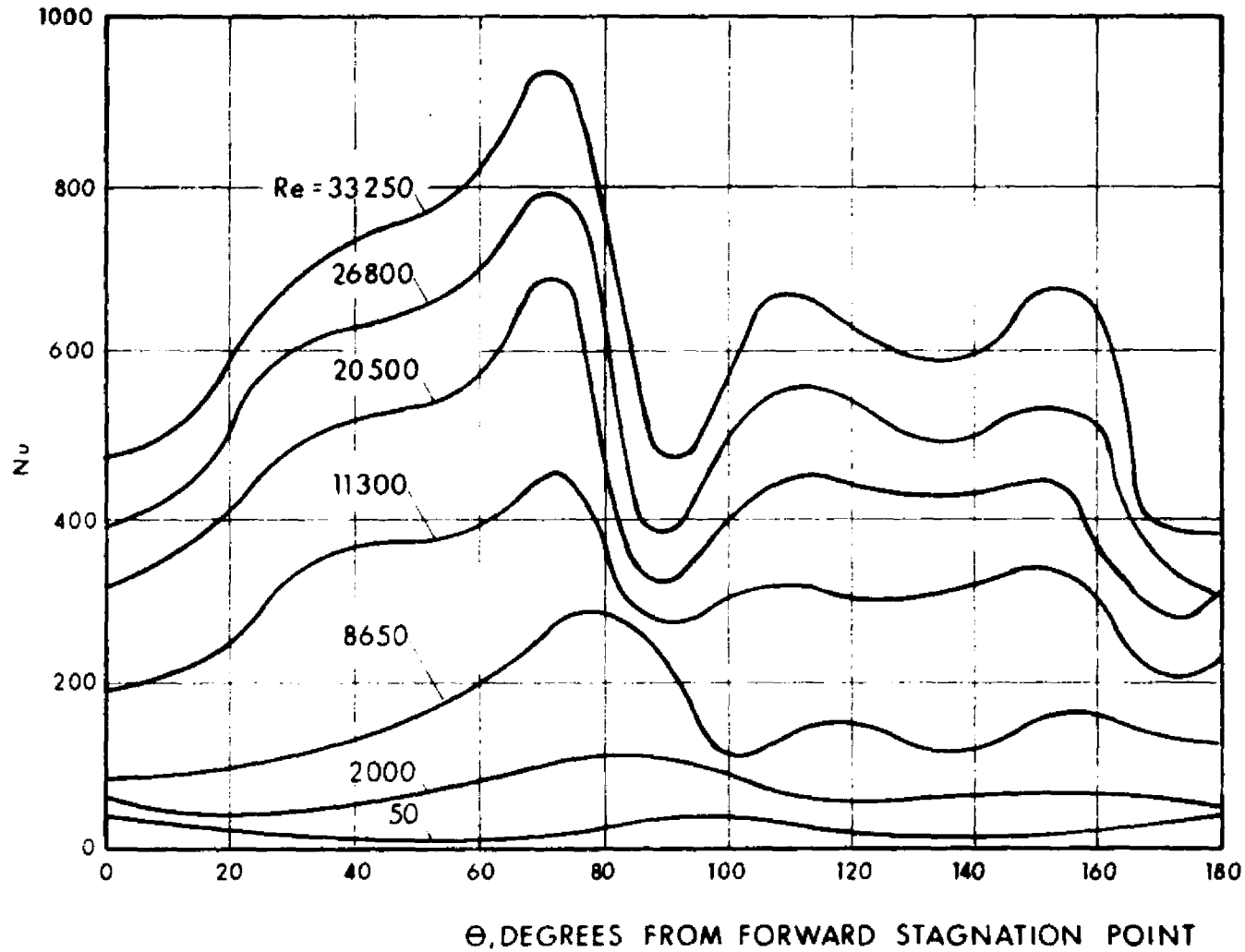

non-uniformities in the beds of commercial units must be accounted for, before any generalized design correlations can be obtained.

The most recent work in this field is that of Wilson and Geankoplis[63]. They measured mass transfer rates from packed beds of benzoic acid spheres to water and propylene glycol solutions in the very low Reynolds number, $\frac{d_p L}{\mu}$, range of 0.0016 to 55. Bed height was found to have only a slight effect on jd. The use of inert spheres to dilute the bed by as much as 10 to 1 was found to have no effect on jd. Varying the Schmidt number from 950 to 70,600 also had no effect on jd when $Sc^{2/3}$ was used. Axial mixing effects were found to be small. They found that at low Reynolds numbers jd is inversely proportional to ϵ. This is in agreement with the gas phase work of Sen Gupta and Thodos and the theoretical result of Pfeffer.

These authors recommend that for liquid-phase mass transfer in the Re range of 0.0016 to 55 and the ϵ range of 0.35 to 0.75 the relation

$$\epsilon \, jd = 1.09 \left(\frac{d_p L}{\mu}\right)^{-2/3} \tag{52}$$

be used. For Re between 55 to 1500 they suggest the equation

$$\epsilon \, jd = 0.250 \left(\frac{d_p L}{\mu}\right)^{-0.31} \tag{53}$$

For gases they recommend the correlation of Sen Gupta and Thodos, equation (36).

Experimental data on fluidized bed systems show an even greater discrepancy between different investigations than the fixed and distended bed data. However, in all cases the mass or heat transfer coefficient was found to decrease from the fixed bed value to that corresponding to a single particle in suspension. This clearly indicates a correlation with voidage as a parameter.

DESCRIPTION OF MATERIALS, APPARATUS, AND EXPERIMENTAL METHOD

Materials

Benzoic acid andbeta naphthol (2 naphthol)were obtained from the Fischer Scientific Company. These reagent grade compounds had the analyses shown in Table VI, as certified by the American Chemical Society.

The physical properties of these materials, pertinent to this investigation, are presented in Appendix A.

Distilled water was prepared by the use of a Barnstead Water Still available in the Marlies Unit Operations Laboratory.

Apparatus

Flow System

A schematic flow sheet of the apparatus used throughout this work appears in Figure 19. Figure 20 shows photographs of various portions of the flow system during an actual experimental run.

The "main-line" of the flow system was made up of three sections of 5-inch inside diameter by 1/4-inch thick lucite tubing fabricated according to the specifications shown in Figure 21 by the Allied Plastics Supply Corporation. Each section was equipped on both ends with 7-inch outside diameter by 1/4-inch thick flanges. The flanges contained six equally

TABLE VI. American Chemical Society Certified Analyses of the Benzoic Acid and Beta Naphthol Used Throughout this Work

Benzoic Acid

Freezing Point	122° - 123°C.
Residue After Ignition	0.0005%
Chlorine Compounds (Cl)	0.001%
Sulfur Compounds (S)	0.0004%
Heavy Metals (as Pb)	0.0000%
Substances Reducing $KMnO_4$	P.T.
Insoluble in Methanol	0.001%

Beta Naphthol

Melting Point Range	122.5 - 123.3°C.
Solubility in Alcohol	P.T.
Residue on Ignition	0.00%
Acids	No Reaction
Alpha Naphthol	No Reaction
Naphthalene	P.T.

FIGURE 19 - SCHEMATIC FLOW DIAGRAM

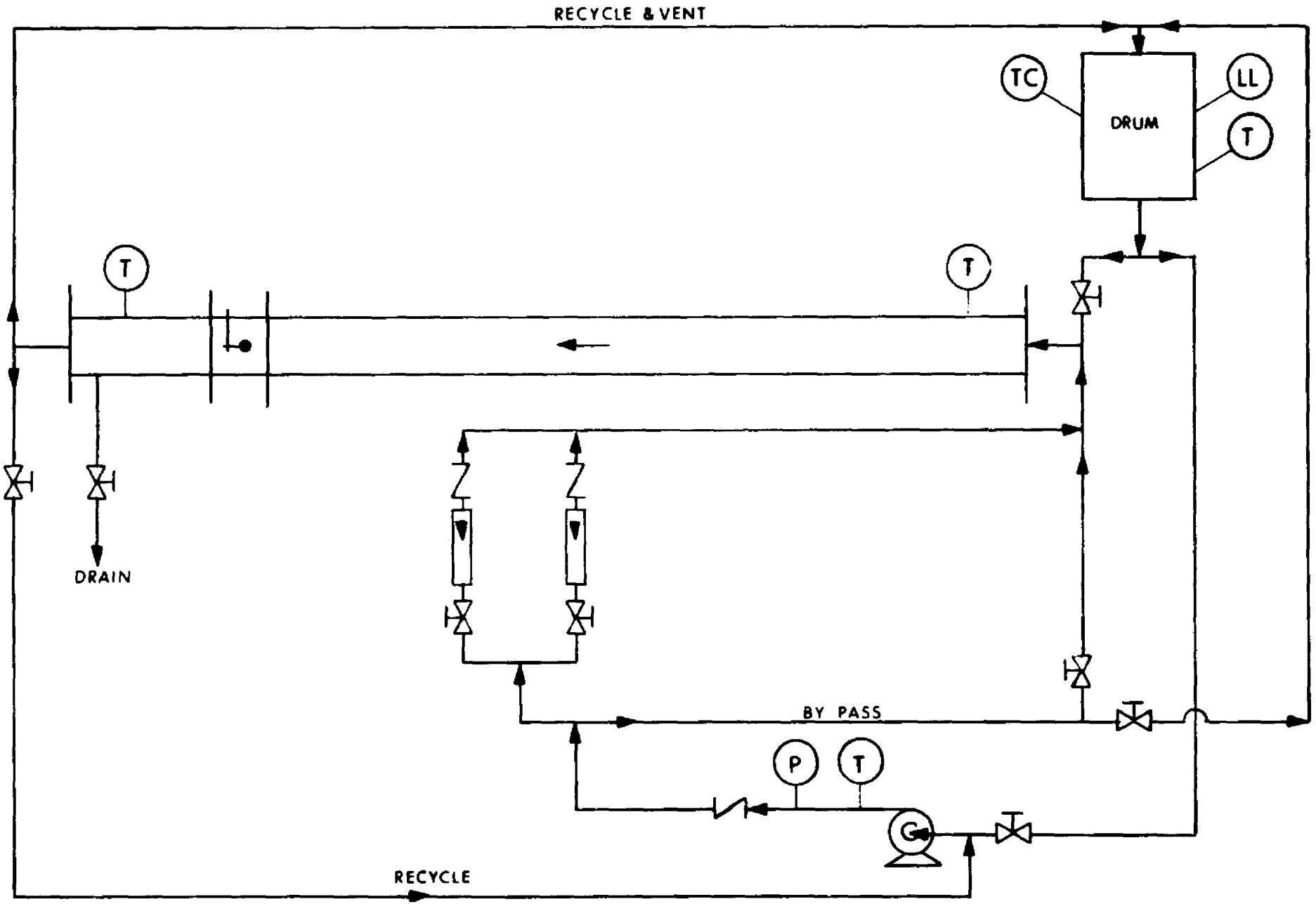

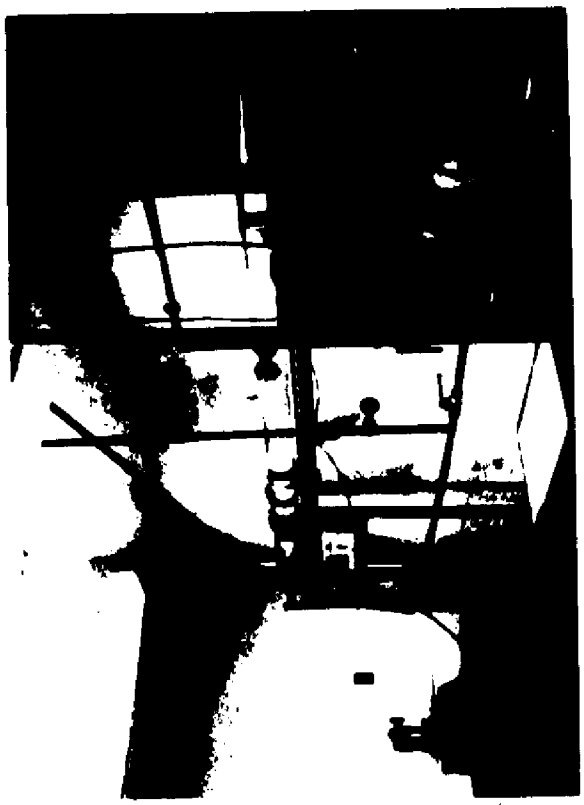

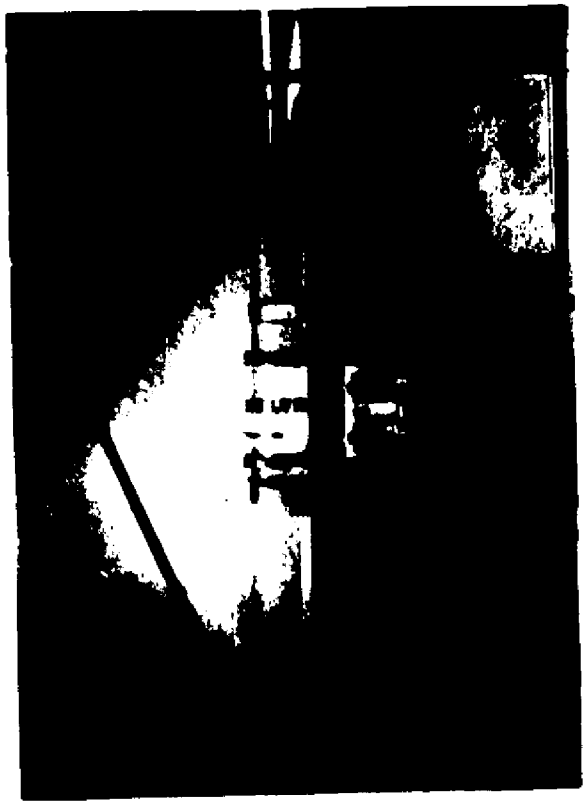

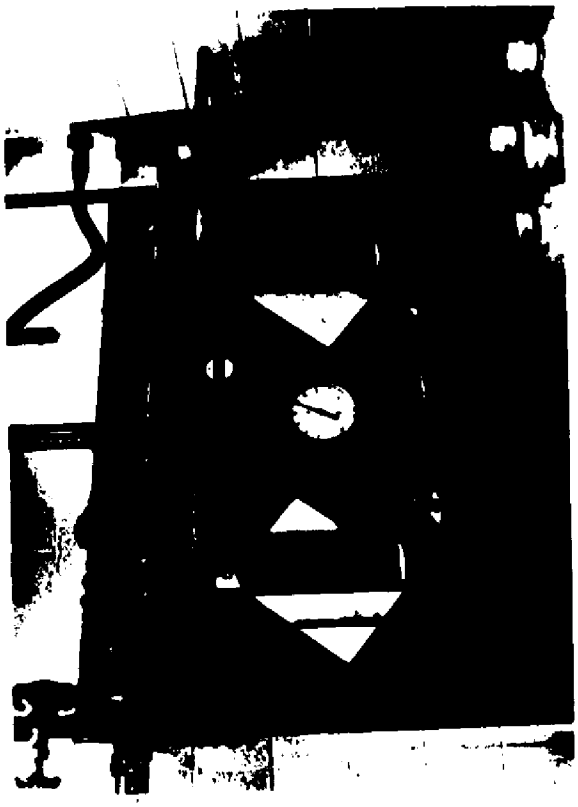

FIGURE 21

DRAWING OF FLOW SYSTEM MAIN

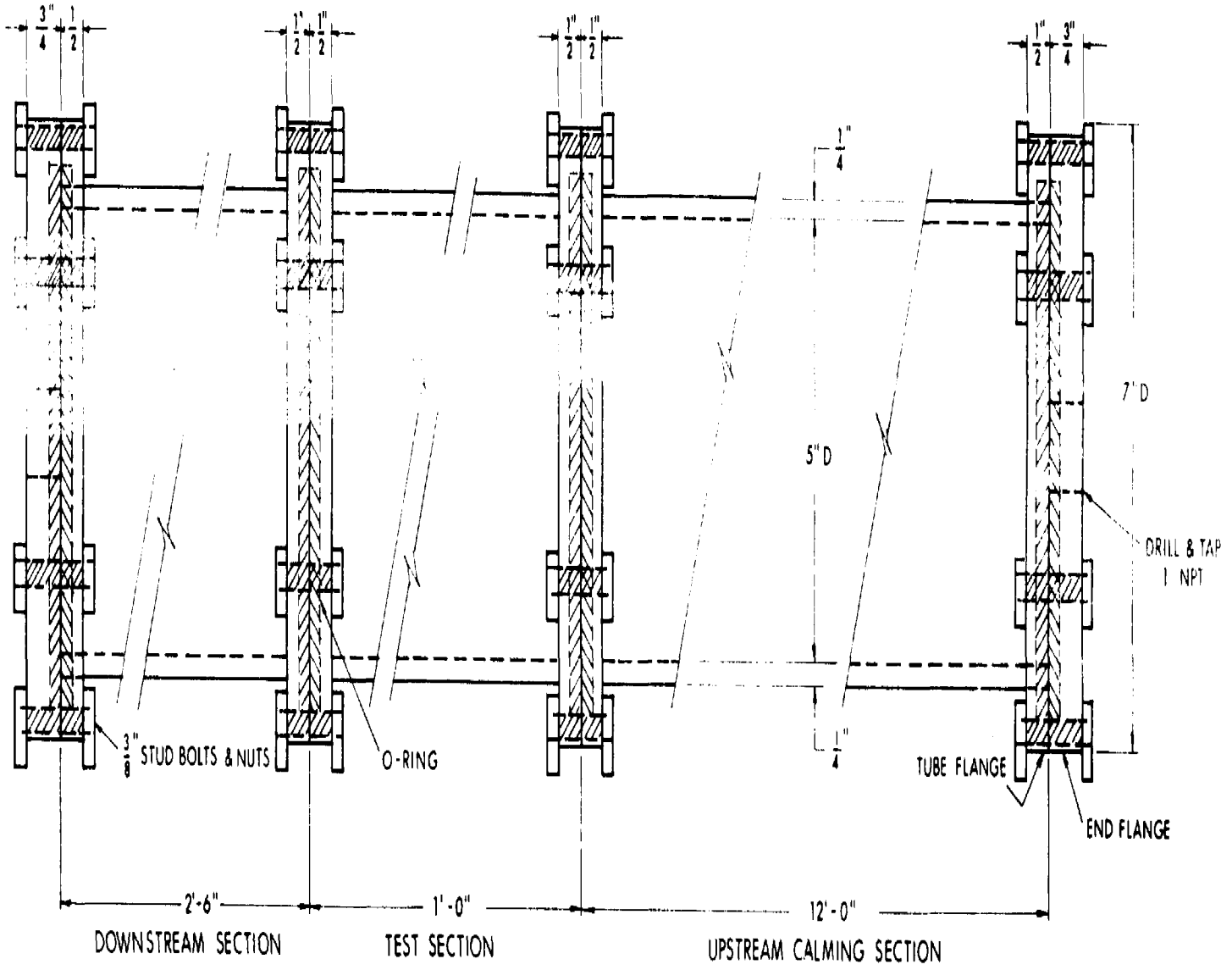

FOR GREATER DETAIL SEE FIGURE 22

SCALE: 1/2" = 1"

spaced 3/8-inch bolt holes on a 6 1/2-inch diameter bolt circle. Grooves for the insertion of Buna-N O-ring gaskets were cut into each flange. The O-rings used were made of 0.275-inch diameter Buna-N O-ring rubber cord stock which was obtained from C. E. Conover and Company. End flanges, 7-in. O. D. x 1-in. I. D. x 1/2-in. thick, also contained an O-ring groove and bolt holes matching those of the tube flanges. In order to facilitate assembly with the fluid supply lines, the end flanges were tapped for 1-inch NPT fittings.

The first section of the 15 1/2 foot long horizontal main was a 12 foot long upstream calming zone to insure fully developed laminar flow in the test section. The second section, or test section, was one foot long and equipped as shown in Figures 22 and 23 with Swagelok male connectors, catalog number 100-1-1, obtained from R. S. Crum and Company, which served as packing glands. These fittings made it possible to position up to three layers of inert spheres in the test zone ahead of the "active" sphere in any desired array. A 400-1-4 Swagelok male connector was used as the packing gland for the "active" sphere support rod. The remaining 2 1/2 foot section was the downstream calming zone.

A 55 gallon tight head aluminum drum served as an overhead fluid reservoir. The drum was mounted on a platform, 12 feet above the floor and was equipped with a top inlet and bottom outlet each being 1 inch in diameter.

FIGURE 22
DRAWING OF TEST SECTION

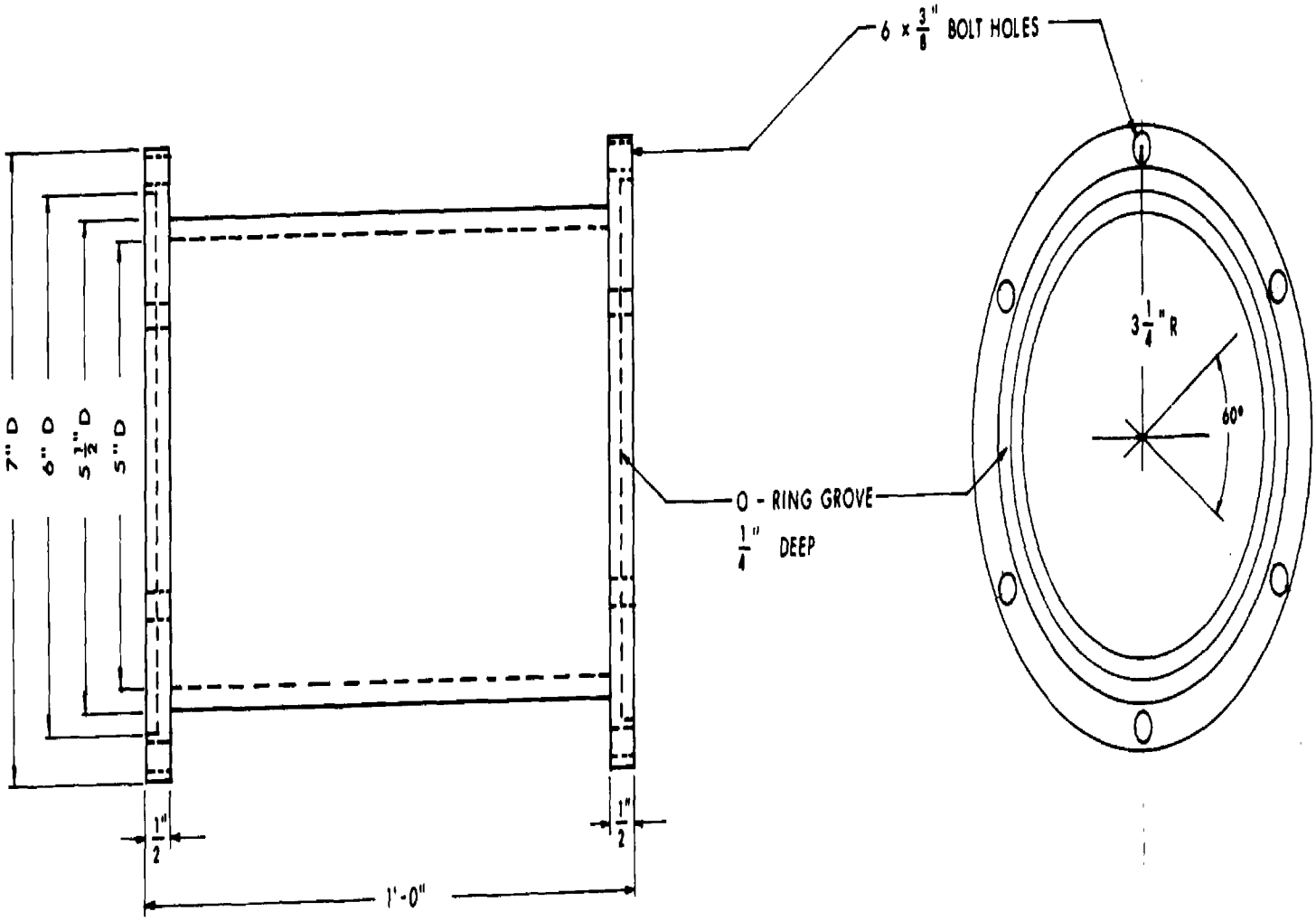

DOWNSTREAM SECTION SAME BUT 2'-6" LONG
UPSTREAM SECTION SAME BUT 12'-0" LONG

SCALE : 1/2" = 1"

END FLANGE SAME BUT 3/4" THICK WITH 1" NPT HOLE IN CENTER.

Figure 23

TEST SECTION

An Aminco Portable Cooling Unit designed for maintaining liquid baths or tanks at or below room temperature with a constancy of $\pm 0.1^{\circ}C$ was obtained from the American Instrument Company. This cooler consisted of a refrigeration unit and a Thermistemp temperature controller which controlled the bath liquid temperature and the regulating action of the refrigeration unit. The portable cooling unit was mounted on the platform next to the aluminum drum. Asbestos board insulation was inserted between these two parts of the system in order to prevent the air, cooling the compressor, from impinging on the reservoir.

The cooling coil was mounted inside the head of the drum so that the inlet water would splash over it. When the drum was filled to capacity the coil was totally submerged. The thermistor probe of the controller and a thermometer, which will later be described, were mounted at the bottom of the drum near the outlet. Swagelok fittings served as packing glands for these mountings. Tests of this assembly showed that a temperature of $20^{\circ}C$. could be maintained $\pm 0.05^{\circ}C$. for an indefinite time interval.

The drum outlet was arranged so that the flow system could be filled either directly from the reservoir or by use of the pumping equipment. In actual operation, the main line was directly filled by gravity and then the pumping system was used to establish the water rate throughout the apparatus.

A 316 stainless steel centrifugal pump with ceramic graphite-neoprene seals and a 1/6 horsepower motor was donated by Sethco Industries. The suction end of the pump was connected to one branch of the overhead drum outlet. The pump discharge led to a bypass line leading back to the drum inlet as well as to the flow control section of the apparatus.

In order to isolate the flow system from pump vibrations, suction and discharge connections were made with flexible metal hose connectors purchased from the Barco Manufacturing Company. All of the end connections on the 15 1/2 foot horizontal main were made with these same fittings.

Flow control was accomplished by the use of two rotameters equipped with needle and check valves and a globe valve on the bypass line. In order to completely bypass the rotameters and fill the system by pumping, another line outfitted with a globe valve was installed.

The rotameters used were the Fischer and Porter, model number 10A2735CA, standard type Flowrator Meter. They each had a tempered borosilicate metering tube, stainless steel float, and Buna-N O-rings. One meter was capable of operation in the range 0.28 to 3.5 gallons of water per minute and the other in the range 0.042 to 0.425 gallons per minute.

Both meters were calibrated and the calibration curves are presented in Figures 24 and 25.

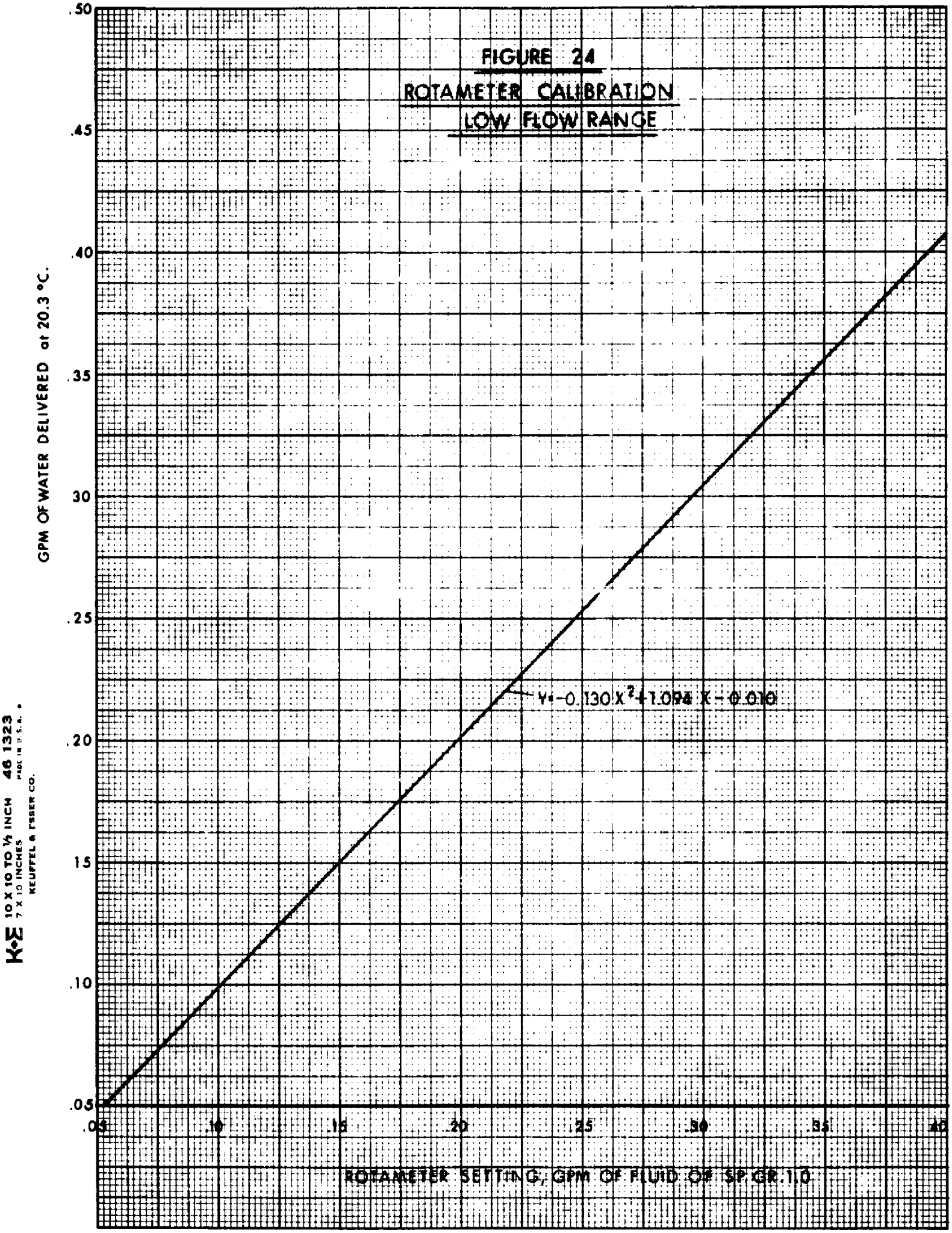
FIGURE 24
ROTAMETER CALIBRATION
LOW FLOW RANGE
GPM OF WATER DELIVERED at 20.3 °C.
.50
.45
.40
.35
.30
.25
.20
.15
.10
.05
Y=-0.130X²+1.094 X-0.010
.05
.10
.15
.20
.25
.30
.35
.40
ROTAMETER SETTING, GPm OF FLUID OF SP GR. 1.0
K•E 10 X 10 TO ½ INCH 46 1323
7 X 10 INCHES
KEUFFEL & ESSER CO.

FIGURE 25

ROTAMETER CALIBRATION - HIGH FLOW RANGE

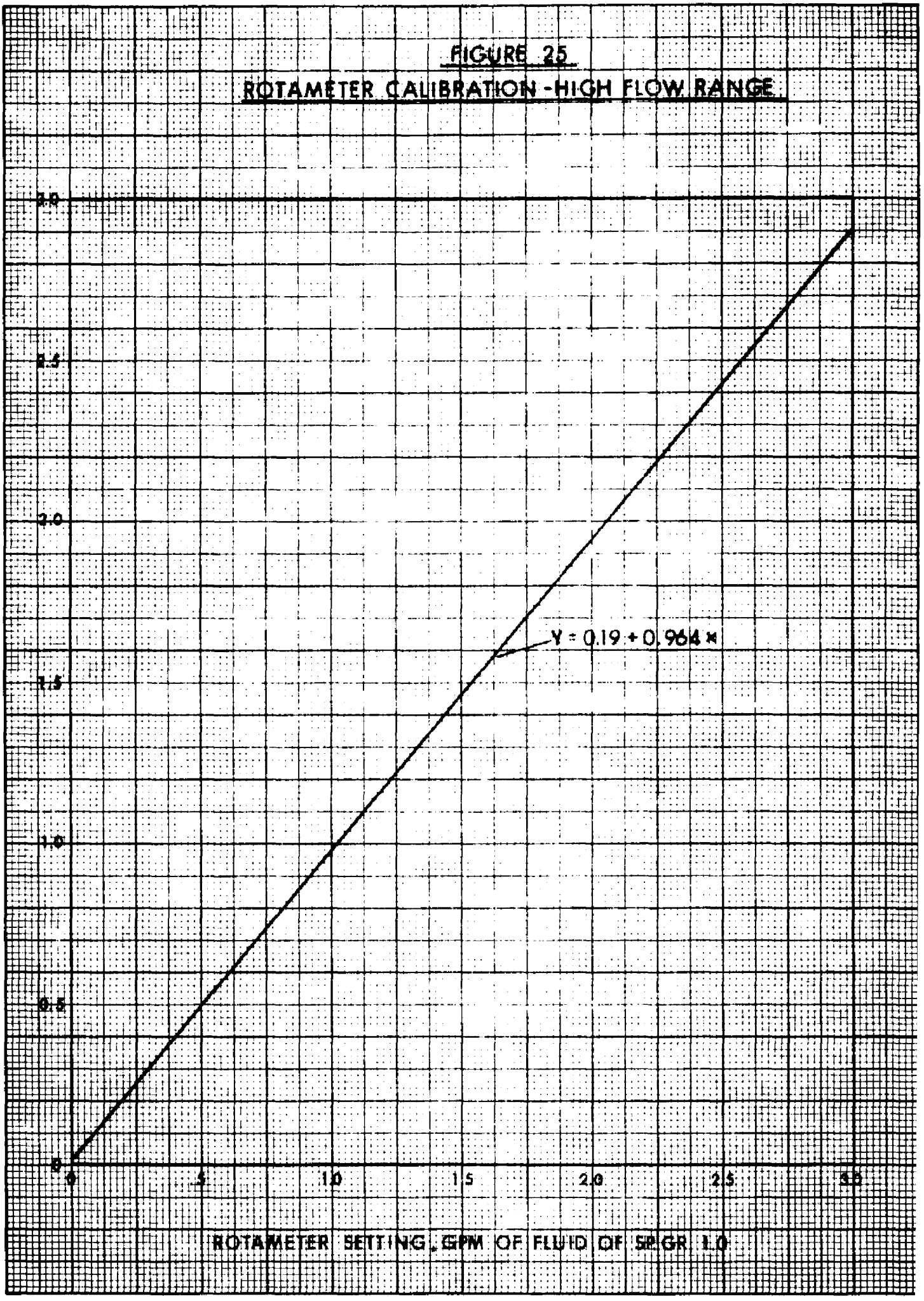

K•E 10 X 10 TO ½ INCH 46 1323
7 X 10 INCHES MADE IN U.S.A.
KEUFFEL & ESSER CO.

At the discharge end of the 5 inch diameter main, provision was made for draining, recycling, and venting. The drain line led to the building drain and faciliatated the emptying of the system and the disposal of contaminated solvent. The recycle line was arranged so that effluent from the main could either be returned to the overhead tank or recycled directly to the pump. Throughout this study effluent was always returned to the reservoir because it permitted better temperature control. As a safety precaution, the entire flow system was vented to the top of the drum.

Subsidiary lines were made by using 1 inch nominal hard drawn copper water tubing and assembly was accomplished by using 1 inch nominal sweat fittings and appropriate threaded adapters.

Temperature was measured at the inlet to the rotameter section, at the inlet and discharge of the 5 inch diameter main, and at the discharge from the overhead vessel. For this purpose, precision thermometers having a range of from -1° to $50^{\circ}C$. and capable of being read directly to the nearest $0.1^{\circ}C$. were used. Run time was determined by means of a Cramer Controls Electronic Elapsed Time Meter.

Particle Measurement System

A Wilder Micro Projector, model number AM20-1194, was donated to the project by the Mechanical Engineering Department. This unit was originally purchased

from the George Scherr Company and the present distributor of such apparatus is Scherr-Tumico, New York, Incorporated.

As obtained, the stage and micrometers were unsatisfactory for the present purposes. Therefore, a new P-1515-1-2" x 2" stage and fixture was purchased from Scherr-Tumico. The stage was equipped with two Tumico micrometer heads, catalog number 1245, which were capable of being read directly to ± 0.0001 inches. A rotary stage insert was designed to enable radii measurement of the active sphere at ten degree intervals. A device for locking the particle in position, was also designed. This device was mounted on the rotary stage. Figures 26 and 27 are detail drawings of the rotary stage and locking device, respectively. Photographs of each item and of the entire assembly are presented in Figures 28 and 29.

When completely assembled, an optical measuring system, capable of measuring particle radii to ± 0.0001 inches at 10° intervals on the particle perimeter was available. Measurement was possible in only a single plane through the particle. Although the unit was capable of motion in both the x and y directions, careful adjustment to make the entire assembly concentric with the axis of the viewing screen allowed the necessity of motion only along the particular radius under consideration.

This unit was extremely sensitive and therefore daily checks were made with a "standard" aluminum sphere.

FIGURE 26
DRAWING OF ROTARY STAGE

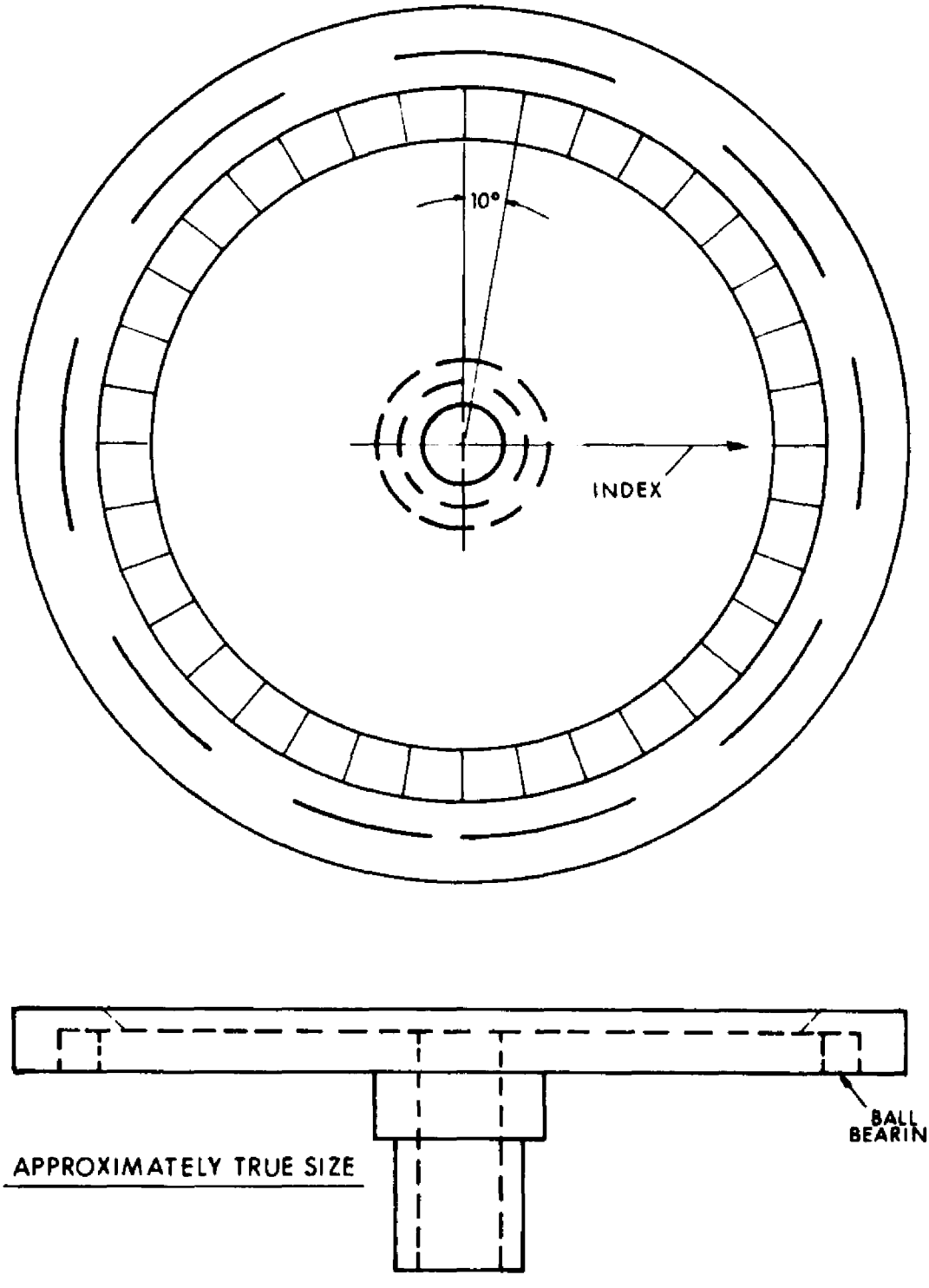

FIGURE 27
DRAWING OF PARTICLE LOCKING DEVICE

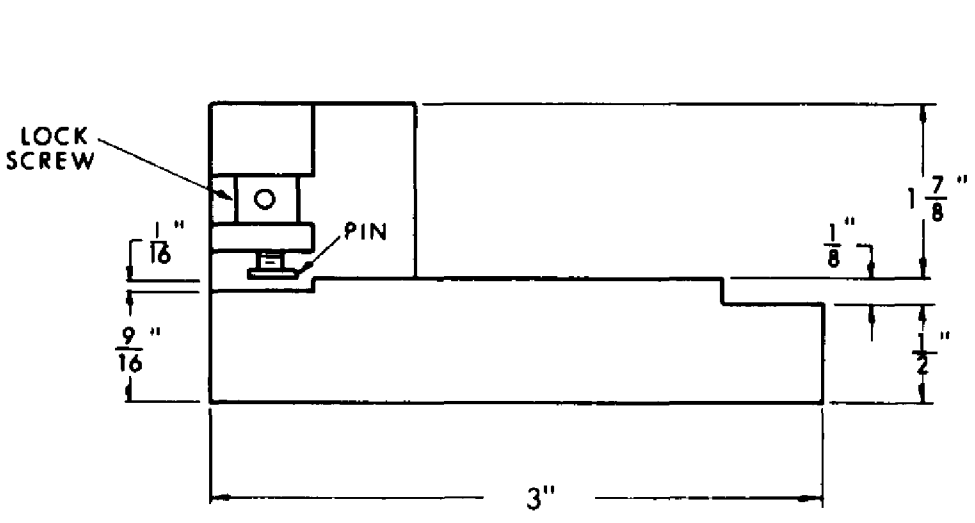

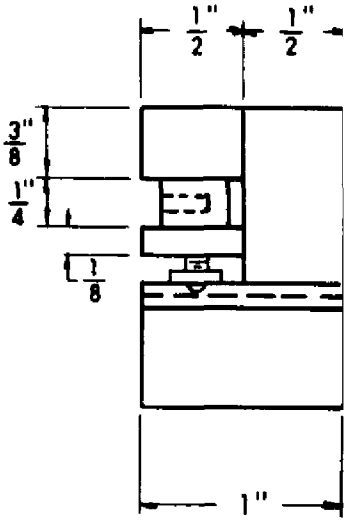

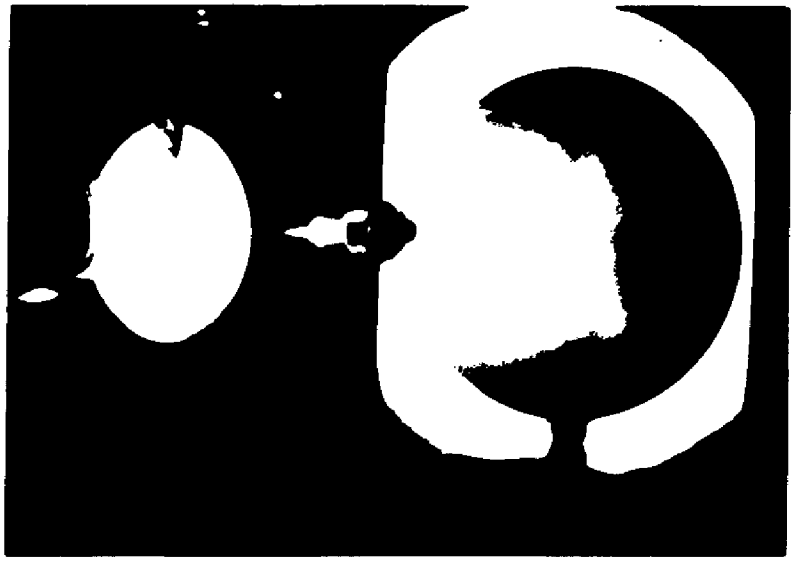

Figure 29

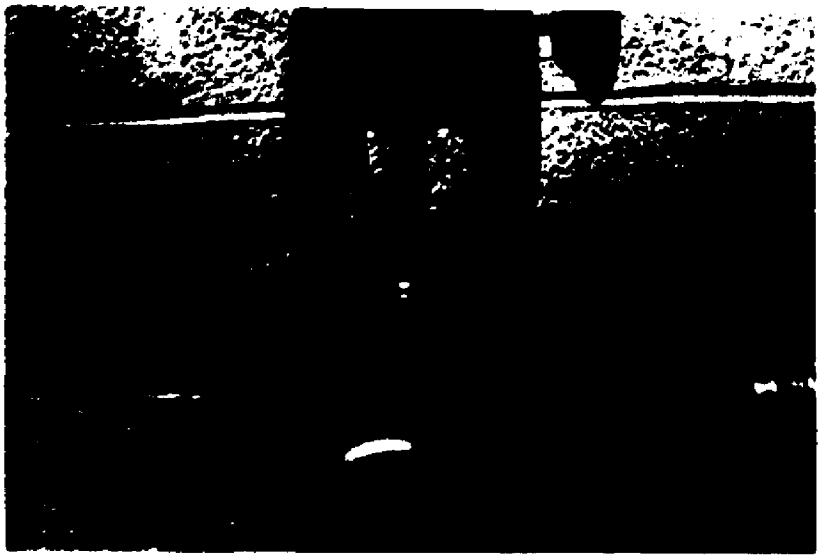

MEASURING ASSEMBLY

Particle Preparation Apparatus

The "active" spherical particles used throughout this investigation were cast, with their central support rods in place, in molds constructed according to the specifications shown in Figure 30. Photographs of the actual molds used are presented in Figure 31.

The mold used for preparing the beta naphthol particles was made of cold rolled steel. The one for use with benzoic acid was also made of cold rolled steel but since molten benzoic acid reacts with iron this mold required nickel plating. In order to insure the good adherence of the nickel, it was necessary to first lay down a layer of copper. For best plating results, the layers of copper and nickel were of equal thickness. The plating was done by the Woodside Metal Finishers Corporation.

The basic design of the molds and the necessary machining operations were identical in all other respects. The molds were constructed by the staff technicians according to the following procedure:

A. Four 10 inch × 2 inch × 1/2 inch thick pieces of cold rolled steel were cut, annealed, and surfaced. Two of these slabs were used for each mold.
B. A pair of slabs, at a time, were placed on the table of a vertical milling machine and the locations of all the details were established by use of an indicating head.
C. Matching hemispheres were milled with 1/2 inch Ball End-End Mill Cutters

FIGURE 30 - DETAIL DRAWING OF MOLDS USED

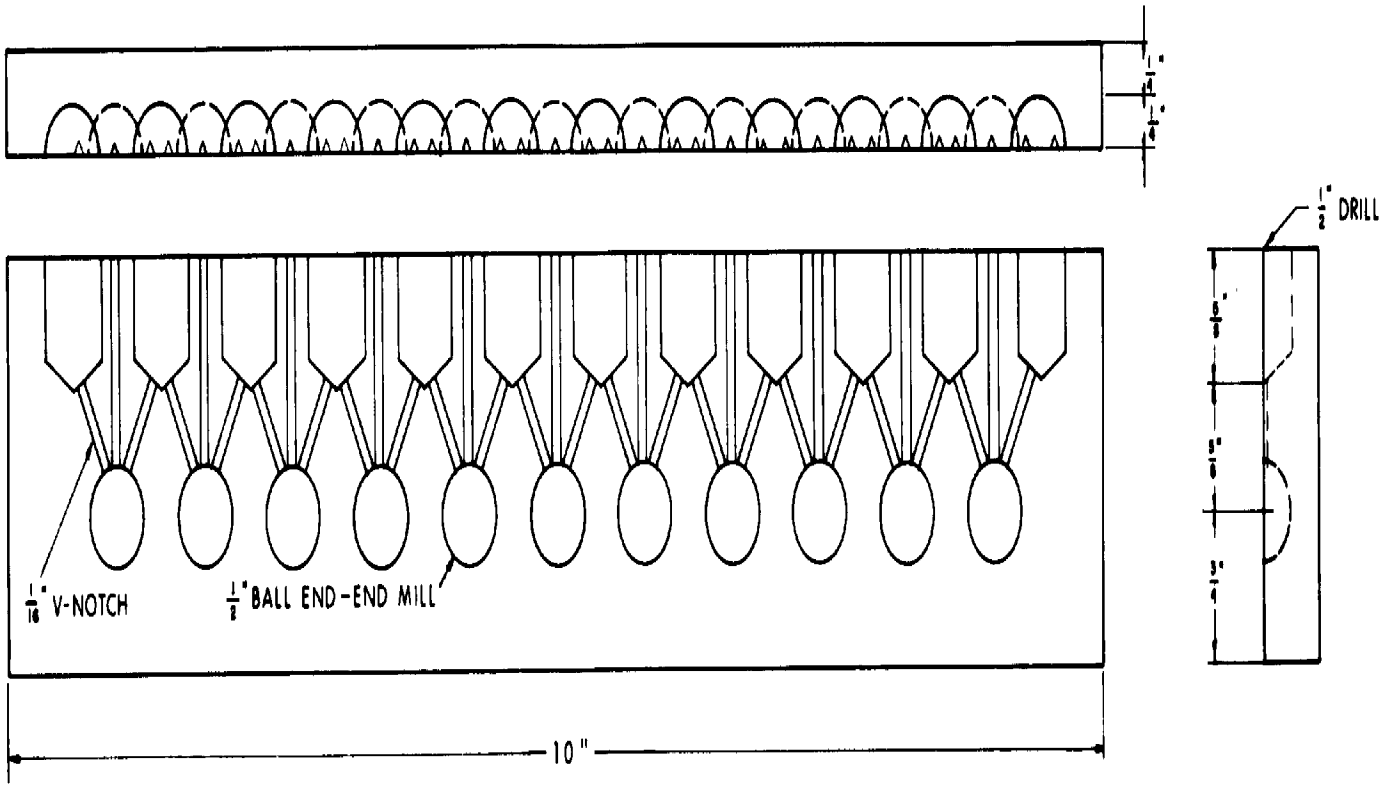

SCALE 1" = 1"
2 MATCHING PAIRS REQ'D

Figure 31

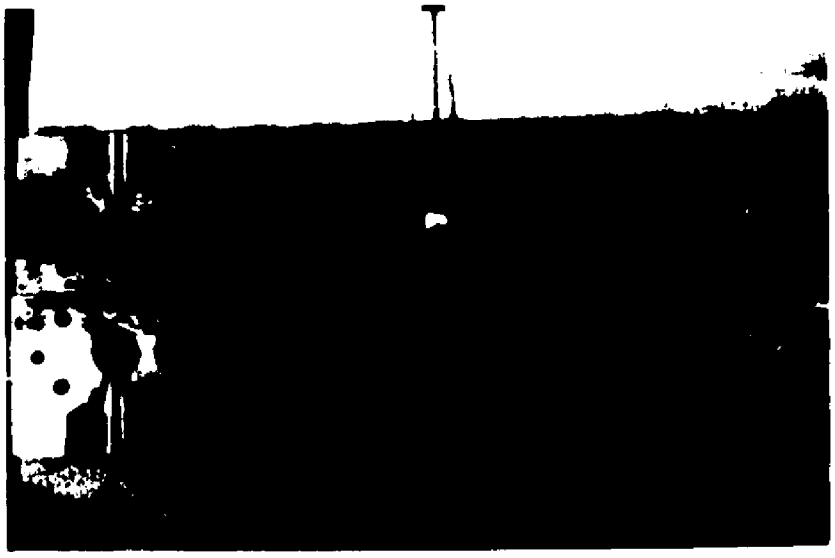

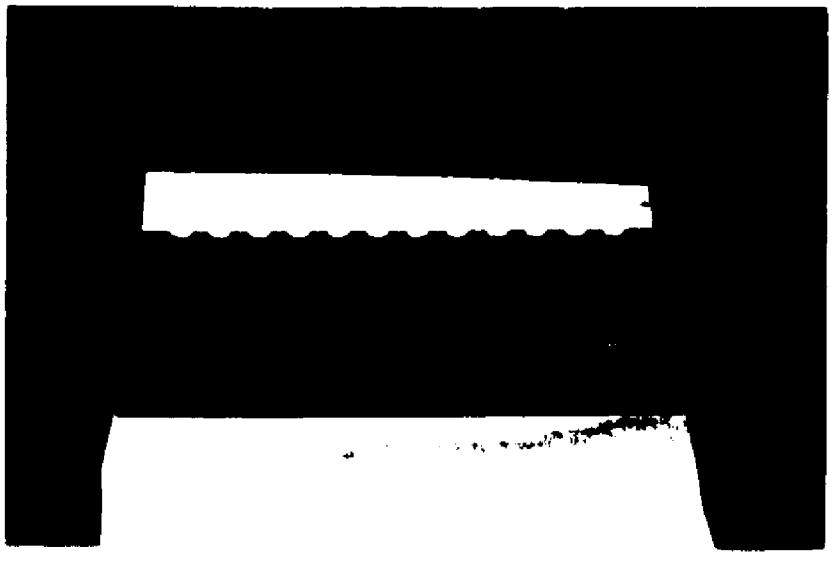

MOLD FOR CASTING
ACTIVE SPHERES

to a depth of 1/4 of an inch.

D. Matching halves of the pouring reservoirs were machined.

E. 90° V-notches were cut to a depth of 1/32 of an inch. These notches were located 170°, 180°, and 190° from the front of each hemisphere. They were cut so that when the mold was assembled they would serve as pour holes, rod insert holes, and vent holes, respectively.

F. Holes for tapered alignment pins were machined.

G. Screw holes were drilled and tapped. Tapping was done on only one half of each mold.

H. The hemispheres of each half mold were hand polished, starting with valve grinding compound and ending with a paste of fine alundum in a light lubricating oil.

I. The four half sections were cleaned and the two molds assembled.

J. One mold was then sent out to be plated; the other was ready for use.

Each of the molds was capable of yielding eleven-half inch diameter spherical particles. Each particle was mounted on a 1/16 inch outside diameter X 0.020 inch inside diameter / 3 inch long seamless 316 stainless steel support rod, located along its central axis. The tubing used for the support rods was obtained from Whitehead Metal Products.

The particles made had smooth-non-powdery surfaces with imperfections located at 170° and 190° from the forward stagnation point. These flaws arose because of the pour and vent holes. There was a slight seam on the spheres

where the two halves of the mold met. All of these defects were trimmed from the surface with a razor blade. Their presence, however, did not cause any discrepancies since all measurements were made in the plane perpendicular to the one in which they were located. The particles were hard and machinable. Sectioning showed them to contain no entrained air bubbles and pycnometric density determinations showed them to have a uniform density. Because the mold was polished, the resulting particles had no surface machining marks, nor did they adhere to the mold surface. Mold release agents were not needed to recover the particles.

Test Section

The test section used in this work was designed to permit a great deal of versatility in particle configuration. Several views of the test section are shown in Figure 23.

The one foot long flanged lucite tube obtained from the fabricator was prepared as a test section in the following manner:

A. "Blind" plywood end flanges were prepared to match the tube end flanges.
B. The tube was then mounted on the table of a vertical miller. The spindles holding it in place were centered along the central axis of the tube and were locked onto the wooden flanges. An indicating head was attached to one of the spindles so that movement of the indicating dial would cause the tube to rotate around its axis.

C. The milling head was fitted with a drill chuck adapter and drill.

D. Holes were drilled at 30° intervals along the surface of the tube.

E. The holes were then tapped in order to allow mounting of the Swagelok fittings.

F. The Swageloks were mounted by hand, care being taken so that they would not penetrate the inner surface of the tube wall. Teflon tape, wrapped around the threads of each fitting, served to give a water tight seal.

Experimental Method

Particle Preparation

The assembled mold was placed on an electric hot plate and heated to the melting point of the material to be cast. At the same time, a clean covered beaker, containing sufficient material to completely fill the mold, was also heated on the hot plate until its contents were molten. The mold was then placed on a wooden stand and the melt was poured into it. After the mold had been filled to capacity it was allowed to stand for several minutes. It was then quenched in cold water for a period of time much longer than that necessary to solidify the melt. The mold was then opened and the particles mounted on support rods were removed and dessicated a minimum of 72 hours.

On the day prior to its use, the particle was taken from the dessicator, the flaws, discussed previously, were removed and the excess material adhering to the support rod was wiped away with a solvent moistened swab.

The apparatus shown in Figure 32 was then used to position the "positive stop" bar on the support rod. The stop bar was held in place by a set screw. This assembly permitted accurate establishment of the distance, 3.0000 inches $\pm$0.0001", between the sphere center and the rear of the bar. This dimension was fixed in order to accurately position the particle in the comparator and in the test section.

The particle prepared in this manner was then returned to the dessicator.

Initial Particle Measurement

Immediately prior to its use the sphere was placed on the stage of the measuring system, see Figure 28, and its radius was measured at 10° intervals along its surface. This measurement was repeated a minimum of three separate times. The measured values at each position were averaged and these averages were recorded as the initial radius profile.

Between radius profile measurements, the assembled rod-sphere system was weighed on an analytical balance to the nearest tenth of a milligram. In all cases, identical weights $\pm$.3 milligrams were obtained for the same unit, regardless of the time interval between weighings. This value was recorded as the initial particle weight.

Mounting of Active and Inert Spheres

The test section, described previously, was arranged so that a single

Figure 32

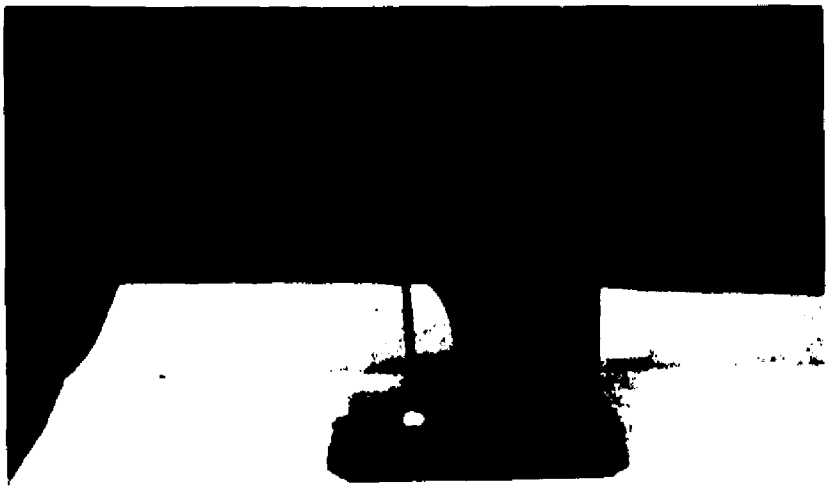

SPHERE POSITIONER

active sphere, when mounted properly, would be located at its exact center.

A 1/4 inch diameter x 4 inch long brass rod was prepared according to the specifications shown in Figure 33a. The support rod of the active sphere unit was inserted into the 1/16 inch diameter hole of this mounting rod and slipped through until the stop bar rested against it. Then the set screw was used to lock this assembly together and the entire unit, shown in Figure 33b, was inserted into the appropriate packing gland and preliminarily centered by eye.

A centering guide, shown in Figure 34a, was used to accurately center the active sphere which was then locked in place in the test section. A final check was made using a Starrett inside micrometer capable of being read to 0.001 inches. If it was found that corrections were necessary, the entire procedure was repeated until the active particle was situated with its center at the center of the test zone.

The test region was outfitted with packing glands, see Figure 23, which would permit anywhere from a single inert particle to three layers of inert particles to be placed in the neighborhood of the active sphere, in a great variety of configurations.

Stainless steel rods, similar to the "active" sphere support rods, were used to position and hold the inert particles at the locations desired.

Lucite spheres, 1/2 inch in diameter, served as the inert particles. These were obtained from the Ace Plastics Company.

FIGURE 33

MOUNTING OF THE ACTIVE SPHERE

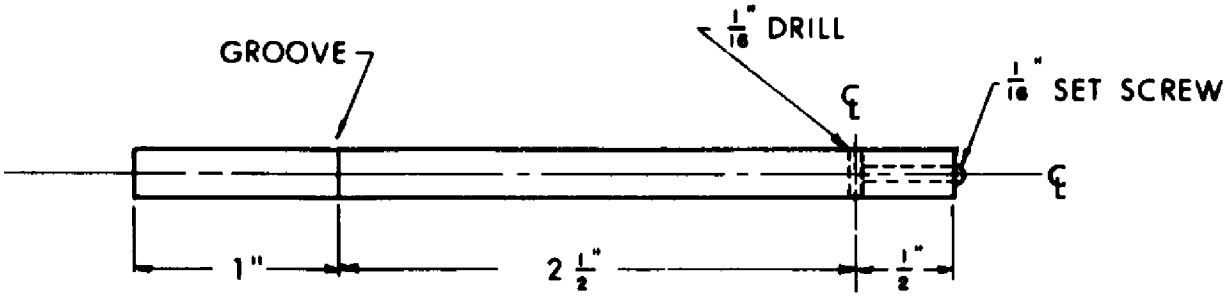

"A"

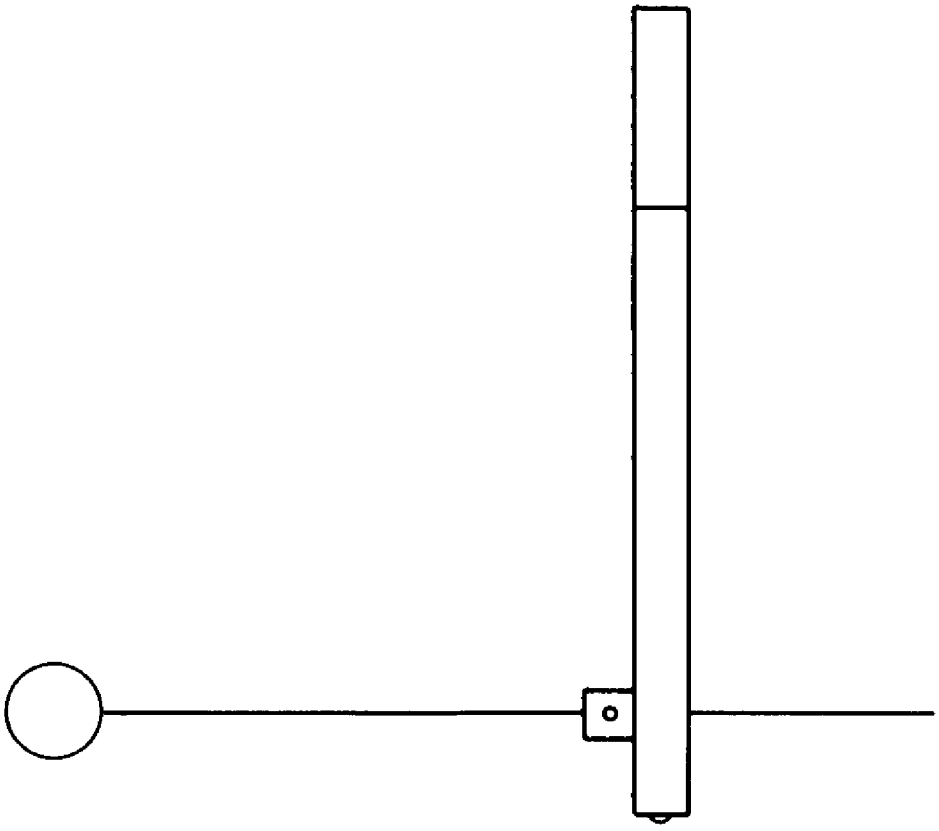

"B"

FIGURE 34

CENTERING AND LOCATION GUIDES

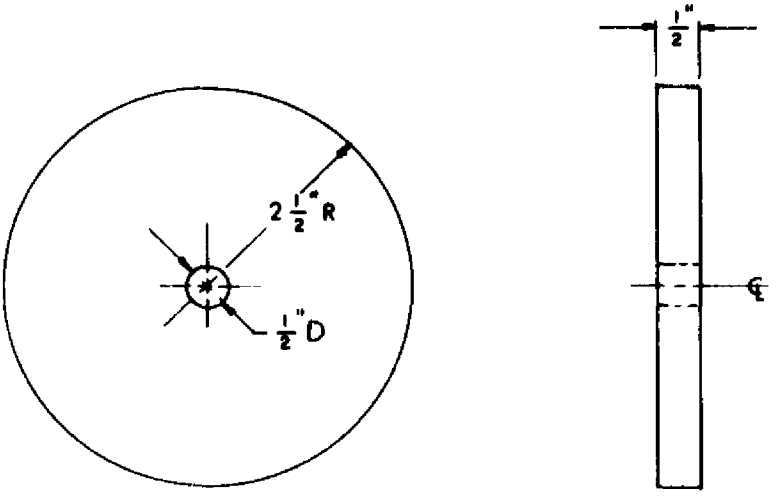

"A"

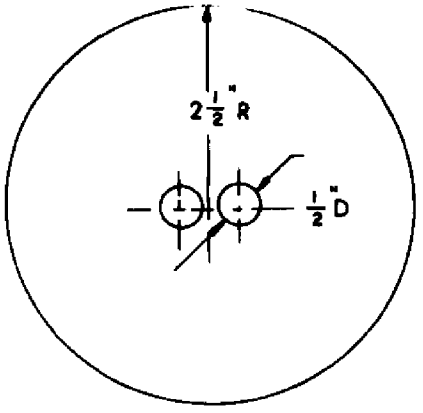

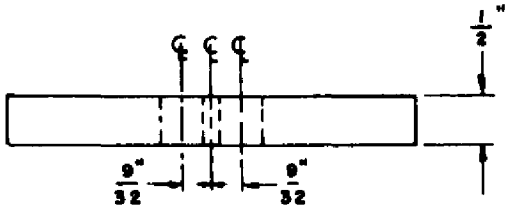

"B"

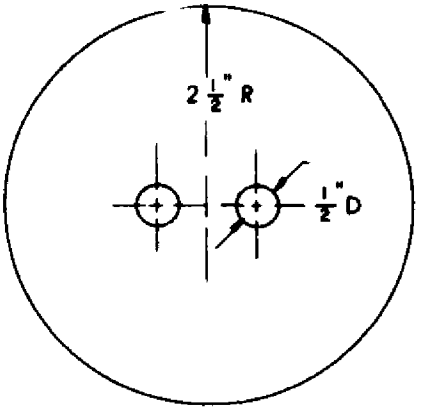

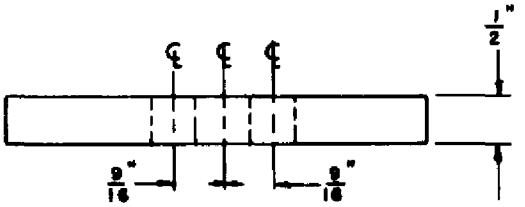

"C"

A gauge, which consisted of an accurately machined half inch diameter sphere, milled out of a block of cold rolled steel, was used to select those lucite particles which most closely could be said to be one half inch in diameter. These particles were then drilled so that through one axis there was a 1/16 inch diameter hole and through a mutually perpendicular axis there was a 1/16 inch diameter hole to the sphere center. It was through these holes that the steel rods were inserted into the inert particles.

The procedure used in mounting the inert spheres was dependent upon the configuration desired. In all cases, except for those where full layers of inert particles were used, the lucite centering and location guides shown in Figure 34a, b, and c were necessary for proper inert sphere positioning.

The guide in Figure 34a was used when it was desired to locate one or more inert particles, directly in front of the active sphere. The guide in Figure 34b was used to establish inert spheres when the particle configuration was an equilateral triangle of half inch height. When it was desired that the composite particle configuration be an equilateral triangle one inch high the guide in Figure 34c was used.

These guides were all prepared by turning down on a lathe, 1/2 inch thick lucite squares so that the the radius of each guide conformed to the radius of the test section, as measured with inside micrometers. This allowed the guides to be slipped into and out of the test zone.

The desired separation between the active and inert particles was accomplished by insertion of the inert particle support rod through a packing gland in the appropriate layer. When not in use, the glands were sealed with 1/16 inch diameter inserts.

Run Procedure

The following procedure was used for all of the experiments :

A. Place the assembled test section into position in the flow system and lock it in place.
B. Completely fill the flow system by gravity from the overhead reservoir.
C. Close the gravity feed valve.
D. Establish the desired flow rate by adjustment of the appropriate rotameter needle valve and the bypass line valve.
E. At periodic intervals throughout the run, record time, temperatures, inlet pressure, and flow rate.
F. Upon conclusion of the desired run interval, empty the system, remove the test section, and recover the active particle. Immediately place the used active particle in a dessicator.

After each run, between three and four gallons of water was lost while removing the test zone. This was replaced with freshly distilled water immediately. Periodically, the system was drained and refilled with newly distilled water.

It should be mentioned, that even without loss, and hence necessary water replenishment, over fifty runs with the same water supply would cause only a one percent error in the mass transfer driving force of the fiftieth run. This calculation was based upon an overall particle diminution of four percent and the subsequent solute buildup in the recirculating water.

Run intervals were determined from information presented in Appendix G at the start of any series of studies and then experience was used to select a run interval for attaining approximately an overall particle diminution of four percent.

From the time of completion 72 hours were allowed to transpire before any further measurements were made on the active sphere.

Final Particle Measurement

Exactly the same procedure described for making the initial run measurements was used to establish the final particle radius profile and weight.

RESULTS AND DISCUSSIONS

Single Sphere Studies

Although the primary aim of this study was the investigation of local and overall mass transfer rates from spheres in multiparticle systems, it was considered important to establish the reliability of the experimental techniques used by comparing the results obtained with the results of previous investigators. It was also desired to extend the earlier single sphere data down to the low Reynolds number range used in this study. For these reasons, a series of single sphere runs were made using both the benzoic acid-water and beta naphthol-water systems. Local and overall mass transfer rates were determined over a particle Reynolds number range of 5 to 175.

The overall single sphere mass transfer results, obtained in this study, along with the pertinent run variables are presented in Table VII. The local mass transfer profiles, plotted as the local Sherwood number versus angle (θ) on the surface of the sphere with particle Reynolds number as a parameter, are presented in Figures 35 and 36 for benzoic acid and in Figures 37 and 38 for beta naphthol. According to boundary layer theory of flow around a single sphere and the experimental results presented by Garner, et. al. [20, 22, and 23] and other investigators, the mass transfer rate decreases from a maximum at the forward stagnation point to a minimum at a position corresponding to the ring of separation of the boundary layer. Behind this ring of separation, in the wake region of flow, the rate of mass transfer increases to a second maximum at the rear stagnation point. At very low

TABLE VII. Overall Mass Transfer Rates for Single Spheres of Beta Naphthol and Benzoic Acid

Run Number	Solute	Run Time, Hours	Weight Loss, Grams	Flow Rate, GPM	Run Temp., °C.	Solute Solubility, Grams/1000 Grams of Solution	Schmidt Number	Initial Surface Average Radius, Inches	Final Surface Average Radius, Inches	Reynolds Number	Sh_o
I-2	BN	17.5	.0509	0.501	22.00	0.65	907.9	0.2507	0.2487	32.75	29.6
I-3	BN	17.5	.0459	0.501	21.90	0.65	910.0	0.2479	0.2441	32.2	27.1
I-5	BN	14.0	.0337	0.549	21.75	0.65	913.4	0.2472	0.2450	35.2	24.8
I-6	BN	13.5	.0371	0.694	21.90	0.65	910.0	0.2483	0.2460	44.8	28.2
I-7	BN	25.0	.0708	0.646	21.90	0.65	910.0	0.2450		41.35	29.3
I-8	BN	25.0	.0648	0.646	21.85	0.65	911.2	0.2501	0.2457	41.8	26.6
I-9	BN	25.0	.0677	0.646	21.80	0.65	912.3	0.2532	0.2484	42.25	27.4
I-10	BN	25.0	.0780	0.646	22.00	0.65	907.9	0.2487	0.2445	41.75	32.1
I-11	BN	74.7	.1104	0.0767	23.10	0.67	870.4	0.2509	0.2426	5.1	14.5
I-12	BN	27.9	.1124	0.790	21.90	0.65	910.0	0.2516	0.2438	51.15	41.3
I-13	BN	24.0	.1084	1.176	21.70	0.65	914.4	0.2543	0.2464	76.55	45.8
I-14	BN	72.0	.1895	0.407	21.85	0.65	911.2	0.2489	0.2366	25.8	27.6
I-15	BN	22.6	.1305	2.428	22.00	0.65	907.9	0.2550	0.2453	159.1	58.7
I-16	BN	22.1	.0854	1.609	22.00	0.65	907.9	0.2532	0.2480	105.6	39.2
I-17	BN	22.0	.1095	1.995	22.20	0.65	903.8	0.2554	0.2494	132.5	50.1
I-18	BN	26.2	.1248	2.428	22.10	0.65	905.9	0.2525	0.2458	158.8	48.6
I-19	BA	25.5	.4624	0.0766	26.90	3.53	860.0	0.2614	0.2301	5.5	37.0
I-20	BA	3.0	.1311	1.608	25.45	3.38	940.0	0.2600	0.2504	116.25	93.8
I-21	BA	2.3	.1188	2.425	25.55	3.39	935.0	0.2569	0.2484	174.05	110.95
I-22	BA	3.2	.1242	1.175	25.55	3.39	935.0	0.2573	0.2482	84.35	83.99
I-23	BA	4.2	.1068	0.406	25.90	3.42	809.5	0.2606	0.2530	29.85	52.38
I-24	BA	2.6	.0834	0.789	25.70	3.41	925.0	0.2561	0.2500	56.9	68.12

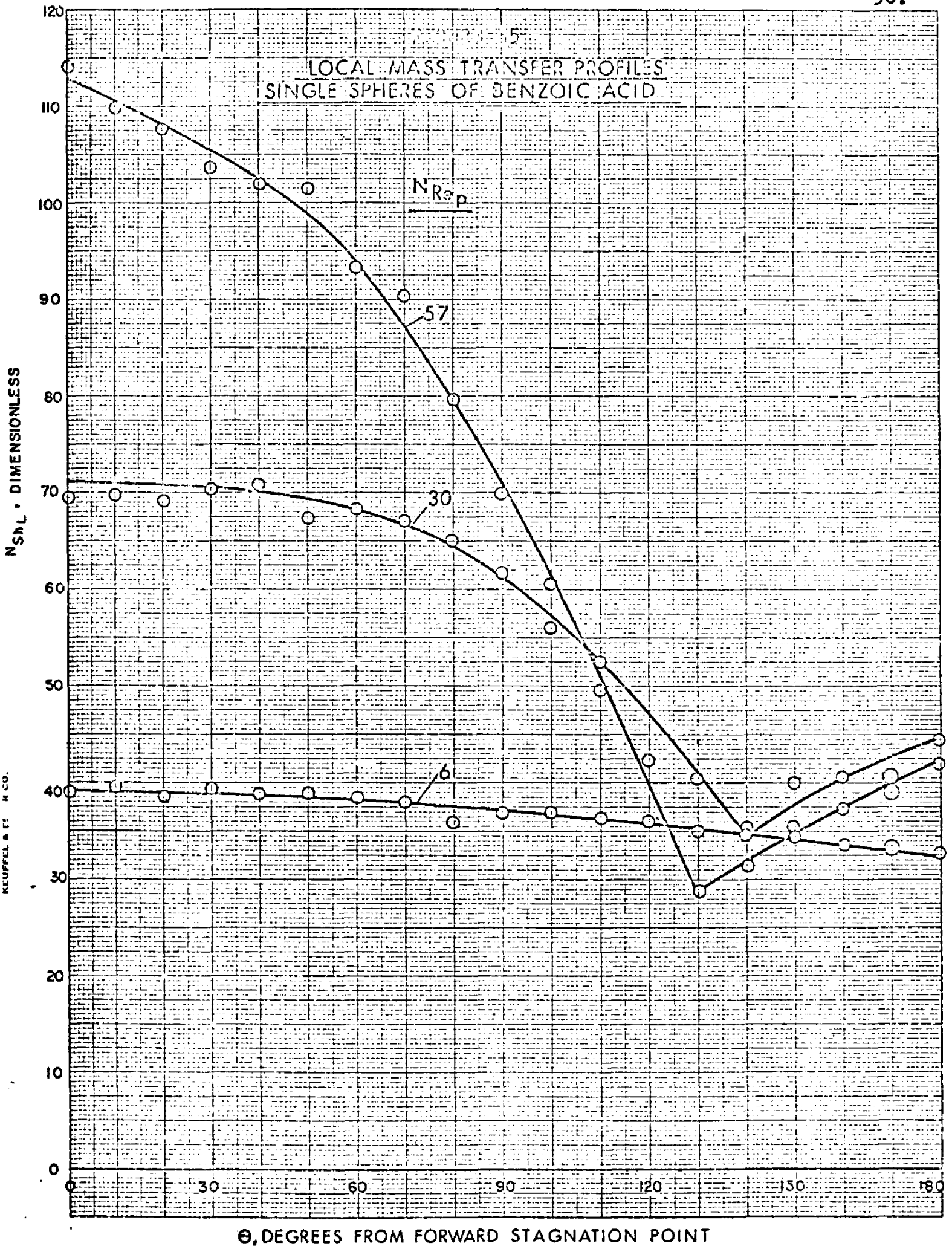
FIG. 5
LOCAL MASS TRANSFER PROFILES
SINGLE SPHERES OF BENZOIC ACID
N_{Re_p}
57
30
6
N_{Sh_L}, DIMENSIONLESS
θ, DEGREES FROM FORWARD STAGNATION POINT
0
10
20
30
40
50
60
70
80
90
100
110
120
30
60
90
120
150
180

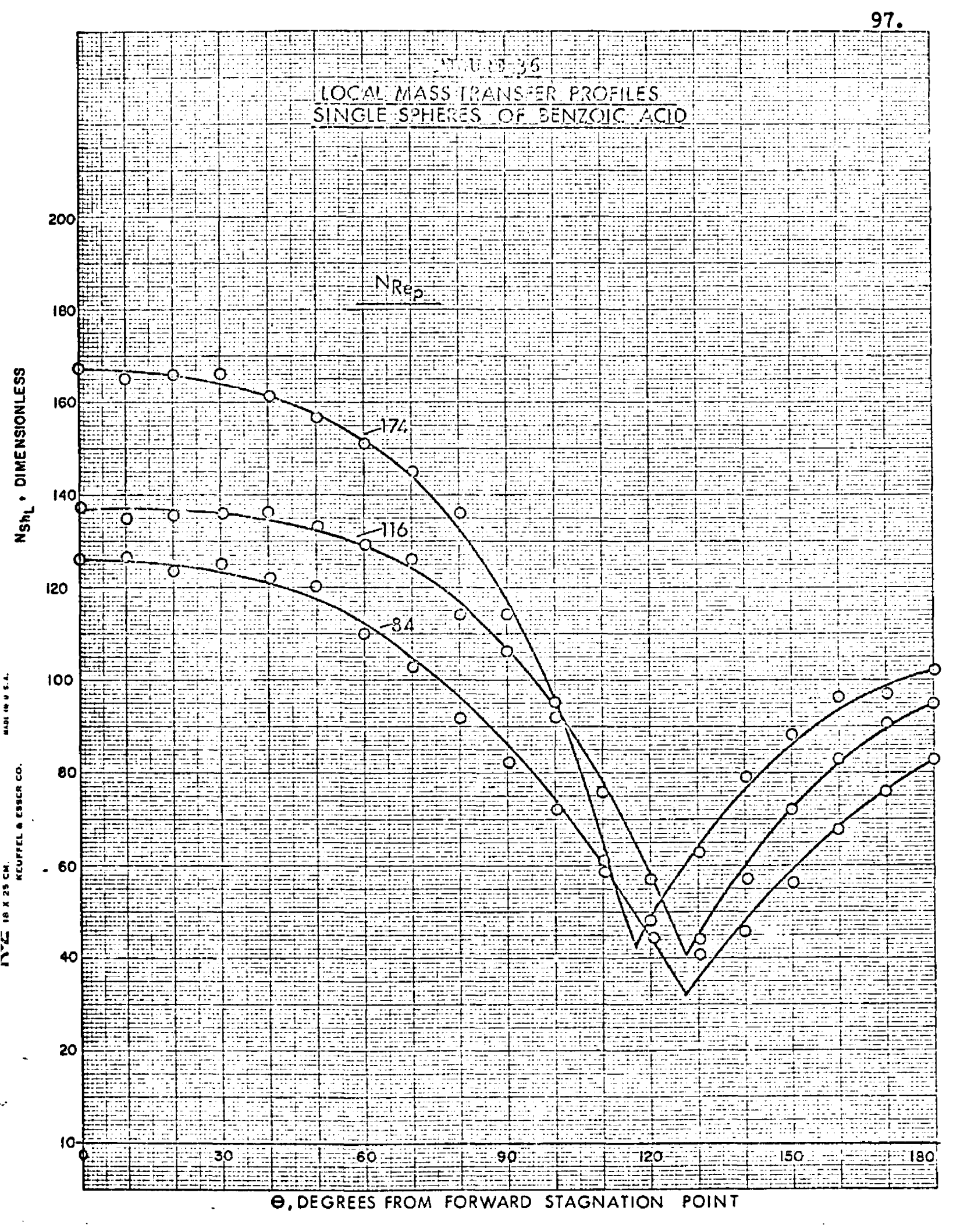
LOCAL MASS TRANSFER PROFILES
SINGLE SPHERES OF BENZOIC ACID
N_{Rep}
174
116
84
N_{Sh_L}, DIMENSIONLESS
200
180
160
140
120
100
80
60
40
20
10
0
30
60
90
120
150
180
θ, DEGREES FROM FORWARD STAGNATION POINT

FIGURE 37

LOCAL MASS TRANSFER PROFILES

SINGLE SPHERES OF BETA NAPHTHOL

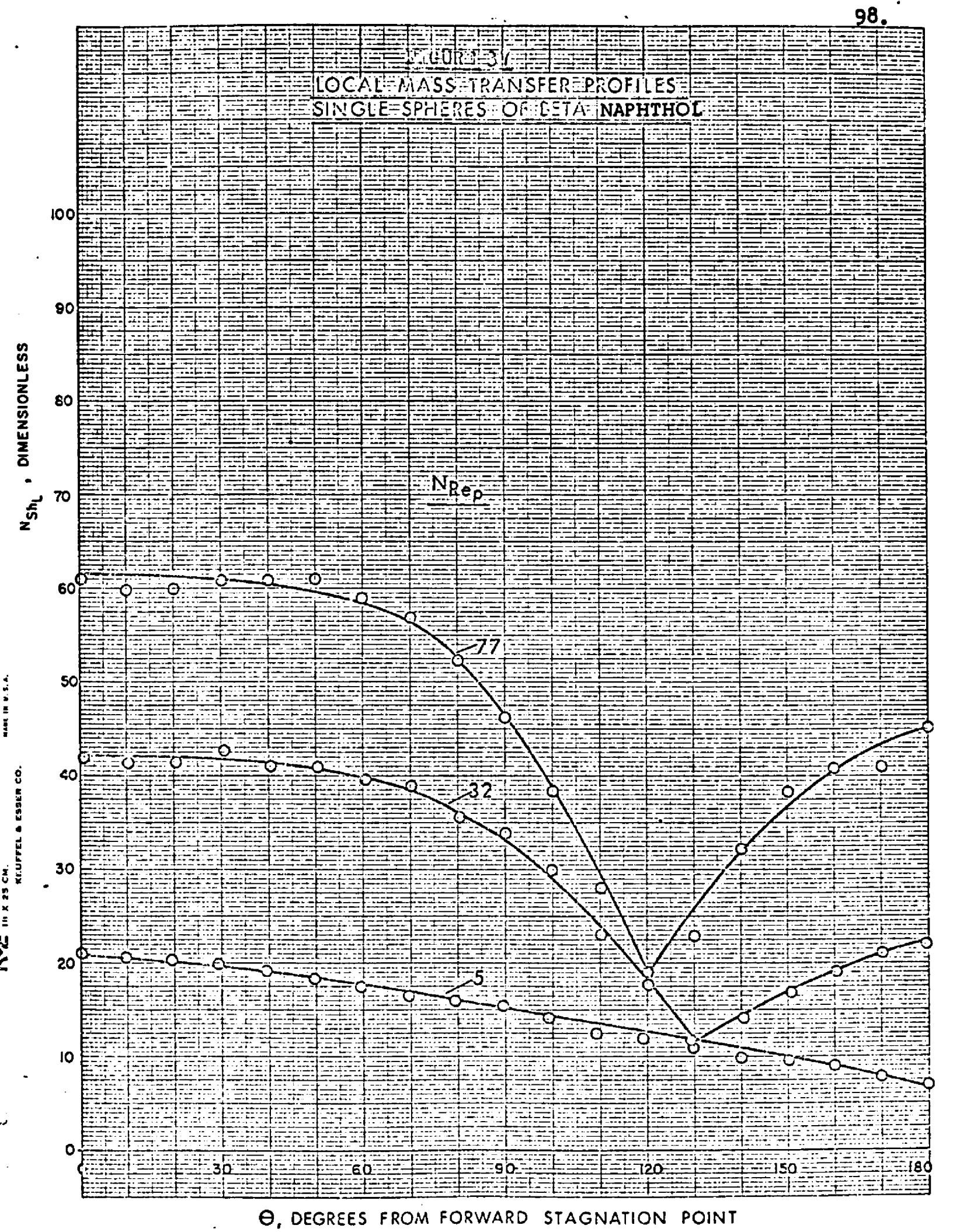

FIGURE 38

LOCAL MASS TRANSFER PROFILES
SINGLE SPHERES OF BETA NAPHTHOL

Reynolds numbers, where boundary layer separation does not occur, the minimum value of the local mass transfer rate occurs at the rear stagnation point. Figures 35 to 38 show that the present single sphere results generally follow the mass transfer profile predicted from boundary layer theory. It was noted that for both systems, at a Reynolds number as high as 5 separation does not appear to occur, while at Reynolds numbers greater than 25 the appearance of the separation point is quite striking. It was also observed that the separation ring shifts forward with increasing Reynolds number. This observation agrees with those reported by Garner, et. al. [20, 22, and 23], Rhodes and Peebles [46], and Wadsworth [60].

Comparisons of the local mass transfer rates obtained for the benzoic acid runs were made with the local mass transfer rate profiles previously reported. In Figure 39 are presented the local Sherwood number profiles obtained in this work at particle Reynolds numbers of 84 and 174 along with the profile reported in (46) at a Reynolds number of 166 and the profiles reported in (55) at Reynolds numbers of 100 and 200. Inspection of the figure shows that there is good agreement between the present work and the earlier investigations for the benzoic acid-water system. No comparison could be made with the beta naphthol results.

By numerically integrating the local Sherwood number over the surface of the sphere, an overall Sherwood number was calculated for each run. For the benzoic acid runs comparisons were made with the overall mass transfer results of Garner, et. al. [20, 22, and 23], Rhodes and Peebles [46], and Rowe, et. al. [47]. The data are presented in Figure 40 on a plot of overall Sherwood number versus

FIG. 39

COMPARISON OF PRESENT LOCAL MASS TRANSFER PROFILES WITH THOSE REPORTED IN (46) AND (55)

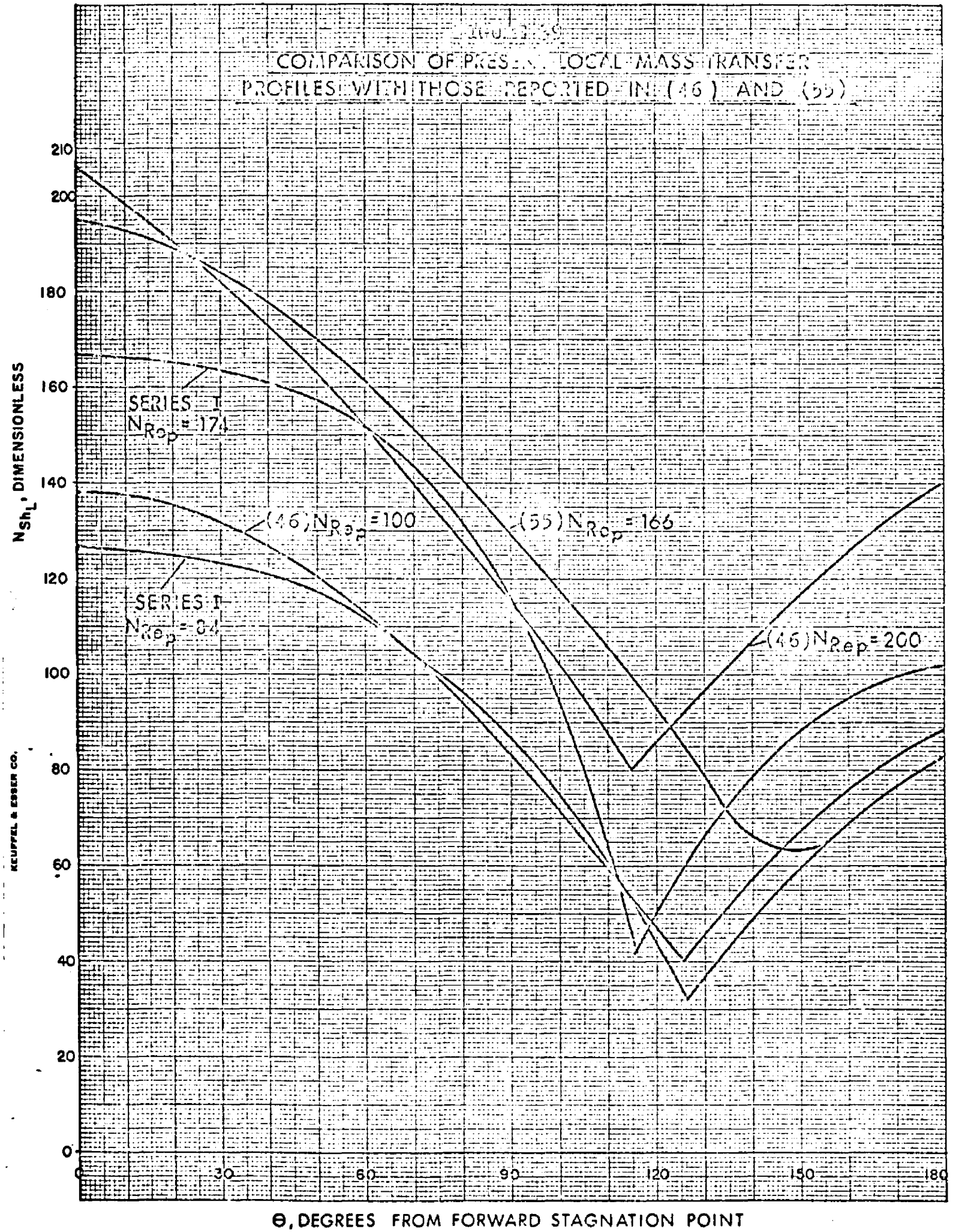

the dimensionless parameter $Re^{1/2}\ Sc^{1/3}$, obtained from boundary layer theory. The beta naphtholdata were compared with the overall mass transfer results of Steele and Geankoplis[53] and McCune and Wilhelm[38] in the same figure. It is apparent from the figure that there is good agreement for both systems with the earlier reported overall mass transfer data. The present results for benzoic acid can be represented by

$$Sh_o = 2 + 0.87\ Re^{1/2}\ Sc^{1/3} \qquad (54)$$

and for beta naphtholby

$$Sh_o = 2 + 0.47\ Re^{1/2}\ Sc^{1/3} \qquad (55)$$

In Figure 41 are presented the overall Sherwood number results of this study, for both systems, plotted as Sh_o vs. Pe. It is seen, in Figures 40 and 41, that the benzoic acid data gives higher results with increasing Reynolds number but that at low Peclet numbers the difference between the values obtained for both systems diminishes. These results are in agreement with those obtained by Steele and Geankoplis[53].

Attempts were made to explain the difference between the overall mass transfer coefficients found for the two systems on the basis of the effect of concentration driving force (flux), the effect of natural convection, and the effect of Schmidt number.

According to the discussion of interphase transport in multicomponent systems presented by Bird, Stewart, and Lightfoot,[4a] systems in which the driving force for mass transfer into a phase is large will exhibit lower mass

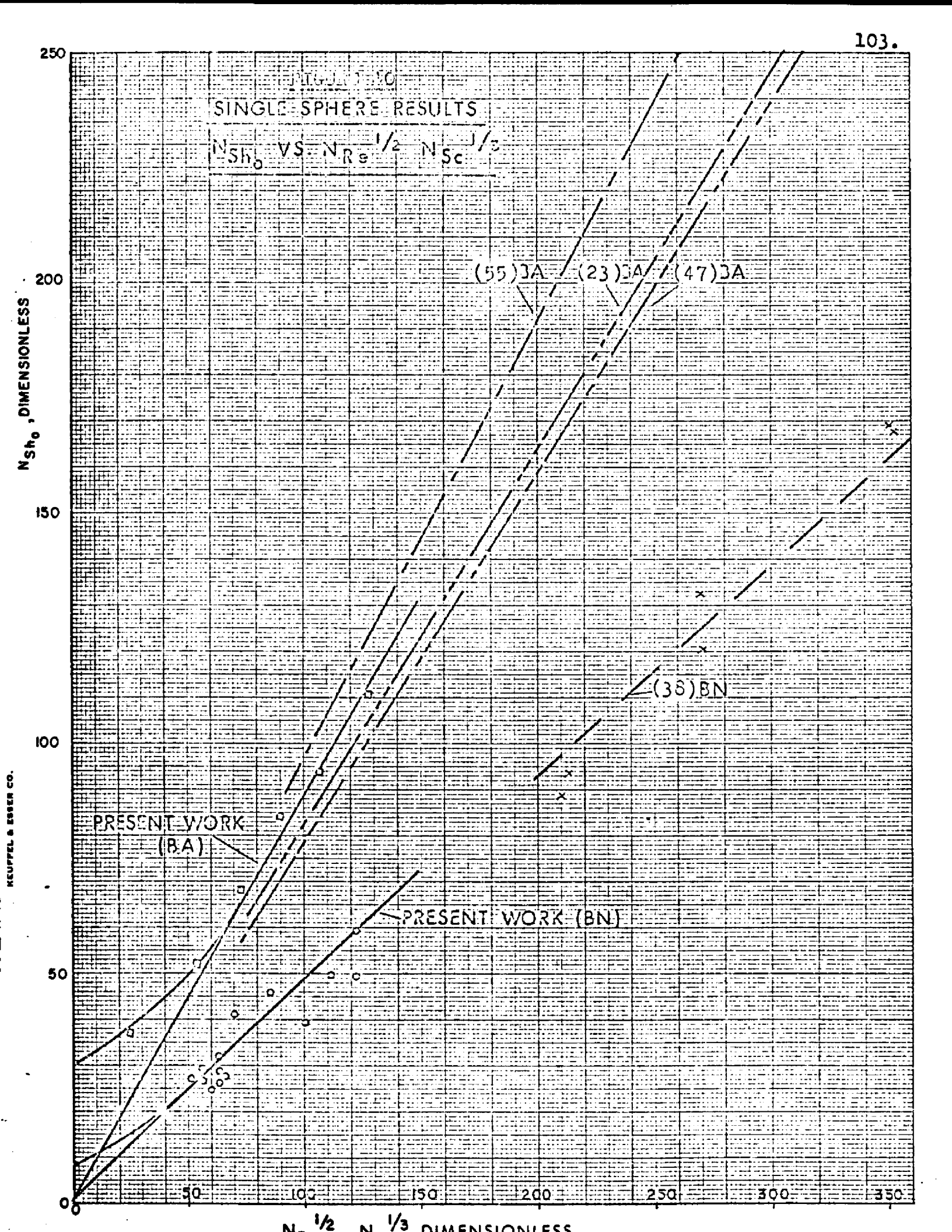
FIGURE 50
SINGLE SPHERE RESULTS
N_{Sh_o} VS $N_{Re}^{1/2}$ $N_{Sc}^{1/3}$
N_{Sh_o}, DIMENSIONLESS
$N_{Re}^{1/2}$ $N_{Sc}^{1/3}$ DIMENSIONLESS
(55)BA
(23)BA
(47)BA
(38)BN
PRESENT WORK (BA)
PRESENT WORK (BN)
0
50
100
150
200
250
300
350
KEUFFEL & ESSER CO.

FIGURE 41 - SINGLE SPHERE RESULTS - Sh_o VS. Pe

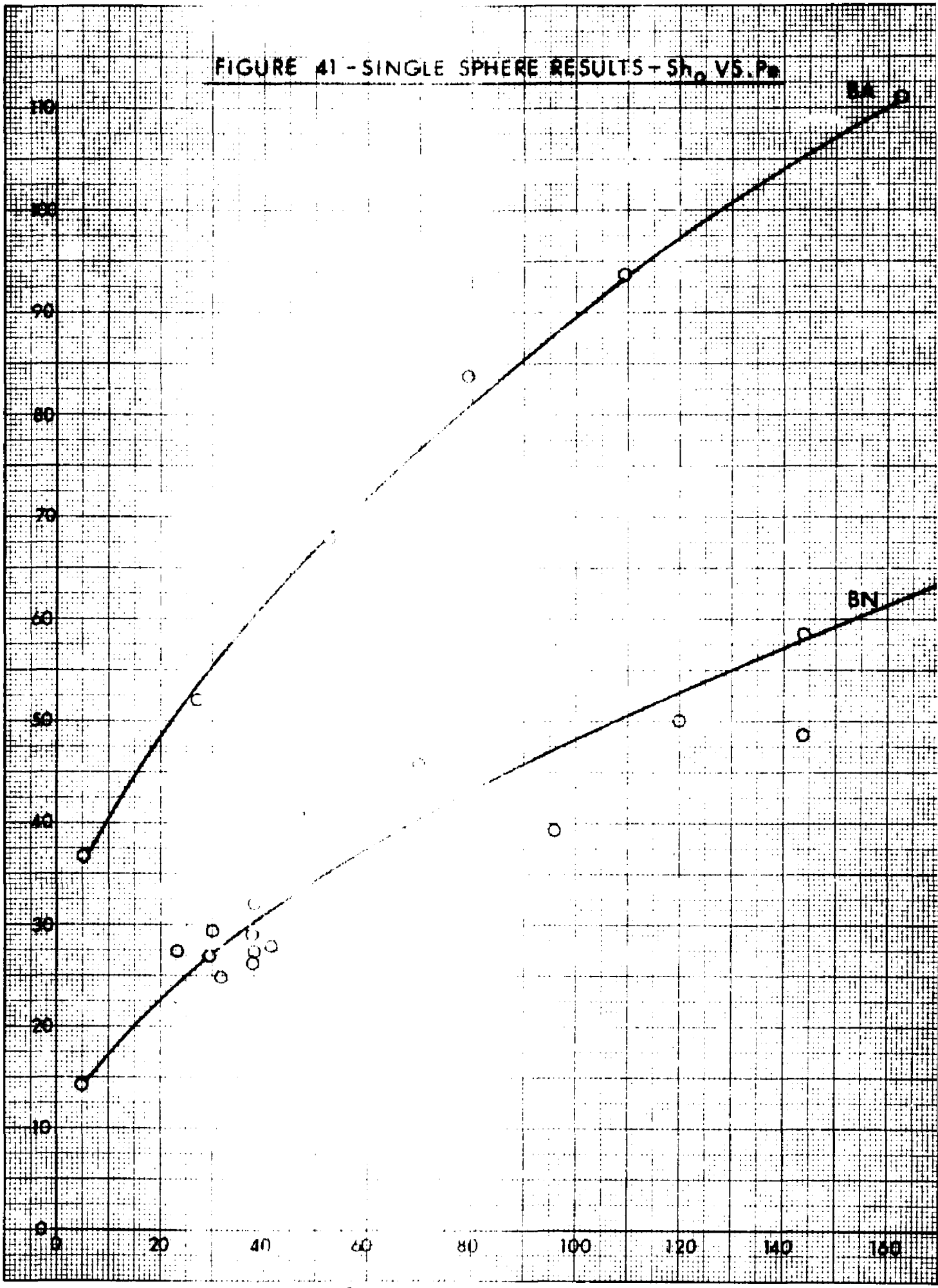

K+E 10 X 10 TO THE CENTIMETER 46 1513
16 X 25 CM. MADE IN U.S.A.
KEUFFEL & ESSER CO.

transfer coefficients than systems in which the driving force is small. This has been shown based on film, boundary layer, and penetration theories. Thus, for two materials such as benzoic acid and beta naphthol, when mass transfer coefficients to water are being measured, the material having the larger equilibrium solubility, and hence the larger driving force, should have a lower mass transfer coefficient than the other material. Under the conditions of the present investigation, benzoic acid had an equilibrium solubility of approximately five times that of beta naphthol. Therefore, due to driving force effects alone, one would expect benzoic acid to have a lower mass transfer coefficient than beta naphthol. Calculations, based on film theory, show that the mass transfer coefficient for benzoic acid should be 98.7% of that for beta naphthol(see Appendix I). These calculations were made, taking into account only the different concentration driving force; all other factors were kept constant. It was observed however, that benzoic acid exhibited larger Sherwood numbers than betanaphthol. Thus, the experimental differences cannot be due to flux effects.

Steele and Geankoplis[53] also found that the j-factor (which automatically compensates for differences in Schmidt number) was appreciably greater for benzoic acid than for betanaphthol. Since these authors worked only at high Reynolds numbers, natural convection was eliminated as a possible cause for this difference. Therefore, they experimentally investigated the effect of differences in driving force. By varying the concentration of the fluid they were able to vary the driving force or flux in their experiments. Their results confirm the theoretical predictions, based on film theory, that a higher flux will lower the

mass transfer coefficient and not raise it. Hence, Steele and Geankoplis concluded that differences in driving force cannot explain the observed differences in mass transfer rate for the benzoic acid and beta naphtholsystems.

Natural convection effects offer another possible explanation for the observed difference in mass transfer coefficients for these two systems. The Grashof number for the benzoic acid-water system is from 4 to 5 times greater than that for the beta naphthol water system, in the temperature range of this work. Thus, the natural convection contribution to the mass transfer process should be more important with the benzoic acid-water system than with the beta naphthol water system.

However, the existing natural convection correlations (see reference 54) give values of Sh for both systems, at zero Reynolds number which are greater than the overall Sherwood numbers found in the present study at finite Reynolds numbers. For example, according to Appendix B, the Sherwood number at zero Reynolds number for the benzoic acid system is approximately 50, whereas present results indicate a value closer to 30. Similarly, for the beta naphthol system the Sherwood number based on natural convection is calculated as 36, whereas present results indicate a value closer to 8. Thus, even though present correlations predict greater natural convection mass transfer coefficients for benzoic acid than for beta naphthol, they do not accurately predict what these values actually are. Hence, one must conclude that, although natural convection effects may cause the observed differences in mass transfer coefficients

for these systems, presently accepted correlations for natural convection do not adequately predict Sh numbers at zero Re and no final decision can be made as to the validity of natural convection as cause of the observed Sh number differences. Furthermore, at higher Reynolds numbers where forced convection effects overshadow any natural convection effects there should be no difference in the Sherwood numbers. However, both the present work and the work of Steele and Geankoplis at very high Re (600 - 140,000) show that the Sherwood numbers do not become identical at the higher Reynolds numbers.

Schmidt number effects may also be used as a possible explanation for the observed differences in the Sherwood numbers obtained for these systems. However, theoretical and experimental investigations indicate that mass transfer coefficients are proportional to $Sc^{1/3}$. Plots of present results against $Re^{1/2}$ $Sc^{1/3}$ and $Pe^{1/3}$ $(Re^{1/3}\ Sc^{1/3})$, do not cause the observed differences to disappear. Therefore, one must conclude that Schmidt number differences cannot explain the observed differences between the Sherwood numbers for benzoic acid and those for beta naphthol.

Since neither flux effects, natural convection effects nor Schmidt number effects can offer an adequate explanation for the difference between the overall mass transfer coeffcients found for the two systems it may be that the physical properties of either one or both of the systems, $\mathcal{D}$ or C^*, is in error. This possibility, of course, cannot be confirmed since the physical properties used in the calculations are believed to be the most accurate, presently available.

Recently, it has come to the attention of the author that this difference may be due to differences in the crystalline nature of the cast particles of these materials. This hypothesis is fully explained in the addendum (page 174).

In Figure 42 the overall mass transfer results are plotted on logarithmic paper as Sh_o vs. Pe. It was found that a line of slope 1/3 could adequately represent the present data, which is in agreement with that predicted by Levich[34] and Pfeffer[40] for low particle Reynolds number flow. The equations obtained from the faired data of the figure are

$$Sh_o = 1.56\ Pe^{1/3} \qquad \text{Benzoic acid-water} \qquad (56)$$

and

$$Sh_o = 0.75\ Pe^{1/3} \qquad \text{Beta naphthol - water} \qquad (57)$$

Multiparticle System Studies

Axial Configurations

The axial configurations of particles studied in this investigation are shown in Figure 43. As can be seen from the figure, two series of runs were made with two spheres (doublets) and two series of runs were made with three spheres (triplets). The overall mass transfer results of these axial studies as well as the important run data are presented in Table VIII.

Typical local mass transfer profiles obtained for series II, III, V and VI using both benzoic acid and beta naphthol test spheres are presented in Figures 44

FIGURE 42

SINGLE SPHERE RESULTS - N_{sh_o} VS. N_{pe}

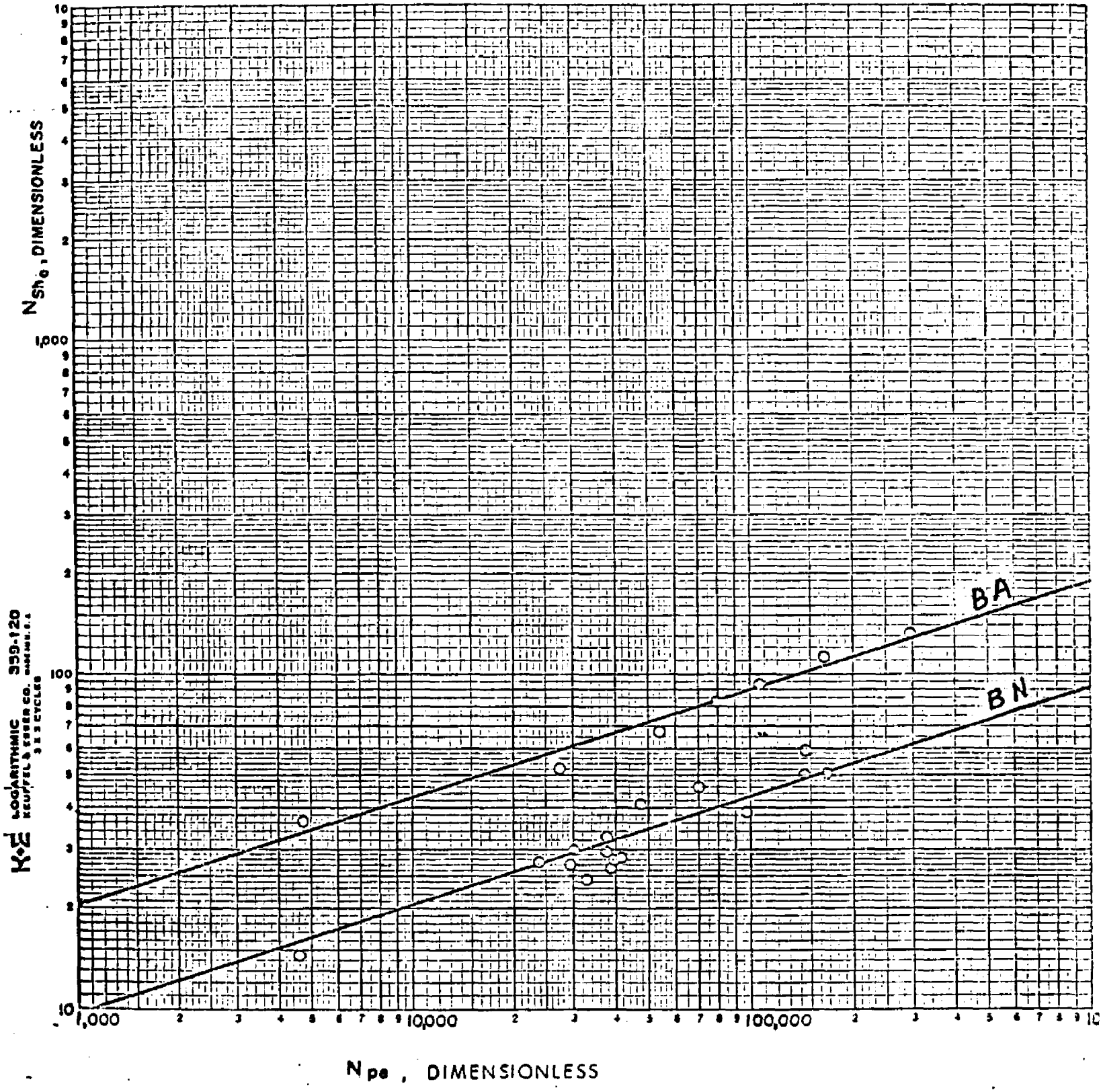

FIGURE 43

AXIAL CONFIGURATIONS USED

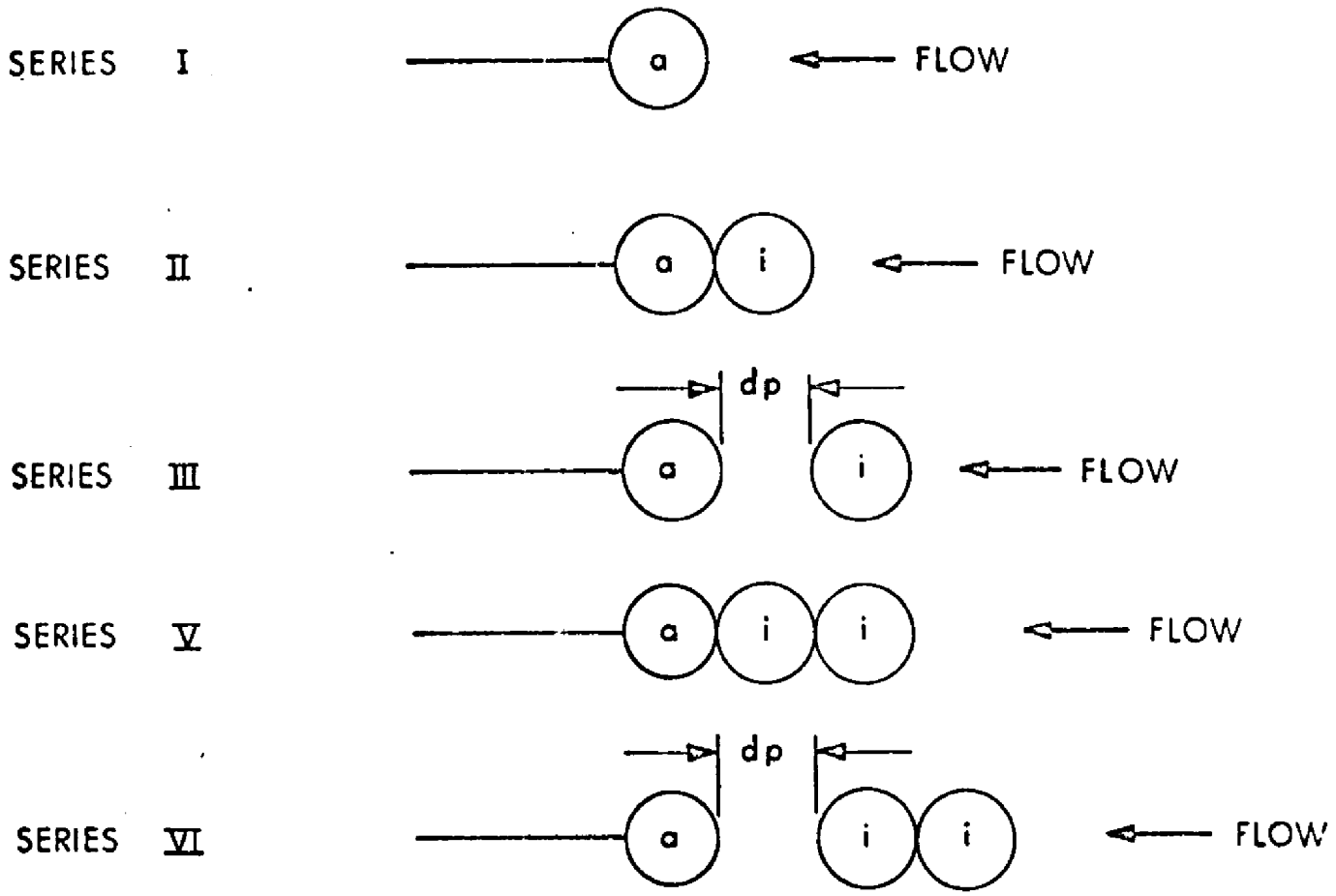

dp = PARTICLE DIAMETER, 1/2"

i = INERT SPHERE

a = ACTIVE SPHERE

TABLE VIII. Overall Mass Transfer Results - Axial Studies

Run Number	Solute	Run Time	Weight Loss	Flow Rate	Run Temperature	Solute Solubility	Schmidt Number	Initial Surface Avg. Radius	Final Surface Avg. Radius	Reynolds Numbers	Sh_o
		Hours	Grams	GPM	°C.	Grams / 1000 Grams		Inches	Inches		
II-1	BN	71.0	.0873	.0757	23.5	0.68	848.3	.2515	.2471	5.2	11.58
II-2	BN	101.2	.1530	.0756	24.84	0.725	803.2	.2541	.2447	5.35	13.04
II-3	BN	47.2	.1318	.406	24.95	0.725	794.7	.2539	.2473	28.5	23.78
II-4	BN	43.3	.1587	.789	24.83	0.725	803.3	.2566	.2472	55.55	31.31
II-5	BN	24.2	.1173	1.608	24.94	0.73	794.9	.2557	.2496	113.8	40.65
II-6	BA	3.0	.1094	2.425	25.77	3.41	920.0	.2502	.2447	171.3	78.74
II-7	BA	3.0	.1008	1.608	25.50	3.39	935.0	.2562	.2515	116.05	72.06
II-8	BA	3.0	.0858	1.174	25.50	3.39	935.0	.2569	.2529	85.1	61.08
II-9	BA	3.5	.0901	0.789	25.50	3.39	935.0	.2559	.2513	56.9	55.25
II-10	BA	3.8	.0775	0.406	25.90	3.42	910.0	.2557	.2514	29.45	42.44
II-11	BA	6.2	.1128	0.0766	26.90	3.52	860.0	.2564	.2493	5.65	35.60
II-12	BA	6.1	.1009	0.0758	24.75	3.31	970.0	.2569	.2508	5.45	36.96
II-14	BA	4.0	.1348	2.432	25.52	3.39	933.0	.2458	.2368	166.55	75.80
III-1	BA	3.7	.1515	2.425	25.80	3.41	910.0	.2513	.2417	170.8	88.05
III-2	BA	2.6	.0911	1.608	25.80	3.41	910.0	.2485	.2443	113.15	75.25
III-3	BA	2.6	.0698	0.791	25.71	3.41	925.0	.2513	.2476	56.25	57.81
III-4	BN	25.8	.1516	1.998	25.80	0.74	758.0	.2536	.2454	142.35	48.50
III-5	BA	3.0	.1192	2.432	25.38	3.37	940.0	.2521	.2430	170.3	87.97
III-6	BA	3.0	.0883	1.601	24.71	3.31	972.0	.2453	.2378	107.75	69.28
III-7	BA	19.3	.2772	.0758	24.27	3.27	1000.0	.2446	.2243	4.95	35.90
III-8	BA	3.1	.0813	.791	24.33	3.27	1000.0	.2511	.2447	54.2	61.68
III-9	BA	20.0	.2795	.0768	24.04	3.25	1020.0	.2454	.2242	4.95	35.82
III-10	BN	50.0	.1347	.407	24.44	0.71	815.0	.2545	.2455	28.2	23.79

TABLE VIII. Continued

Run Number	Solute	Run Time	Weight Loss	Flow Rate	Run Temperature	Solute Solubility	Schmidt Number	Initial Surface Avg. Radius	Final Surface Avg. Radius	Reynolds Numbers	Sh_o
		Hours	Grams	GPM	°C.	$\frac{\text{Grams}}{1000 \text{ Grams}}$		Inches	Inches		
III-11	BN	18.7	.0556	1.177	24.77	0.725	800.0	.2459	.2412	80.0	30.83
III-12	BN	5.9	.0375	1.998	24.92	0.73	796.0	.2533	.2504	140.9	53.60
III-13	BN	53.5	.0895	.0768	23.98	0.74	820.0	.2530	.2472	5.25	14.13
III-16	BN	6.0	.0413	2.432	25.37	0.74	788.0	.2578	.2553	176.5	56.07
V-1	BA	24.5	.3483	.0768	25.32	3.37	940.0	.2486	.2211	5.1	33.49
V-2	BA	4.1	.0889	.791	24.09	3.25	1010.0	.2508	.2461	54.0	51.70
V-3	BA	3.5	.1031	1.511	23.54	3.20	1035.0	.2602	.2543	112.4	69.71
V-4	BA	3.0	.1045	2.431	23.84	3.23	1020.0	.2599	.2537	171.05	81.59
V-5	BN	24.6	.0639	0.407	24.51	0.71	810.0	.2538	.2496	28.45	22.66
V-6	BN	23.5	.0902	1.997	24.60	0.72	810.0	.2455	.2393	134.55	34.40
V-7	BN	24.4	.0882	1.177	24.57	0.72	810.0	.2508	.2449	80.1	31.58
V-9	BN	6.9	.0341	2.432	25.40	0.74	785.0	.2555	.2524	174.8	46.62
VI-1	BN	20.1	.0939	1.177	24.99	0.73	794.0	.2532	.2472	82.6	39.56
VI-2	BN	22.0	.1230	1.997	24.84	0.73	800.0	.2536	.2456	139.35	47.62
VI-3	BN	51.7	.1274	0.407	24.54	0.72	805.0	.2516	.2433	28.05	21.50
VI-4	BA	3.0	.1066	2.432	25.03	3.34	950.0	.2474	.2405	166.55	81.58
VI-5	BA	3.0	.1179	1.612	25.25	3.45	895.0	.2614	.2540	119.85	78.99
VI-6	BA	2.9	.0771	0.791	25.65	3.40	925.0	.2584	.2531	57.6	55.90
VI-7	BA	4.0	.0764	0.0768	25.17	3.45	901.0	.2602	.2561	5.7	38.35

through 51 as Sh_L versus the angle θ from the forward stagnation point with particle Reynolds number as a parameter. Overall mass transfer results for these series are presented in Figures 52 through 55 as Sh_o versus Peclet number.

From the local mass transfer profile figures, the following observations can be made. At points of contact between the spheres a minimum mass transfer rate is obtained. As the separation between spheres increases the spheres have a smaller effect upon one another. Thus, for two particles in direct axial contact, as in series II with the active sphere behind the inert one, a minimum transfer rate at the forward stagnation point is found. The transfer rate then increases because of exposure to the flow of fluid and then decreases to a minimum again at the location of the separation ring. In the wake area the transfer rate again increases up to the rear stagnation point. If separation does not occur, a minimum transfer rate is observed at the rear stagnation point. The presence of the single inert sphere also has an effect on the location of the separation point.

With two inert spheres directly in front of the active sphere (all three touching), as in series V, an accentuation of the effects described above for doublets are obtained.

With increasing separation between active and inert spheres, as in series III and VI, the effect of the inert particle on the mass transfer in the forward flow area and at the forward stagnation point decreases. In fact, at sufficiently

FIGURE 44

LOCAL MASS TRANSFER PROFILES - SERIES II -

BENZOIC ACID RESULTS - N_{Sh_L} VS. θ

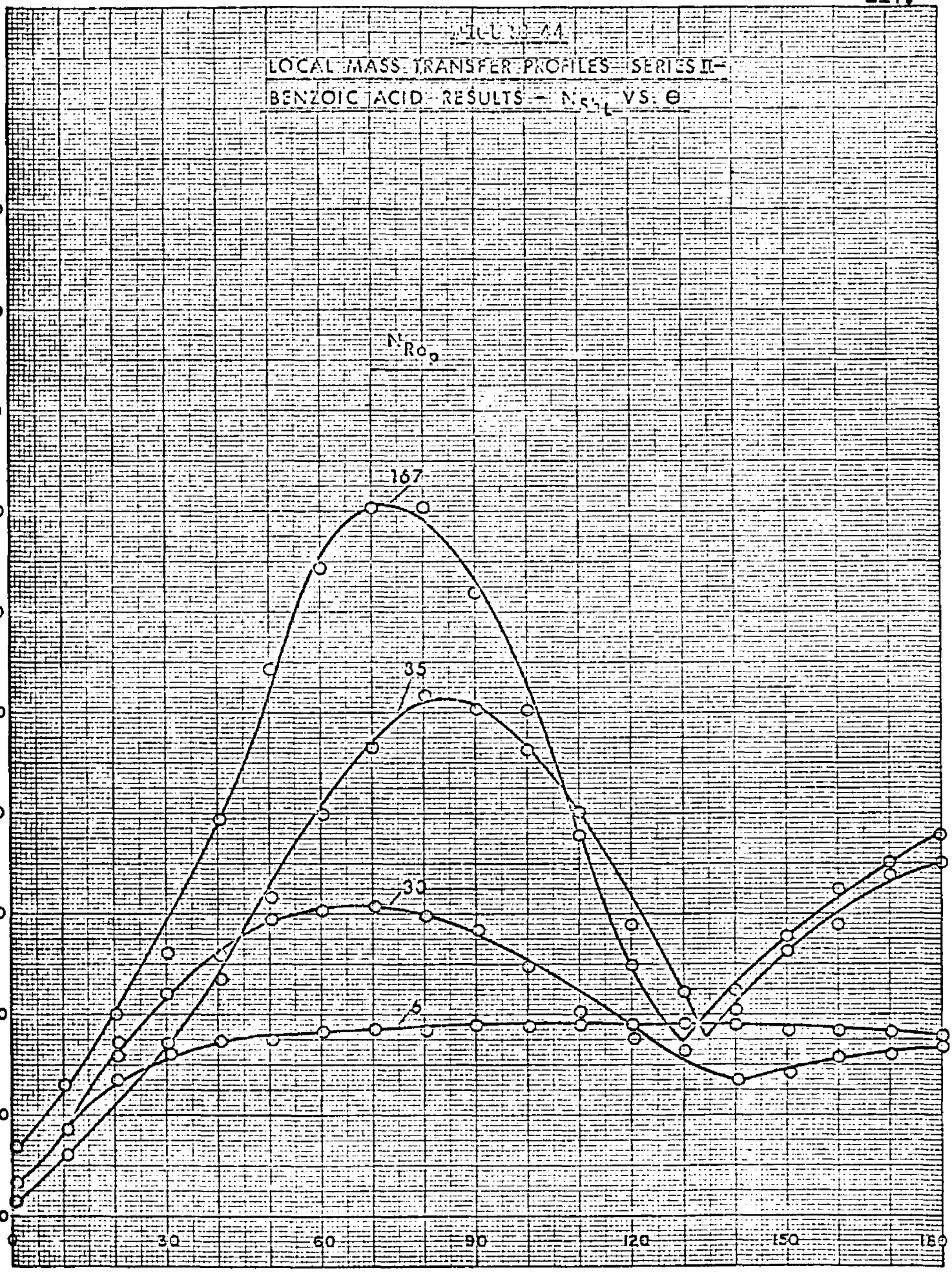

K&E 10 X 10 TO THE CENTIMETER 46 1513
18 X 25 CM. KEUFFEL & ESSER CO. MADE IN U.S.A.

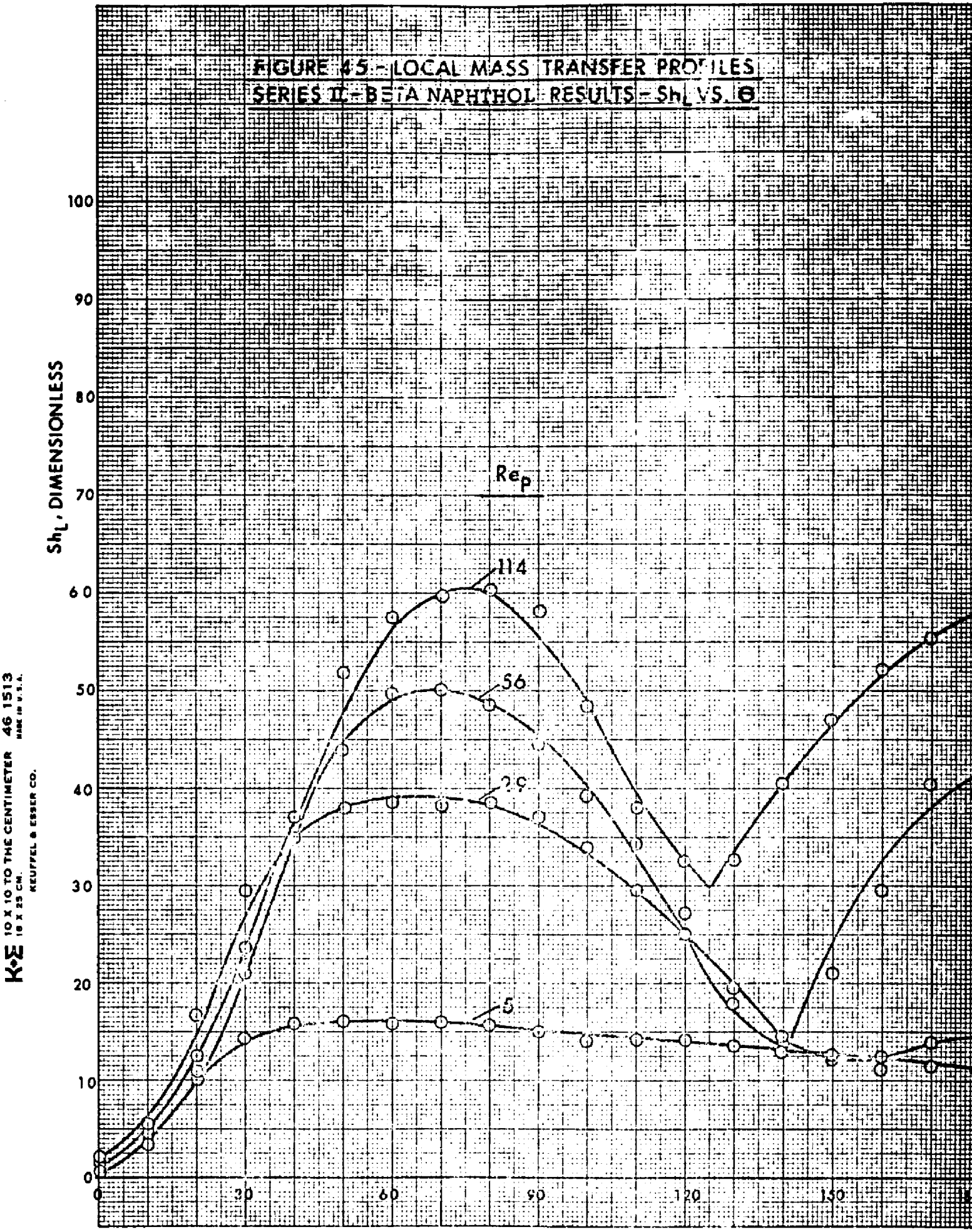
FIGURE 45 - LOCAL MASS TRANSFER PROFILES
SERIES II - BETA NAPHTHOL RESULTS - Sh_L VS. θ
Sh_L, DIMENSIONLESS
Re_p
114
56
29
5
0
10
20
30
40
50
60
70
80
90
100
30
60
90
120
150
θ DEGREES FROM THE FORWARD STAGNATION POINT
K+E 10 X 10 TO THE CENTIMETER 46 1513
18 X 25 CM.
KEUFFEL & ESSER CO.

FIGURE 22

LOCAL SHERWOOD NUMBER PROFILES
SERIES III - BENZOIC ACID RESULTS - N_{Sh_L} VS. θ

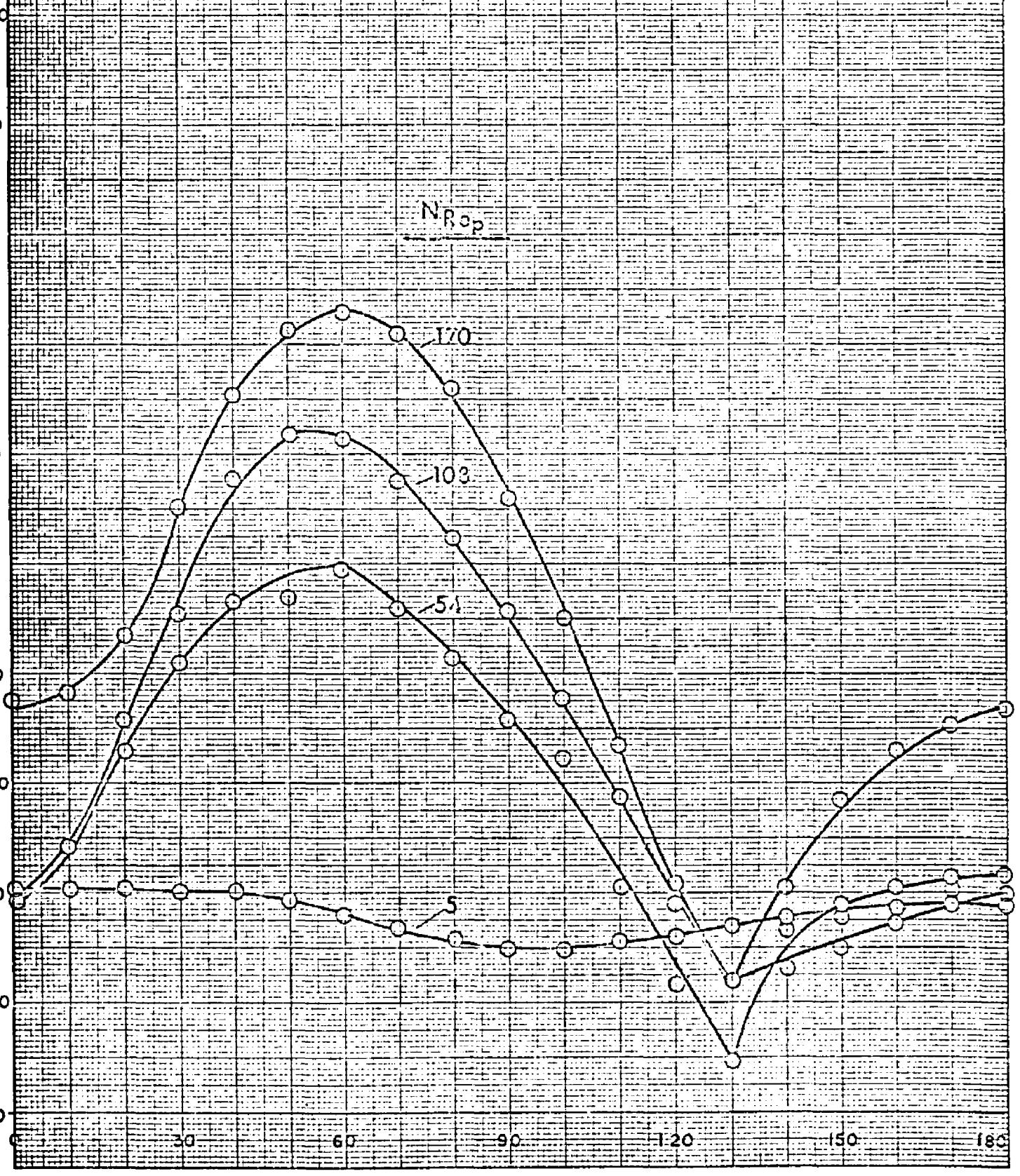

K+E 10 X 10 TO THE CENTIMETER 46 1513
18 X 25 CM.
KEUFFEL & ESSER CO.

FIGURE 47 - LOCAL SHERWOOD NUMBER PROFILES
SERIES III - BETA NAPHTHOL RESULTS - Sh VS Θ

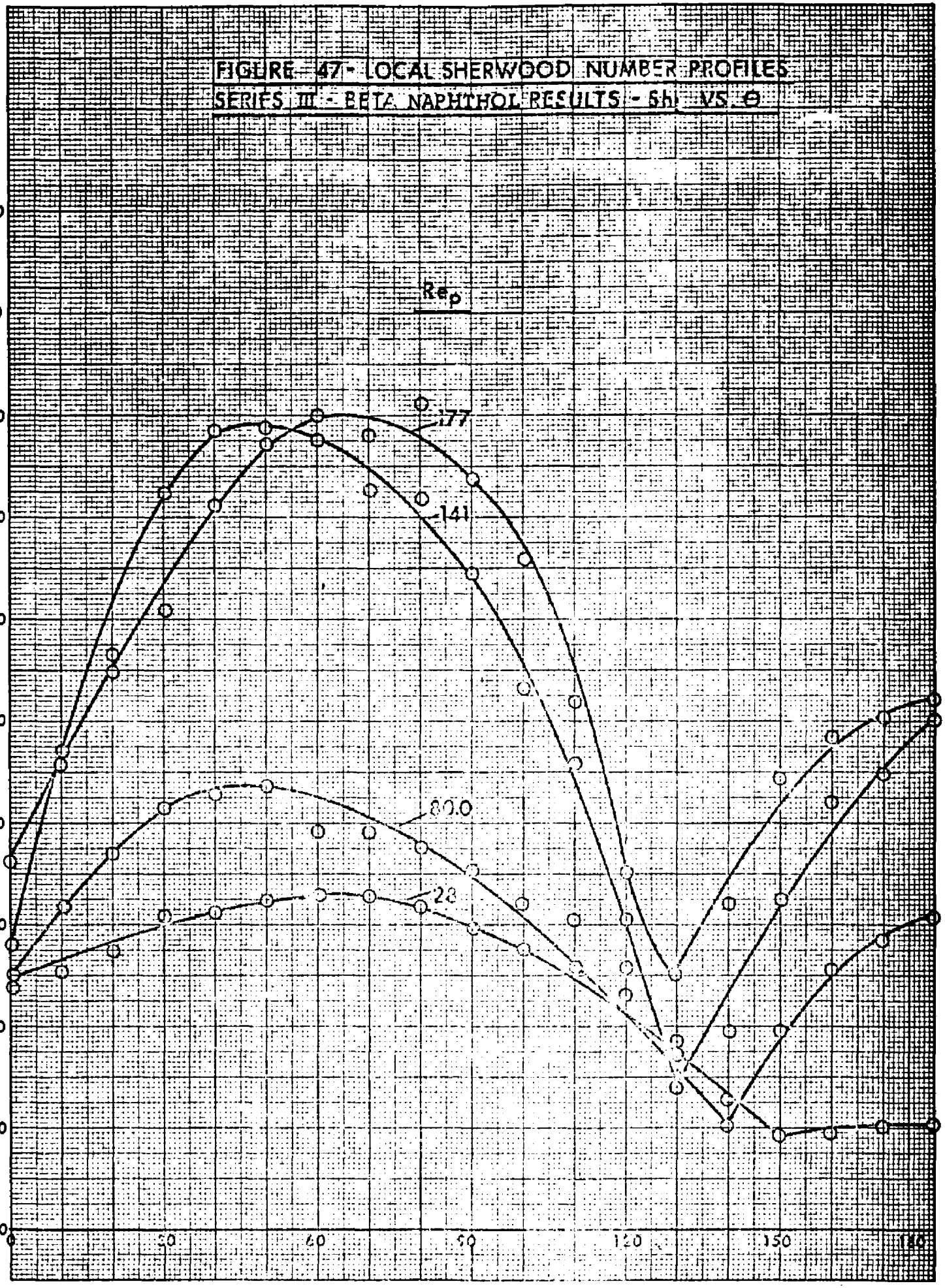

K+E 10 X 10 TO THE CENTIMETER 46 1513
18 X 25 CM.
KEUFFEL & ESSER CO.

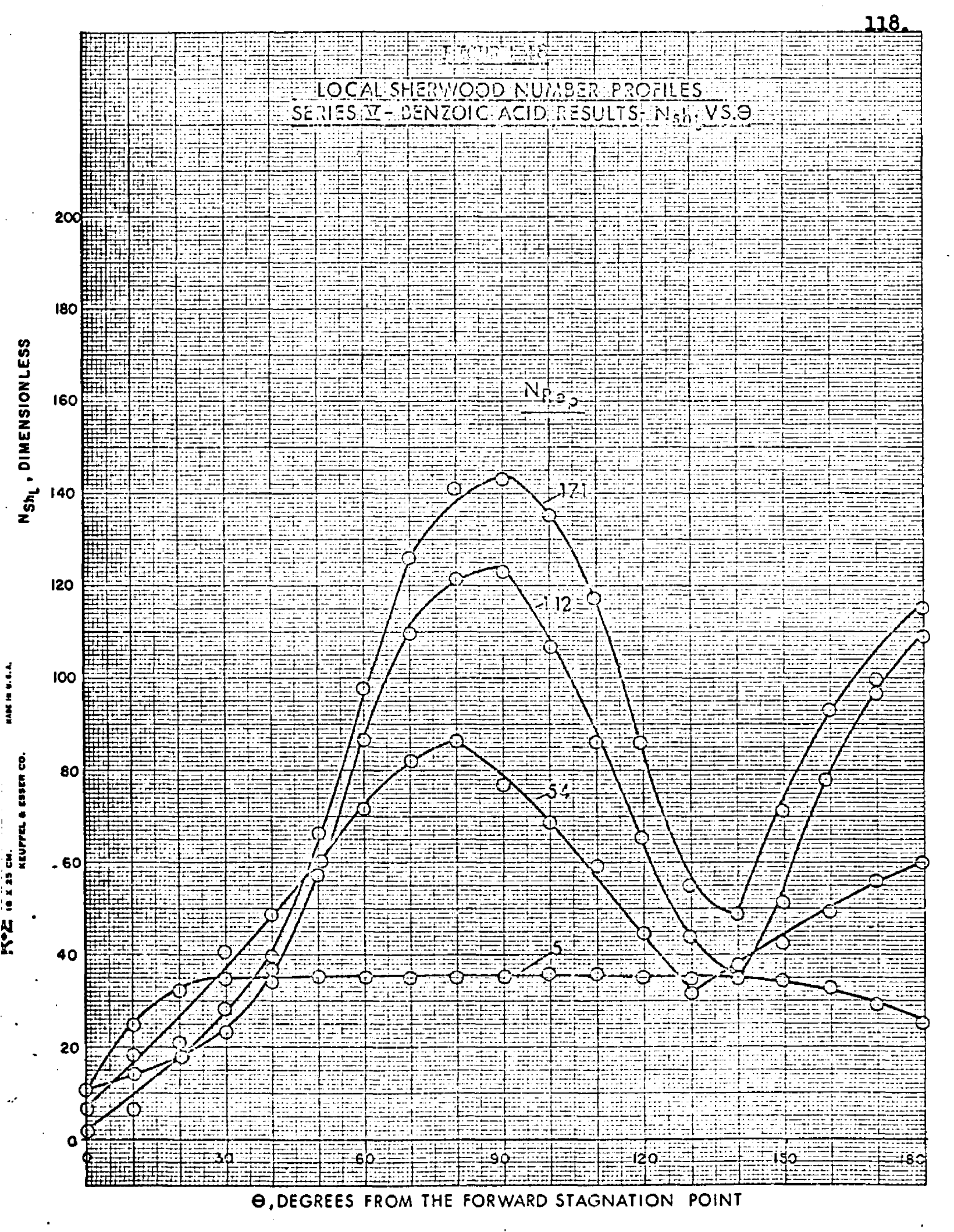
LOCAL SHERWOOD NUMBER PROFILES
SERIES V - BENZOIC ACID RESULTS - N_{Sh_L} VS. Θ
N_{Re_D}
171
112
54
5
N_{Sh_L}, DIMENSIONLESS
0
20
40
60
80
100
120
140
160
180
200
0
30
60
90
120
150
180
Θ, DEGREES FROM THE FORWARD STAGNATION POINT

FIGURE 49 LOCAL SHERWOOD NUMBER PROFILES
SERIES V - BETA NAPHTHOL RESULTS - Sh_θ VS θ

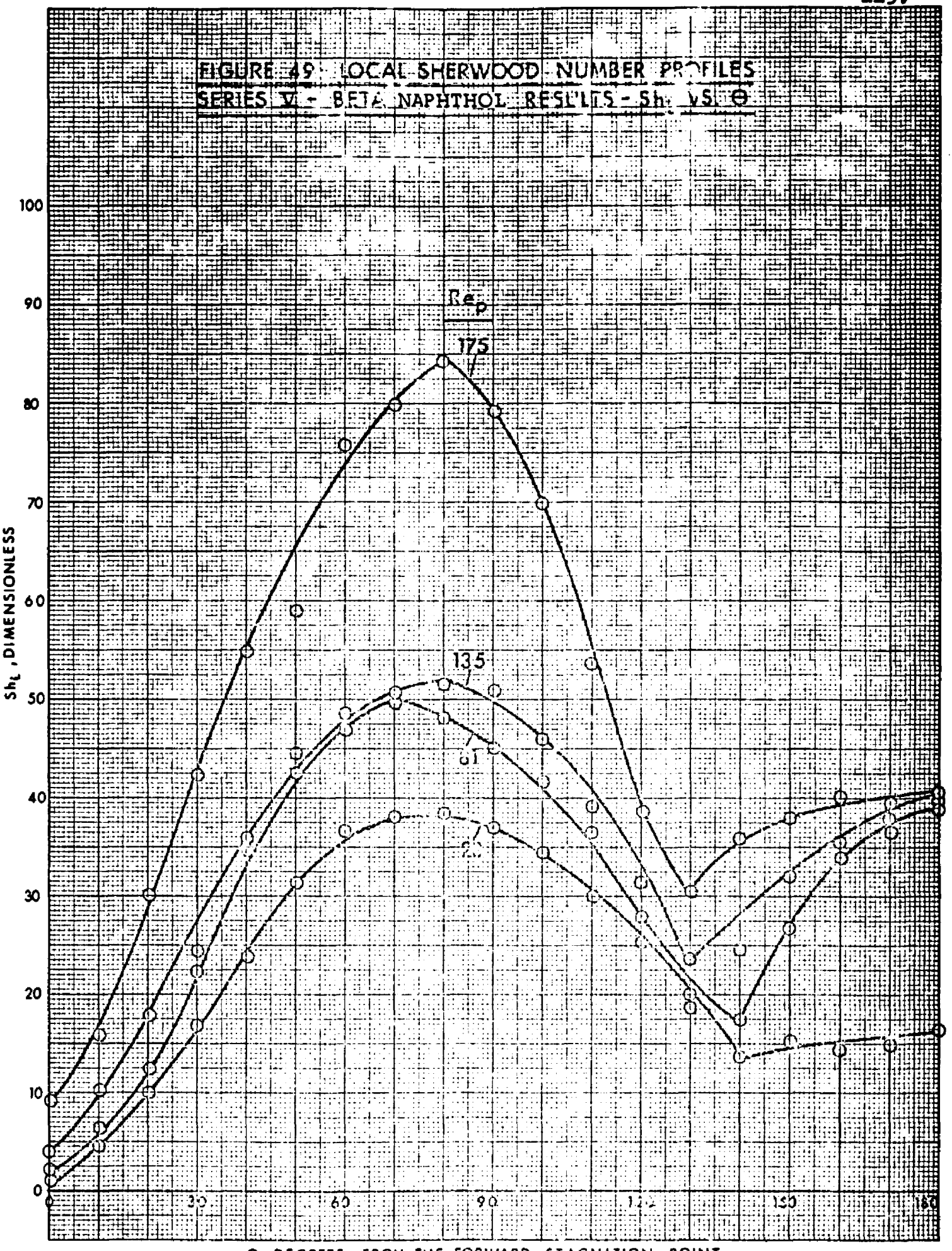

K+E 10 X 10 TO THE CENTIMETER 46 1513
18 X 25 CM. KEUFFEL & ESSER CO.

FIGURE 50

LOCAL SHERWOOD NUMBER PROFILES SERIES VI - BENZOIC ACID RESULTS N_{Sh_L} VS. θ

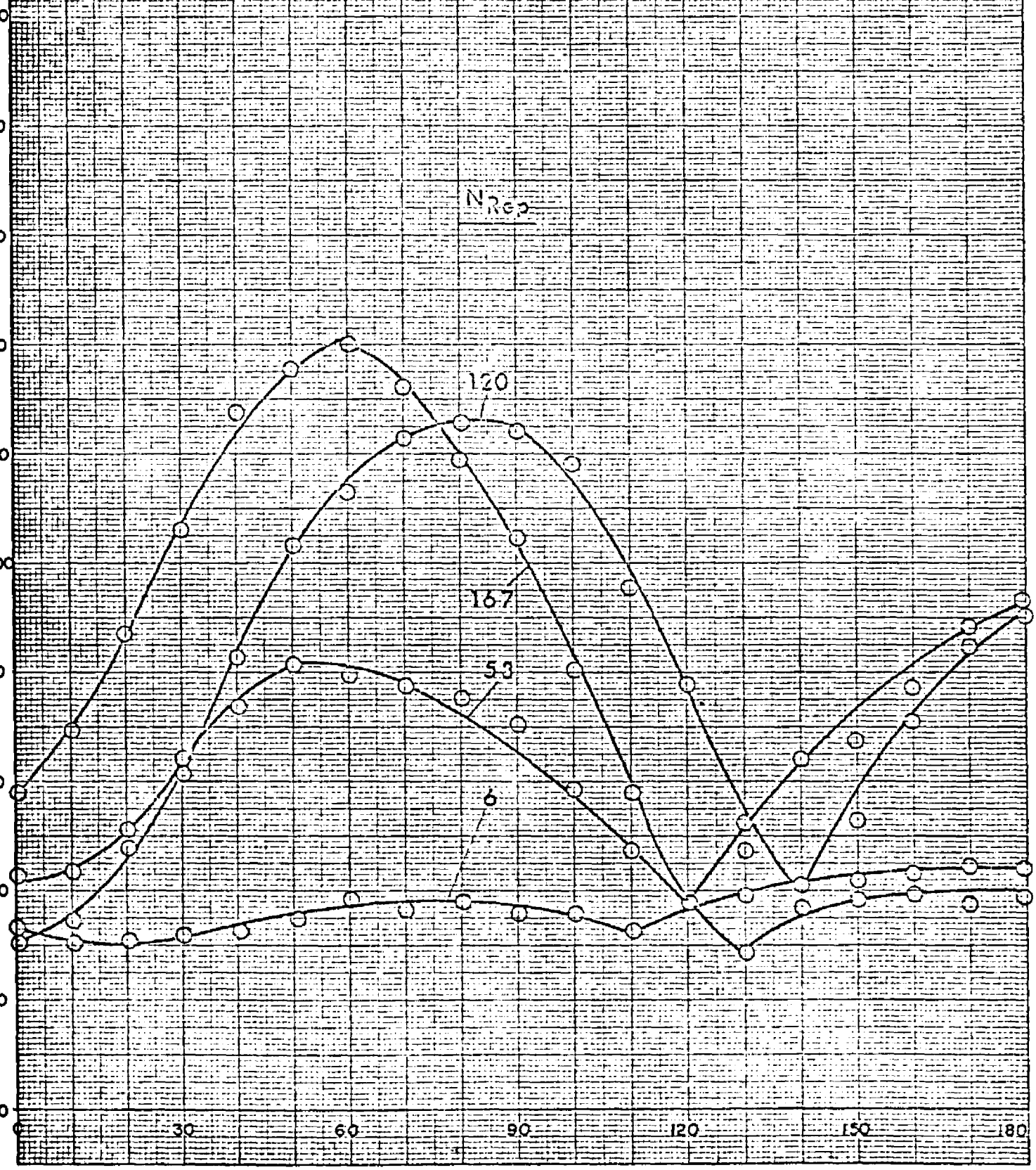

K&E 10 X 10 TO THE CENTIMETER 46 1513
18 X 25 CM. KEUFFEL & ESSER CO.

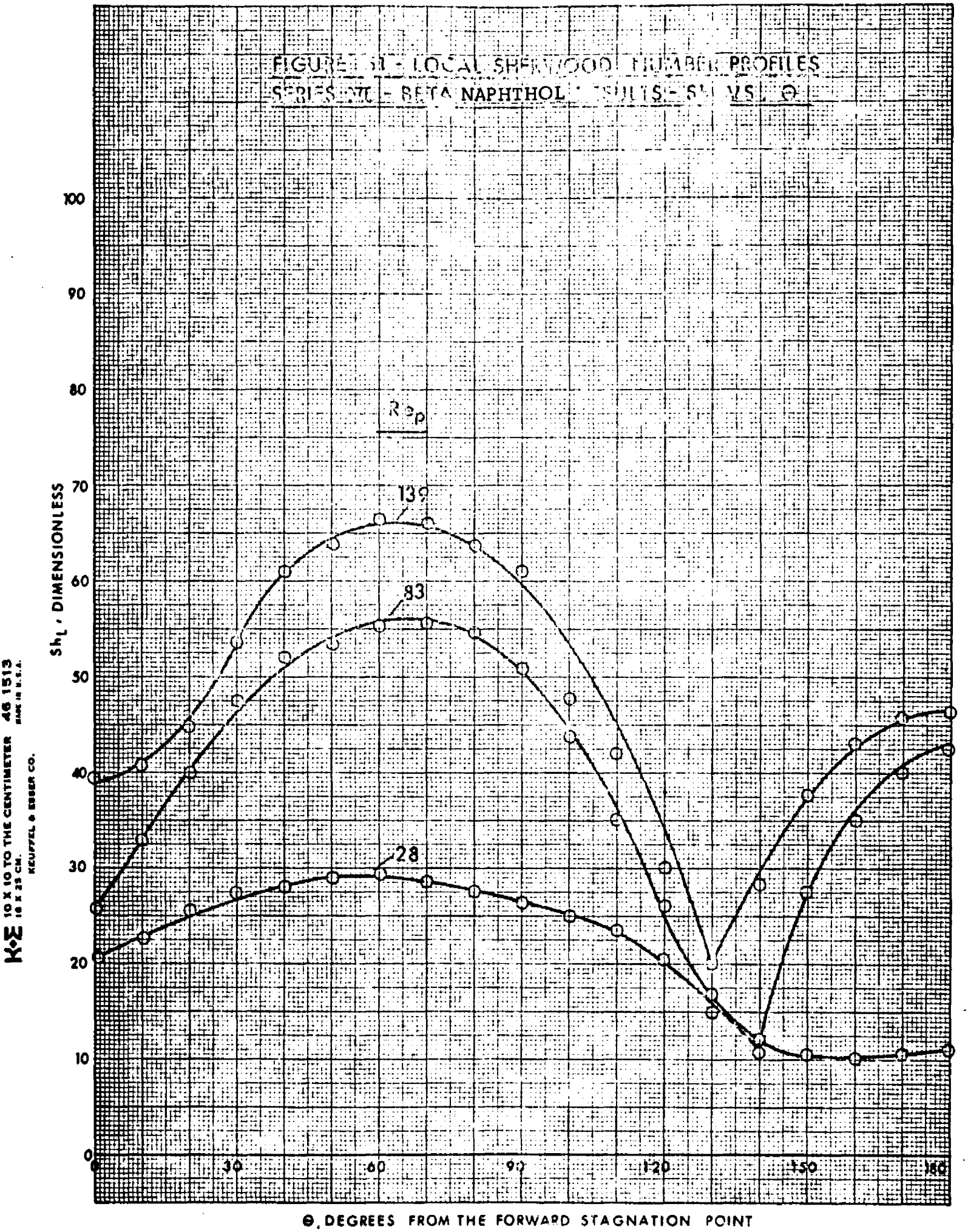
FIGURE 31 - LOCAL SHERWOOD NUMBER PROFILES
SERIES VII - BETA NAPHTHOL RESULTS - Sh VS. Θ
Re_p
139
83
28
Sh_L , DIMENSIONLESS
0
10
20
30
40
50
60
70
80
90
100
30
60
90
120
150
180
Θ, DEGREES FROM THE FORWARD STAGNATION POINT
K&E 10 X 10 TO THE CENTIMETER 46 1513
16 X 25 CM.
KEUFFEL & ESSER CO.

FIGURE 42 - SERIES II RESULTS - Sh_o V.S. Pe

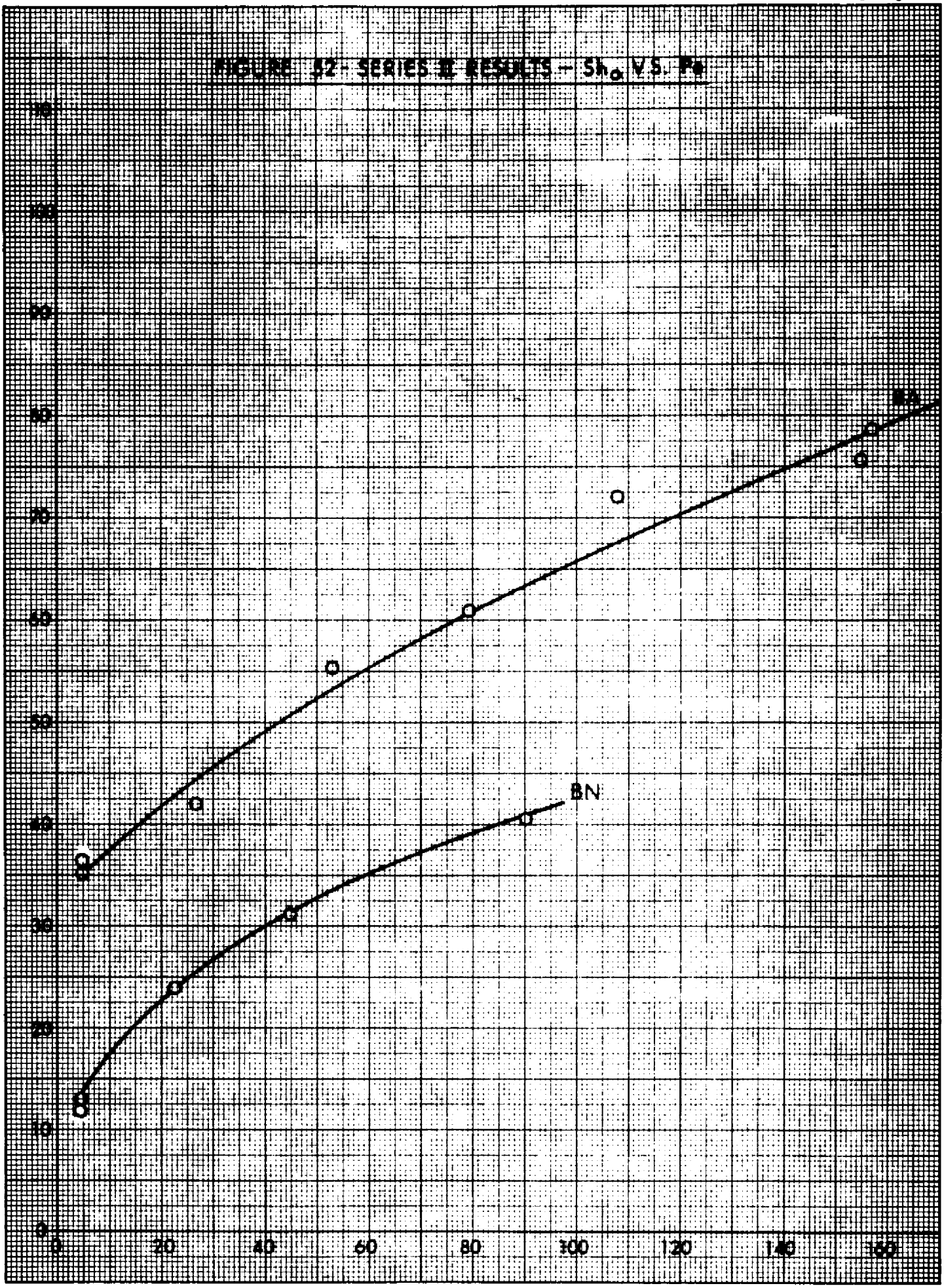

K&E 10 X 10 TO THE CENTIMETER 46 1513
18 X 25 CM. MADE IN U.S.A.
KEUFFEL & ESSER CO.

FIGURE 53 - SERIES III RESULTS - Sh_o VS. Pe

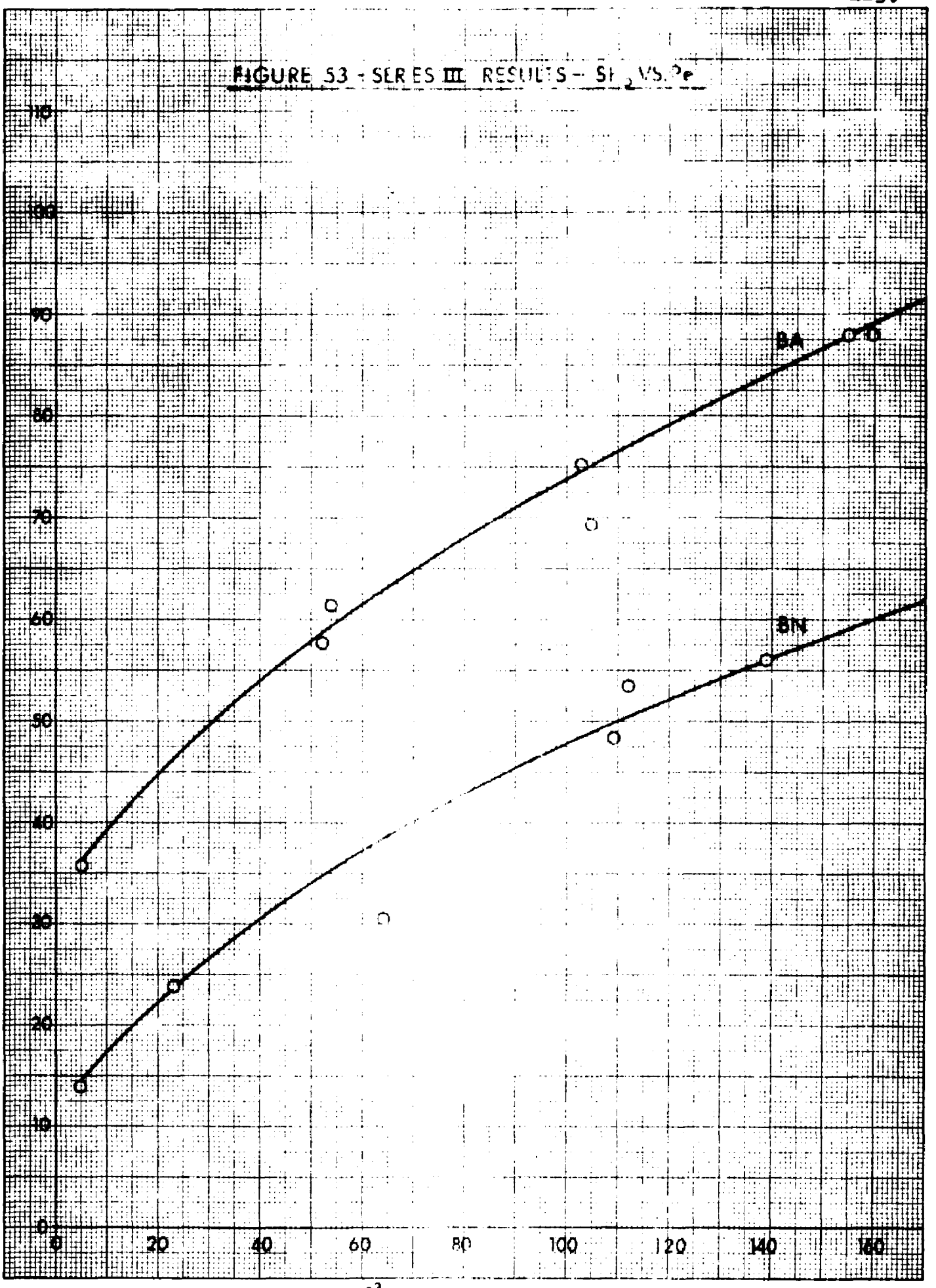

K+E 10 X 10 TO THE CENTIMETER 46 1513
18 X 25 CM
KEUFFEL & ESSER CO.

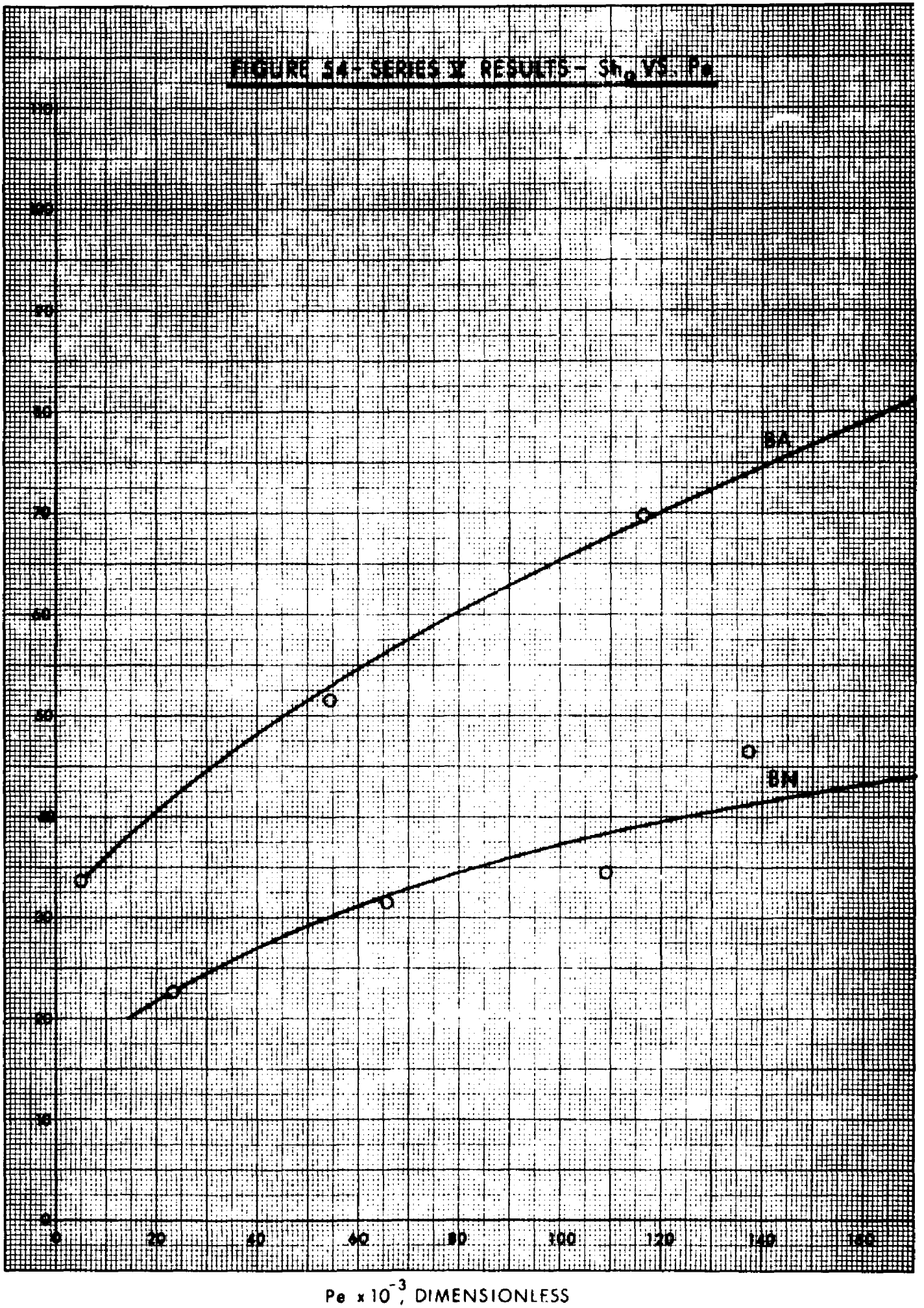

K•E 10 X 10 TO THE CENTIMETER 46 1513
18 X 25 CM. MADE IN U.S.A.
KEUFFEL & ESSER CO.

FIGURE 55 - SERIES XI RESULTS - Sh_o VS. Pe

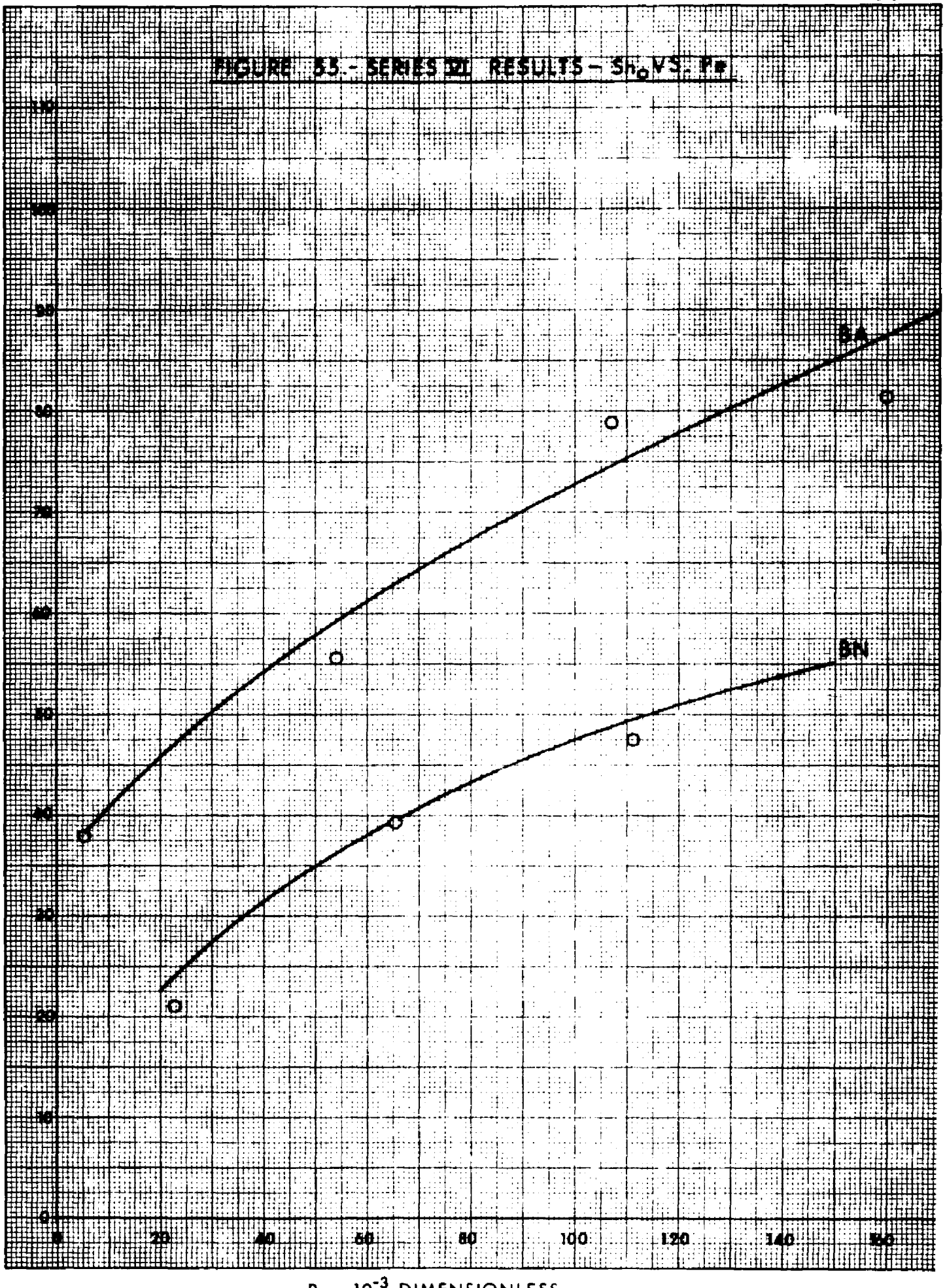

Sh_o, DIMENSIONLESS

$Pe \times 10^{-3}$, DIMENSIONLESS

K•E 10 X 10 TO THE CENTIMETER 46 1513
18 X 25 CM. MADE IN U.S.A.
KEUFFEL & ESSER CO.

large separation the active sphere should not be affected at all by the presence of the inert spheres. The increased separation between active and inert spheres, characterized by series III and VI, also shows a decreasing effect upon the location of the separation ring and hence upon the contribution of the wake region to the total transfer rate.

In order to compare the local mass transfer results, Figures 56 and 57 were prepared. In these figures the local transfer profiles, Sh_L vs. θ , obtained for benzoic acid runs at a particle Reynolds number of approximately 75 in series I, II, and III and in series I, V, and VI are presented. A study of these figures shows that the variation of the local coefficients agrees with the discussion presented above.

The effects of the inert spheres on the overall mass transfer rate are similar to those found for the local mass transfer rates. For example, the overall mass transfer coefficient for the series II runs is less than that found for the single sphere runs; whereas, the overall coefficients of series III are less than those obtained for a single sphere but greater than those obtained for series II. Similarly, the overall transfer rates of series V are much less than those found for series I and less than those found for series II; whereas, the overall results of series VI are greater than those of series V, less than those of series III, and even less than those of series I.

The overall mass transfer coefficients obtained for the benzoic acid and

FIGURE 56

COMPARISON OF LOCAL MASS TRANSFER PROFILES

SERIES I, II, AND III – BENZOIC ACID – $N_{Re} \doteq 75$ – N_{Sc} – V.S. θ

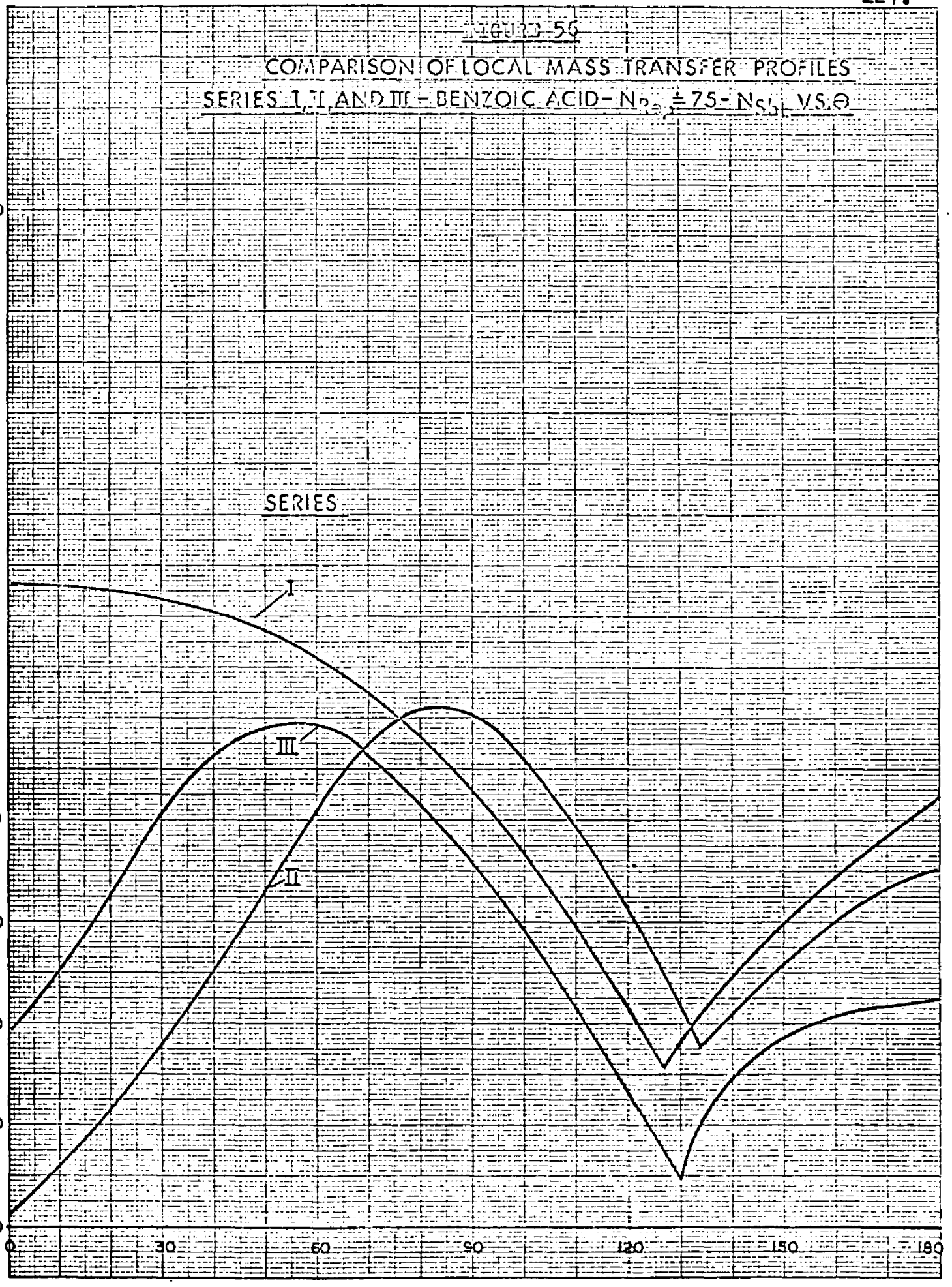

FIGURE 57

COMPARISON OF LOCAL MASS TRANSFER PROFILES

SERIES I, V AND VI - BENZOIC ACID - $N_{Re_p} = 75$ - N_{Sh_L} VS. Θ

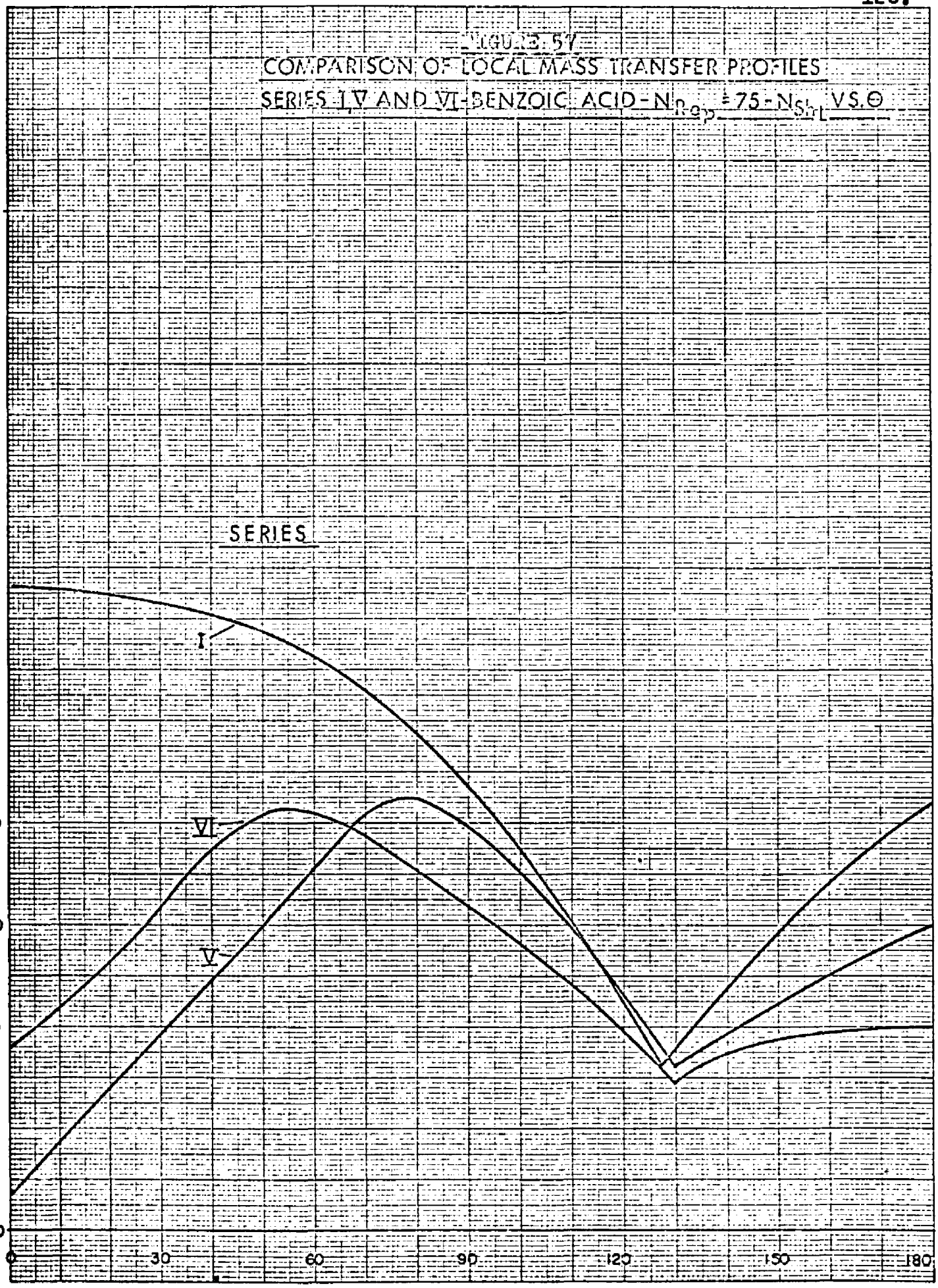

K·E 10 X 10 TO THE CENTIMETER 46 1513
MADE IN U.S.A.
10 X 25 CM.
KEUFFEL & ESSER CO.

betanaphtholruns of series I, II, and III are compared in Figure 58 by plotting Sh_o vs. Pe. This figure shows that at low Peclet numbers, the number of inert particles has a small effect on the overall mass transfer process; whereas, increasing Pe leads to increasing dependence of the overall transfer rate on the number of particles present. That the curves obtained for both systems studied for the same number of inert particles are different is again an indication of the effect discussed earlier. This figure also shows that the single sphere gives the largest overall transfer rate while the doublet in contact gives the smallest, and the overall Sh numbers are seen to decrease in the order of series I, III, and II. This is in agreement with the earlier discussion.

As another comparison, Figure 59 shows the overall transfer results obtained for series I, V, and VI. The order of decreasing overall mass transfer rate is seen to be series I, VI, and V. The decreasing effect of the number of inert particles with decreasing Pe is also seen and the difference in Sh which is also dependent on Pe is noted by comparing the results for benzoic acid and betanaphtholat the same particle configuration.

Equilateral Triangular Configurations

The two equilateral triangular geometries (series VIII and IX) used in this investigation are shown in Figure 60. The overall equilateral triangular array mass transfer results, obtained in this study, along with the pertinent run data are presented in Table IX.

FIGURE 58

SERIES I, II AND III

COMPARISON OF OVERALL MASS TRANSFER RESULTS

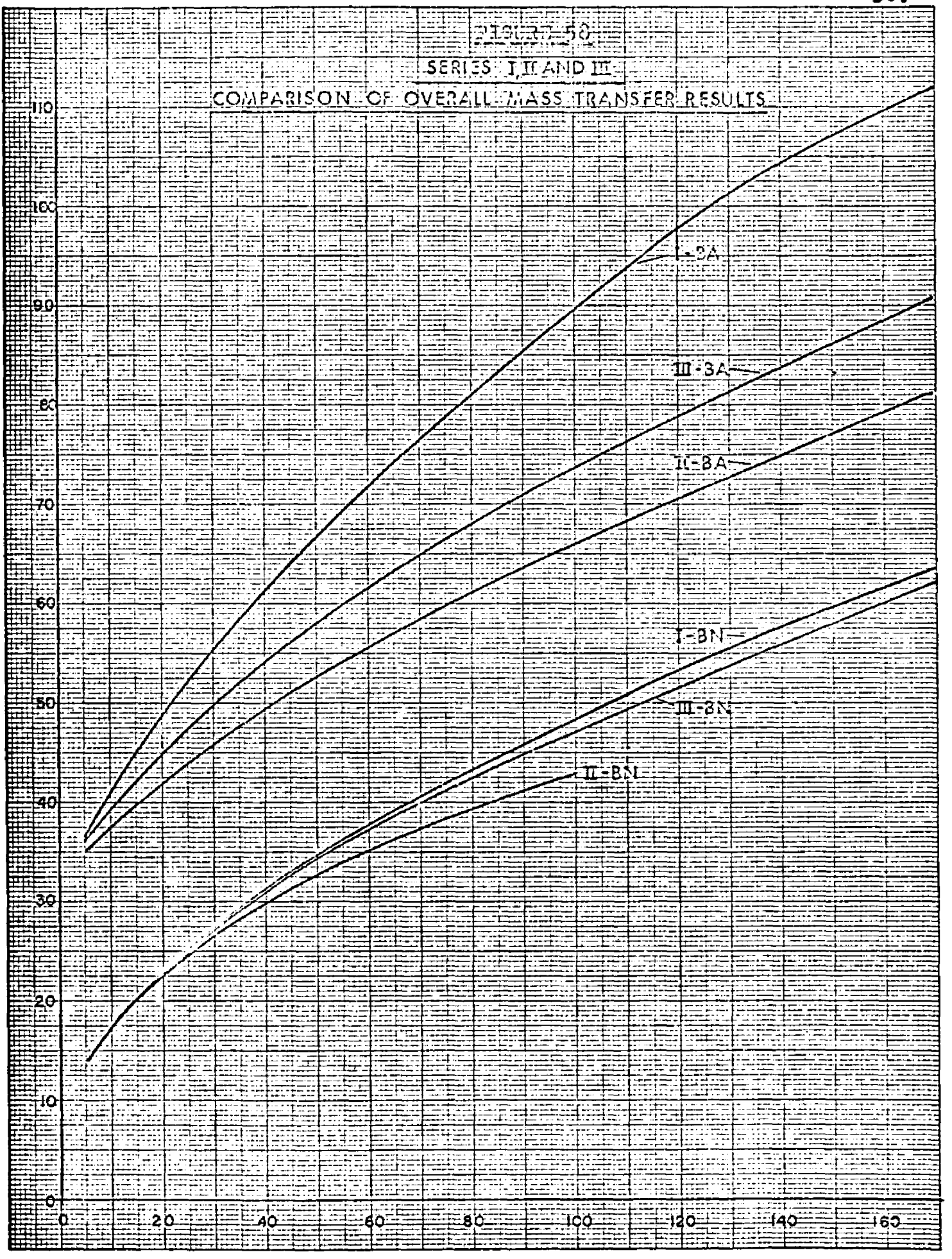

K+E 10 X 10 TO THE CENTIMETER 46 1513
18 X 25 CM.
KEUFFEL & ESSER CO.

FIGURE 52

SERIES I, V & VI

COMPARISON OF OVERALL MASS TRANSFER RESULTS

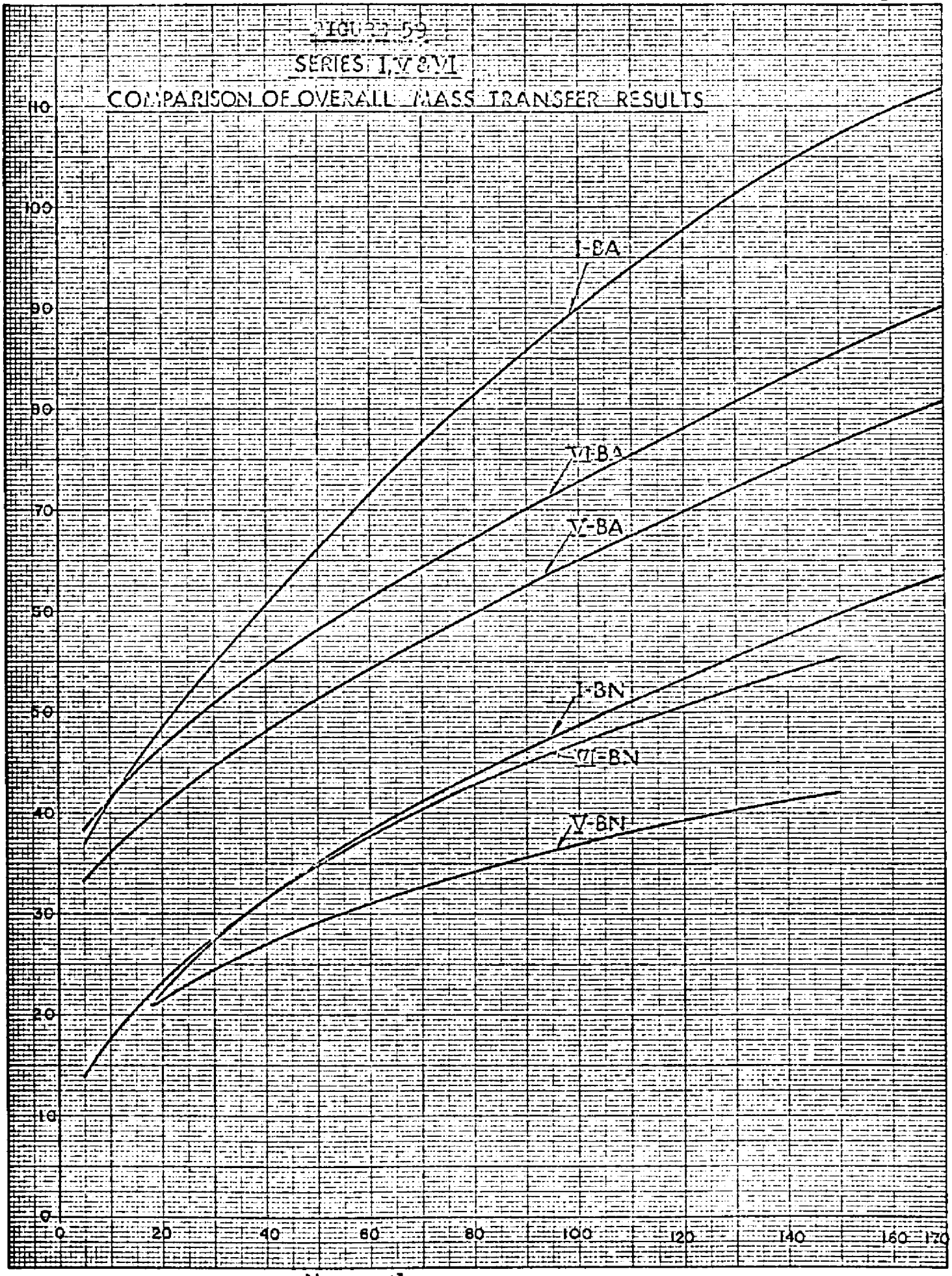

K&E 10 X 10 TO THE CENTIMETER 46 1513
10 X 25 CM. MADE IN U.S.A.
KEUFFEL & ESSER CO.

FIGURE 60 EQUILATERAL TRIANGLE CONFIGURATIONS USED

SERIES VIII

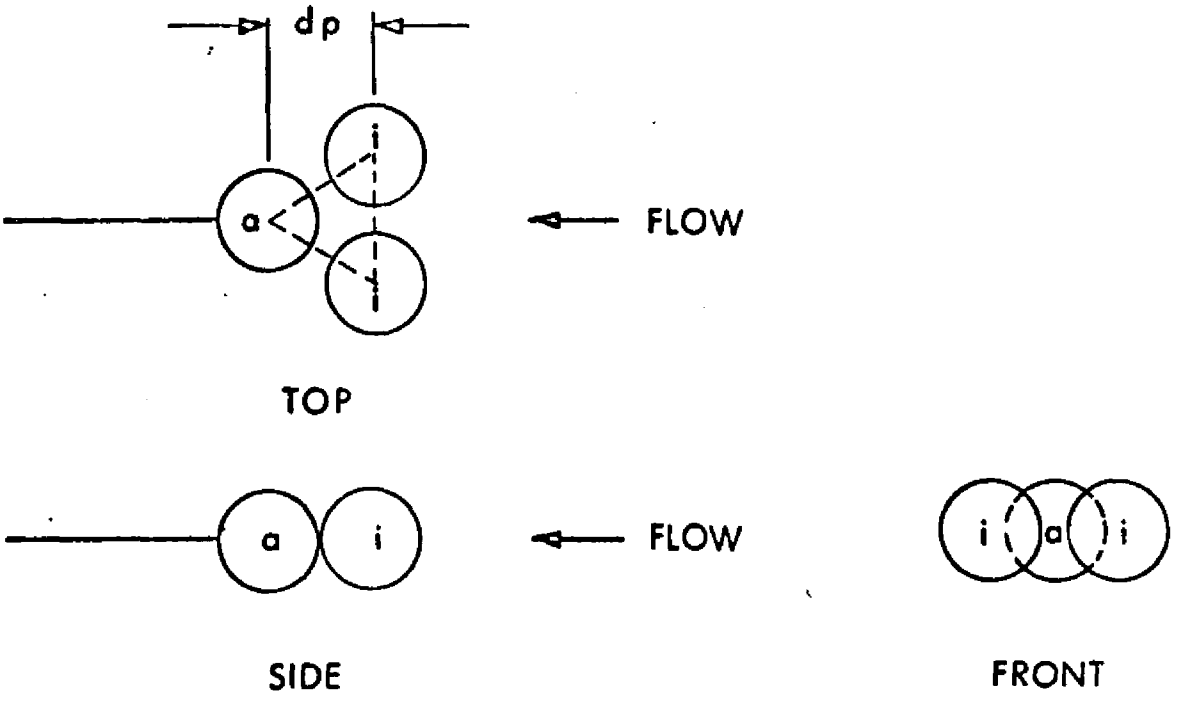

SERIES IX

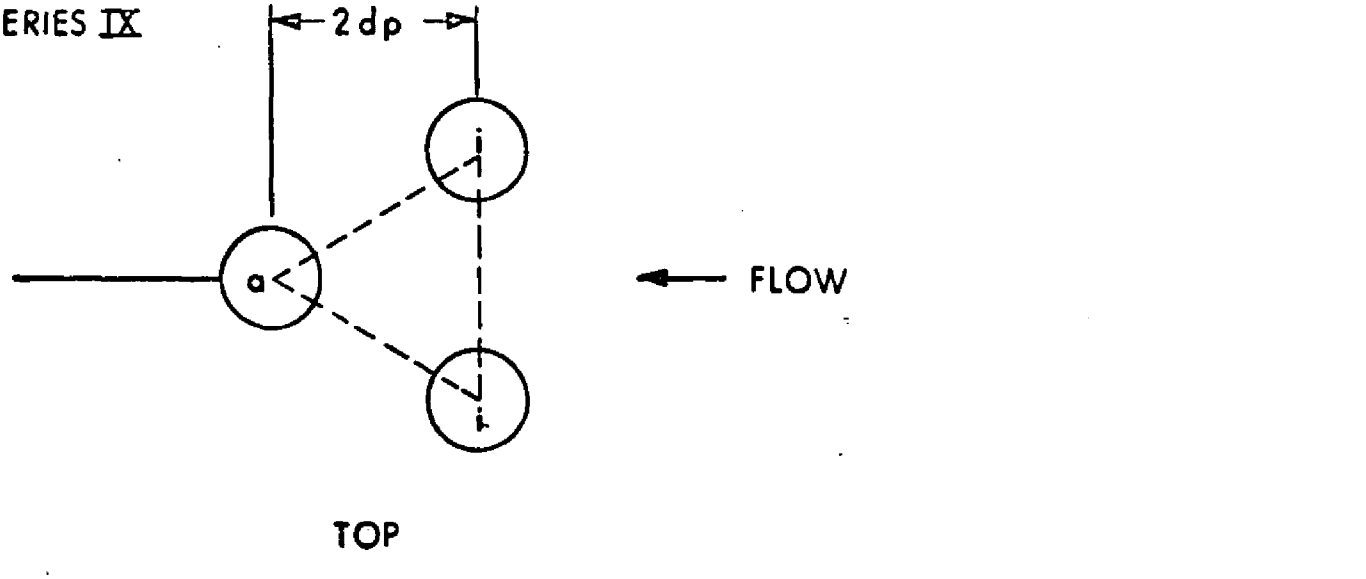

TABLE IX. Overall Mass Transfer Results - Equilateral Triangle Studies

Run Number	Solute	Run Time	Weight Loss	Flow Rate	Run Temperature	Solute Solubility	Schmidt Number	Initial Surface Avg. Radius	Final Surface Avg. Radius	Reynolds Number	Sh_o
		Hours	Grams	GPM	°C.	Grams/1000 Grams of solution		Inches	Inches		
VIII-1	BA	25.1	.3910	0.407	24.69	3.31	980.0	.2570	.2309	27.65	36.87
VIII-2	BN	23.5	.1129	1.998	24.63	0.72	805.0	.2551	.2489	140.0	41.17
VIII-3	BN	29.0	.1012	1.177	24.81	0.73	800.0	.2547	.2481	82.65	29.51
VIII-4	BN	96.0	.1702	0.407	23.11	0.67	863.0	.2532	.2437	27.2	17.16
VIII-7	BA	3.0	.1135	2.433	25.87	3.42	915.0	.2522	.2456	173.2	80.68
VIII-8	BA	3.0	.0928	1.612	26.40	3.47	885.0	.2522	.2469	116.4	63.54
VIII-9	BA	6.0	.1023	0.0768	25.48	3.38	940.0	.2562	.2500	5.5	36.65
VIII-10	BA	4.8	.0938	0.791	25.06	3.34	955.0	.2500	.2443	54.9	44.10
IX-1	BN	21.9	.1303	1.998	23.98	0.695	830.0	.2527	.2445	136.15	54.14
IX-2	BN	24.4	.1194	1.177	24.25	0.70	821.0	.2459	.2377	78.5	45.15
IX-3	BN	77.0	.2134	0.407	24.78	0.73	805.0	.2498	.2355	27.55	24.45
IX-4	BA	7.1	.1156	0.0768	24.54	3.29	990.0	.2558	.2482	5.4	37.46
IX-5	BA	3.4	.1368	1.511	24.03	3.24	1017.0	.2570	.2476	111.55	95.39
IX-7	BA	3.2	.1441	2.432	25.22	3.36	940.0	.2445	.2341	154.05	103.1
IX-8	BA	3.1	.1010	0.791	25.68	3.43	920.0	.2484	.2415	55.2	71.15
IX-9	BA	6.4	.0978	0.0768	24.98	3.34	964.0	.2420	.2349	5.15	35.97

The local mass transfer profiles obtained, with benzoic acid and beta naphthol, for these series are presented in Figures 61 through 64. The figures show that the two inert particles placed horizontally in front of the active sphere have a greater effect on the local mass transfer coefficients in the more closed configuration (series VIII) than in the more open configuration (series IX). In fact, the local transfer profiles for series IX are quite similar in appearance to those presented earlier for single spheres. The more closed configuration, series VIII, shows a much smaller forward flow area with a minimum mass transfer rate occurring before 90^{o} from the forward stagnation point. This is due to the presence of the inert spheres which block the forward flow area.

In Figure 65, the overall mass transfer rates for both systems studied and for both geometrical configurations are plotted as Sh_o vs. Pe. The overall Sherwood number results for the closed triangular arrangement are smaller than for the single sphere at all Peclet numbers because of the area blockage effect. For the open triangular arrangement, the overall Sherwood number results are somewhat higher than for the single sphere. Thus, the more open arrangement begins to simulate the behavior of a large array of particles for which the Sherwood number is always higher than that for a single sphere.

The equilateral triangular runs show the combined effect of both axial and radical proximity of inert spheres upon the local and overall mass transfer rates from the test sphere. It appears that axial proximity has a much greater

FIGURE 61.

LOCAL SHERWOOD NUMBER PROFILES SERIES VIII-

BENZOIC ACID RESULTS - N_{Sh_L} VS. Θ

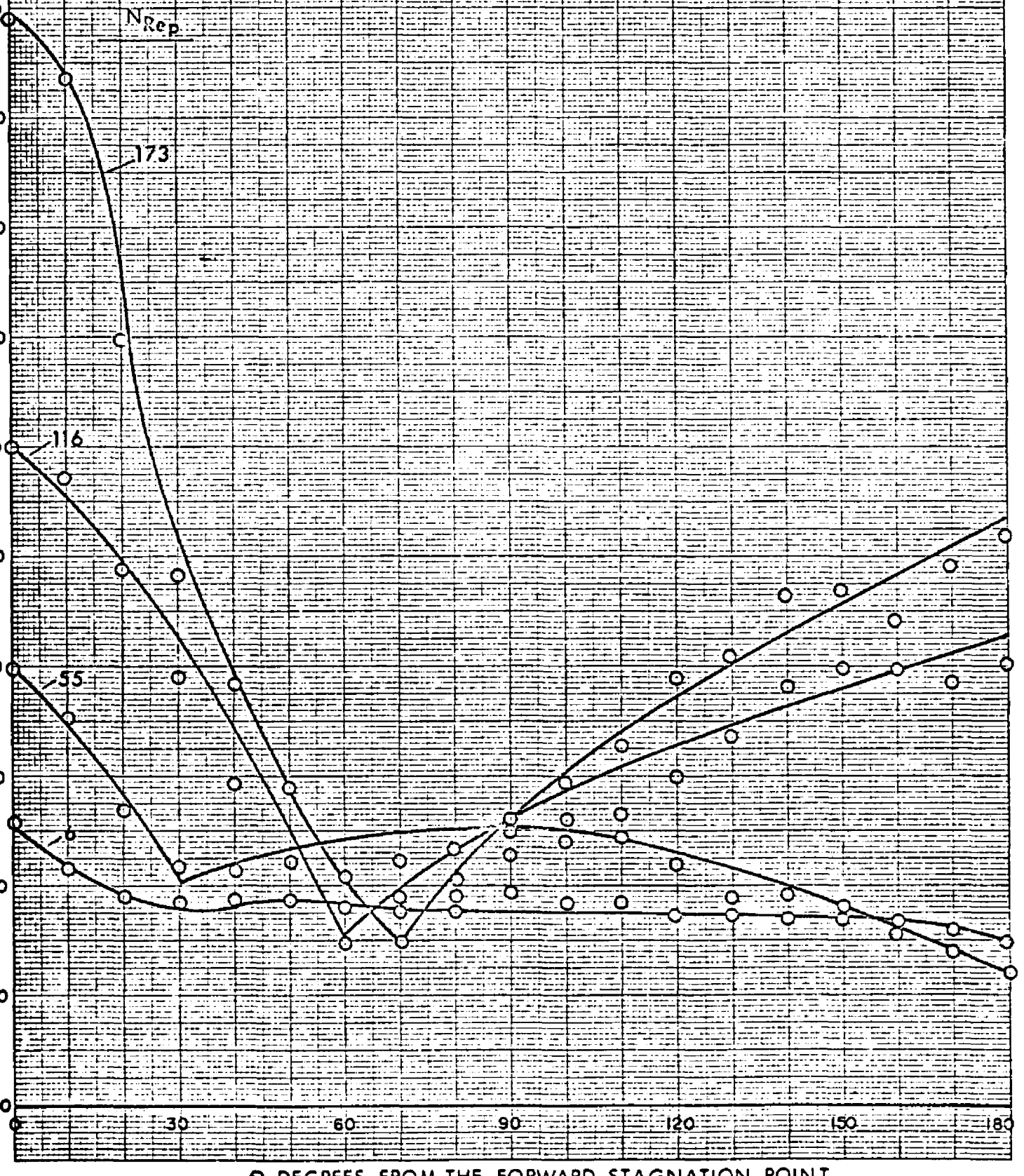

K·E 10 X 10 TO THE CENTIMETER 46 1513
18 X 25 CM.
KEUFFEL & ESSER CO.

FIGURE 62 - LOCAL SHERWOOD NUMBER PROFILES
BETA NAPHTHOL RESULTS - SERIES VIII Sh_L VS θ

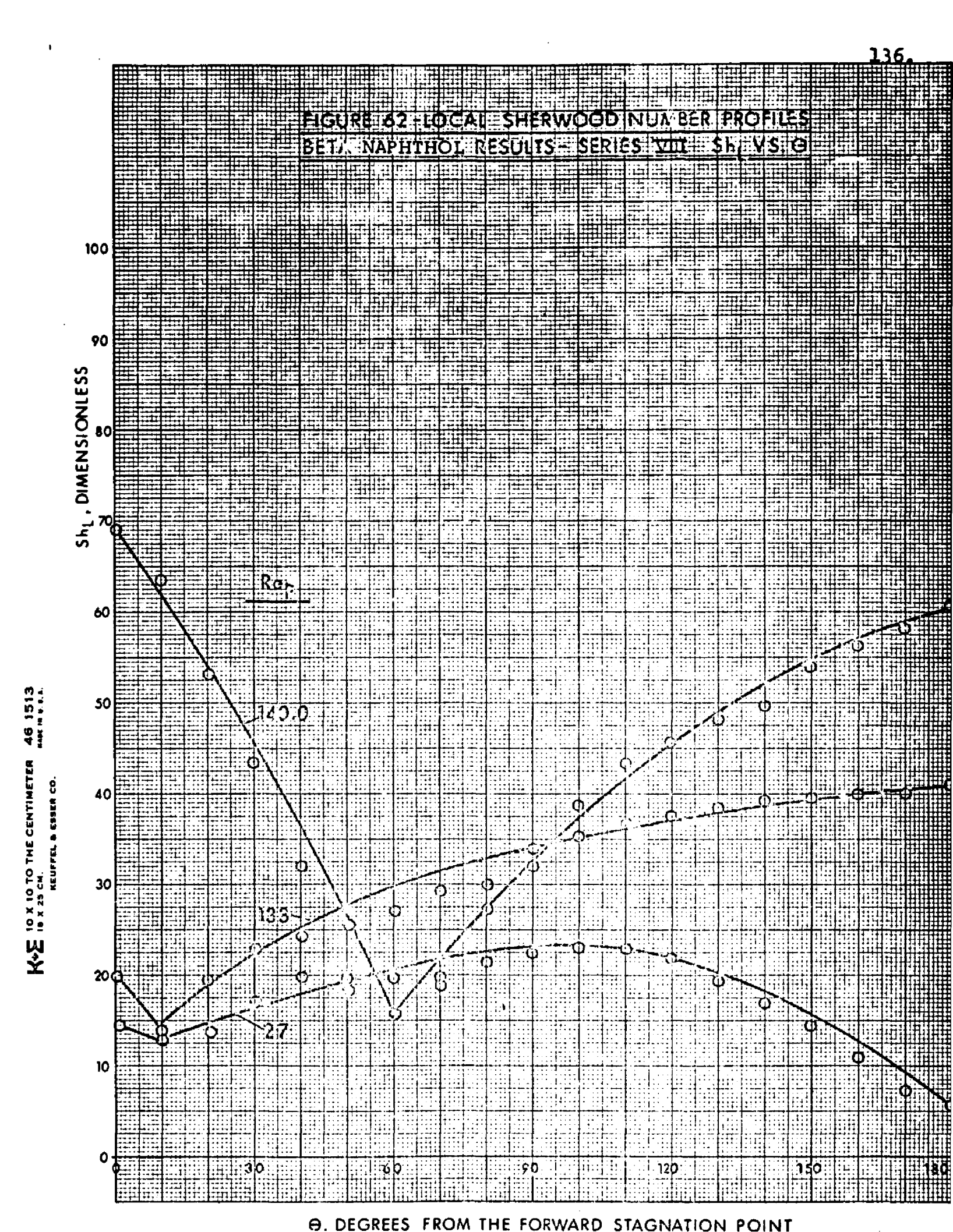

K+E 10 X 10 TO THE CENTIMETER 46 1513
18 X 25 CM. KEUFFEL & ESSER CO.

FIGURE 63

LOCAL SHERWOOD NUMBERS PROFILES

SERIES TC - BENZOIC ACID RESULTS

N_{sh_L} VS. Θ

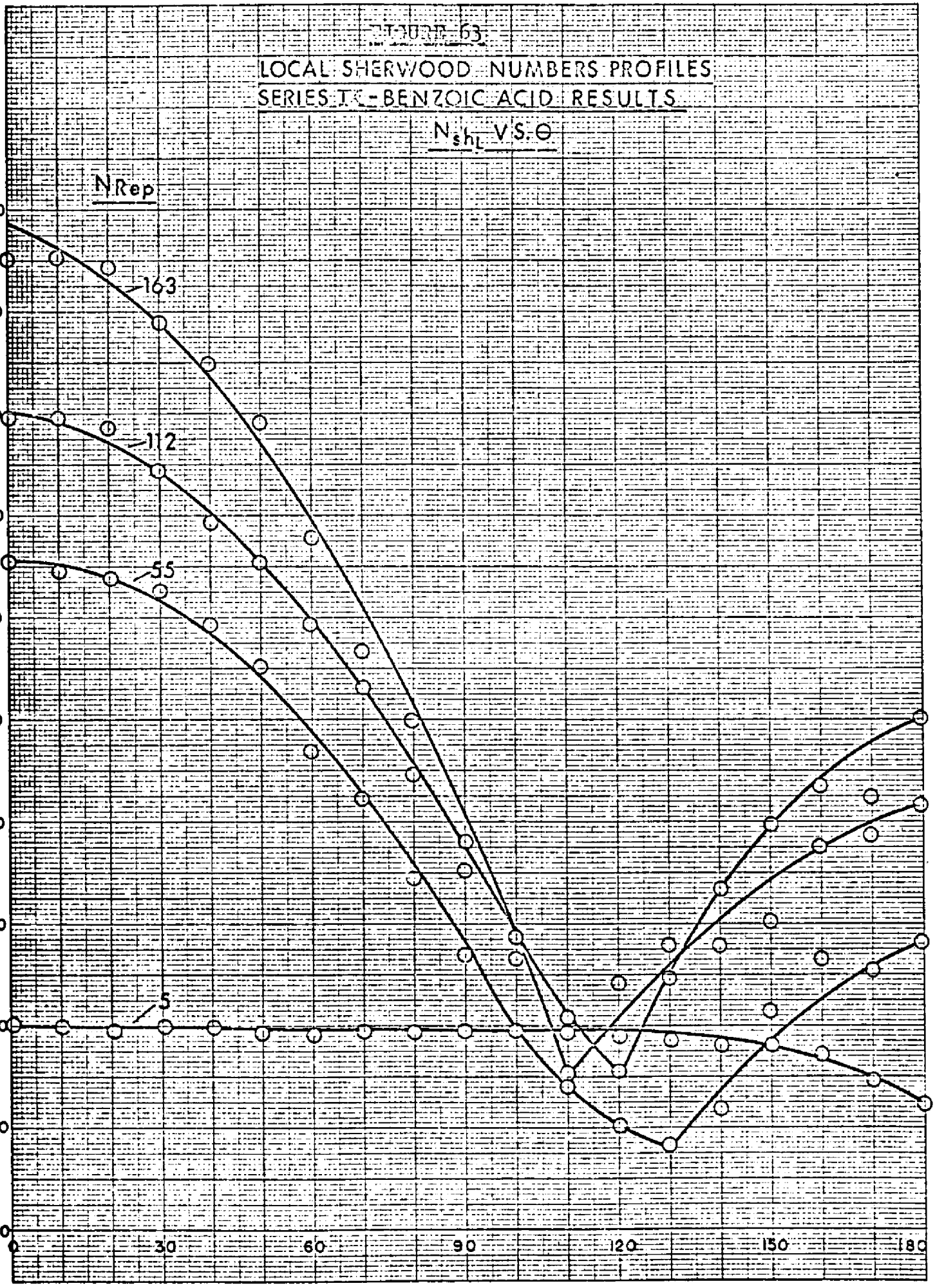

K•E 10 X 10 TO THE CENTIMETER 46 1513
16 X 25 CM.
KEUFFEL & ESSER CO.

FIGURE 64 - LOCAL SHERWOOD NUMBER PROFILES
BETA NAPHTHOL RESULTS - SERIES IX - Sh_L VS. Θ

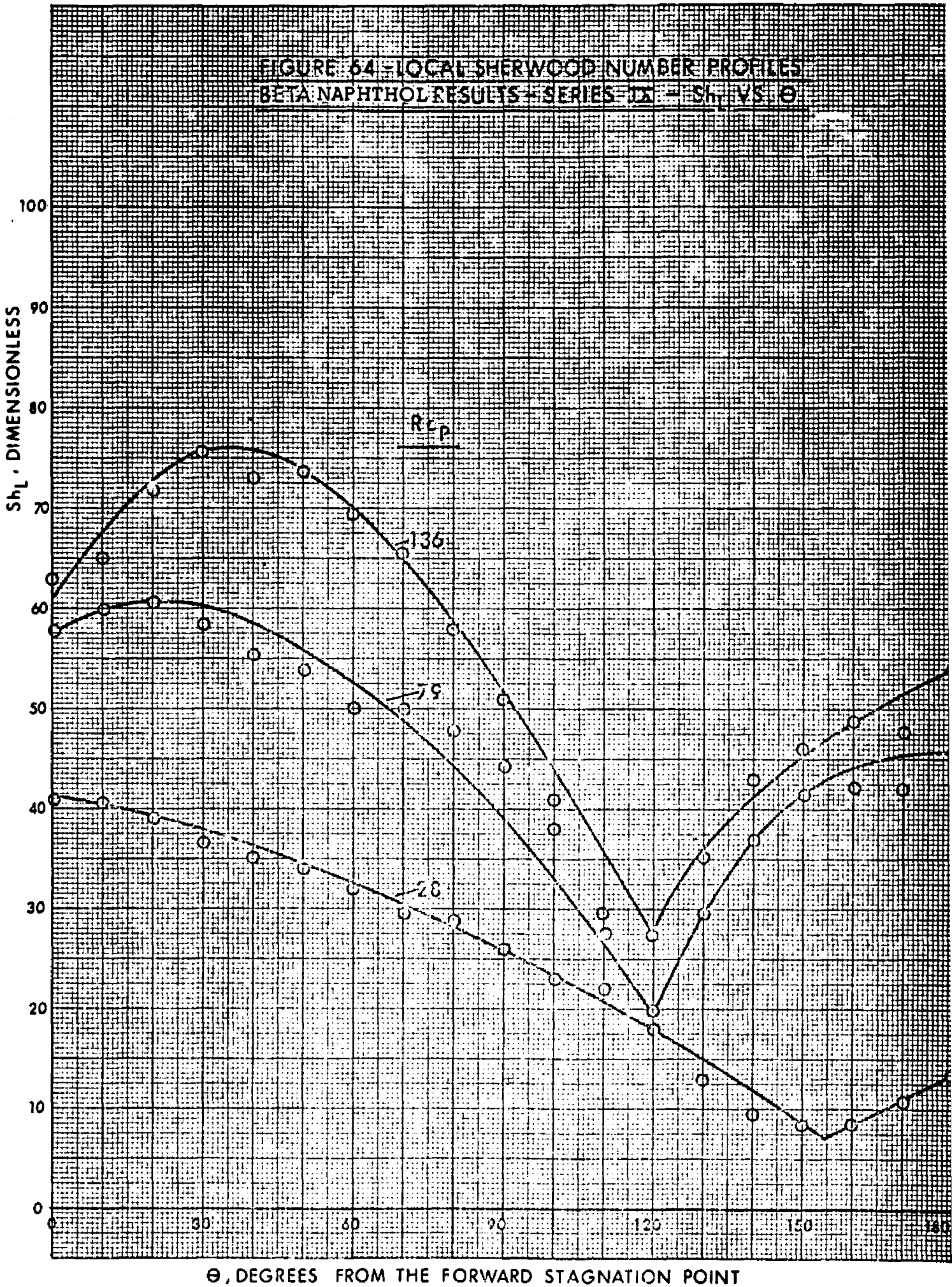

K+E 10 X 10 TO THE CENTIMETER 46 1513
18 X 25 CM.
KEUFFEL & ESSER CO.

FIGURE 65

RESULTS - SERIES VIII AND IX - Nsh_o VS. N_{pe}

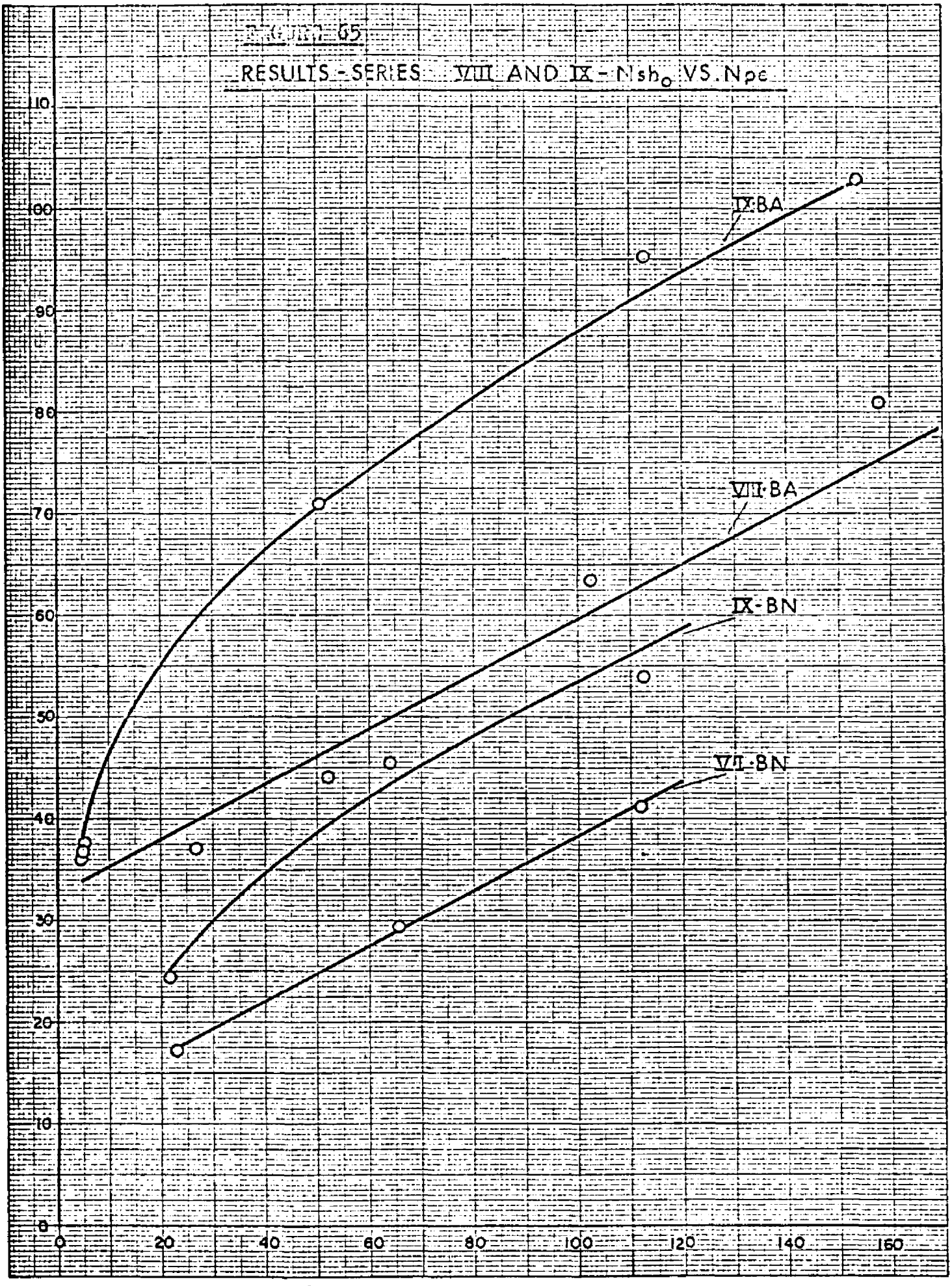

K•E 10 X 10 TO THE CENTIMETER 46 1513
16 X 25 CM.
KEUFFEL & ESSER CO.

effect on the mass transfer rate. That is, at the same separation between particles the axially located one will have a more pronounced effect on the test sphere than a radially located one. In order to more fully study the effect of radial proximity, the hexagonal series of runs were performed.

Hexagonal Configurations

Figure 66 summarizes the hexagonal geometries used in this work. The series VII runs, at three different "pseudo" voidages, were carried out with a single layer hexagonal array of particles; the active sphere being at the center of the array. The series X runs, also at three different "pseudo" voidages, were carried out with a two layer hexagonal array of particles; the test sphere being at the center of the downstream layer. Thus, series VII studies the effect of a radial arrangement of particles; whereas, series X studies the effect of a combination radial and axial configuration. In Table X are presented the overall mass transfer results of these hexagonal configuration studies along with the pertinent run information.

The local mass transfer profiles for the Series VII runs are presented in Figures 67 through 69. Each figure is at a constant "pseudo" voidage and is plotted as Sh_L vs. θ with particle Reynolds number as a parameter. Figures 67 and 68 are similar in appearance to those obtained for single spheres and the open equilateral triangle configuration. However, Figure 69, which presents the results obtained when the inert spheres touched the test

FIGURE 66 HEXAGONAL GEOMETRIES USED

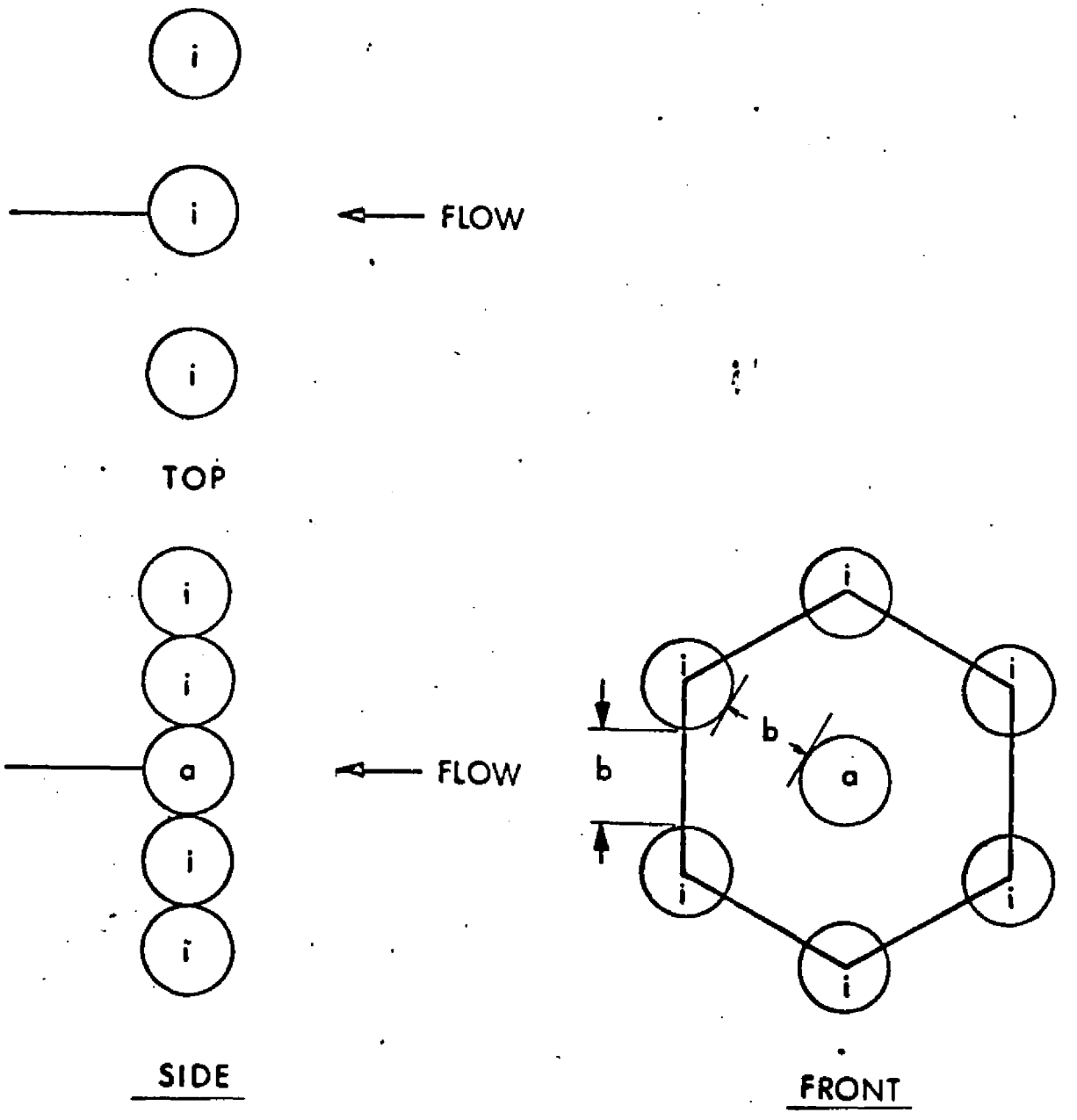

SERIES NUMBER	b INCHES	ϵ' VOIDAGE	
VII a	1/2 = dp	0.85	SHOWN
VII b	1/4 = $\frac{dp}{2}$	0.73	NOT SHOWN
VII c	ZERO	0.40	NOT SHOWN

THE TWO-LAYER HEXAGONAL ARRAYS ARE MADE BY ADDING A SECOND LAYER OF INERT SPHERES IN FRONT OF THE ONE SHOWN. VOIDAGE IS MAINTAINED BY SEPARATING THE LAYERS BY "b".

TABLE X. Overall Mass Transfer Results - Benzoic Acid Test Spheres - Hexagonal Studies

Run Number	Pseudo Voidage	Run Time	Weight Loss	Flow Rate	Run Temperature	Solute Solubility	Schmidt Number	Initial Surface Avg. Radius	Final Surface Avg. Radius	Reynolds Number	Sh_o
		Hours	Grams	GPM	°C.	Grams/1000 Grams of solution		Inches	Inches		
VII-1	.85	3.5	.1758	2.432	25.80	3.41	914.0	.2531	.2402	171.30	108.4
VII-2	.85	3.0	.1257	1.612	25.24	3.46	895.0	.2403	.2297	109.25	92.45
VII-3	.85	3.0	.0952	0.791	25.63	3.40	925.0	.2539	.2469	56.35	68.17
VII-4	.85	6.0	.1013	0.0768	25.54	3.39	935.0	.2555	.2487	5.50	36.40
VII-5	.80	3.0	.1581	2.433	25.81	3.41	913.0	.2496	.2376	169.25	115.1
VII-6	.73	3.0	.1335	1.613	27.05	3.54	854.0	.2354	.2236	108.65	95.52
VII-7	.73	3.0	.1448	2.432	25.71	3.41	920.0	.2458	.2349	166.55	107.2
VII-8	.73	4.0	.1164	0.791	24.50	3.29	990.0	.2297	.2185	49.15	75.23
VII-9	.73	22.5	.3421	0.0768	24.53	3.30	975.0	.2564	.2334	5.25	35.49
VII-10	.40	4.0	.1697	2.432	25.05	3.34	960.0	.2607	.2508	174.70	92.96
VII-11	.40	3.0	.0889	1.611	24.85	3.32	965.0	.2335	.2274	103.80	72.60
VII-12	.40	3.0	.0699	0.791	24.87	3.32	965.0	.2469	.2427	54.15	53.72
VII-13	.40	6.0	.0972	0.0768	25.52	3.39	934.0	.2598	.2543	5.50	34.19
VII-14	.85	6.2	.0978	0.0768	25.22	3.36	945.0	.2430	.2358	5.20	36.28
VII-15	.73	4.0	.1895	2.432	25.55	3.39	933.0	.2496	.2370	168.05	105.8
VII-16	.73	4.0	.2117	2.673	25.75	3.41	920.0	.2576	.2431	190.85	113.2
X-1	.85	3.0	.1237	2.432	25.64	3.40	927.0	.2573	.2495	175.40	87.69
X-2	.85	3.5	.1203	1.612	25.50	3.38	934.0	.2571	.2505	116.05	73.69
X-3	.85	6.0	.1494	0.791	25.53	3.39	933.0	.2494	.2404	55.00	55.18
X-4	.85	6.2	.1143	0.0768	26.15	3.45	900.0	.2605	.2536	5.70	37.39
X-5	.40	3.0	.0631	2.432	25.43	3.38	935.0	.2567	.2514	175.00	45.04

TABLE X. Continued

Run Number	Pseudo Voidage	Run Time	Weight Loss	Flow Rate	Run Temperature	Solute Solubility	Schmidt Number	Initial Surface Avg. Radius	Final Surface Avg. Radius	Reynolds Number	Sh_o
		Hours	Grams	GPM	$^{o}C.$	Grams/1000 Grams of solution		Inches	Inches		
X-6	.40	3.0	.0549	1.612	25.36	3.37	938.0	.2606	.2575	118.10	38.51
X-7	.40	5.0	.0764	0.791	25.49	3.38	934.0	.2508	.2462	55.75	33.44
X-8	.40	19.5	.2855	0.0768	26.08	3.44	910.0	.2532	.2366	5.40	31.54
X-9	.82	3.0	.1221	2.432	25.37	3.37	938.0	.2534	.2472	172.15	88.93
X-10	.82	3.0	.0966	1.612	25.37	3.37	938.0	.2492	.2438	112.40	71.41
X-11	.82	5.0	.1163	0.791	25.43	3.38	937.0	.2447	.2389	54.15	52.44

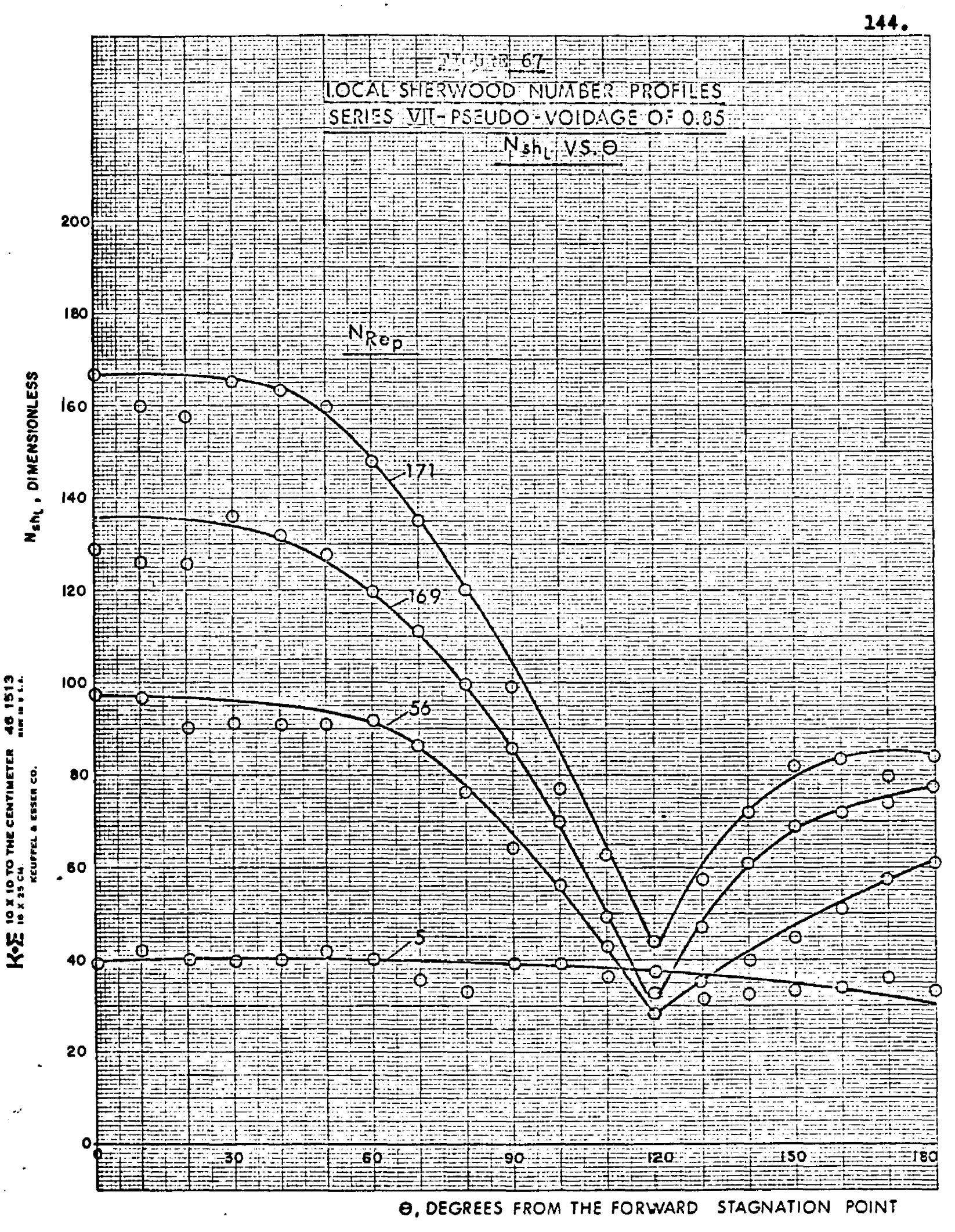
LOCAL SHERWOOD NUMBER PROFILES
SERIES VII - PSEUDO-VOIDAGE OF 0.85
N_{sh_L} V.S. θ
N_{Rep}
171
169
56
5
N_{sh_L}, DIMENSIONLESS
0
20
40
60
80
100
120
140
160
180
200
0
30
60
90
120
150
180
θ, DEGREES FROM THE FORWARD STAGNATION POINT
K+E 10 X 10 TO THE CENTIMETER 46 1513
16 X 25 CM.
KEUFFEL & ESSER CO.

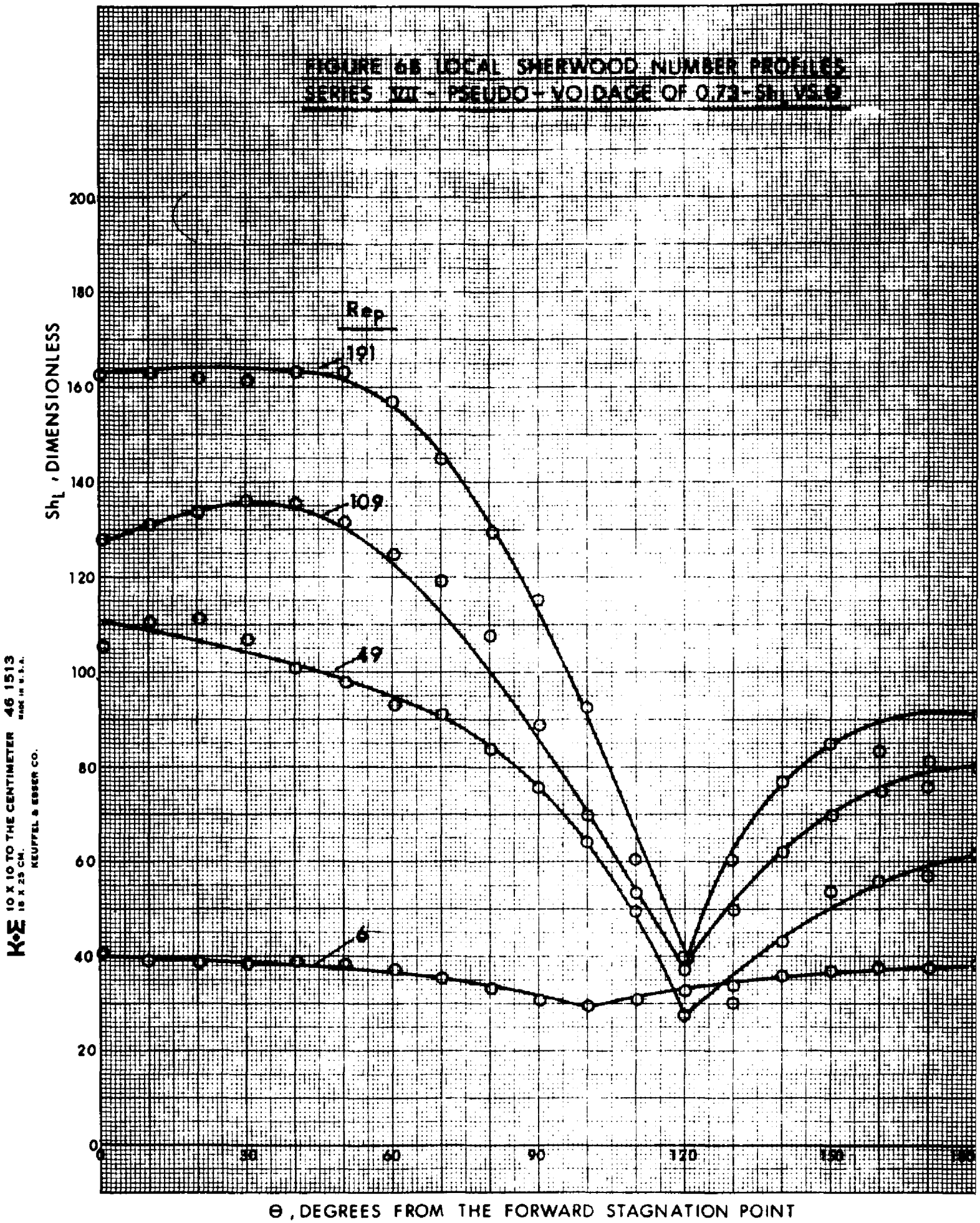
FIGURE 68 LOCAL SHERWOOD NUMBER PROFILES
SERIES VII - PSEUDO - VO DAGE OF 0.73 - Sh_L VS. Θ
Re_P
191
109
49
6
Sh_L , DIMENSIONLESS
200
180
160
140
120
100
80
60
40
20
0
30
60
90
120
150
Θ , DEGREES FROM THE FORWARD STAGNATION POINT
K&E 10 X 10 TO THE CENTIMETER 46 1513
18 X 25 CM.
KEUFFEL & ESSER CO.

FIGURE 69

LOCAL SHERWOOD NUMBER PROFILES

SERIES VII - PSEUDO-VOIDAGE OF 0.40

N_{sh_L} VS. θ

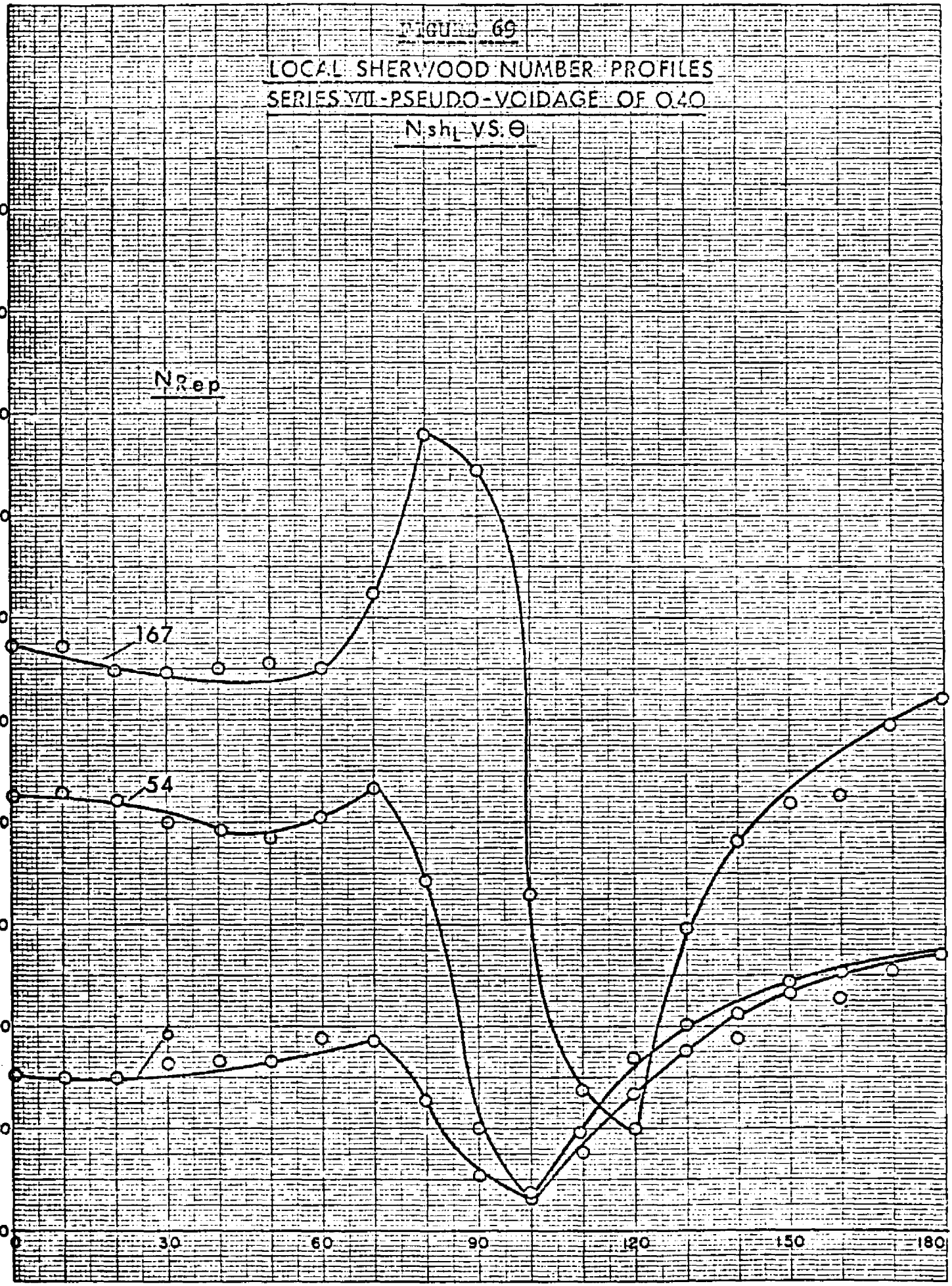

K+E 10 X 10 TO THE CENTIMETER 46 1513
18 X 25 CM. MADE IN U.S.A.
KEUFFEL & ESSER CO.

sphere, shows the large effect on the mass transfer coefficient due to the points of contact normal to the flow direction.

In Figure 70 are presented the overall transfer rates obtained for all series VII runs, plotted as Sh_o vs. Pe with "pseudo" voidage, ϵ', as parameter. The single sphere benzoic acid data are plotted at ϵ' equal to 1.0 as a comparison. The figure shows that at Pe of about 5,000 all configurations give similar results. At Pe greater than 45,000 and a "pseudo" voidage of 0.85 (one diameter between the spheres) the overall mass transfer rate appears greater than that obtained for single spheres; whereas, at lower Pe the mass transfer rate is approximately the same as that for a single sphere. At a "pseudo" voidage of 0.73 (one-half diameter between spheres) the overall mass transfer rates are greater than those obtained for a single sphere for Pe less than 150,000. For all Peclet numbers studied, a "pseudo" voidage of 0.40 gave the minimum overall transfer rates due to contact between particles. The higher mass transfer coefficients found for the "pseudo" voidages of 0.73 and 0.85, which are in agreement with the open equilateral triangle results, are an indication of the increased mass transfer rates which are observed in multiparticle systems such as packed and fluidized beds.

In Figures 71, 72 and 73, the local mass transfer profiles obtained for the series X runs are presented. These results are in close agreement with the results of series II and series III at the same axial separation and show

FIGURE 70

SERIES I (EA) RESULTS AND SERIES VII RESULTS -

N_{Sh_o} VS. N_{P_e}, ϵ' IS PARAMETER

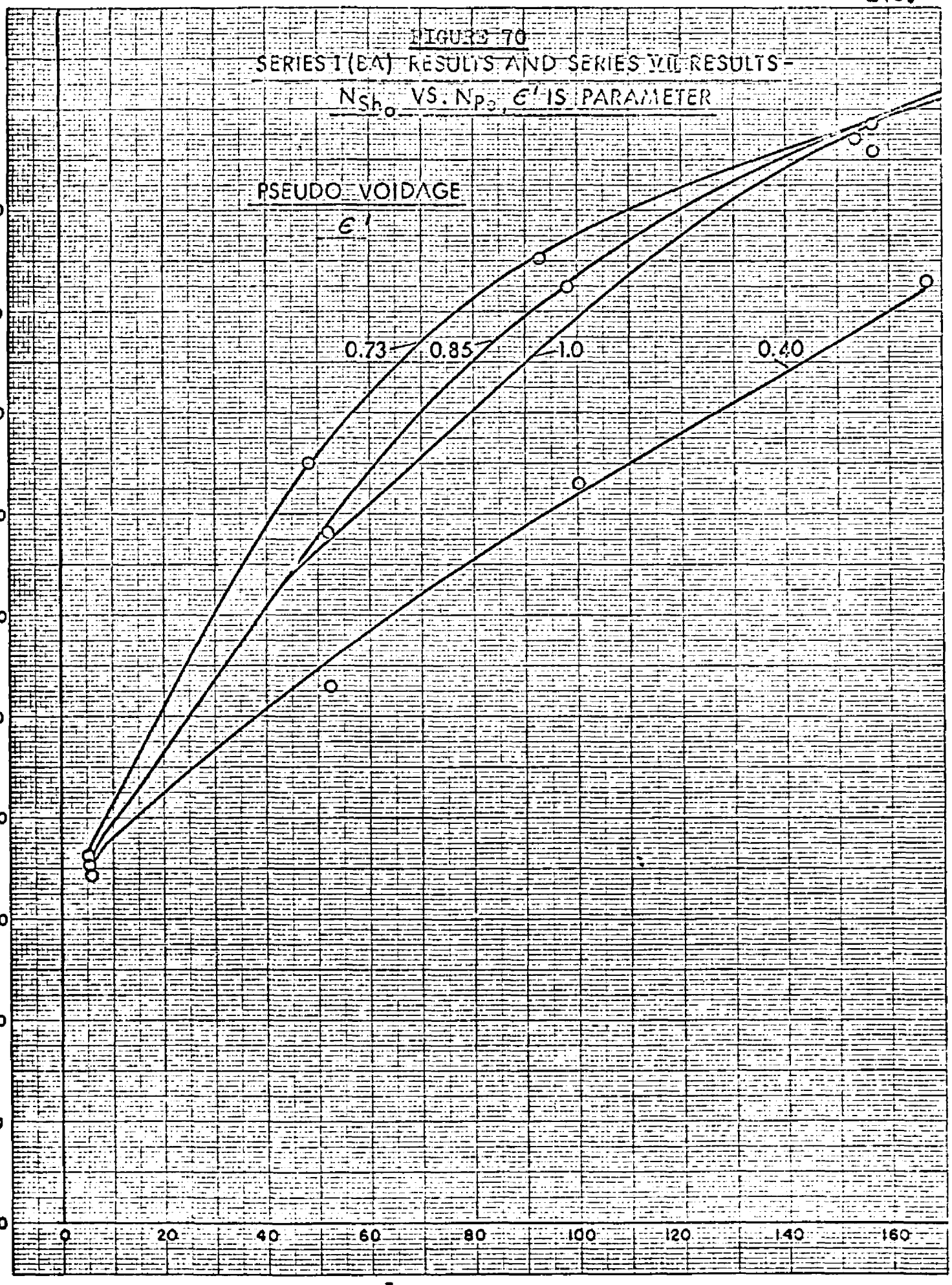

K•E 10 X 10 TO THE CENTIMETER 46 1513
18 X 25 CM. MADE IN U.S.A.
KEUFFEL & ESSER CO.

FIGURE 71

LOCAL SHERWOOD NUMBER PROFILES

SERIES X - PSEUDO-VOIDAGE OF 0.85 - N_{Sh_L} VS. θ

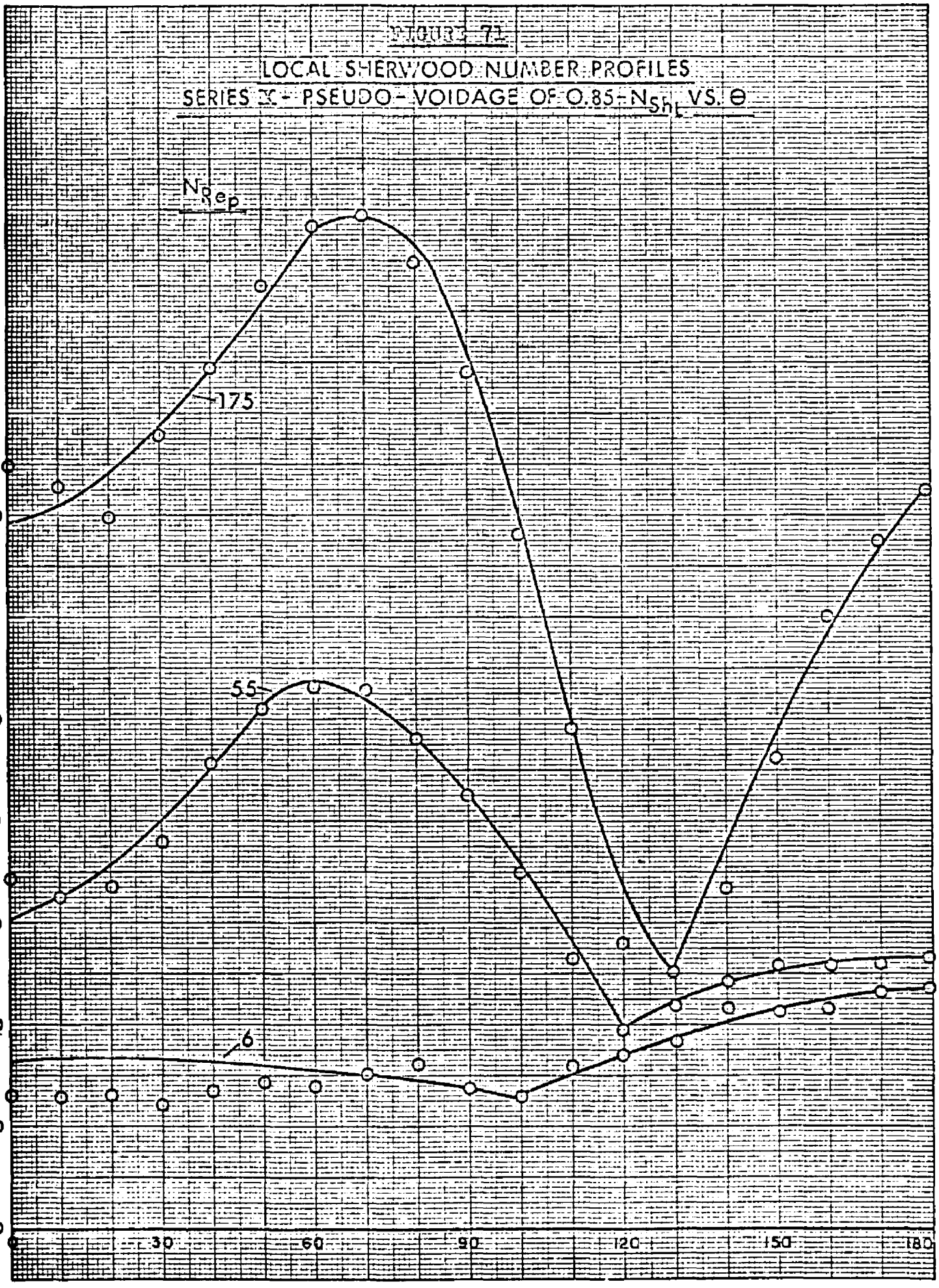

K+E 10 X 10 TO THE CENTIMETER 46 1513 MADE IN U.S.A. 10 X 25 CM. KEUFFEL & ESSER CO.

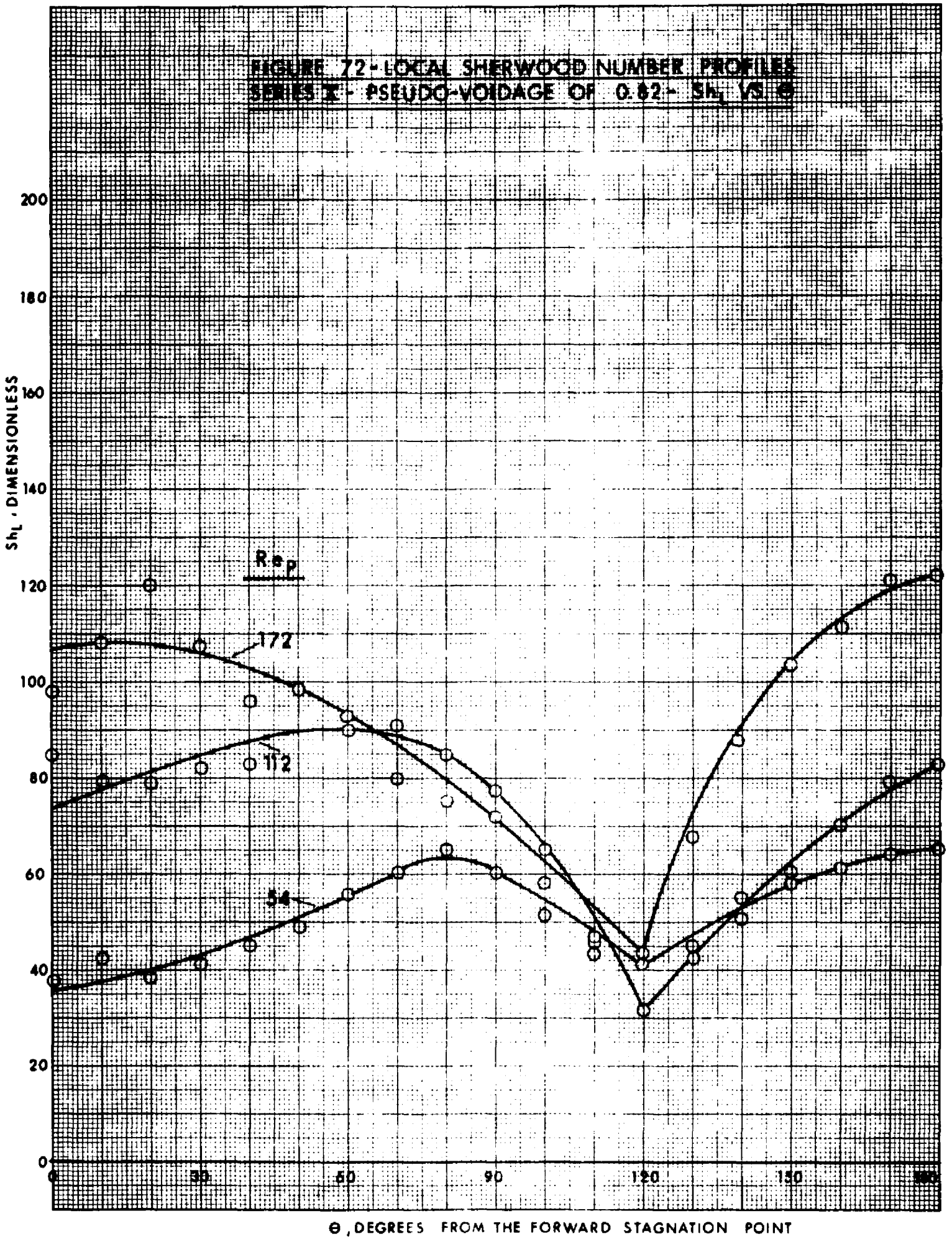

K•E 10 X 10 TO THE CENTIMETER 46 1513
18 X 25 CM. KEUFFEL & ESSER CO. MADE IN U.S.A.

FIGURE 73

LOCAL SHERWOOD NUMBER PROFILES SERIES X-

PSEUDO-VOIDAGE OF 0.70 - N_{Sh_L} VS. Θ

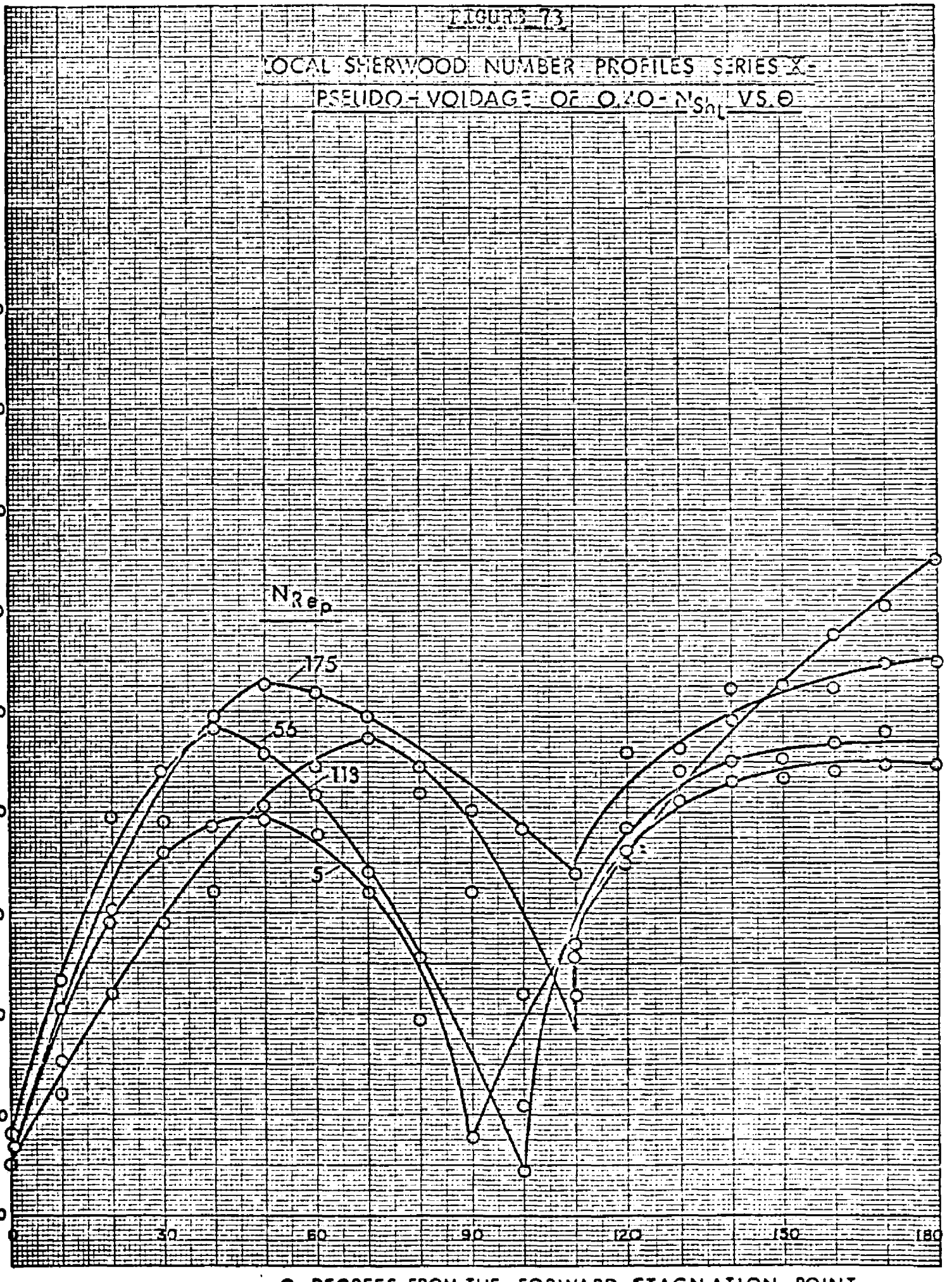

that the effect of axial proximity is much greater than that of radial proximity for small numbers of particles around the test sphere.

In Figure 74, the overall mass transfer coefficient for series X, with the single sphere results included for comparison, are presented as Sh_o vs. Pe with ϵ' as parameter. The curve at ϵ' equal to 0.82 (one diameter between spheres axially and one half diameter radially) was predicted from a cross-plot of the results at ϵ' of 0.40, 0.85 and 1.0, which is shown in Figure 75. Three runs at a "pseudo" voidage of 0.82 were then made and the results are also plotted on Figure 74. It should be noted that the three points obtained are in good agreement with the predicted curve. At an ϵ' of 0.40 a marked reduction in overall transfer rates was observed. The figure shows that at all values of ϵ' investigated for this series, the overall mass transfer rates are less than those obtained for a single sphere. This is due to the large area blockage effect obtained with the touching two layer hexagonal configuration.

Figure 76, which is a comparison of the overall mass transfer results obtained from the series I, III, VII ($\epsilon' = 0.85$) and X ($\epsilon' = 0.85$) benzoic acid runs, shows how closely series X is related to series III. Figure 77, which compares the overall benzoic acid mass transfer results for series I, II, VII ($\epsilon' = 0.40$) and X ($\epsilon' = 0.40$) shows how strongly the close packing of the inert particles has reduced the overall transfer rate from the benzoic acid test sphere. These observations are in complete agreement with the local coefficient results discussed above.

FIGURE 74.

SERIES I (BA) RESULTS & SERIES X RESULTS-

N_{Sh_o} VS. N_{P_e}, ϵ' IS PARAMETER

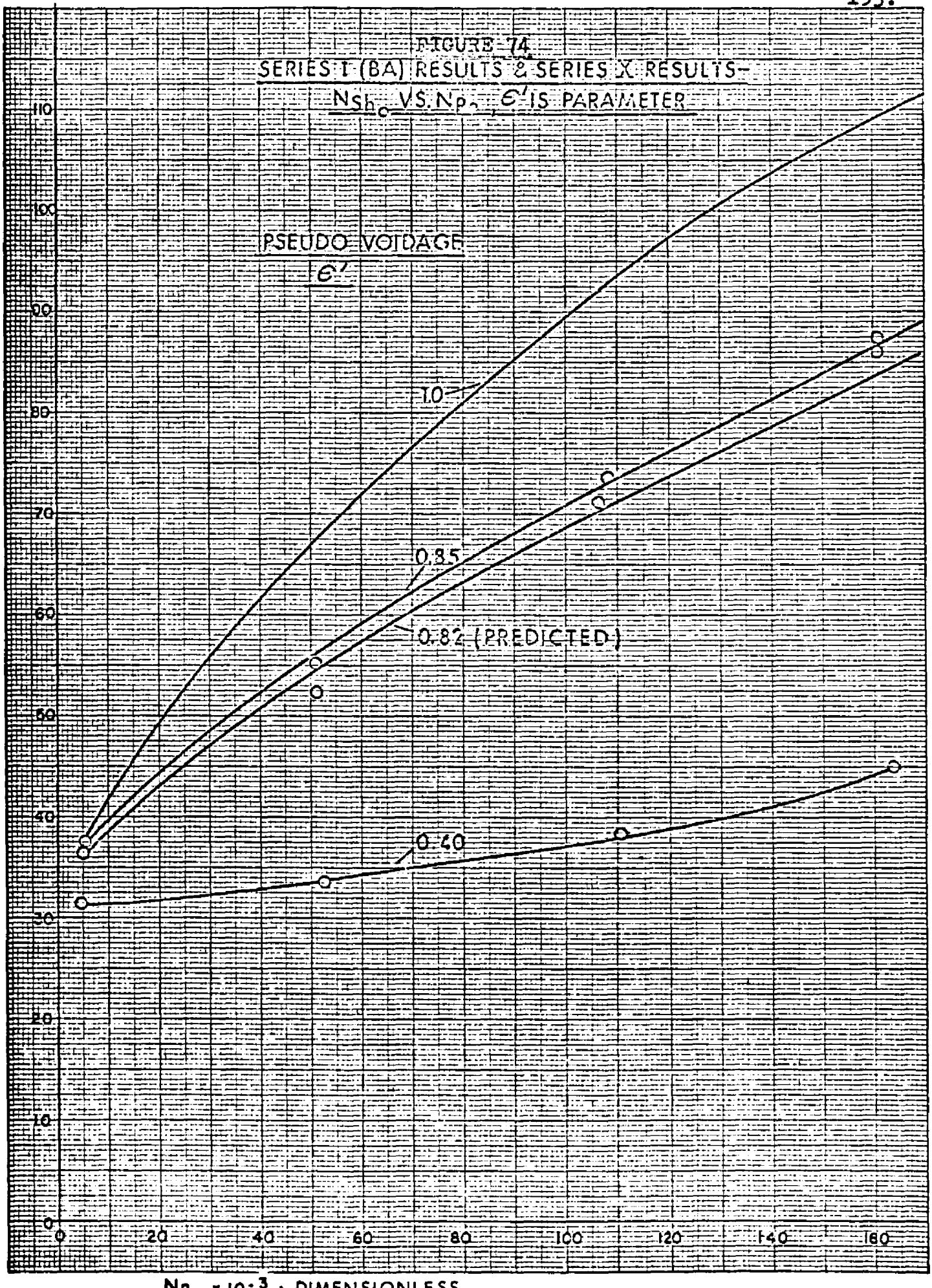

K+E 10 X 10 TO THE CENTIMETER 46 1513
18 X 25 CM. MADE IN U.S.A.
KEUFFEL & ESSER CO.

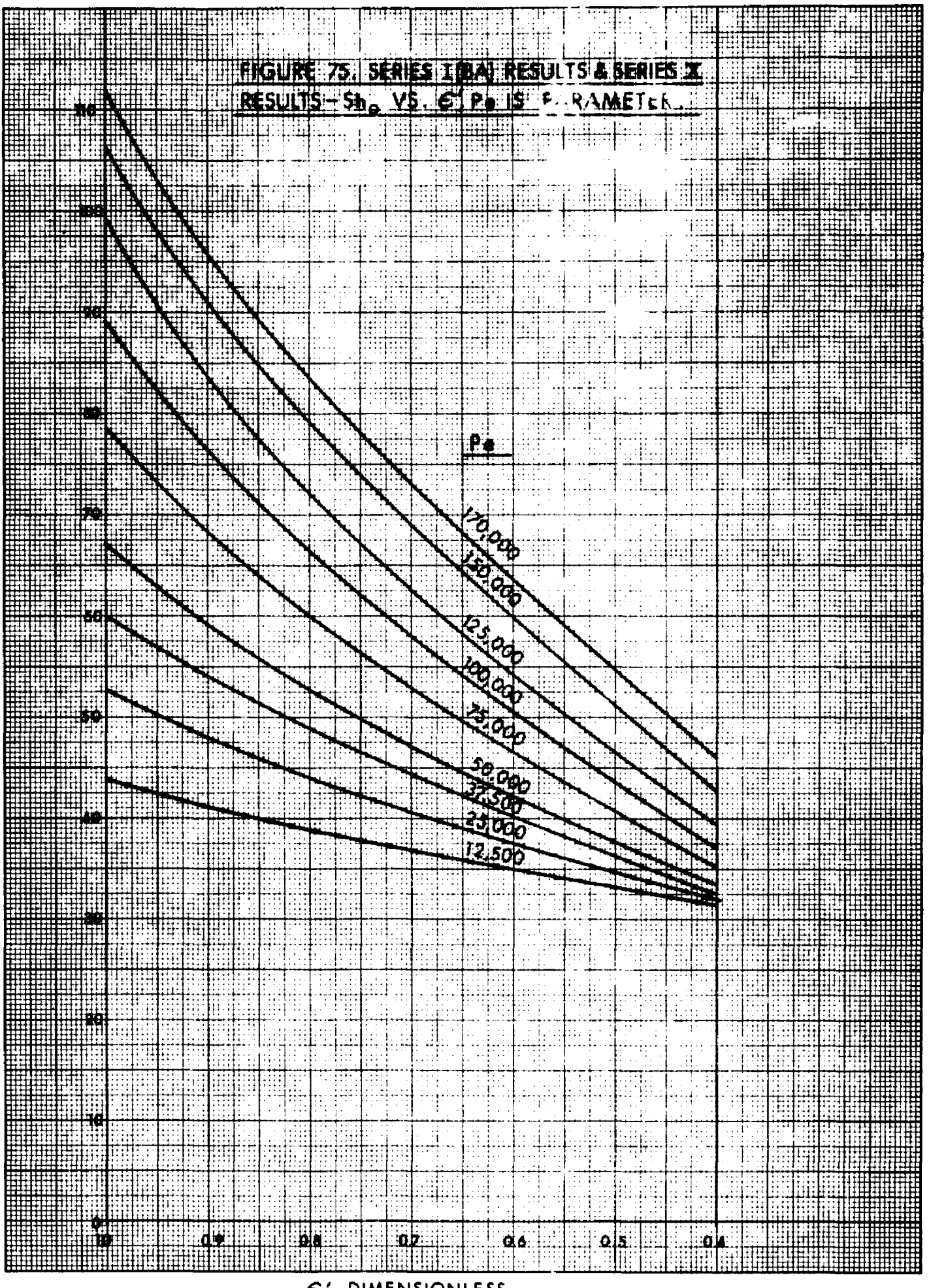

K+E 10 X 10 TO THE CENTIMETER 46 1513
MADE IN U.S.A.
KEUFFEL & ESSER CO.

FIGURE 76

COMPARISON OF BENZOIC ACID RESULTS

SERIES I, III, VII ($\epsilon' = 0.85$), & X ($\epsilon' = 0.85$) N_{Sh_o} VS. N_{P_e}

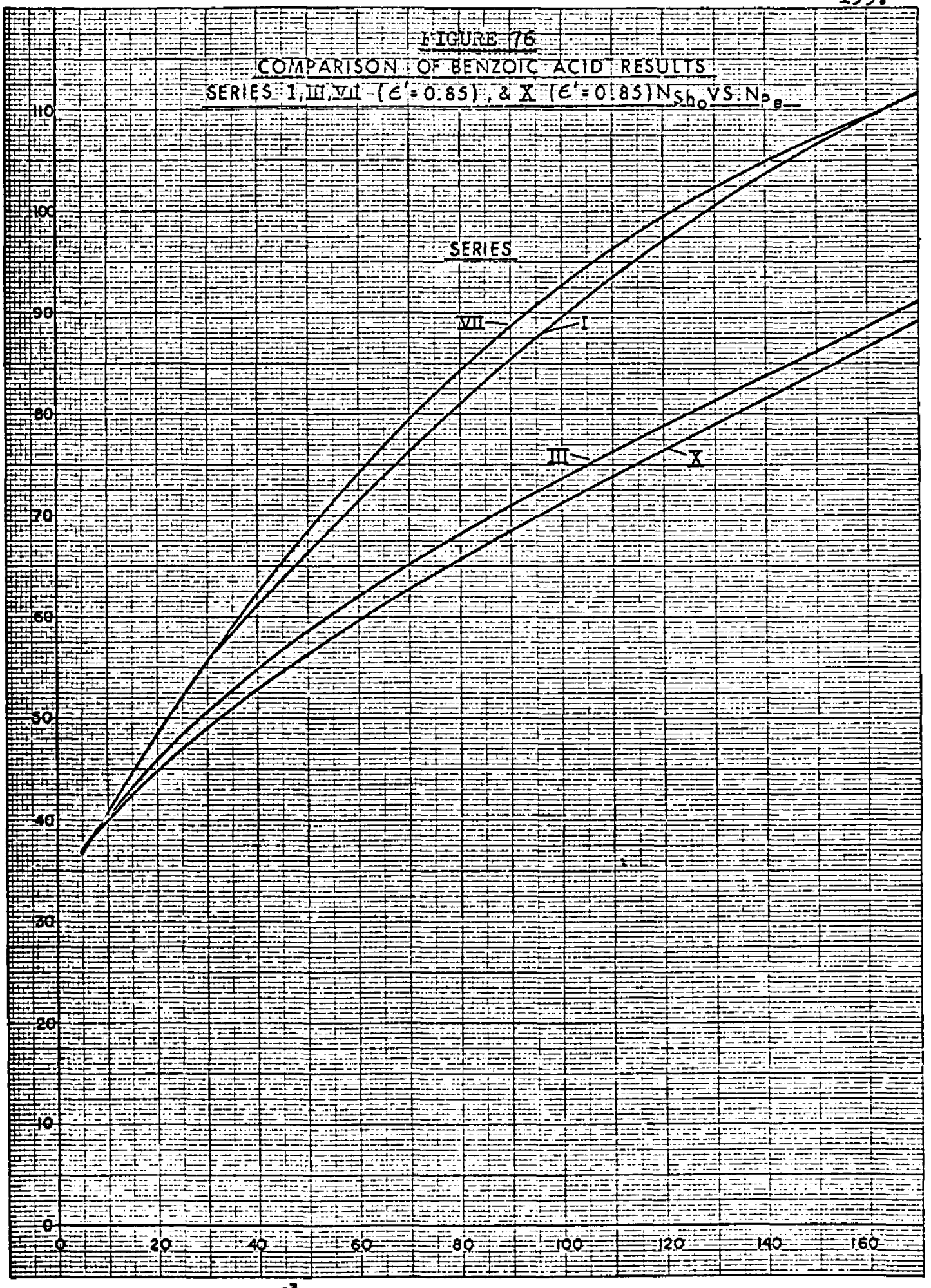

K·E 10 X 10 TO THE CENTIMETER 46 1513
10 X 25 CM. MADE IN U.S.A.
KEUFFEL & ESSER CO.

FIGURE 77

COMPARISON OF BENZOIC ACID RESULTS

SERIES I, II, VII ($\mathcal{C}'$=0.10) & X ($\mathcal{C}'$=0.40)

N_{Sh_o} VS. N_{Re}

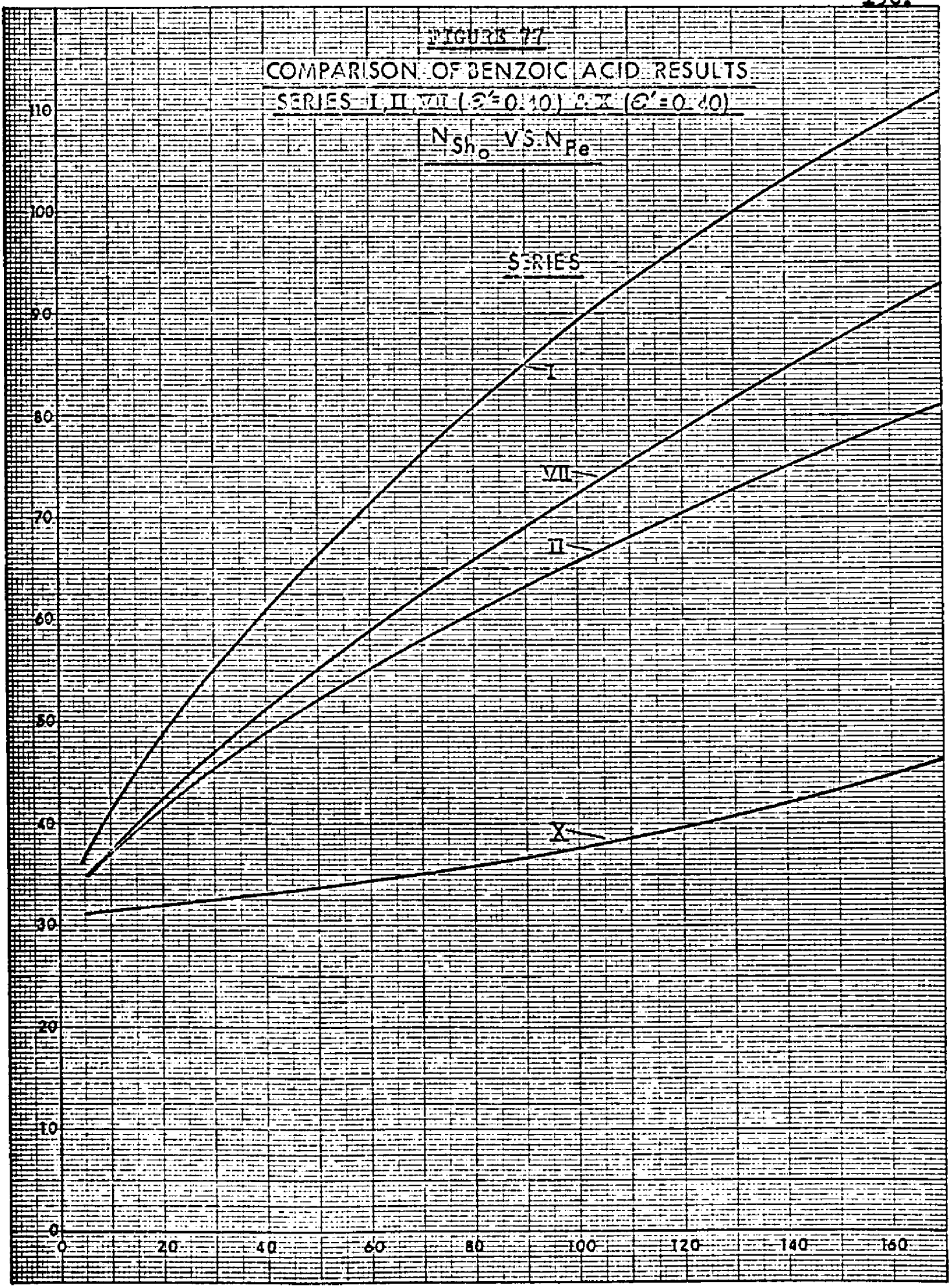

K•E 10 X 10 TO THE CENTIMETER 46 1513
18 X 25 CM.
KEUFFEL & ESSER CO.

Relationship Between Local and Overall Mass Transfer Rates for All Studies

It should be noted that, in all cases, the overall mass transfer rates obtained from the local Sherwood number profiles by graphical integration, using a planimeter, were within 10% of the overall Sherwood number based on the weight loss of the particles. This result is confirmed by inspection of Table XI. The average difference between Sh_o calculated by both methods is 3.33%.

TABLE XI. Comparison Between Overall Sherwood Numbers Calculated from Local Mass Transfer Profiles and Particle Weight Loss

Series No.	Solute	Re_p	Integrated Avg. Sh	Avg. Sh based on Wt. Loss	Percent Difference
I	BA	6	36.6	37.0	-2.05
		30	57.2	52.4	+9.18
		57	71.0	68.0	+4.44
		84	81.5	84.0	-3.00
		116	99.0	93.8	-5.50
		174	105.3	110.95	-5.50
	BN	5	15.1	14.5	+4.00
		32	28.7	27.1	+6.00
		77	48.0	45.8	+5.00
		106	39.8	39.2	+1.50
		133	50 9	50.1	+1.50
		159	62.2	58.7	+6.00
II	BA	6	33.5	35.6	-5.75
		30	40.7	42.4	-4.00
		85	59 7	61.1	-2.50
		167	75.5	75.8	-1.50
	BN	5	13.0	13.0	----
		29	24.1	23.8	+1.50
		56	31.6	31.3	+1.00
		114	41.1	40.7	+1.00
III	BA	5	36 2	35.9	+1.00
		54	58 4	61.7	-5.55
		108	69 3	69.3	----
		170	88.8	88.0	+1.00
	BN	28	24.4	23.8	+2.50
		80	32.2	30.8	+4.50
		141	54.1	53.6	+1.00
		177	58.7	56.1	+4.50

TABLE XI. Continued

Series No.	Solute	Re_p	Integrated Avg. Sh	Avg. Sh based on Wt. Loss	Percent Difference
V	BA	5	34.6	33.5	+3.00
		54	56.6	51.7	+9.50
		112	69.7	69.7	------
		171	82.4	81.6	+1.00
	BN	28	22.1	22.7	-2.50
		81	31.4	31.6	-0.05
		135	36.0	34.4	+4.50
		175	49.9	46.6	+7.00
VI	BA	6	37.0	38.4	-4.00
		58	52.2	55.9	-6.50
		167	86.9	81.6	+6.25
		120	78.6	79.0	-0.50
	BN	28	21.7	21.5	+1.00
		83	40.3	39.6	+2.00
		139	49.1	47.6	+3.00
VIII	BA	6	35.4	36.7	-3.50
		55	45.1	44.1	+2.00
		116	68.6	63.5	+8.00
		173	85.2	80.7	+5.50
	BN	27	18.0	17.2	+5.00
		133	32.0	29.5	+8.50
		140	43.6	41.2	+6.00
IX	BA	5	38.3	37.5	+2.00
		55	73.9	71.2	+3.50
		112	101.7	95.4	+7.00
		163	111.3	103.1	+8.00
	BN	28	25.7	24.5	+5.00
		79	47.1	45.2	+4.50
		136	57.5	54.1	+6.00

TABLE XI. Continued

Series No.	Solute	Re_p	ε	Integrated Avg. Sh	Avg. Sh Based on Wt. Loss	Percent Difference
VII	BA	5	0.85	37.7	36.3	+4.00
		56		69.4	68 2	+2.00
		109		91.9	92.5	-1.00
		171		112.8	108.4	-4.00
		6	0.73	35.2	35.5	-1.00
		49		74.2	75.2	-1.50
		109		95.7	95.5	———
		191		116.	113.2	+2.50
		6	0.40	33.6	34.2	-2.00
		54		56.6	53.7	+5.50
		167		96.0	93.0	+3.00
X	BA	6	0.85	37.1	37.4	———
		55		55.0	55.2	———
		175		88.0	87.7	———
		54	0.82	52.1	52.4	———
		112		72.0	71.4	———
		172		88.7	88.9	———
		5	0.40	32.6	31.6	+3.00
		56		35.5	33.4	+6.00
		118		37.6	38.6	-3.00
		175		43.1	45.0	-4.50

CONCLUSIONS AND RECOMMENDATIONS

Axial, radial, and combined axial-radial arrangements of inert spheres were used to investigate the effect of small numbers of particles on the local and overall mass transfer rates from a single sphere at low Reynolds numbers. Studies were made using two or three spheres axially oriented, seven spheres radially arranged in a single layer hexagon, three spheres in an axial-radial combination forming an equilateral triangle, and fourteen spheres in a two layer hexagonal array exhibiting a combined axial-radial arrangement. The following conclusions can be drawn based on the results of this work.

Single Sphere Studies

1. Separation does not appear to occur at a particle Reynolds number of 5. However, separation is quite striking at a Reynolds number of 25. The location of the separation ring is dependent upon Re_p. This dependence of separation on Reynolds number is in agreement with the results of previous investigators.

2. The mass transfer coefficient of benzoic acid is always greater than that of beta naphtholat the same Peclet number. Attempts to explain this based on considerations of differences in natural convection, driving force, and Schmidt number, did not succeed.

3. The overall mass transfer rate, in the Reynolds number range investigated, can be adequately represented either as a function of $Pe^{1/3}$ or $Re^{1/2}\,Sc^{1/3}$ in agreement with theoretical predictions.

Multiparticle System Studies

Axial Configurations

1. At points of contact between spheres minimum mass transfer rates occur.

2. As the separation between spheres increases the spheres have a smaller effect upon one another.

3. At a particle Reynolds number of 5 separation does not appear to occur. The occurrence of separation is dependent upon Re_p and as the Reynolds number increases the location of the separation ring shifts forward. The presence of inert spheres, directly in front of the test sphere, causes the separation ring to move back toward the rear stagnation point. Thus, with a sufficiently large number of spheres in an axial arrangement it is possible that separation may not occur until the particle Reynolds number is substantially increased.

4. The overall mass transfer rates found in all cases were less than those obtained for a single sphere at all particle Reynolds numbers investigated. This is in agreement with drag data for small numbers of spheres.

5. At low Peclet numbers, the number of inert spheres in the array has only a minor effect on the overall mass transfer process. Increasing Peclet number leads to an increasing dependence of the overall transfer rate on the number of inert particles.

6. The axial effect of the inert spheres appears to be due to area blockage as well as to a disturbance of the hydrodynamic flow profile around

the test sphere.

Equilateral Triangular Configurations

1. An open equilateral triangular arrangement of spheres gives local mass transfer profiles similar in appearance to those for single spheres. The more closed configuration results in a much smaller forward flow area with a minimum mass transfer rate occuring before 90° from the forward stagnation point. This greatly reduced forward flow area is due to the blockage effect caused by the close proximity of the inert spheres.

2. The overall Sherwood numbers for a closed equilateral triangular arrangement are smaller than for a single sphere at all Peclet numbers because of the area blockage effect. For an open triangular arrangement the overall Sherwood numbers are somewhat higher than for a single sphere. The more open arrangement begins to simulate the behavior of a large array of particles for which the Sherwood number is always higher than that for a single sphere.

3. At the same separation between particles an axially located particle has a more pronounced effect on a test sphere than a radially located one.

Hexagonal Configurations

1. Open single layer hexagonal configurations of particles give local mass transfer profiles similar to those obtained for single spheres and open equilateral triangular arrays. Single layer hexagonal arrays, in which the

inert spheres touch the test sphere, give much smaller mass transfer rates, showing the large effect that points of contact between spheres normal to the flow direction have on the mass transfer process.

2. At a Peclet number of 5,000, all single layer hexagonal arrangements give similar overall Sherwood number results. Thus, at this low Pe, geometry effects are minimal.

3. At Peclet numbers greater than 45,000, the single layer hexagon studies where the particles were separated by one diameter give Sh_o results higher than those for single spheres. For those single layer hexagon runs, where the particles were separated by one-half a diameter, the overall mass transfer results are greater than those obtained for single spheres up to a Peclet number of 150,000. Thus, slight separation begins to improve the overall Sherwood numbers and the beginnings of the multiparticle effect of higher Sh_o for all particle packings is seen.

4. Very close contact of particles in a single layer hexagon gives minimum overall mass transfer results because of the area blockage effect.

5. Two layer hexagonal arrays, at the same axial separation of particles as in the doublet and triplet studies, give similar mass transfer profiles. Thus, axial proximity has a much larger effect than radial proximity for small numbers of particles around the test sphere.

6. The area blockage effect leads to greatly reduced overall transfer rates for all two layer hexagonal geometries studied. The addition of more layers of particles should improve the overall mass transfer rate until it

becomes equal to and eventually exceeds that for a single sphere. This must occur since in actual multiparticle systems the Sherwood number has been shown to always be greater than that for a single sphere at all voidages.

Recommendations

1. The separation between two axially located particles, necessary for single sphere behavior, should be exactly determined.

2. Studies should be made with inert spheres placed behind the test sphere, since, it is believed that this arrangement will enhance the mass transfer process by creating turbulence in the wake area.

3. Additional work should be carried out in order to determine the size of the bed at which the overall transfer rate becomes identical to that for a single sphere and then surpasses it.

4. The effect of a larger number of particles on the location of the separation ring should be studied in order to determine whether particles will cause separation to be surpressed at low Reynolds numbers ($\lesssim 50$) as believed to be the case by Pfeffer and Happel.

5. The reasons for the difference in the mass transfer rates observed for the benzoic acid and beta naphthol systems should be further investigated by working with materials whose physical properties are different from those of the materials used in this study.

NOMENCLATURE

Symbol	Meaning	Units
a	- coefficient of density change per unit density, per unit of concentration of solute added	- dimensionless
A_p	- surface area of a particle	- $ft.^2$
BA	- benzoic acid	
BN	- beta naphthol (2 naphthol)	
c	- molar concentration	- $lb.\ moles/ft.^3$
C^*	- solute solubility at equilibrium	- $lbs./lb._{solution}$
C_p	- specific heat of fluid	- $Btu/lb.\ ^oF.$
ΔC	- concentration driving force	- $lbs./lb._{solution}$
$\mathcal{D}$, D_L	- diffusion coefficient	- $ft.^2/hr.$
d, d_c	- conduit diameter	- ft.
d_p, D_p	- particle diameter	- ft.
f	- area availability factor	- dimensionless
f	- Ergun friction factor defined by equation (24)	- dimensionless
f_{ox}	- drag on a body defined in equation (12)	- dimensionless
f_4'	- constant in equation (8)	- $radians^{-4}$
g_c	- gravity constant	- $32.2\ ft./sec.^2$
g_o'	- constant in equation (8)	- $radians^{-1}$
g_2'	- constant in equation (8)	- $radians^{-2}$
G	- mass rate of flow	- $lb./hr.\ ft.^2$

Symbol	Meaning	Units
G	- volumetric rate of flow	- GPM
Gr, N_{Gr}	- Grashof number = $d_p^3 \rho^2 g_c a \Delta c / \mu^2$	- dimensionless
h	- convective heat transfer coefficient	- Btu/hr. ft.^{2} ^oF.
j	- Colburn j factor	- dimensionless
jd	- mass transfer factor = Sh $Sc^{2/3}$/Re Sc	- dimensionless
j_E	- Ergun j factor defined by equation (24)	- dimensionless
jh	- heat transfer factor = Nu $Pr^{2/3}$ / Re Pr	- dimensionless
j_{α}	- modified Colburn j factor = j x	- dimensionless
k	- thermal conductivity of fluid	- Btu/ hr. ft. ^oF.
k_l	- convective mass transfer coefficient	- lbs. of sol'n / hr. x sq. ft.
k_{avg}, k_o	- average (or overall) convective mass transfer coefficient	- lbs. of sol'n / hr. x sq. ft.
k_L	- local convective mass transfer coefficient	- lbs. of sol'n / hr. x sq. ft.
K_c	- convective mass transfer coefficient	- ft./hr. or lbs. of sol'n / hr.x sq. ft.
L	- mass flow rate of liquid	- lbs./hr. ft.^{2}
m	- molecular weight	- lbs./lb. mole
M	- mass transfer group defined by equation (15)	- dimensionless
Nu, N_{Nu}	- Nusselt number = h d_p / k	- dimensionless
Nu_{avg}, Nu_o	- average (or overall) Nusselt number	- dimensionless

Symbol	Meaning	Units
Nu_L	- local Nusselt number	- dimensionless
Nu_o'	- Nusselt number at zero Reynolds number	- dimensionless
Pe, N_{Pe}	- Peclet number = Re x Sc	- dimensionless
Pr, N_{Pr}	- Prandtl number = $C_p \mu / k$	- dimensionless
r	- radial direction in a spherical coordinate system	- ft.
Re, Re_p N_{Re}, N_{Re_p}	- Reynolds number = $d_p V \rho / \mu$	- dimensionless
Re_m	- modified Reynolds number = $\sqrt{A_p}\ G / \mu (1 - \epsilon)$	- dimensionless
Re'	- modified Reynolds number = $\sqrt{A_p}\ G / \mu$	- dimensionless
Re_ϵ	- modified Reynolds number = Re / ϵ	- dimensionless
Sc, N_{Sc}	- Schmidt number = $\mu / \rho \mathcal{D}$	- dimensionless
Sh, Sh_{avg} Sh_o, N_{Sh_o}	- average (or overall) Sherwood number = $k_o d_p / \mathcal{D} \rho_f$	- dimensionless
Sh_L, N_{Sh_L}	- local Sherwood number = $k_L d_p / \mathcal{D} \rho_f$	- dimensionless
Sh_o'	- Sherwood number at zero Reynolds number	- dimensionless
t	- temperature	- ^oC.
t	- time	- hours
V	- superficial velocity of flow in a packed bed	- ft./sec.
V_∞	- main-stream velocity	- ft./sec.
W	- weight	- lbs.
$\mathcal{Z}$	- parameter describing the hydrodynamic conditions surrounding a particle, defined by equation (14)	- dimensionless

Greek Letters

Symbol	Meaning	Units
Δ	- change in value	
ϵ	- fractional void volume	- dimensionless
ϵ_d	- fractional void volume of dense packing	- dimensionless
ϵ_l	- fractional void volume of loose packing	- dimensionless
ϵ'	- pseudo fractional void volume	- dimensionless
ρ	- density	- lbs./ft.^{3}
ϑ	- angular position on the surface of a particle as measured from the forward stagnation point	- degrees
θ	- spherical angle in a spherical coordinate system	- radians
θ_{sep}	- location of the separation point (or ring)as measured from the forward stagnation point	- degrees
μ	- viscosity of fluid	- lbs./ft. sec.

Subscripts

Symbol	Meaning
f	- fluid property
g	- gas phase property
l	- liquid phase property
s	- solid or solute property

LITERATURE CITED

1. Acrivos, A., and Taylor, T. D., Physics of Fluids, 5, 387 (1962).

2. Allander, G., Trans. Royal Institute of Tech., Stockholm, 70, (1953).

3. Bar-Ilan, M., and Resnick, W., Ind. Eng. Chem., 49, 313 (1957).

4. Baumeister, E. B., and Bennett, C. O., A.I.Ch.E. Journal, 4, 69 (1958).

4a. Bird, R. B., Stewart, W.E., and Lightfoot, E.N., "Transport Phenomena", John Wiley & Sons, New York (1960).

5. Breiman, L., Norman Bridge Laboratory, California Institute of Tech., Rept. No. 2F-2 (1952).

6. Brenner, H., Chem. Eng. Sci., 18, 109 (1963).

7. Carberry, J. J., A.I.Ch.E. Journal, 6, 460 (1960).

8. Chu, J.D., Kalil, J., and Wetteroth, W.A., Chem. Eng. Prog. 49, 141 (1953).

9. Dryden, C.E., Strang, D.A., and Withrow, A.E., Chem. Eng. Prog., 49, 191 (1953).

10. Eichorn, J., and White, R.R., Chem. Eng. Prog., 48, Symposium Ser. No. 4, 11 (1952).

11. Ergun, S., Chem. Eng. Prog., 48, 227 (1952).

12. Friedlander, S.K., A.I.Ch.E. Journal, 3, 43 (1957).

13. Friedlander, S.K., A.I.Ch.E. Journal, 7, 347 (1961).

14. Frisch, H.L., J. Chem. Phys., 22, 123 (1954).

15. Frossling, N., Ger. Beit. Geophysik, 52. 170 (1938).

16. Frossling, N., Lunds Univ. Arsskr. N.F. AVD. 36. 4, (1940).

17. Fuchs, N., J. Phys. (U.S.S.R.), 6, 224 (1934).

18. Gaffney, B.W., and Drew, T.B., Ind. Eng. Chem., 42, 1120 (1950).

19. Gamson, B.W., Thodos, G., and Hougen, O.A., Trans. Am. Inst. Chem. Engrs., 39, 1 (1943).

20. Garner, F.H., and Grafton, R.W., Proc. Roy. Soc., A224, 64 (1954).

21. Garner, F.H., and Hoffman, J. M., A.I.Ch.E. Journal, 6, 579 (1960).

22. Garner, F.H., and Keey, R., Chem. Eng. Sci., 9, 119 (1958).

23. Garner, F.H., and Suckling, R.D., A.I.Ch.E. Journal, 4, 114 (1958).

24. Glaser, M.B., and Thodos, G., A.I.Ch.E. Journal, 4, 63 (1958).

25. Grafton, R.W., Chem. Eng., Sci., 18, 457 (1963).

26. Hobson, M., and Thodos, G., Chem. Eng. Prog., 45, 517 (1949).

27. Hobson, M., and Thodos, G., Chem. Eng. Prog., 47 370 (1951).

28. Hurt, P.M., Ind. Eng. Chem., 35, 522 (1943).

29. Illingworth, C.R., J. Fluid Mechanics, 7 , 442 (1960).

30. Kramers, H., Physica, 12, 61 (1946).

31. Kronig, R., and Bruijsten, J., Applied Scientific Research, 2, 439 (1951).

32. Kusik, C.L., and Happel, J., Ind. Eng. Chem. Fundamentals, 2, 163 (1962).

33. Langmuir, I., Phys. Rev., 12, 368 (1918).

34. Levich, V.G., "Physicochemical Hydrodynamics," Prentice Hall, New York, 1962.

35. Lochiel, A.C., and Calderbank, P.H., Chem. Eng. Sci., 19, 471 (1964).

36. Lof, G.O., and Hawley, R.W., Ind. Eng. Chem., 40, 1061 (1948).

37. McConnachie, J.T.L., and Thodos, G., A.I.Ch.E. Journal, 9, 60 (1963).

38. McCune, C.K., and Wilhelm, R.H., Ind. Eng. Chem., 41, 1124 (1949).

39. Nielson, A.E., J. Phys. Chem., 65, 46 (1961).

40. Pfeffer, R., Ind. Eng. Chem. Fundamentals, 3, 380 (1964).

41. Pfeffer, R., and Happel, J., A.I.Ch.E. Journal, 5, 605 (1964).

42. Pfeffer, R., and Huang, C.Y., "A Boundary Layer Model for Mass or Heat Transport in Multiparticle Systems at Low Reynolds Numbers", submitted to Ind. Eng. Chem. Fundamentals for publication (1964).

43. Ogiwara, J., Meteorological Society of Japan, 22, 127 (1944).

44. Ranz, W.E., and Marshall, W.R., Chem. Eng. Prog., 48, 141 (1952).

45. Resnick, W., and White, R.R., Chem. Eng. Prog., 48 Symposium Ser. No. 4, 11 (1952).

46. Rhodes, J.M., and Peebles, F.N., A.I.Ch.E. Journal, 11, 481 (1965).

47. Rowe, P.N., Claxton, K.T., and Lewis, J.B., United Kingdom Atomic Energy Authority, Chemical Engineering Division, AERE - R. 4674, Harwell (1964).

48. Rudenberg, R., Elekrotech. Z., 46, 1342 (1925).

49. Sen Gupta, A., and Thodos, G., Chem. Eng. Prog., 58, 58 (1962).

50. Sen Gupta, A., and Thodos, G., A.I.Ch.E. Journal, 8, 608 (1962).

51. Sen Gupta, A., and Thodos, G., 56th Annual Meeting A.I.Ch.E., Houston (1963).

52. Sen Gupta, A., and Thodos, G., A.I.Ch.E. Journal 9,751 (1963).

53. Steele, L.R., and Geankoplis, C.J., A.I.Ch.E. Journal, 5, 178 (1959).

54. Steinberger, R.L., and Treybal, R.E., A.I.Ch.E. Journal, 6, 227 (1960).

55. Suckling, R.D., Ph. D. Thesis, Univ. of Birmingham, England (1956).

56. Taecker, R.G. and Hougen O.A., Chem. Eng. Prog., 45 188 (1949).

57. Tang, Y.,Duncan, J., and Schweyer, H., NACA-TN 2867 (1953).

58. Thoenes, D., and Kramers, H. Chem. Eng. Sci., 8, 271 (1958).

59. Tomotika, S., A.R.C.R. & M., No. 1678 (1936).

60. Tomotika, S., and Aoi T., Quart. J. Mech. Appl. Math., 3, 140 (1950).

61. Wadsworth, J., Natl. Res. Council (Canada) Rept. MT-39, (Sept. 12, 1958).

62. Williamson, J.E., Bazaire, K.E., and Geankoplis, C.J., Ind. Eng. Chem. Fundamentals 2 126 (1963).

63. Wilson, E.J., and Geankoplis, C.J., Ind. Eng. Chem. Fundamentals, 5 9 (1966).

64. Yuge, T., Rept. Inst High Speed Mechanics of Tohoku Univ., 6, 143 (1956).

65. Yuge, T. Transactions A.S.M.E. 82, 214 (1960).

66. Zhitkavich, E.K., and Zabrodsky, S.S., "Model Investigation of Heat Transfer Between the Fluid and the Spherical Particle in Packings Under Atmospheric and Lower Pressures.", Heat and Mass Transfer Institute of the U.S.S.R. Academy of Sciences, Minsk, U.S.S.R.

ADDENDUM

It has recently come to the attention of the author that a possible explanation for the observed difference between the mass transfer coefficients for benzoic acid and beta naphthol (at the same value of $Re^{1/2}Sc^{1/3}$) may be due to differences in grain size of the cast spheres of these materials. It is well established that the chemical activity of metals at the grain boundaries is generally higher than that in the bulk of the individual grains. This phenomenon is used by metallurgists in order to examine the grain size and structure of metals, the grain boundaries being preferentially attacked by etching materials. The reason for the greater chemical activity of the boundaries between grains is due to the fact that the interface between grains represents a disordered structure rather than the ordered arrangement of atoms characteristic of the bulk of the grains.

The number and size of the grains present in a metallic solid are influenced by the rate of cooling of the material from the liquid state. The number and size of the grains further determine the amount of grain boundary present in the solid, smaller grains resulting in more grain boundaries. The grain size, being related to the rate of cooling of the material is also related to the thermal conductivity of the material. The nature of the boundary between grains should also be influenced by the crystal structure of the material. The granular nature of a solid in essence is related to the nucleation and growth process.

It is reasonable therefore to expect that the solidification of crystalline organic materials from the liquid state would behave in a manner quite analagous to that of metals. If the nature of the grains of the cast benzoic acid spheres is such that it will cause greater disorder at grain boundaries than that of the beta naphthol spheres, then it is possible that "grain dropping" of the benzoic acid may occur. That is, some benzoic acid grains could fall from the particle surface before they are completely dissolved. This would result in a greater solubility than the true value used in the data analysis and hence would result in a greater mass transfer coefficient.

In order to establish whether or not grain dropping may have occurred the surface roughness exhibited by the particles before and after exposure to the flow was examined microscopically. Photographic results of these tests are shown in Figure 78. The figure shows that the surface roughness of the benzoic acid particle has increased quite strikingly during the exposure to the water flow while the roughness of the beta naphthol particle has not changed to any apparent extent. These results imply that some grain dropping may be occurring in the benzoic acid-water system but is not occurring in the beta naphthol-water system.

It is also possible that the rate of grain dropping may be an increasing function of the particle Reynolds number so that with increasing flow the difference between the benzoic acid and beta naphthol mass transfer coefficients will increase.

FIGURE 78

RESULTS OF ROUGHNESS TESTS

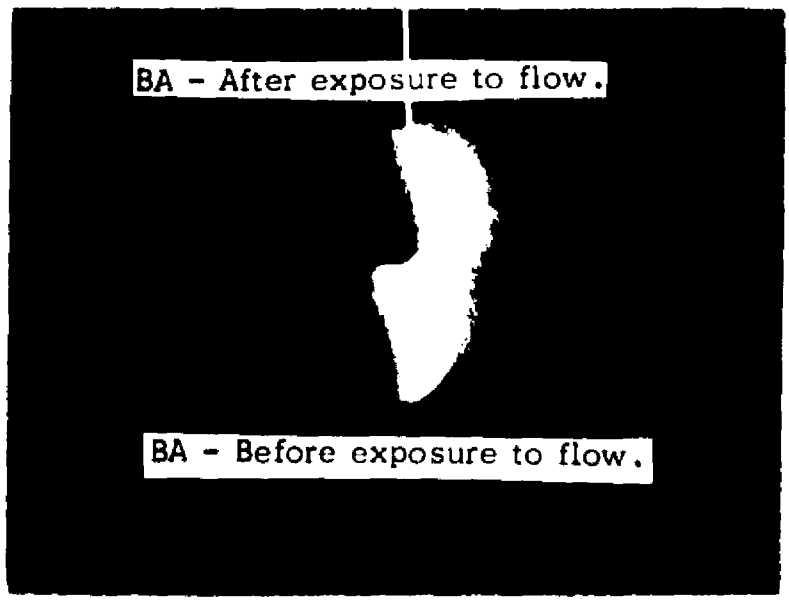

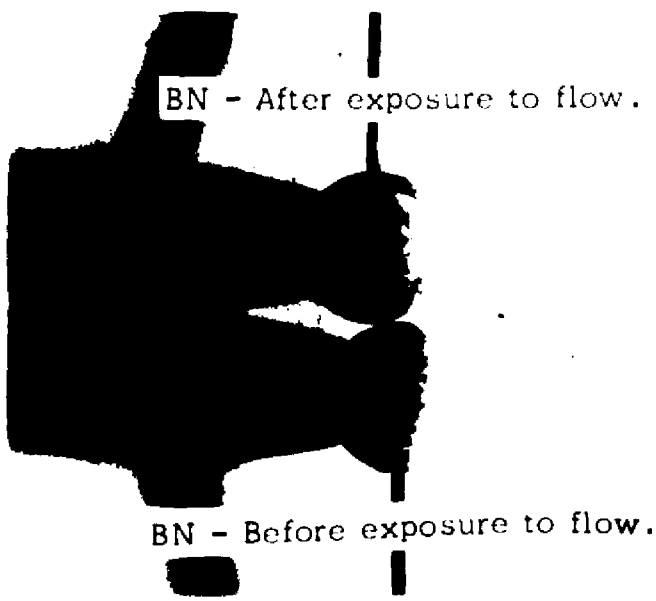

Steele and Geankoplis[53] while studying the effect of flux on mass transfer coefficients found that at zero driving force (in a saturated solution) the benzoic acid-water system showed measurable mass transfer rates. This phenomenon can be explained by the grain dropping theory even though it cannot be explained by mass transfer theory.

It is therefore concluded that the grain dropping phenomenon can satisfactorily explain the observed difference between the mass transfer coefficients of benzoic acid and those of beta naphthol. Further roughness tests, using highly polished surfaces of benzoic acid and beta naphthol before exposure to water flow, should be made to confirm the preliminary tests which were performed.

PRESENTATION AND PUBLICATION

A condensed version of this thesis was presented by the author at the 59th Annual Meeting of the A.I.Ch.E. in Detroit, Michigan during December, 1966. The condensed version has been accepted for publication, co-authored by the author and Professor Robert Pfeffer, in an A.I.Ch.E. Symposium Series volume entitled "Fundamental Research on Heat and Mass Transfer" edited by Professor William N. Gill. The publication will appear in print shortly.

VITA

The author attended the City College of New York and received his Bachelor's degree in Chemical Engineering in February, 1960. With the help of a research assistantship sponsored by the United States Air Force Office of Scientific Research, he continued his studies at New York University. He conducted research which led to his master's thesis, entitled "The Effects of Donor Compounds on the Thermal Decomposition of Aluminum Triethyl." In addition, he conducted process development studies for the Engineering Research Division. He received his Master of Chemical Engineering degree in 1964.

In September, 1962, the author returned to City College to pursue his graduate work, thus becoming the first doctoral student in the Chemical Engineering Department. His research was supported by the National Science Foundation and the City University of New York. During the spring of 1965, the author had the experience of teaching a Unit Operations Laboratory course at the City University. He is a member of both the American Institute of Chemical Engineers and the American Chemical Society.

In September, 1966, he accepted a position in the Development Department of Halcon International, Inc. He plans to reside with his wife in the metropolitan area and continue to be employed by this company.

APPENDIX

A. PHYSICAL PROPERTIES OF EXPERIMENTAL MATERIALS

The physical properties of the experimental materials used in this investigation are summarized in this section. Included are the density and viscosity of water and the equilibrium solubility, the diffusivity, and the Schmidt number of betanaphtholand benzoic acid in water. This information was obtained from the literature.

TABLE App I. Density of Water

Chemical Engineers' Handbook, Perry J. H., 3rd Edition, pg. 175, Table 45, McGraw-Hill, New York (1950).

Temp. °C.	Density g/cc	Temp. °C.	Density g/cc	Temp. °C.	Density g/cc
20.0	.9982323	20.1	.9982117	20.2	.9981909
20.3	.9981701	20.4	.9981490	20.5	.9981280
20.6	.9981068	20.7	.9980855	20.8	.9980641
20.9	.9980426	22.0	.9980210	21.1	.9979993
21.2	.9979775	21.3	.9979556	21.4	.9979335
21.5	.9979114	21.6	.9978892	21.7	.9978669
21.8	.9978444	21.9	.9978219	22.0	.9977993
22.1	.9977765	22.2	.9977537	22.3	.9977308
22.4	.9977077	22.5	.9976846	22.6	.9976613
22.7	.9976380	22.8	.9976145	22.9	.9975910
23.0	.9975674	23.1	.9975437	23.2	.9975198
23.3	.9974959	23.4	.9974718	23.5	.9974477
23.6	.9974235	23.7	.9973991	23.8	.9973747
23.9	.9973502	24.0	.9973256	24.1	.9973009
24.2	.9972760	24.3	.9972511	24.4	.9972261
24.5	.9972010	24.6	.9971758	24.7	.9971505
24.8	.9971250	24.9	.9970995	25.0	.9970739
25.1	.9970482	25.2	.9970225	25.3	.9969966
25.4	.9969706	25.5	.9969445	25.6	.9969184
25.7	.9968921	25.8	.9968657	25.9	.9968393
26.0	.9968128	26.1	.9967861	26.2	.9967594
26.3	.9967326	26.4	.9967057	26.5	.9966786
26.6	.9966515	26.7	.9966243	26.8	.9965970
26.9	.9965696	27.0	.9965421	27.1	.9965146
27.2	.9964869	27.3	.9964591	27.4	.9964313
27.5	.9964033	27.6	.9963753	27.7	.9963472
27.8	.9963190	27.9	.9962907	28.0	.9962623
28.1	.9962338	28.2	.9962052	28.3	.9961766
28.4	.9961478	28.5	.9961190	28.6	.9960901
28.7	.9960610	28.8	.9960319	28.9	.9960027
29.0	.9959735	29.1	.9959440	29.2	.9959146
29.3	.9958850	29.4	.9958554	29.5	.9958257
29.6	.9957958	29.7	.9957659	29.8	.9957359
29.9	.9957059	30.0	.9956756		

TABLE App II Viscosity of Water

Chemical Engineers' Handbook, Perry, J. H., 3rd Edition, pg. 374, Table 7, McGraw-Hill, New York (1950).

TEMPERATURE °C.	VISCOSITY CENTIPOISE
20	1.0050
21	0.9810
22	0.9579
23	0.9358
24	0.9142
25	0.8937
26	0.8737
27	0.8545
28	0.8360
29	0.8180
30	0.8007

FIGURE APP. 1

SOLUBILITY OF 2-NAPHTHOL IN WATER

(MOYLE, M.P. & TYNER, M., J. & E.C., 45, 1794 (1953))

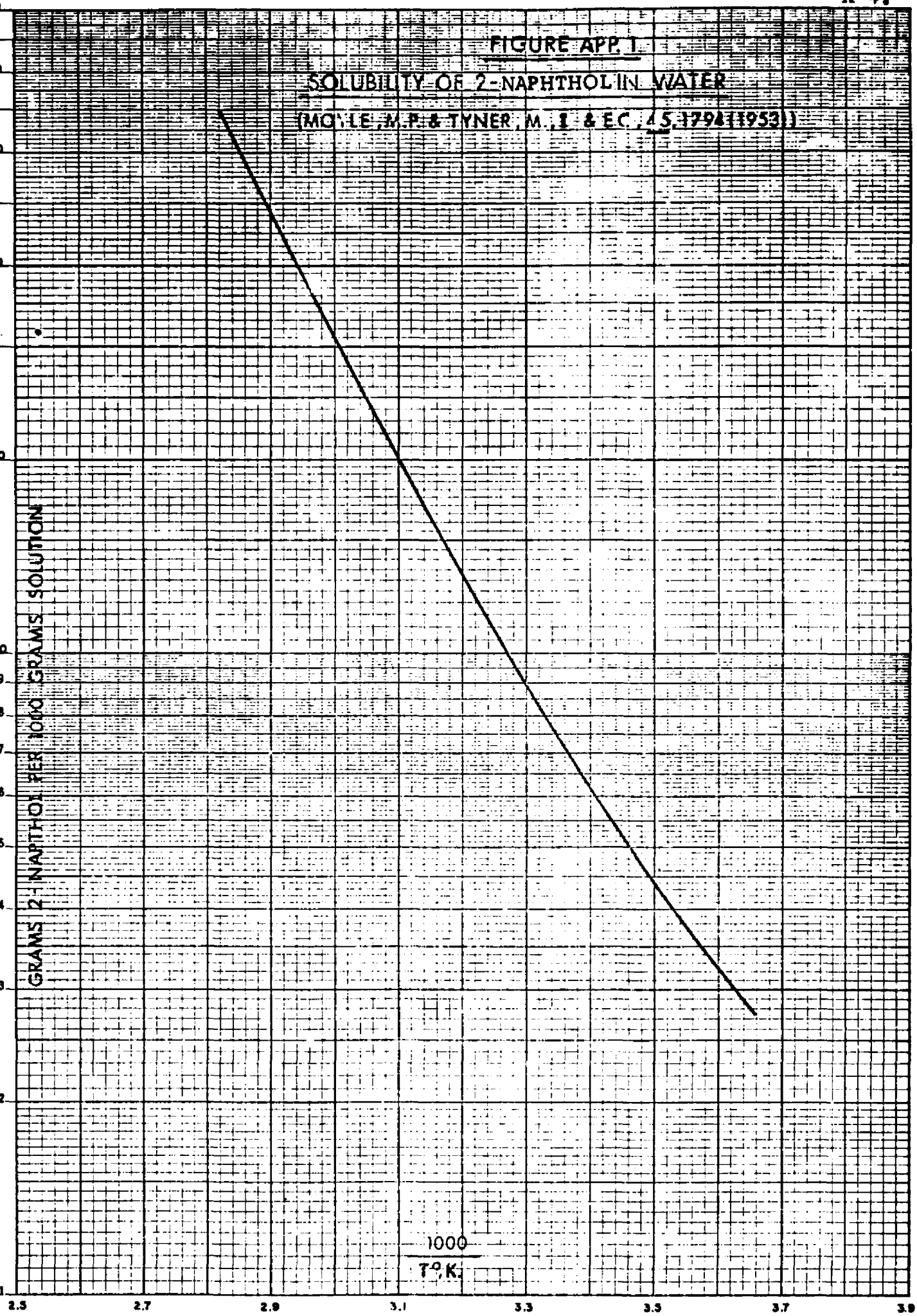

K•E SEMI-LOGARITHMIC 46 4973
2 CYCLES X 70 DIVISIONS MADE IN U.S.A.
KEUFFEL & ESSER CO.

FIGURE APP.2

DIFFUSIVITY OF 2-NAPHTHOL IN WATER

(MOYLE, M.P., & TYNER, M., I & EC, 45, 1794 (1953))

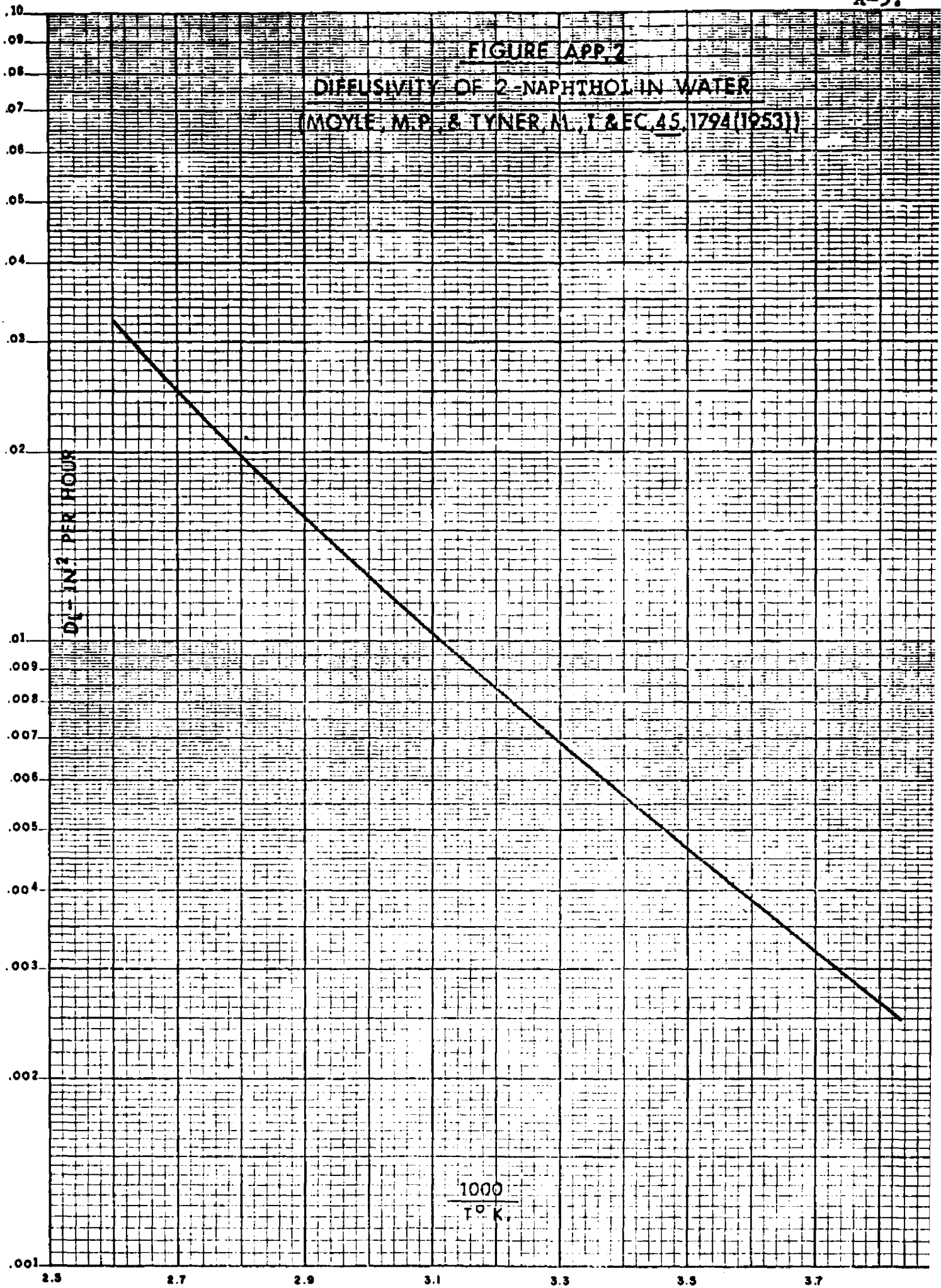

K&E SEMI-LOGARITHMIC 46 4973
2 CYCLES X 70 DIVISIONS
KEUFFEL & ESSER CO.

FIGURE APP 3

SCHMIDT NUMBER OF 2-NAPHTHOL IN WATER

(MOYLE, M.P. & TYNER, M., I & EC, 45, 1794 (1953))

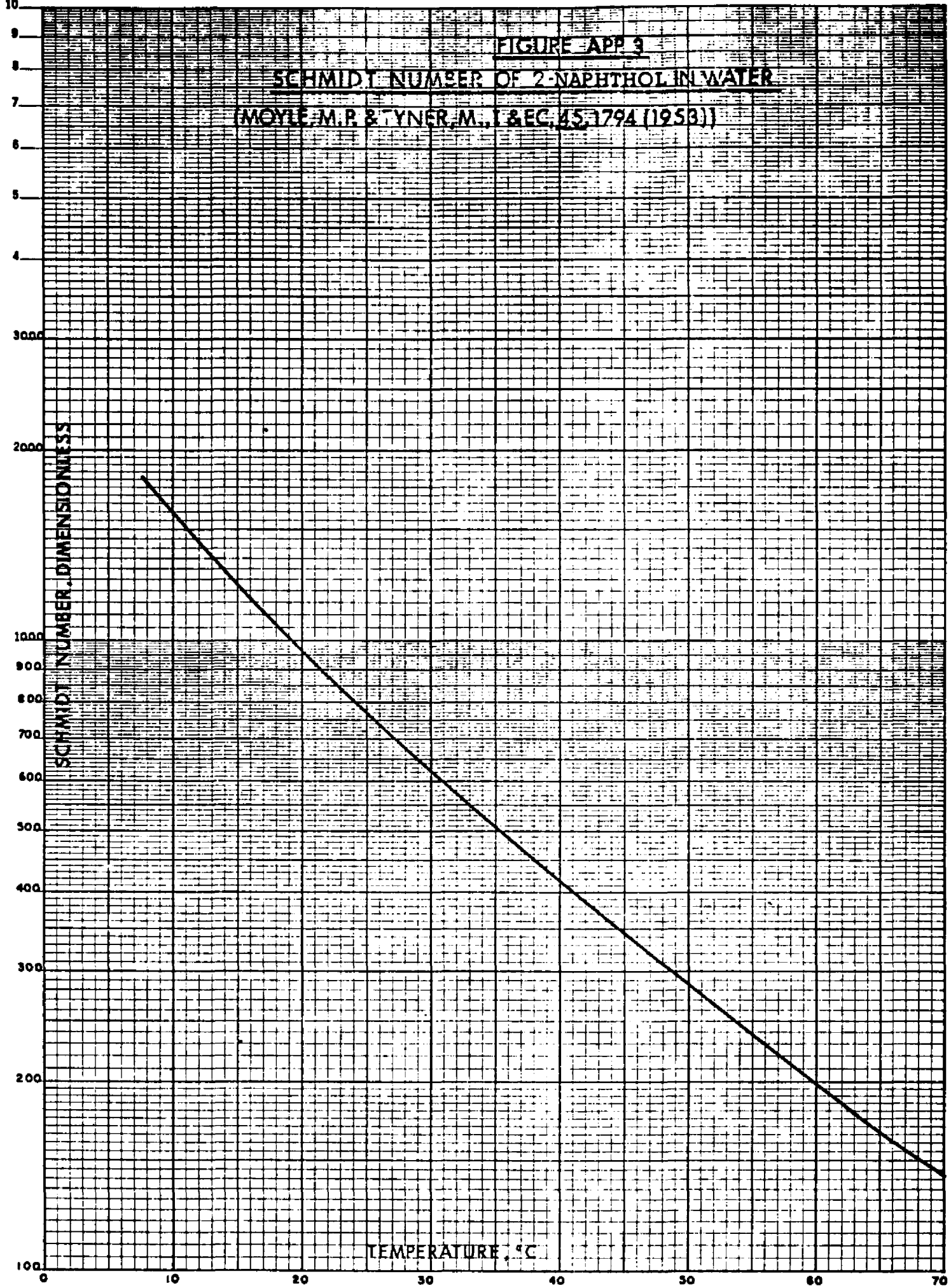

K•E SEMI-LOGARITHMIC 46 4973
2 CYCLES X 70 DIVISIONS MADE IN U.S.A.
KEUFFEL & ESSER CO.

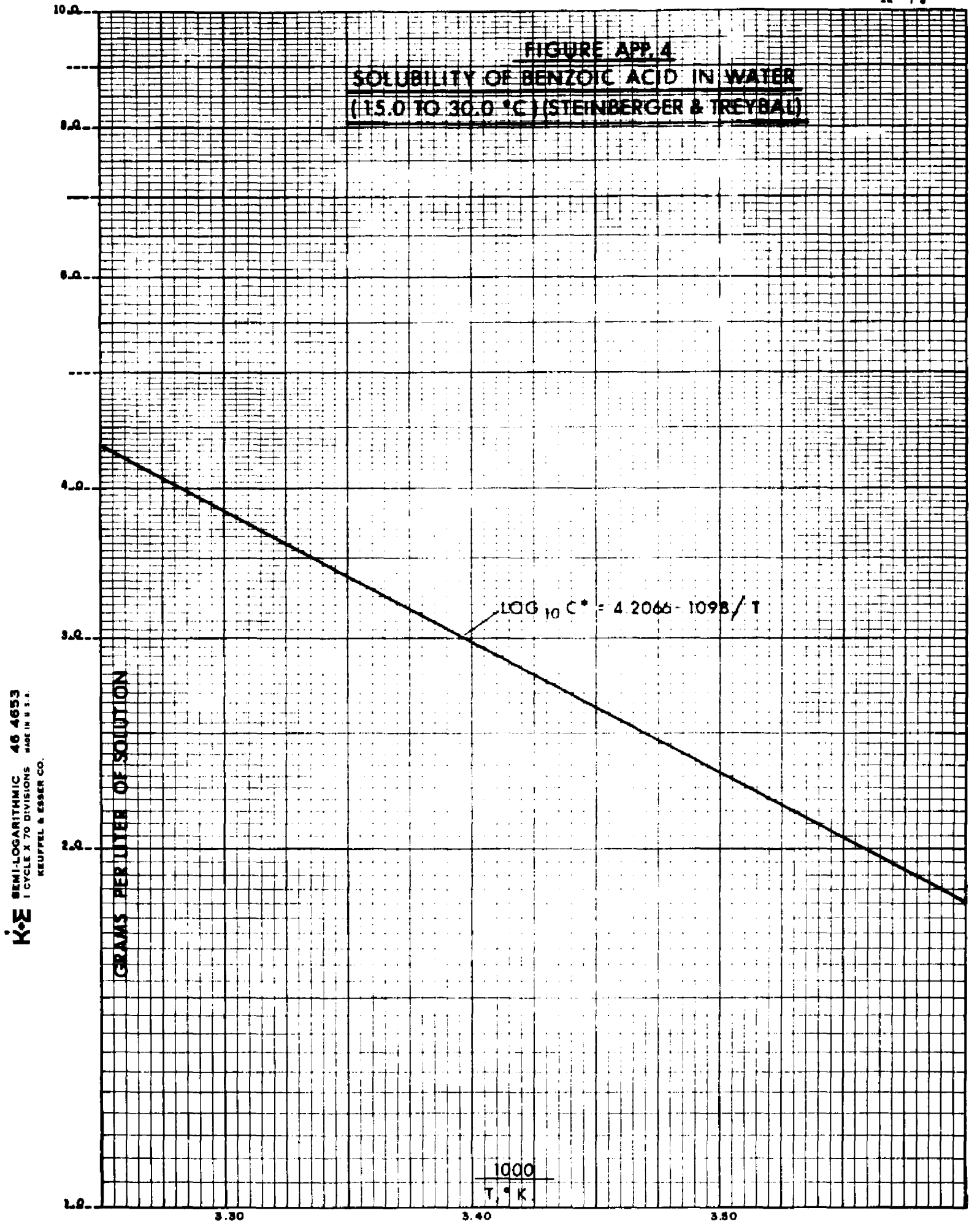
FIGURE APP.4
SOLUBILITY OF BENZOIC ACID IN WATER
(15.0 TO 30.0 °C) (STEINBERGER & TREYBAL)
LOG 10 C* = 4.2066 - 1098 / T
GRAMS PER LITER OF SOLUTION
10.0
8.0
6.0
4.0
3.0
2.0
1.0
3.30
3.40
3.50
1000 / T, °K
K&E 46 4653
SEMI-LOGARITHMIC
1 CYCLE X 70 DIVISIONS
KEUFFEL & ESSER CO.

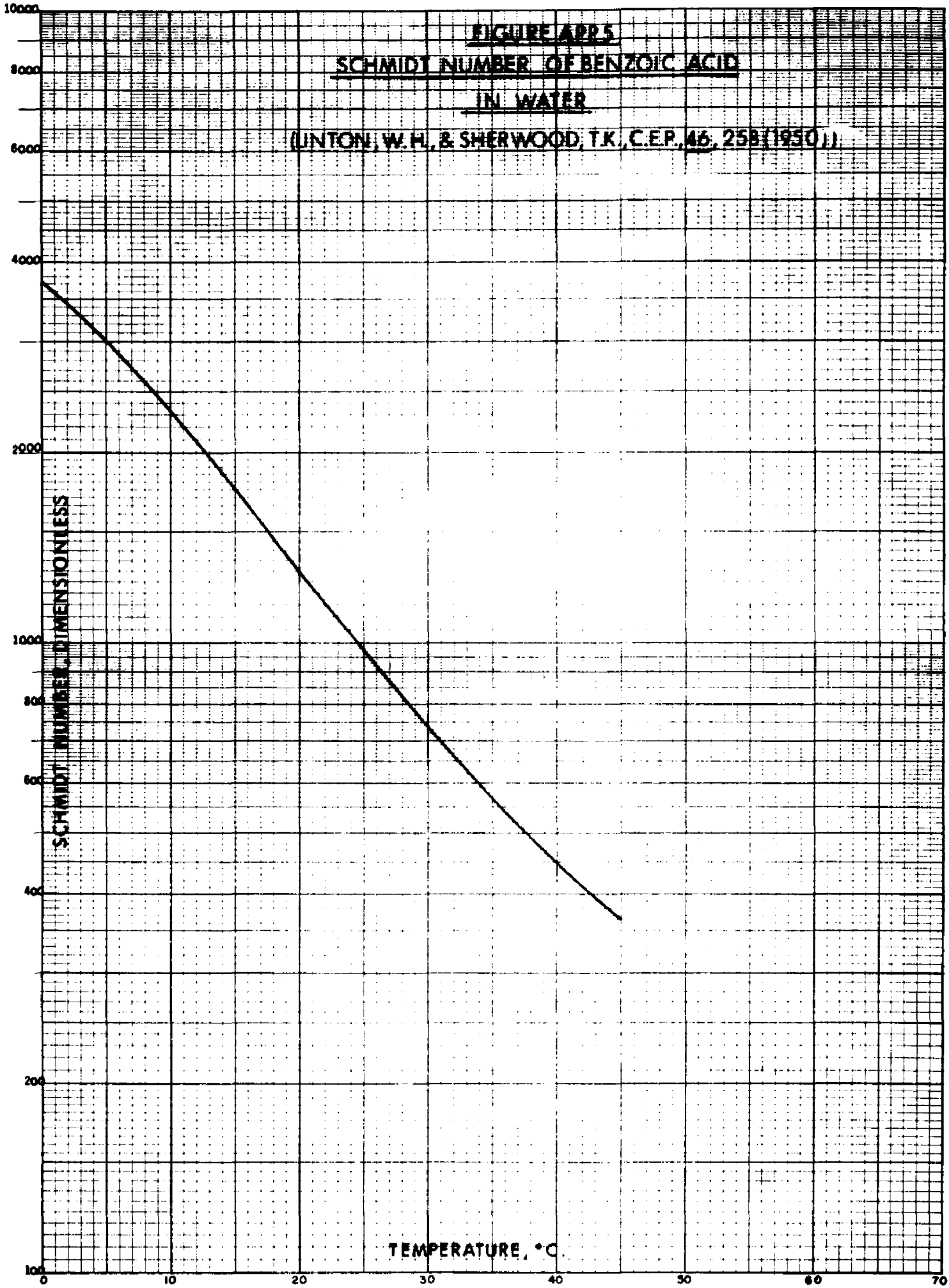

K+E SEMI-LOGARITHMIC 46 4973
2 CYCLES X 70 DIVISIONS MADE IN U.S.A.
KEUFFEL & ESSER CO.

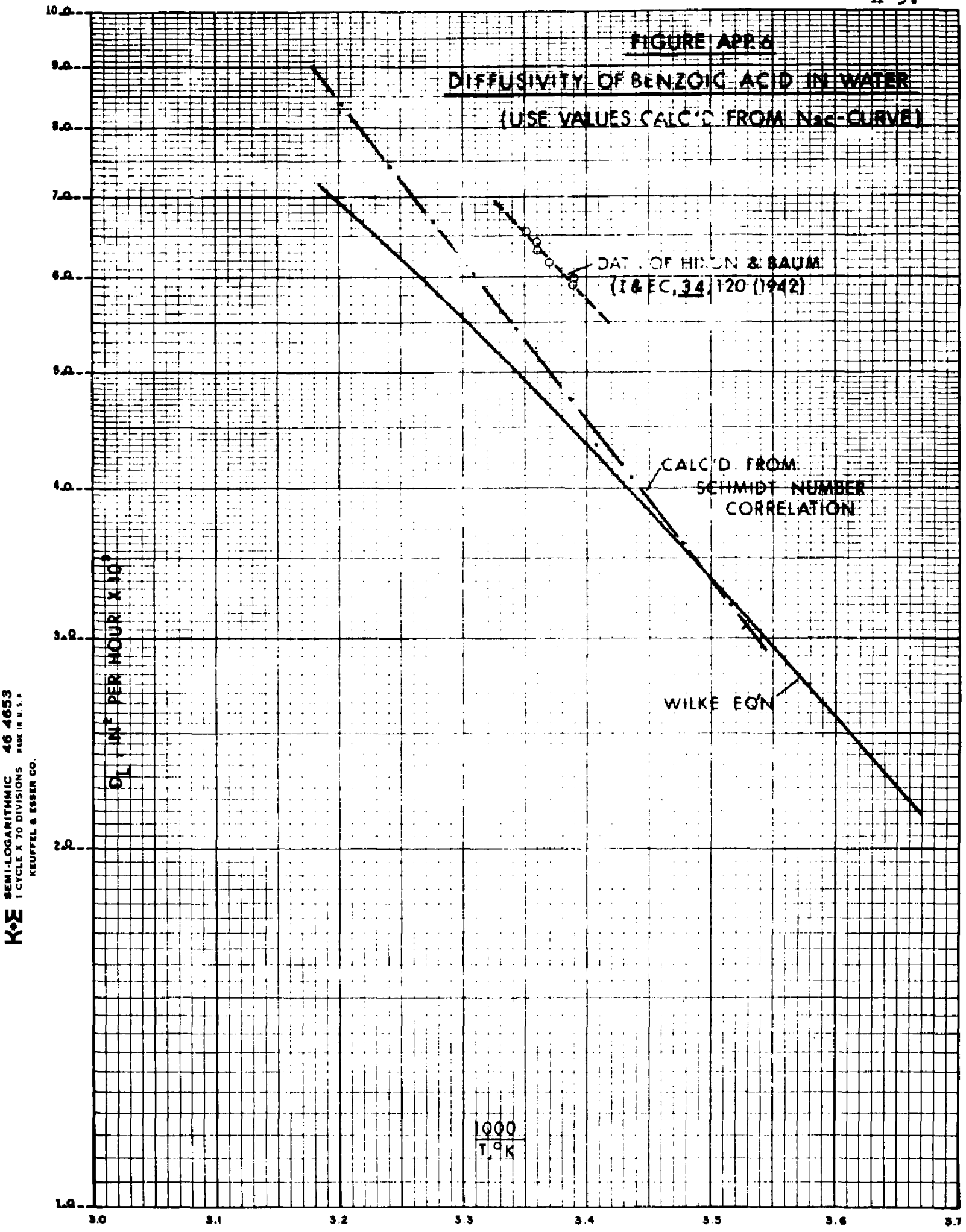
FIGURE APP.6
DIFFUSIVITY OF BENZOIC ACID IN WATER
(USE VALUES CALC'D FROM Nsc-CURVE)
DAT. OF HIXON & BAUM
(I & EC, 34, 120 (1942)
CALC'D FROM
SCHMIDT NUMBER
CORRELATION
WILKE EQN
D_L, IN² PER HOUR X 10⁵
10.0
9.0
8.0
7.0
6.0
5.0
4.0
3.0
2.0
1.0
3.0
3.1
3.2
3.3
3.4
3.5
3.6
3.7
1000/T, °K
K+E SEMI-LOGARITHMIC 46 4653
1 CYCLE X 70 DIVISIONS
KEUFFEL & ESSER CO.

B. GRASHOF NUMBER CALCULATION

The Grashof number, G_r, is a dimensionless group which arises from consideration of the conservation equations with no external flow. The fluid is put into motion due to convection currents which are caused by density differences. Therefore, G_r is a measure of the heat or mass transferred by natural convection. It was computed from the physical properties of the experimental materials and the physical dimensions of the particles used in this investigation.

The method of calculation and the values of the Grashof number, as a function of temperature, for the systems studied are summarized and presented in this section.

The Grashof number was calculated as follows:

$$G_r = \frac{D_p^3 \rho^2 g_c a \Delta c}{\mu^2} \qquad (B.1)$$

where

a = The coefficient of density change per unit density, per unit of concentration of solute added, dimensionless.

Δc = Concentration driving force, lbs. of solute per lb. of solution.

D_p = Particle diameter, ft.

g_c = Gravity constant, ft./sec.^{2}

ρ = Fluid density, lbs./ft.^{3}

μ = Fluid viscosity, lbs./ft.-sec.

For this investigation

$$a = 1.0$$

$$\Delta c = C^*$$

Therefore

$$Gr = \frac{D_p^3 \rho^2 g_c C^*}{\mu^2} \qquad (B.2)$$

with

$$D_p = .0417 \text{ ft.}$$

$$g_c = 32.2 \text{ ft./sec.}^2$$

The physical properties C^*, ρ and μ were known as a function of temperature. Table App. III summarizes the results of the calculation of Gr.

Now let us calculate the Sherwood number at zero Re for these two systems, according to the correlation for natural convection of Steinberger and Treybal, to be expected for the present single sphere studies.

Benzoic Acid Runs

$$t_{avg} = 25.8^{\circ}C.$$

$$Sc_{avg} = 917.4$$

$$Gr = 8.803 \times 10^4$$

$$Sc \times Gr = 8.09 \times 10^7$$

$$Sh'_o = 2 + 0.569 (8.09 \times 10^7)^{1/4}$$

$$Sh'_o = 56$$

TABLE App. III. Grashof Numbers for Benzoic Acid and Beta Naphthol as a Function of Temperature

Benzoic Acid		Beta Naphthol	
t °C.	$Gr \times 10^{-4}$	t °C.	$Gr \times 10^{-4}$
20.0	5.771	20.0	1.194
21.0	6.270	21.0	1.306
22.0	6.789	22.0	1.424
23.0	7.099	23.0	1.534
24.0	7.680	24.0	1.668
25.0	8.283	25.0	1.807
26.0	8.908	26.0	1.952
27.0	9.864	27.0	2.192
28.0	10.582	28.0	2.388
29.0	11.362	29.0	2.571
30.0	11.856	30.0	2.808

FIGURE APP.

G_r VS. t FOR BENZOIC ACID-WATER AND BETA-NAPHTHOL-WATER SYSTEM.

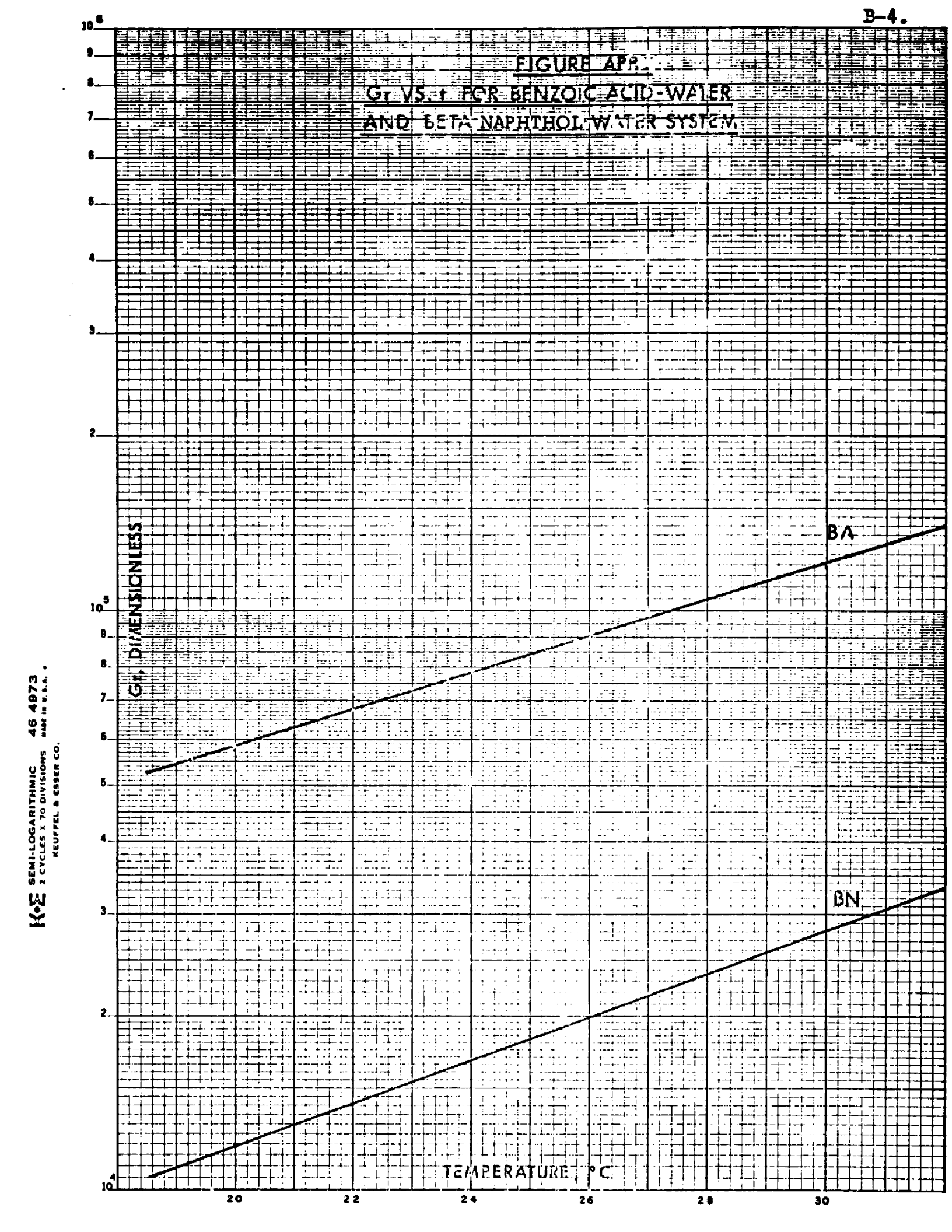

K•E SEMI-LOGARITHMIC 46 4973
2 CYCLES X 70 DIVISIONS
KEUFFEL & ESSER CO.

Beta Naphthol Runs

$t_{avg} = 22.0^{\circ}C.$

$Sc_{avg} = 908$

$Gr = 14.24 \times 10^{3}$

$Sc \times Gr = 1.295 \times 10^{7}$

$Sh'_{o} = 2 + .569 (1.295 \times 10^{7})^{1/4}$

$Sh'_{o} = 36$

C. ROTAMETER CALIBRATION

The Fischer-Porter flow meters were calibrated by establishing a constant flow rate in the loop (at constant temperature). The effluent water was collected for a time interval measured by an electronic stopwatch capable of being read to $\pm$ 0.2 seconds. Weighings were carried out on a scale capable of being read to $\pm$ 0.25 pounds. In order to minimize errors, weights were determined by difference.

According to this procedure, the actual flow rate at a given rotameter setting was obtained from the following equation

$$G = \frac{W \alpha}{\rho t} \qquad (C.1)$$

where

G = the actual volumetric flow rate, $\frac{\text{gal.}}{\text{min.}}$

t = the collection time, seconds

ρ = the fluid density, lbs./gal.

α = conversion factor, 60 sec./min.

An analysis of equation (C.1) shows that the relative error in each measurement of the flow rate was

$$\frac{dG}{G} = \frac{dW}{W} + \frac{dt}{t} + \frac{d\rho}{\rho} \qquad (C.2)$$

where

dW = the error in W, ± 0.25 lbs.

dt = the error in t, ± 0.2 seconds

$d\rho$ = the error in ρ, $\pm 1 \times 10^{-5} \frac{\text{grams}}{\text{cc}}$

The percent relative error in the measured flow rate was then found to be $100\ (dG/G)$.

The data obtained and the error analysis resulting from the calibration of the low flow range rotameter are given in Table App. IV. The percent relative error in this calibration procedure was between $\pm 0.980\%$ and $\pm 1.183\%$. The standard least squares technique was used to correlate this data with the result that

$$y = -0.130x^2 + 1.094x - 0.010 \qquad \text{(C.3)}$$

where

y = the actual flow rate, gal./min.

x = the rotameter setting, gal./min.

The standard deviation in this correlation was 1.15×10^{-4} and the average deviation was 3.7×10^{-4}.

The data obtained and the error analysis resulting from calibration of the high flow range rotameter are presented in Table App. V. The percent relative error in this procedure was between $\pm 1.056\%$ and $\pm 1.358\%$. Standard

TABLE App. IV. Calibration Data - Low Flow Range Rotameter

Rotameter Setting	Water Temperature	W	t	ρ	G	$\frac{dW}{W}$	$\frac{dt}{t}$	$\frac{d\rho}{\rho}$	$\frac{dG}{G}$
GPM	$^{o}C.$	lbs.	seconds	lbs/gal	GPM				
0.05	20.3	21.25	3599.2	8.34	0.042	.01176	.00006	.00001	.01183
0.10	20.3	24.60	1800.4	8.34	0.098	.01016	.00011	.00001	.01028
0.15	20.3	25.00	1200.2	8.34	0.150	.01000	.00017	.00001	.01018
0.20	20.3	25.25	899.2	8.34	0.202	.00990	.00022	.00001	.01013
0.25	20.3	25.00	720.0	8.34	0.250	.01000	.00028	.00001	.01029
0.30	20.3	25.50	600.1	8.34	0.306	.00980	.00033	.00001	.01014
0.35	20.3	25.50	522.5	8.34	0.351	.00980	.00038	.00001	.01019
0.40	20.3	25.40	449.5	8.34	0.407	.00984	.00044	.00001	.01029
0.40	20.3	25.50	451.5	8.34	0.406	.00980	.00044	.00001	.01025
0.35	20.3	25.625	519.8	8.34	0.355	.00977	.00038	.00001	.01016
0.30	20.3	25.75	601.6	8.34	0.308	.00971	.00033	.00001	.01005
0.25	20.3	25.50	722.1	8.34	0.254	.00980	.00028	.00001	.01009
0.20	20.3	25.50	901.2	8.34	0.204	.00980	.00022	.00001	.01003
0.15	20.3	25.375	1200.7	8.34	0.152	.00985	.00017	.00001	.01003
0.10	20.3	25.25	1800.9	8.34	0.101	.00990	.00011	.00001	.01002
0.05	20.3	21.25	3600.2	8.34	0.042	.01176	.00006	.00001	.01183
0.05	20.3	21.60	3599.2	8.34	0.043	.01157	.00006	.00001	.01164
0.10	20.3	25.20	1800.2	8.34	0.101	.00992	.00011	.00001	.01004
0.15	20.3	25.45	1199.9	8.34	0.153	.00982	.00017	.00001	.01000
0.20	20.3	25.50	900.4	8.34	0.205	.00977	.00022	.00001	.01000
0.25	20.3	25.50	720.5	8.34	0.255	.00980	.00028	.00001	.01009
0.30	20.3	25.50	600.4	8.34	0.306	.00980	.00033	.00001	.01014
0.35	20.3	25.75	518.4	8.34	0.357	.00971	.00039	.00001	.01011
0.40	20.3	25.50	450.5	8.34	0.407	.00980	.00044	.00001	.01025
0.075	20.3	25.75	2551.5	8.34	0.073	.00971	.00008	.00001	.00980
0.375	20.3	25.75	482.0	8.34	0.384	.00971	.00042	.00001	.01014
0.325	20.3	25.75	555.7	8.34	0.333	.00971	.00036	.00001	.01008
0.275	20.3	25.75	656.7	8.34	0.282	.00971	.00031	.00001	.01003
0.225	20.3	25.625	801.8	8.34	0.230	.00976	.00025	.00001	.01002

TABLE App. V. Calibration Data - High Flow Range Rotameter

Rotameter Setting GPM	Water Temperature °C	W lbs.	t seconds	ρ lbs/gal.	G GPM	$\frac{dW}{W}$	$\frac{dt}{t}$	$\frac{d\rho}{\rho}$	$\frac{dG}{G}$
0.5	20.3	24.0	351.2	8.34	0.478	.01000	.00055	.00001	.01056
1.0	20.3	24.75	181.5	8.34	0.981	.01010	.00071	.00001	.01082
1.5	20.3	24.625	120.9	8.34	1.465	.01015	.00165	.00001	.01181
2.0	20.3	24.625	91.2	8.34	1.943	.01015	.00219	.00001	.01235
2.5	20.3	25.125	74.3	8.34	2.433	.00995	.00269	.00001	.01265
3.0	20.3	24.500	61.0	8.34	2.889	.01020	.00328	.00001	.01349
3.0	20.3	24.500	61.0	8.34	2.889	.01020	.00328	.00001	.01349
2.5	20.3	24.500	72.3	8.34	2.438	.01020	.00277	.00001	.01298
2.0	20.3	24.750	90.7	8.34	1.963	.01010	.00221	.00001	.01232
1.5	20.3	24.800	120.6	8.34	1.479	.01008	.00166	.00001	.01175
1.0	20.3	25.000	181.2	8.34	0.993	.01000	.00110	.00001	.01111
0.5	20.3	24.750	351.4	8.34	0.493	.01010	.00055	.00001	.01056
0.5	20.3	24.800	352.3	8.34	0.492	.01008	.00055	.00001	.01064
1.0	20.3	25.000	181.1	8.34	0.993	.01000	.00110	.00001	.01111
1.5	20.3	26.750	130.7	8.34	1.472	.00935	.00153	.00001	.01089
2.0	20.3	24.750	90.9	8.34	1.959	.01010	.00220	.00001	.01231
2.5	20.3	24.750	73.3	8.34	2.429	.01010	.00273	.00001	.01284
3.0	20.3	24.400	60.2	8.34	2.916	.01025	.00332	.00001	.01358

least squares analysis of this data resulted in the following correlating equation.

$$y = 0.964x + 0.019 \qquad (C.4)$$

where x and y were defined as for equation (C.3). The standard deviation in this correlation was 26.29×10^{-4} and the average deviation was 27.77×10^{-4}.

The average maximum error in the calibration of the low flow range meter was $\pm 0.74\%$ and that for the calibration of the high range flow meter was $\pm 0.55\%$.

D. DENSITY DETERMINATION DATA

In order to check the suitability of the particle preparation procedure as well as to establish the particle density for computational purposes it was necessary to determine the densities of the benzoic acid and beta naphthol spheres used in this investigation.

Since the two materials are slightly soluble in water it was necessary to modify the usual pycnometric procedure. Saturated solutions of both substances were used as the liquid medium for these determinations and their densities were established relative to distilled water by using a Westphal Balance. It was found that these solutions exhibited essentially the same density as water.

With these saturated solutions of known density available, the densities of the solid particles were established by using a wide mouth solids pycnometer. The data obtained as a result of the density determinations are summarized in Table App. VI. The method of computation used to evaluate the density of the particles was as follows:

Let

V_s = Volume of solid, milliliters

W_1 = Weight of pycnometer + liquid, grams

W_2 = Weight of empty pycnometer, grams

W_3 = Weight of pycnometer + solid, grams

TABLE App. VI. Particle Density Data

Beta Naphthol

W_1 Grams	W_2 Grams	W_3 Grams	W_4 Grams	W_5 Grams	W_6 Grams	ρ_L gm/ml.	t °C.	V ml	ρ_s gm./ml.	$\frac{2}{W_3}$	$\frac{2}{W_2}$	$\frac{1}{W_1}$	$\frac{1}{W_4}$	$\frac{d\rho}{\rho_s}$
42.1583	34.7863	35.9480	42.2769	1.1617	1.0431	.9975674	23.0	0.9510	1.2088	.0555	.0575	.0237	.0237	.00002
41.5025	34.1947	35.3427	41.6714	1.1480	0.9791	.9975674	23.0	1.0238	1.1213	.0555	.0585	.0241	.0240	.00002
42.1775	34.7863	35.9444	42.3313	1.1581	1.0043	.9975674	23.0	0.9982	1.1602	.0556	.0575	.0237	.0236	.00002
41.5246	34.1949	35.3445	41.6535	1.1496	1.0207	.9975674	23.0	0.9821	1.1706	.0556	.0585	.0241	.0240	.00002
42.1746	34.7864	35.9980	42.3490	1.2116	1.0372	.9975674	23.0	0.9565	1.2535	.0556	.0575	.0237	.0235	.00002
41.5312	34.1949	35.4019	41.6530	1.2070	1.0852	.9975674	23.0	0.9237	1.3057	.0565	.0585	.0241	.0240	.00002
41.9789	34.6522	35.7985	42.1109	1.1464	1.0144	.9975674	23.0	0.9882	1.1601	.0559	.0577	.0238	.0238	.00002
41.3915	34.0642	35.2114	41.5172	1.1472	1.0315	.9975674	23.0	0.9718	1.1805	.0558	.0587	.0242	.0241	.00002
41.9790	34.6514	35.8576	42.1028	1.2052	1.0824	.9975674	23.0	0.9261	1.3025	.0558	.0577	.0238	.0238	.00002
41.3408	34.0643	35.2707	41.4621	1.2064	1.0851	.9975674	23.0	0.9238	1.3059	.0557	.0587	.0242	.0241	.00002
41.9921	34.6514	35.8005	42.1084	1.1491	1.0328	.9975674	23.0	0.9706	1.1839	.0559	.0577	.0238	.0238	.00002
41.3432	34.0643	35.2137	41.4608	1.1494	1.0318	.9975674	23.0	0.9715	1.1831	.0568	.0587	.0242	.0241	.00002

Benzoic Acid

41.3852	34.1257	35.3407	41.5105	1.2150	1.0897	.9975437	23.1	1.0924	1.1122	.0566	.0586	.0242	.0241	.00002
41.3852	34.1257	35.3373	41.5138	1.2116	1.0830	.9975437	23.1	1.0857	1.1160	.0566	.0585	.0242	.0241	.00002
41.3852	34.1257	35.3808	41.5253	1.2551	1.1150	.9975437	23.1	1.1528	1.0887	.0555	.0586	.0242	.0241	.00002
41.3852	34.1257	35.3400	41.5030	1.2143	1.0965	.9975437	23.1	1.0992	1.1047	.0566	.0586	.0242	.0241	.00002
41.3852	34.1257	35.3851	41.5213	1.2594	1.1233	.9975437	23.1	1.1261	1.1184	.0555	.0586	.0242	.0241	.00002
41.3852	34.1257	35.3524	41.5324	1.2367	1.0894	.9975437	23.1	1.0921	1.1324	.0556	.0586	.0242	.0241	.00002

W_4 = Weight of pycnometer + solid + liquid, grams

W_5 = Weight of solid, grams

W_6 = Weight of liquid displaced, grams

ρ_L = Density of liquid, grams/milliliter

ρ_s = Density of solid, grams/milliliter

Then

$$W_5 = W_3 - W_2 \tag{D.1}$$

$$W_6 = (W_2 - W_1) - (W_4 - W_3) \tag{D.2}$$

$$V_s = \frac{W_6}{\rho_L} \tag{D.3}$$

$$\rho_s = \frac{W_5}{V_s} \tag{D.4}$$

An error analysis of this procedure, assuming that the liquid density measurement was not subject to error, yielded the following equation for the relative error in the solid density.

$$\frac{d\rho_s}{\rho_s} = 2\frac{dW_3}{W_3} + 2\frac{dW_2}{W_2} + \frac{dW_1}{W_1} + \frac{dW_4}{W_4} \tag{D.5}$$

Since the weighings were made on an analytical balance, the possible deviation in any measurement was ± 0.0001 grams.

Therefore

$$\frac{d\rho_s}{\rho_s} = 10^{-4}\left[\frac{2}{W_3} + \frac{2}{W_2} + \frac{1}{W_1} + \frac{1}{W_4}\right] \tag{D.6}$$

The percent relative error, E, was then obtained by the following relation

$$E = \left(\frac{d\rho_s}{\rho_s}\right) 100 = 10^{-2}\left[\frac{2}{W_3} + \frac{2}{W_2} + \frac{1}{W_1} + \frac{1}{W_4}\right] \qquad (D.7)$$

This procedure did not permit taking into account the effects of air buoyancy or adsorped air in the particles. However, buoyancy effects were small and even minimized by weighing by difference. The effect of adsorped air was also small and further minimized by handling all the particles in the same manner.

It was thus established that the density of the benzoic acid particles was 1.1121 grams/ml. with a standard deviation of $\pm$0.0146 grams/ml., an average deviation of $\pm$ 0.0102 grams/ml., a probable error of $\pm$0.0099 grams/ml., and a percent relative error of $\pm$0.002%.

The beta naphthol particles were found to have a density of 1.2114 grams /ml. with a standard deviation of $\pm$0.0644 grams/ml., an average deviation of $\pm$0.0538 grams/ml., a probable error of $\pm$0.0435 grams/ml., and a relative error of $\pm$0.002%.

E. VIBRATIONAL CONSIDERATIONS

If a pulse with the same fundamental frequency as the natural frequency of the sphere support system was present in the flow system, the support would vibrate severely, approaching a condition of resonance. This vibration would eventually decay, but until it did it might have caused a serious error in the results of the present investigation. It was therefore necessary to establish the lowest normal mode of free vibration of the particle mounting system shown in Figure App. 8-a.

The system was simplified to a horizontal beam as shown in Figure App. 8-b. The deflection of this simplified unit was determined for the system under inertia loading. The entire structure was represented as a cantilever beam loaded as shown in Figure App. 8-c. The loads on the beam are shown as P_L and P_f/L where

P_L = Weight of the spherical particle and its mounting rod, lbs.

$\frac{\Delta P_f}{L}$ = Weight of the brass rod per unit length, lbs./in.

The weight of the 316 stainless steel rod used was computed from its volume and density. The rod was 2.875 inches long X 0.063 inches O.D. X 0.020 inches I.D. and its density was 0.283 lbs./in.^{3} [Mechanics of Materials", Higdon, Ohlsen, and Stiles, John Wiley & Sons, New York (1962)]. Accordingly, its weight was found to be 22.8 X 10^{-4} lbs. The weight of a 1/2 inch diameter spherical particle of either benzoic acid or beta naphthol was between 29.0 X 10^{-4} and 30.0 X 10^{-4} lbs. It was

FIGURE APP. 8

SIMPLIFICATION OF SPHERE SUPPORT SYSTEM FOR VIBRATION CALCULATIONS

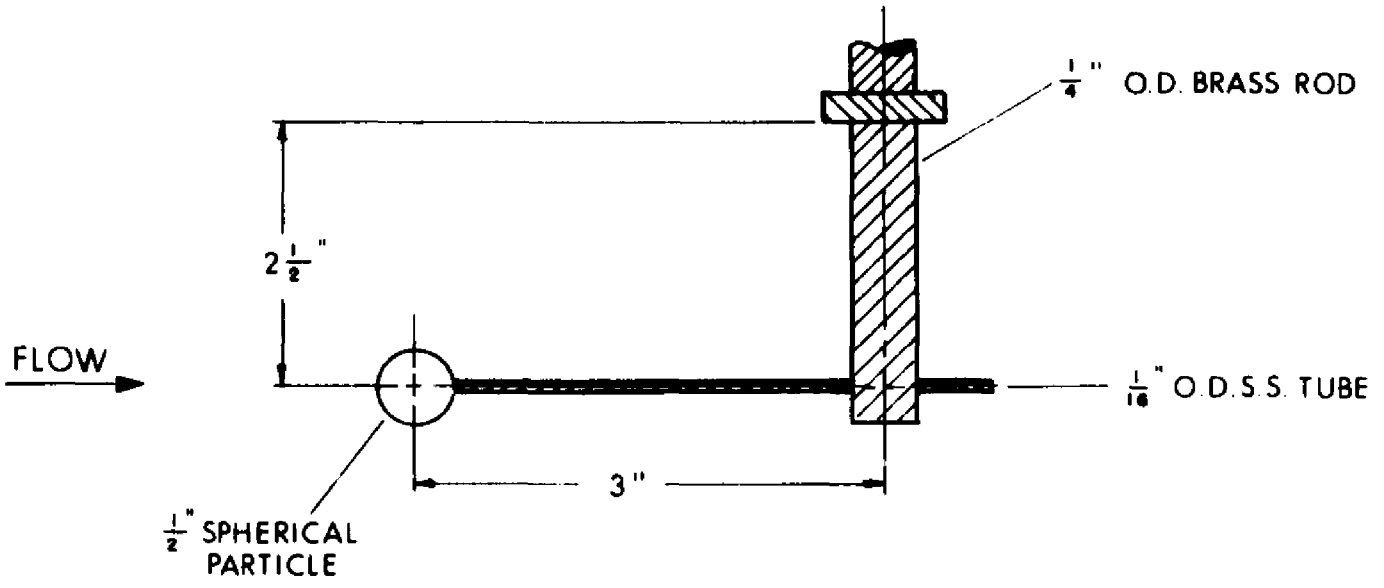

"A"

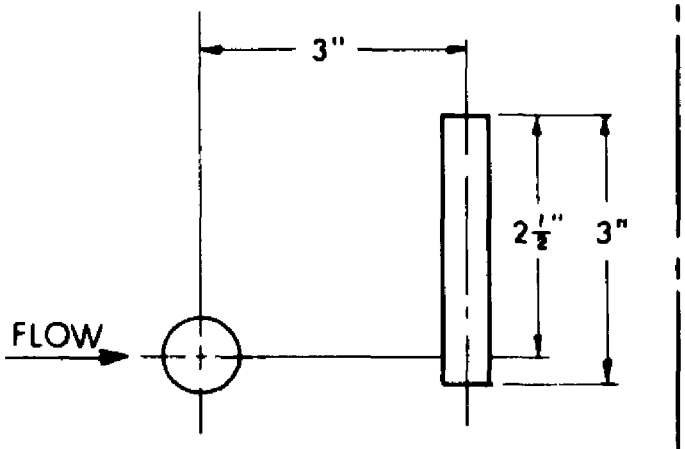

"B"

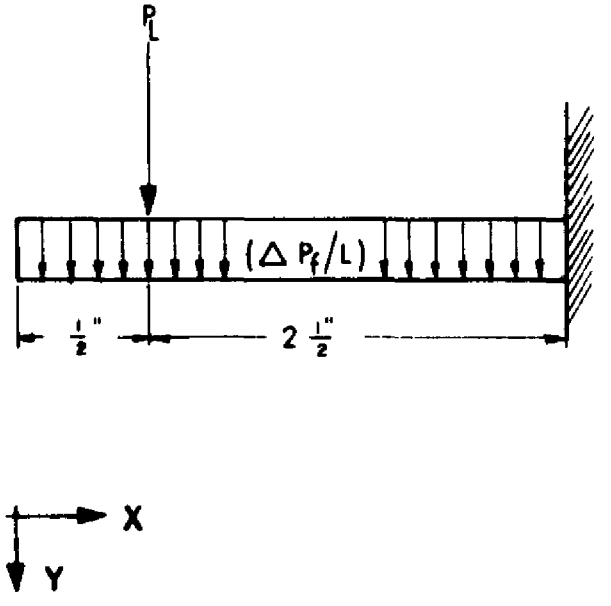

"C"

assumed, for calculating, that the weight of the particle was 29.5×10^{-4} lbs. Therefore,

$$P_L = 52.3 \times 10^{-4} \text{ lbs.} \qquad \text{(E.1)}$$

The weight per unit length of the brass rod was computed from its cross sectional area and density. The brass rod used was 3.00 inches long X 0.250 inches in diameter and it had a density of 0.455 lbs./in^3. Accordingly,

$$\frac{\Delta P}{L}_f = 2.23 \times 10^{-2} \frac{\text{lbs.}}{\text{in.}} \qquad \text{(E.2)}$$

In order to use the Rayleigh quotient to determine the natural frequency we chose to represent the maximum dynamic deflection by the static deflection curve.

Having established the loadings on the beam it was necessary to analyze the system, according to standard techniques of structural analysis, in order to obtain its deflection profile. The principle of superposition was applied to this problem and the solution to each component loading was found in the "Steel Construction Manual". Thus, the deflection profile for this system could be summarized as follows:

<u>For $x < 1/2$ inch:</u>

$$y(x) = \frac{\frac{\Delta P}{L}_f}{24EI} (x^4 - 108x + 243) + \frac{25P_L}{24EI} (6.5 - 3x) \qquad \text{(E.3)}$$

For $x > 1/2$ inch:

$$y(x) = \frac{\frac{\Delta P_f}{L}}{24EI}(x^4 - 108x + 243) + \frac{P_L}{6EI}(x^3 - 1.5x^2 - 18x + 40.5) \qquad (E.4)$$

where E = the modulus of elasticity of the material, lbs./in.^{2}

I = the moment of inertia, in.^{4}

x = any location along the length of the beam, in.

y = deflection, in.

For brass the modulus of elasticity, E, is 14×10^6 lbs./in.^{2} The moment of inertia, I, of this beam was found to be

$$I = \frac{\pi r^4}{4} = 1.91 \times 10^{-4} \text{ in.}^4 \qquad (E.5)$$

Therefore, the constant EI in equations (E.3) and (E.4) was found to have a value of 2674 lbs.-in.^{2}

At this point all the information was available for calculating the natural frequency of the composite sphere support system as

$$\frac{p^2}{g_c} = \frac{\sum PE_{max}}{\sum KE_{max}} \qquad (E.6)$$

where p = the natural frequency, cycles/sec.

g_c = the graviational constant.

$\sum PE_{max}$ = the maximum energy stored in the deflected beam.

$\sum KE_{max}$ = the maximum kinetic energy dissipated by the beam in returning to its original position.

Therefore, according to "Engineering Vibrations" by L. S. Jacobson and R. S. Ayres, McGraw-Hill, New York (1958)

$$\frac{p^2}{g_c} = \frac{\frac{1}{2}\int_o^l EI\left(\frac{d^2y}{dx^2}\right)^2 dx}{\frac{1}{2}\left(\frac{\Delta P_f}{L}\right)\int_o^l y^2 dx + P_L \angle y(x)\Big|_{x=1/2}^2} \qquad (E.7)$$

After carrying out the necessary mathematical operations and substituting the appropriate terms into equation (E.7) it was found that the natural frequency of this system was 385 cycles per second with a maximum amplitude of 9.7×10^{-5} inches.

It was possible that only the horizontal portion of the sphere support system (particle and mounting rod) would be subject to vibration. The situation considered is depicted in Figure App. 9. Essentially, this portion of the system behaved as a cantilever beam with a fixed load W_s, the weight of the sphere, at its free end and a uniformly distributed load, w, running its entire length.

The physical constants, pertinent to the vibrational computation for the horizontal member are:

A = rod cross section, 2.80×10^{-3} in.^{2}

d = rod diameter, 0.0625 in.

E = rod modulus of elasticity, 29×10^6 lbs./in.^{2}

I = rod moment of inertia, 77.6×10^{-8} in.^{4}

L = rod length, 2.875 in.

V = flow velocity, $0.c \times 10^{-2}$ to 7.8×10^{-2} ft./sec.

FIGURE APP. 9

SIMPLIFICATION OF SPHERE SUPPORT SYSTEM FOR VIBRATION CALCULATIONS

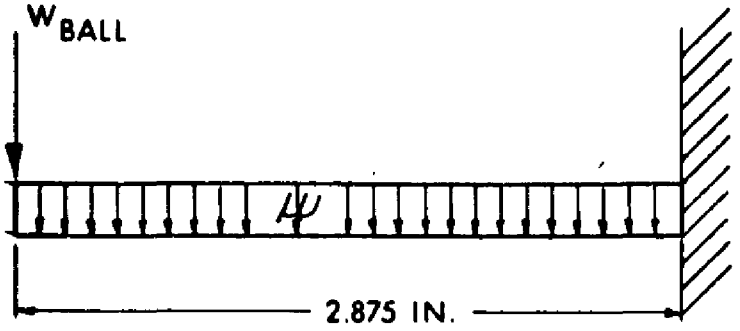

ρ_r = rod density, 0.283 lbs./in.^{3}

ρ_w = fluid density, 62.5 lbs./ft.^{3}

μ_w = fluid viscosity, 2.42 lbs./ft.-hour

From this physical data, its was possible to compute the natural frequency of this system according to the relation

$$p = \frac{\pi g_c EI}{2 \rho_r AL^4} \qquad (E.8)$$

as 635 cycles per second.

Equations (E.7) and (E.8) were derived for systems in an atmospheric environment. Since the system under consideration was immersed in a medium of much greater viscosity than air, a certain damping of the natural frequency would take place. It is the usual practice to assume that for systems in a water environment this damping would reduce the natural frequency by twenty percent. Thus, the composite system of Figure App. 8-a has a natural frequency of 308 cycles per second and the horizontal portion consisting of the particle and mounting tube of Figure App. 9 has a natural frequency of 508 cycles per second.

The amplitude of the natural frequency of the horizontal member was established using the correlation presented by Burgreen, "Vibration of Rods in Parallel Flow", Nucleonics, 17, 78, No. 8 (1959). It was found that the amplitude of the natural frequency of the horizontal member was from 3×10^{-13} to 7.5×10^{-10} inches, depending on the Reynolds number.

The two basic sources of pulses in the apparatus were the pump and spurious building vibrations. The pump rotates at 3400 revolutions per minute and could send pulses through the fluid with a frequency of 56.67 cycles per second. The frequency of the spurious building vibrations although not predictable would be low, about 2-20 cps.

In order to insure against the presence of any vibrations in the test pipeline, the pump and the main horizontal section were connected to the remainder of the apparatus by flexible connectors. The horizontal main itself was shock-mounted so that any spurious vibrations could not be transmitted to the system. Finally, the 12-1/2 foot upstream calming zone acted as a surge tank which would eliminate disturbances transmitted through the fluid.

Visual observation of the sphere and its mounting and support system throughout the course of this study showed that serious vibrations were not present in the test section.

F. METHOD OF DATA ANALYSIS

The data available at the conclusion of any given experiment in this investigation consisted of the length of the run, Δt, the weight loss of the "active" particle, ΔW, the initial, S/1, and final, S/2, radii as a function of angular position, θ, on the sphere surface as measured from the forward stagnation point, the volumetric flow rate, G, and the run temperature, T.

From the known value of T and from the physical properties of the experimental materials presented in Appendix A, it was possible to determine the fluid density, ρ_f, and viscosity, μ_f, the solid density, ρ_s, the equilibrium solubility of the solid in the liquid, C*, the diffusivity, $\mathcal{D}$, and the Schmidt number, Sc , of the solid-liquid system under investigation.

Knowledge of the initial and final radii, as a function of angular position, permitted the computation of the diminution and percent diminution as a function of location and enabled the evaluation of the initial and final particle surface areas and volumes. The initial and final surface average radii were also determined. The diminution as a function of position was obtained as

$$\Delta r_\theta = (S/1)_\theta - (S/2)_\theta \qquad (F.1)$$

The percent diminution as a function of position was calculated as

$$P_\theta = \frac{100 \times \Delta r_\theta}{(S/1)_\theta} \qquad (F.2)$$

An approximate average surface area for the particle was calculated by integrating the measured radius profile from 0 to 2π.

$$A_{avg} = 2 \int_{0}^{2\pi} r^2 \, d\theta \qquad (F.3)$$

When evaluating the initial surface area, the initial radius distribution was used and the integral in equation (F.3) was evaluated numerically by Simpson's rule. The same procedure was used to evaluate the final surface area based on the final radius distribution.

Surface average radii were calculated using the relation

$$r_{SA} = \sqrt{\frac{A_{avg}}{4\pi}} \qquad (F.4)$$

Particle volumes were determined by use of the relation

$$V = \frac{2}{3} \int_{0}^{2\pi} r^3 \, d\theta \qquad (F.5)$$

The integral in equation (F.5) was also evaluated numerically by Simpson's rule; initial volumes were calculated from initial radii profiles and final volumes from final radii profiles.

From the known fluid flow rate the average water velocity was computed by the relation

$$V_s = 0.0163G \qquad (F.6)$$

Sufficient information was then available for establishing the particle Reynolds number as

$$Re_p = \frac{2\, r_{SA}\, V_s\, \rho_f}{\mu_f} \qquad (F.7)$$

Using this relation, initial, final, and average particle Reynolds numbers were obtained.

The Peclet number was then computed from its definition as

$$Pe = Re_p \times Sc \qquad (F.8)$$

Again, initial, final, and average values were calculated.

The overall mass transfer rate was the amount of solute which passed from the solid to the liquid per unit time.

$$\left(\mathcal{N}_A\right)_o = \frac{\Delta W}{\Delta t} \qquad (F.9)$$

By definition, however, the overall mass transfer rate is related to the overall mass transfer coefficient, mass transfer driving force, and particle surface area as

$$\left(\mathcal{N}_A\right)_o = k_o \times A_{avg} \times \Delta C \qquad (F.10)$$

Thus, it was possible to evaluate the overall mass transfer coefficient as

$$k_o = \frac{\Delta W}{\Delta t \times A \times \Delta C} \qquad (F.11)$$

In general, it is possible to express the relation between mass transfer rate and mass transfer coefficient as

$$W_A = k A \Delta C = \frac{\Delta W}{\Delta t} = \frac{\rho_s \times \Delta V}{\Delta t} \qquad (F.12)$$

Thus, the local mass transfer coefficient was obtained by rearrangement of equation (F.12) so that

$$k_L = \frac{\rho_s \times \Delta V_L}{\Delta t \times A_L \times \Delta C} \qquad (F.13)$$

The density of the solid and the run length were known. The concentration driving force, ΔC, is defined as

$$C = C^* - C_B \qquad (F.14)$$

where C_B is the bulk concentration of solute. In this study the bulk concentration of solute was essentially zero; thus, the mass transfer driving force was also known. The local volume change of the solute, ΔV_L, (over a 20^o sector) and the local particle surface area, A_L, were calculated from the initial and final particle radii profiles.

It was decided, at the start of this investigation, to base the local coefficients on the average particle surface area. Hence, A_L was determined

from the initial and final radii distributions as

$$A_L = \frac{1}{2}\left[2\int_{\theta_{L-}}^{\theta_{L+}} r_i^2\, d\theta + 2\int_{\theta_{L-}}^{\theta_{L+}} r_f^2\, d\theta\right] \qquad (F.15)$$

Similarly, the local change of volume of the particle was defined as

$$V_L = V_{1L} - V_{2L} \qquad (F.16)$$

where V_{1L} and V_{2L} were found by the relation

$$V_{nL} = \frac{2}{3}\int_{\theta_{L-}}^{\theta_{L+}} r_n^3\, d \quad , n = 1 \text{ or } 2 \qquad (F.16a)$$

The integrals in equations (F.15) and (F.16a) were evaluated numerically by Simpson's rule using a theta interval of 20°.

In order to check the results and the method of calculation, the density of the solid was calculated from the particle weight loss and change in volume and the overall mass transfer coefficient was calculated from the local mass transfer profile. The density was evaluated from the expression

$$\rho_s = \frac{\Delta W}{V_1 - V_2} \qquad (F.17)$$

and was compared with the particle density measured by the technique described in Appendix D. The overall mass transfer coefficient was calculated by use of the relation

$$k_{avg} = \frac{1}{2\pi}\int_0^{2\pi} k_L(\theta)\, d\theta \qquad (F.18)$$

and was compared with the overall coefficient calculated using equation (F.11) and the experimental data.

With the local mass transfer coefficient profile available it was possible to determine the local Sherwood number as

$$N_{Sh_L} = \frac{k_L\, 2r_{SA}}{\mathcal{D}} \qquad (F.19)$$

The overall Sherwood number was calculated as

$$N_{Sh_o} = \frac{k_{avg}\,(2\, r_{SA})}{\mathcal{D}} \qquad (F.20)$$

The local mass transfer rate profiles, presented in the results section, were plotted by averaging the results for both hemispheres of the particle. Graphical integration, using a Keuffel & Esser Co. Model 62-0000 Compensating Polar Planimeter, permitted evaluation of average values of the mass transfer coefficient and Sherwood number, for the forward flow area, the wake area, and the total surface.

The "separation point" for mass transfer is defined as the point at which the minimum transfer from the particle occurs. This point, θ_{sep}, was obtained from plots of diminution vs. θ, k_L vs. θ, and N_{Sh_L} vs. θ.

All of the computations for the analysis of the present data, except the determination of the separation point and the graphical integrations, were amenable to machine computation. A MAD source language program was written for these computations for use with the IBM 7090 machine, available at the City College Computation Center.

G. CALCULATIONS OF ESTIMATED REQUIRED RUN TIME

It was necessary, at the start of this study, to obtain an estimate of the time required for a given run to achieve a desired average particle diminution of about 4%. Using the experimental results of Garner and Suckling for single spheres, the theoretical results of Pfeffer, and a knowledge of the physical properties of the materials to be studied, the plots shown in Figures App.10 and App. 11 were prepared.

It was assumed that experiments would be conducted at 20°C. and the calculations were carried out as follows:

$$N_{Sh_o} = \frac{k_o d_p}{\mathcal{D}} \qquad (G.1)$$

$$k_o = \frac{\mathcal{W}_A^{\rho}}{AC^*} \qquad (G.2)$$

$$\mathcal{W}_A^{\rho} = \frac{\rho \Delta V}{\theta} \qquad (G.3)$$

$$j_{d_o} = \frac{N_{Sh_o}}{N_{Re_p} (N_{Sc})^{1/3}} \qquad (G.4)$$

Combining equations (G.1), (G.2), and (G.3) it was found that

$$\theta = \frac{d_p \rho \Delta V}{(N_{Sh_o}) \mathcal{D} AC^*} \qquad (G.5)$$

If the mass transfer information was available as the j-factor, by combining (G.4) with (G.5) we found that

$$\theta = \frac{d_p \rho \Delta V}{j d_o \, N_{Re_p} (N_{Sc})^{1/3} \mathcal{D} AC^*} \qquad (G.6)$$

Using the physical properties at 20°C. and assuming a 4% overall change in particle diameter, equation (G .5) for benzoic acid becomes

$$\theta = \frac{531.53}{(N_{Sh})_o}, \text{ hours} \qquad (G.7)$$

and equation (G.6) becomes

$$\theta = \frac{48.76}{j d_o \, N_{Re_p}}, \text{ hours} \qquad (G.8)$$

and for beta naphthol

$$\theta = \frac{1195.81}{(N_{Sh})_o}, \text{ hours} \qquad (G.9)$$

and

$$\theta = \frac{119.58}{j d_o \, N_{Re_p}}, \text{ hours} \qquad (G.10)$$

Garner and Suckling correlated their results for single spheres as

$$(N_{Sh})_o = 2 + 0.95 (N_{Re_p})^{0.5} (N_{Sc})^{0.33} \qquad (G.11)$$

Although this equation was obtained for work with benzoic acid it was assumed to be equally applicable for beta naphthol. Table App. VII summarizes the results of the calculation for single spheres of benzoic acid and beta naphthol.

Pfeffer's results were presented graphically with plots of j_D vs. Re_p with ϵ, fractional void volume, as a parameter. Information was taken from these plots and used with equations (G.8) and (G.10) to establish the values of θ for multiparticle work. Pfeffer's results for $\epsilon = 1.0$ were also computed for comparison with Garner and Suckling's correlation. Table App. VIII summarizes the calculations of estimated run times for single and multiparticle sphere studies.

The information presented in Tables App. XV and XVI was plotted in Figures App. 10 and App. 11. These plots show a relation between θ, the length of the run necessary in hours, vs. the particle Reynolds number, Re_p, with the fractional void volume of the bed as a parameter. They served as a guide for run times to be used for a given particle Reynolds number and particle configuration.

TABLE App. VII. Estimated Required Run Times - Single Sphere Studies

Beta Naphthol

Re_p	$(N_{sh})_o$	θ
10	32.1	37.0
20	44.6	26.7
40	62.0	19.2
60	75.6	15.7
80	86.9	13.7
100	97.0	12.25
200	136.2	8.75
300	166.0	7.2

Benzoic Acid

10	34.7	15.3
20	48.4	10.95
40	67.9	8.04
60	82.1	6.05
80	94.4	5.725
100	105.5	5.04
200	148.0	3.59
300	180.25	2.94

TABLE App. VIII. Estimated Required Run Times--Multiparticle Studies

	Re_p	jd_o	θ Beta Naphthol	θ Benzoic Acid
			Hours	Hours
1.0	10	0.21	56.7	23.1
	20	0.13	45.7	18.7
	40	0.083	36.0	14.7
	60	0.063	31.8	13.0
	80	0.051	29.2	12.0
	100	0.044	27.0	11.0
	200	0.028	21.2	8.7
	300	0.022	18.5	7.5
0.9	10	0.31	39.0	15.9
	20	0.19	31.4	12.9
	40	0.12	24.8	10.1
0.8	10	0.37	32.2	13.2
	20	0.23	25.9	10.6
	40	0.15	20.6	8.4
	60	0.11	18.1	7.4
0.7	10	0.43	27.7	11.3
	20	0.27	22.1	9.0
	40	0.17	17.5	7.2
	60	0.13	15.3	6.2
	80	0.11	14.2	5.8
0.6	10	0.50	23.8	9.8
	20	0.31	19.2	7.8
	40	0.20	15.3	6.3
	60	0.15	13.2	5.4
	80	0.12	12.3	4.6
	100	0.11	11.1	4.5
0.5	10	0.59	20.2	8.3
	20	0.37	16.1	6.6
	40	0.23	13.0	5.3
	60	0.18	11.4	4.6
	80	0.15	10.3	4.2
	100	0.13	9.5	3.9

TABLE App. VIII. Continued

	Re_p	jd_o	θ Beta Naphthol	θ Benzoic Acid
			Hours	Hours
0.4	10	0.70	17.0	6.9
	20	0.44	13.5	5.5
	40	0.28	10.8	4.4
	60	0,21	9.5	3.9
	80	0.18	8.5	3.5
	100	0.15	8.0	3.2

FIGURE APP. 10

ESTIMATED REQUIRED RUN TIMES - SINGLE SPHERE STUDIES

ASSUMPTIONS: —

1. GARNER & SUCKLING'S CORRELATION IS APPLICABLE
2. A 4 % OVERALL CHANGE IN SPHERE DIAMETER
3. OPERATION at 20 °C.

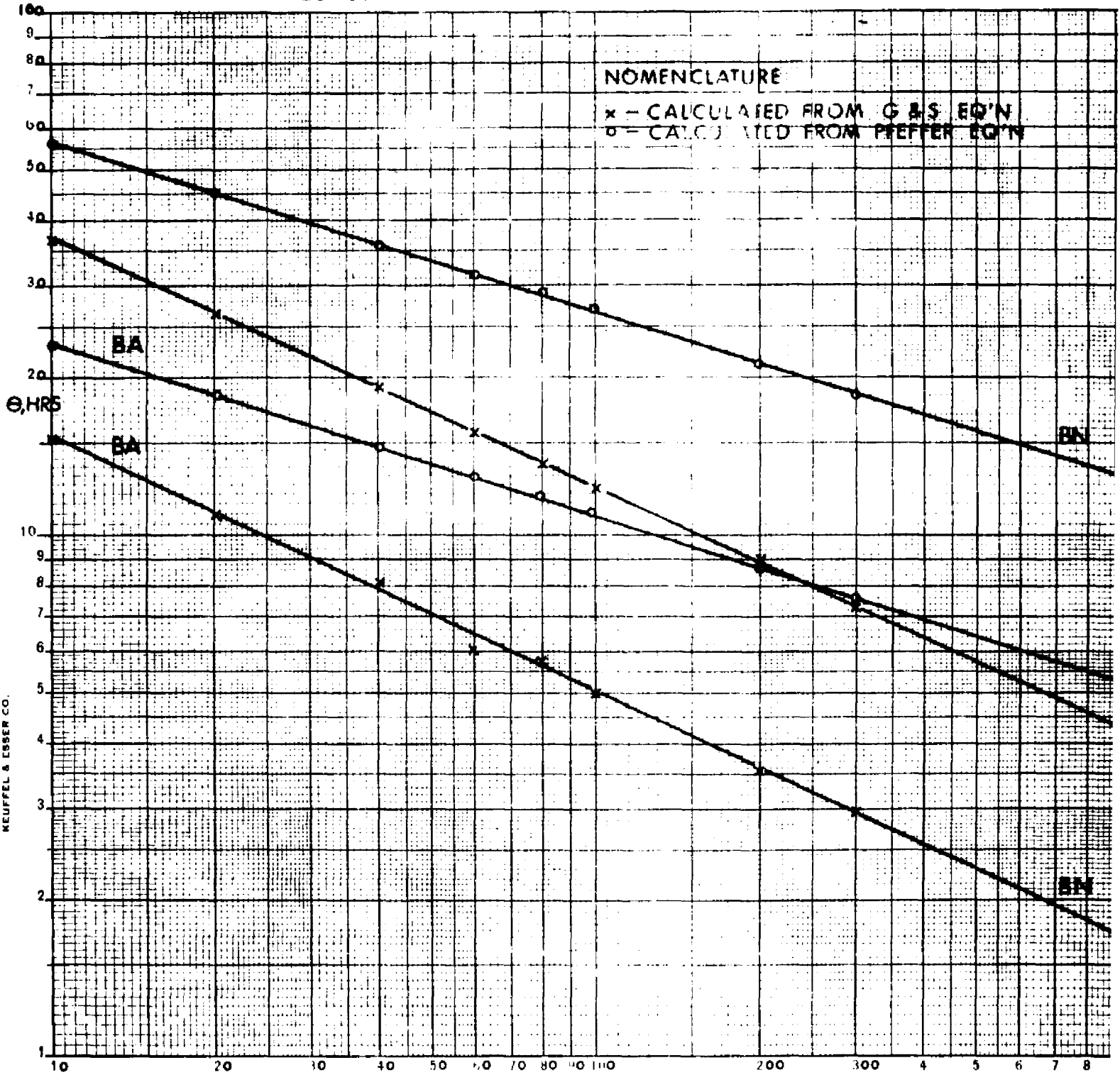

K+E LOGARITHMIC 46 7203
2 X 2 CYCLES MADE IN U.S.A.
KEUFFEL & ESSER CO.

FIGURE APP. 11a

ESTIMATED REQUIRED RUN TIMES - MULTIPARTICLE STUDIES BENZOIC ACID

ASSUMPTIONS: —

1. PFEFFER'S CORRELATION IS APPLICABLE
2. A 4 % OVERALL CHANGE IN SPHERE DIAMETER
3. OPERATION at 20°C.

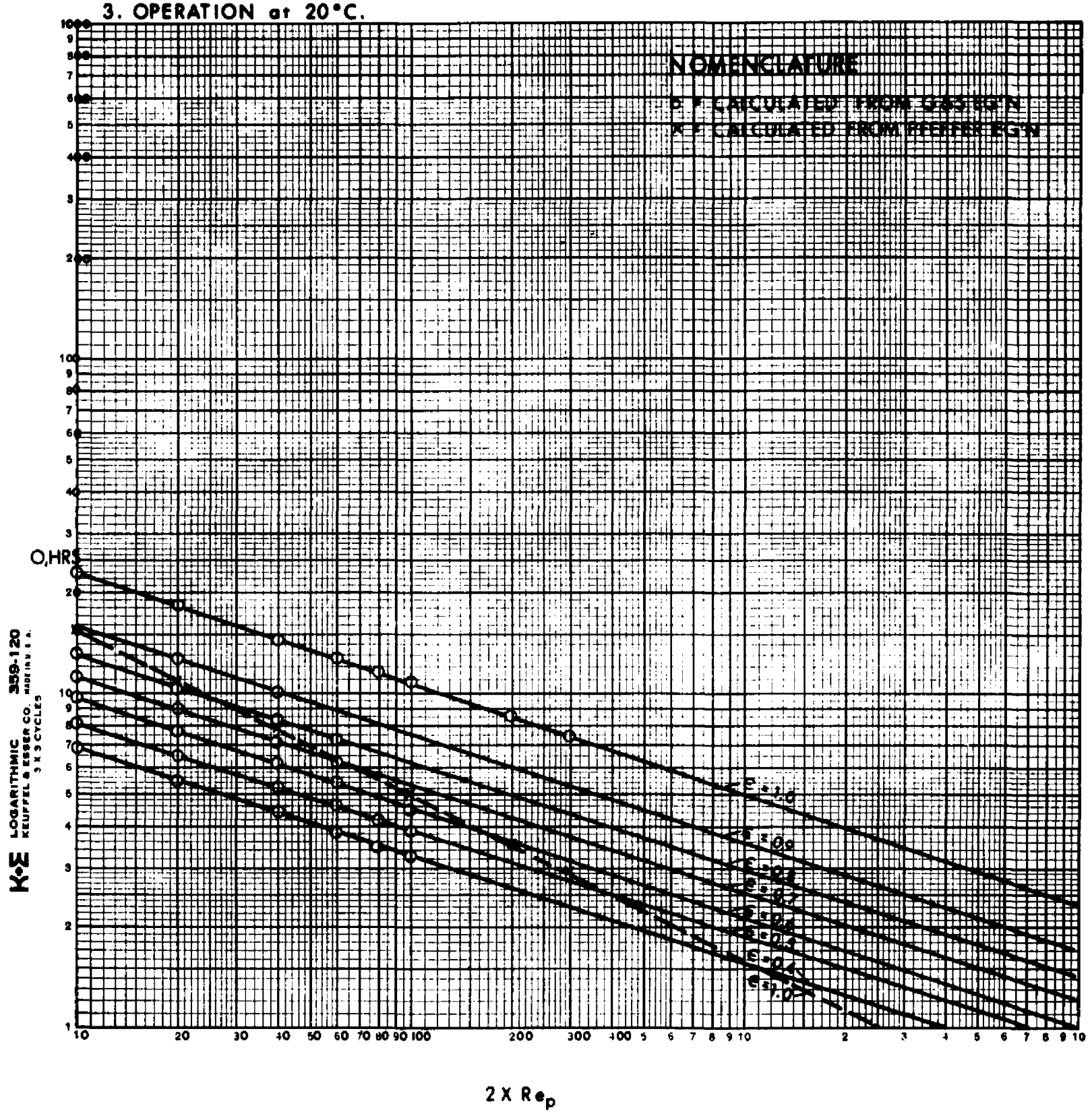

FIGURE APP. 11b

ESTIMATED REQUIRED RUN TIMES - MULTIPARTICLE STUDIES BETA NAPHTHOL

ASSUMPTIONS:—

1. PFEFFER'S CORRELATION IS APPLICABLE
2. A 4 % OVERALL CHANGE IN SPHERE DIAMETER
3. OPERATION at 20 °C.

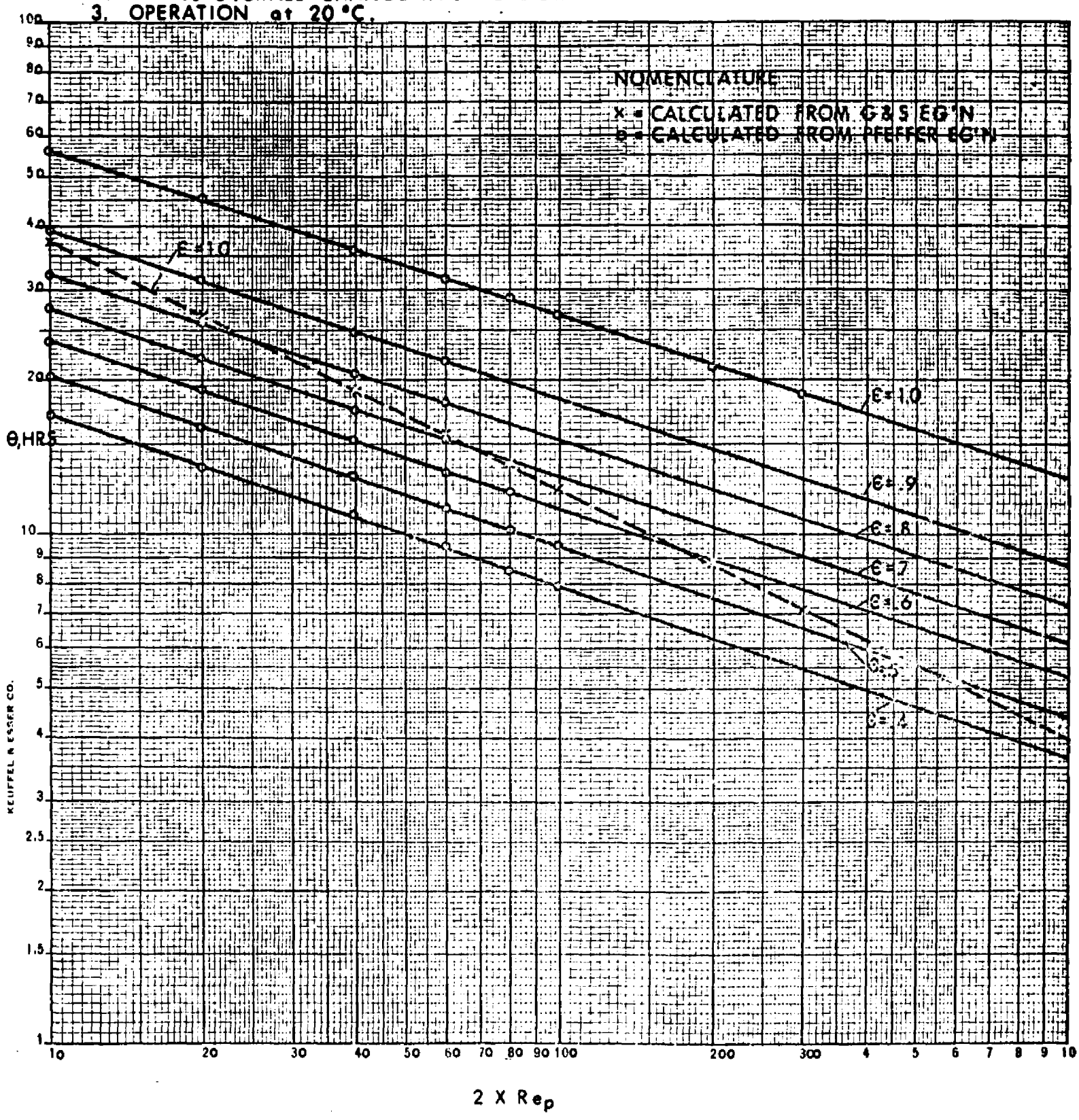

H. ERROR ANALYSIS

In this section are presented the general error analysis for this study and a sample error calculation for a typical run.

Error in the average velocity, V_{avg}:

$$V_{avg} = 0.0163G \tag{H.1}$$

and

$$\frac{dV_{avg}}{V_{avg}} = \frac{dG}{G} \tag{H.2}$$

From the rotameter calibration data

$$\frac{dG}{G} = 0.0120;\ 0.5 \leqslant G \leqslant 0.30 \tag{H.3}$$

$$\frac{dG}{G} = 0.0103;\ 0.05 \leqslant G \leqslant 0.40 \tag{H.4}$$

and therefore the relative error in V_{avg} has been defined.

Error in Diminution; r:

$$\Delta r = r_i - r_f \tag{H.5}$$

and

$$\frac{d\,\Delta r}{\Delta r} = \frac{d\,r_i + d\,r_f}{\Delta r} \tag{H.6}$$

but $$d r_i = d r_f = 1 \times 10^{-4} \text{ inches}$$

therefore,

$$\frac{d \Delta r}{\Delta r} = \frac{2 \times 10^{-4}}{\Delta r} \tag{H.7}$$

If one averages the diminution over both hemispheres of the particle to obtain Δr_{avg}, then the relative error in Δr_{avg} can be shown to be twice that for Δr.

Error in Surface Area; A_{avg}:

$$A_{avg} = 2 \int_0^{2\pi} r^2 \, d\theta \tag{H.8}$$

Using Simpson's rule and evaluating the integral over 20° theta elements it can be shown that

$$A_{avg} = 2 \sum_{k=1}^{k=18} \text{Int } (k) \tag{H.9}$$

where

$$\text{Int } (k) = \frac{\pi}{54} \left[r^2 (I) + 4(r^2 (I + 1)) + r^2 (I + 2) \right] \tag{H.10}$$

From (H.9) it was found that

$$\frac{d A_{avg}}{A_{avg}} = \sum_{k=1}^{k=18} \frac{d (\text{Int } (k))}{\text{Int } (k)} \tag{H.11}$$

and it can be shown that

$$\frac{d(\text{Int }(k))}{\text{Int }(k)} = 2 \times 10^{-4}\left[\frac{\left(r\,(I) + 4r\,(I+1) + r\,(I+2)\right)}{\left(r^2\,(I) + 4(r^2\,(I+1)) + r^2\,(I+2)\right)}\right] \qquad (H.12)$$

Initial radii profiles were used to compute the initial values of A_{avg} and the final values of A_{avg} were computed from the radii profiles obtained at the end of the runs. Similarly, initial values of dA_{avg}/A_{avg} were calculated from initial radii profiles; final values from final radii profiles.

Error in Surface Average Radius: r_{SA}:

$$r_{SA} = \sqrt{\frac{A_{avg}}{4\pi}} \qquad (H.13)$$

and it can be shown that

$$\frac{d\,r_{SA}}{r_{SA}} = \frac{1}{2}\,\frac{d\,A_{avg}}{A_{avg}} \qquad (H.14)$$

Error in Particle Volume; V:

$$V = \frac{2}{3}\int_0^{2\pi} r^3\,d\theta \qquad (H.15)$$

Using Simpson's rule and integrating over 20° volume elements it can be shown that the relative error in V is

$$\frac{dV}{V} = 2 \times 10^{-4} \sum_{k=1}^{k=18} \sum_{m=1}^{m=18} \frac{\text{Int (k)}}{\text{Int (m)}} \qquad \text{(H.16)}$$

where Int (k) is defined in equation (H.10) and

$$\text{Int (m)} = \frac{\pi}{54} \left[r^3 (I) + 4 (r^3 (I + 1)) + r^3 (I + 2) \right] \qquad \text{(H.17)}$$

Initial and final values of V were computed from initial and final radius profiles. Similarly, initial and final values of dV/V were computed.

Error in Reynolds Number; Re_p:

$$Re_p = \frac{2 r_{SA} V_{avg} \rho_f}{\mu_f} \qquad \text{(H.18)}$$

and therefore

$$\frac{d Re_p}{Re_p} = \frac{d r_{SA}}{r_{SA}} + \frac{d V_{avg}}{V_{avg}} + \frac{d\rho_f}{\rho_f} + \frac{d\mu_f}{\mu_f} \qquad \text{(H.19)}$$

Reynolds numbers were computed based on the initial, final and average values of r_{SA} and initial and final values of the relative error in Re_p were calculated using equation (H.19). The relative error in the average value of Re_p was calculated as

$$\frac{d (\overline{Re_p})}{\overline{Re_p}} = \frac{d (Re_p)_i + d (Re_p)_f}{(Re_p)_i + (Re_p)_f} \qquad \text{(H.20)}$$

Error in Peclet Number; Pe:

$$Pe = Re_p \times Sc \tag{H.21}$$

and

$$\frac{d\,Pe}{Pe} = \frac{d\,Re_p}{Re_p} + \frac{d\,Sc}{Sc} \tag{H.22}$$

Peclet numbers were calculated based on initial, final, and average values of Re_p. The relative error in Pe therefore was computed using equation (H.22) and the appropriate value for the relative error in Re_p.

Error in Mass Transfer Rate: $\mathscr{N}_A$:

$$\mathscr{N}_A = \frac{\Delta W}{\Delta t} \tag{H.23}$$

and

$$\frac{d\mathscr{N}_A}{\mathscr{N}_A} = \frac{d\,\Delta W}{\Delta W} + \frac{d\,\Delta t}{\Delta t} \tag{H.24}$$

where $d\,\Delta W = \pm 2 \times 10^{-4}$ grams

$d\,\Delta t = \pm 0.01$ hours

Error in Overall Mass Transfer Coefficient, k_o:

$$k_o = \frac{\mathscr{N}_A}{A_{avg}\, C^*} \tag{H.25}$$

and

$$\frac{d\,k_o}{k_o} = \frac{d\rho_A}{\rho_A} + \frac{d\,A_{avg}}{A_{avg}} + \frac{d\,C^*}{C^*} \qquad (H.26)$$

Overall mass transfer coefficients were calculated based on initial, final, and average values of average surface area and therefore relative errors for k_o were computed using equation (H.26) and the appropriate value of $d\,A_{avg}/A_{avg}$.

Error in Overall Sherwood Number: Sh_o:

$$Sh_o = \frac{k_o \times 2\,r_{SA}}{\mathcal{D}\,\rho_f} \qquad (H.27)$$

and

$$\frac{d\,Sh_o}{Sh_o} = \frac{d\,k_o}{k_o} + \frac{d\,r_{SA}}{r_{SA}} + \frac{d\mathcal{D}}{\mathcal{D}} + \frac{d\rho_f}{\rho_f} \qquad (H.28)$$

Error in Local Mass Transfer Coefficient: k_L

$$k_L = \frac{\rho_s \times \Delta V_L}{\Delta t \times A_L \times C^*} \qquad (H.29)$$

and

$$\frac{d\,k_L}{k_L} = \frac{d\rho_s}{\rho_s} + \frac{d\,C^*}{C^*} + \frac{d\,\Delta t}{\Delta t} + \frac{d\,\Delta V_L}{\Delta V_L} + \frac{d\,A_L}{A_L} \qquad (H.30)$$

Error in Local Sherwood Number; Sh_L:

$$\frac{d\,Sh_L}{Sh_L} = \frac{d\,k_L}{k_L} + \frac{d\,\bar{r}}{\bar{r}} + \frac{d\mathcal{D}}{\mathcal{D}} + \frac{d\,\rho_f}{\rho_f} \qquad (H.31)$$

The following are the results of the error analysis for Run No. I-3, which is typical of this study.

Relative Error in the Average Velocity = 0.0120

Relative Error in the Initial Average Surface Area = 0.00081

Relative Error in the Initial Surface Average Radius = 0.00041

Relative Error in the Final Average Surface Area = 0.00082

Relative Error in the Final Surface Average Radius = 0.00041

Relative Error in the Initial Average Volume = 0.00121

Relative Error in the Final Average Volume = 0.00123

Relative Error in the Initial Reynolds Number = 0.0146

Relative Error in the Final Reynolds Number = 0.0146

Relative Error in the Average Reynolds Number = 0.0146

Relative Error in the Initial Peclet Number = 0.0256

Relative Error in the Final Peclet Number = 0.0256

Relative Error in the Average Peclet Number = 0.0256

Relative Error in the Average Mass Transfer Rate = 0.0031

Relative Error in the Initial Overall Mass Transfer Coefficient = 0.0193

Relative Error in the Final Overall Mass Transfer Coefficient = 0.0193

Relative Error in the Average Overall Mass Transfer Coefficient = 0.0193

Relative Error in the Overall Sherwood Number = 0.0282

The tabulation below summarizes the relative error in the average local diminution, the relative error in the local mass transfer coefficients, and the relative error in the local Sherwood numbers as a function of position on the particle surface.

θ Degrees	$\frac{d\Delta r}{\Delta r}$	$\frac{d\, k_L}{k_L}$	$\frac{d\, Sh_L}{Sh_L}$
0, 360	.030	.058	.067
10, 350	.098	.059	.067
20, 340	.061	.059	.068
30, 330	.082	.059	.069
40, 320	.034	.060	.069
50, 310	.035	.061	.070
60, 300	.039	.061	.071
70, 290	.037	.063	.073
80, 280	.045	.064	.073
90, 270	.047	.065	.076
100, 260	.053	.067	.078
110, 250	.070	.069	.080
120, 240	.047	.071	.083
130, 230	.063	.074	.085
140, 220	.130	.076	.088
150, 210	.088	.080	.091
160, 200	.079	.083	.099
170, 190	.071	.090	.099
180	.067	.095	.103

I. FLUX EFFECT CALCULATIONS

These calculations were made according to the relations presented in Bird, et. al. For benzoic acid-water

$$C^* = 0.00353 \text{ grams/gram of solution} \tag{I.1}$$

$$R_{AB} = \frac{0.00353}{1.0 - 0.00353} = 0.00354 \tag{I.2}$$

$$\phi_{AB} = \ln (1 + R_{AB}) = \ln (1.00354) \tag{I.3}$$

For beta naphthol - water

$$C^* = 0.00065 \text{ grams/gram of solution} \tag{I.4}$$

$$R_{AB} = \frac{0.00065}{1.0 - 0.00065} = 0.00065 \tag{I.5}$$

$$\phi_{AB} = \ln(1.00065) \tag{I.6}$$

By definition

$$\theta_{AB} = \frac{k_{corrected}}{k_{uncorrected}} = \frac{\phi_{AB}}{R_{AB}} \tag{I.7}$$

and therefore

$$\frac{\theta_{BA}}{\theta_{BN}} = \frac{\phi_{BA} R_{BN}}{R_{BA} \phi_{BN}} = \frac{\ln (1.00354) \times .00065}{\ln (1.00065) \times .00354} \tag{I.8}$$

From which we find that

$$\frac{\theta_{BA}}{\theta_{BN}} = 0.987 \qquad \text{(I.9)}$$